Quantum Science and Technology

Georgios M. Nikolopoulos
Igor Jex *Editors*

# Quantum State Transfer and Network Engineering

Springer

# Quantum Science and Technology



For further volumes:
http://www.springer.com/series/10039

# Quantum Science and Technology

## Aims and Scope

The book series Quantum Science and Technology is dedicated to one of today's most active and rapidly expanding fields of research and development. In particular, the series will be a showcase for the growing number of experimental implementations and practical applications of quantum systems. These will include, but are not restricted to: quantum information processing, quantum computing, and quantum simulation; quantum communication and quantum cryptography; entanglement and other quantum resources; quantum interfaces and hybrid quantum systems; quantum memories and quantum repeaters; measurement-based quantum control and quantum feedback; quantum nanomechanics, quantum optomechanics and quantum transducers; quantum sensing and quantum metrology; as well as quantum effects in biology. Last but not least, the series will include books on the theoretical and mathematical questions relevant to designing and understanding these systems and devices, as well as foundational issues concerning the quantum phenomena themselves. Written and edited by leading experts, the treatments will be designed for graduate students and other researchers already working in, or intending to enter the field of quantum science and technology.

Georgios M. Nikolopoulos • Igor Jex
Editors

# Quantum State Transfer and Network Engineering

Springer

*Editors*

Georgios M. Nikolopoulos
Institute of Electronic Structure and Laser
Foundation for Research
and Technology - Hellas

Igor Jex
Faculty of Nuclear Sciences
and Physical Engineering
Czech Technical University in Prague
Prague, Czech Republic

ISBN 978-3-642-39936-7 ISBN 978-3-642-39937-4 (eBook)
DOI 10.1007/978-3-642-39937-4
Springer Heidelberg New York Dordrecht London

Library of Congress Control Number: 2013950265

# Preface

The field of Quantum Information Processing and Technology was born in obscurity in the 1980s, at the intersection of physics, mathematics and computer science. In the decades that followed, the field experienced an explosive growth, with numerous theoretical and experimental scientific breakthroughs. The use of quantum mechanical principles in computation and communication tasks has changed our perception of the nature of information, and has led us to a reconsideration of its processing. Nowadays Quantum Information Processing and Technology is a well established discipline, with many ideas and discoveries that pave the way to more efficient and faster information processing, and more secure quantum networks and communication.

In contrast to classical information processing, where the information is typically coded into sequences of zeros and ones, in the framework of quantum information processing one deals with quantum states of physical systems, such as atoms, ions, quantum dots, Josephson junctions, topological defects, etc. Individual physical systems can be interconnected in various configurations, giving rise to large clusters and networks that are designed so as to perform efficiently certain information processing tasks, by exploiting fundamental principles of quantum mechanics. Faithful transfer of quantum states between two distant points is a necessary precondition for large-scale quantum information processing and networking, irrespective of the physical platform. Hence, the problems of quantum-state transfer and quantum-network engineering have attracted enormous interest over the last decade, and constitute one of the most active areas of research in Quantum Information Processing and Technology.

The present book is a representative collection of contributions dealing with various aspects of this exciting research area. The authors are leading figures in the field who have contributed significantly to its development and are responsible for some of the chief achievements. The chapters illustrate the interdisciplinary character of this research area which has links to transport phenomena, complex systems and spintronics. Possible physical platforms for the realization of quantum networks and studies of quantum-state transfer schemes include liquid and solid-state NMR systems, condensed-matter systems, and quantum optical systems. Each

chapter of this book is a review of theoretical or experimental achievements on a particular topic. We emphasize here that the present book is devoted to a rapidly changing research area and despite the efforts of the authors, some of the recent developments and publications may have not been covered. We hope, however, that the book will serve the interested reader as a welcome reference and introduction to quantum networks and the problem of quantum-state transfer, and will stimulate the scientific community toward new developments in the field.

Heraklion, Greece — Georgios M. Nikolopoulos
Prague, Czech Republic — Igor Jex
June 2013

# Contents

# List of Contributors

**Gonzalo A. Álvarez** Department of Chemical Physics, Weizmann Institute of Science, Rehovot, Israel

**Leonardo Banchi** ISI Foundation, Torino, Italy

**Abolfazl Bayat** Department of Physics and Astronomy, University College London, London, UK

**Matthieu Bellec** Laboratoire Physique de la Matière Condensée, CNRS UMR 7336, Université Nice-Sophia Antipolis, Nice, France

**Sougato Bose** Department of Physics and Astronomy, University College London, London, UK

**Thomas Brougham** Department of Physics, University of Strathclyde, Glasgow, Scotland, UK

**Daniel Klaus Burgarth** Institute of Mathematics and Physics, Aberystwyth University, Physical Sciences Building, Penglais Campus, Aberystwyth, UK

**Paola Cappellaro** Nuclear Science and Engineering Department and Research Laboratory of Electronics, Massachusetts Institute of Technology, Cambridge, USA

**Carlo Di Franco** Centre for Theoretical Atomic, Molecular and Optical Physics, School of Mathematics and Physics, Queen's University Belfast, Belfast, UK

**Vittorio Giovannetti** NEST, Scuola Normale Superiore and Istituto Nanoscienze-CNR, Pisa, Italy

**Antonin Hoskovec** Department of Physics, Faculty of Nuclear Sciences and Physical Engineering, Czech Technical University in Prague, Praha 1, Staré Město, Czech Republic

**Igor Jex** Department of Physics, Faculty of Nuclear Sciences and Physical Engineering, Czech Technical University in Prague, Praha 1, Staré Město, Czech Republic

**Myungshik Kim** QOLS, Blackett Laboratory, Imperial College London, London, UK

**Georgios M. Nikolopoulos** Institute of Electronic Structure and Laser, Foundation for Research and Technology – Hellas, Heraklion, Greece

**Omar Osenda** Facultad de Matemática, Astronomía y Física, Universidad Nacional de Córdoba, Córdoba, Argentina

**Mauro Paternostro** Centre for Theoretical Atomic, Molecular and Optical Physics, School of Mathematics and Physics, Queen's University Belfast, Belfast, UK

**Pasquale Sodano** International Institute of Physics, Universidade Federal do Rio Grande do Norte, Natal, Brazil

**Joachim Stolze** Institut für Physik, Technische Universität Dortmund, Dortmund, Germany

**Stelios Tzortzakis** Institute of Electronic Structure and Laser, Foundation for Research and Technology – Hellas, Heraklion, Greece

**Paola Verrucchi** Istituto dei Sistemi Complessi, Consiglio Nazionale delle Ricerche, Sesto Fiorentino, Italy

**Analia Zwick** Department of Chemical Physics, Weizmann Institute of Science, Rehovot, Israel

# Chapter 1
# Spin Chains as Data Buses, Logic Buses and Entanglers

**Sougato Bose, Abolfazl Bayat, Pasquale Sodano, Leonardo Banchi, and Paola Verrucchi**

**Abstract** In this contribution, we describe some uses of the nonequilibrium dynamics of a spin chain in connecting remote registers for scalable quantum information processing. We first present a brief motivation, and a basic scheme to illustrate the idea of quantum state transfer through a spin chain. This is followed by an outline survey (by no means exhaustive) of the progress to date. We then describe one of the recently proposed methods which provides a high fidelity state transfer

S. Bose (✉) · A. Bayat
Department of Physics and Astronomy, University College London, Gower Street, London WC1E 6BT, UK
e-mail: s.bose@ucl.ac.uk; abolfazl.bayat@ucl.ac.uk

P. Sodano
International Institute of Physics, Federal University of Rio Grande do Norte, A. Odilon Gomes de Lima 1722, Capim Macio, Natal, RN, 59078-400, Brazil

INFN, Sezione di Perugia, Via A. Pascoli, 06123, Perugia, Italy
e-mail: pasquale.sodano02@gmail.com

L. Banchi
ISI Foundation, Via Alassio 11/c, I-10126 Torino (TO), Italy

Dipartimento di Fisica, Università di Firenze, Via G. Sansone 1, I-50019 Sesto Fiorentino (FI), Italy

INFN Sezione di Firenze, via G.Sansone 1, I-50019 Sesto Fiorentino (FI), Italy
e-mail: leonardo.banchi@isi.it

P. Verrucchi
Istituto dei Sistemi Complessi, Consiglio Nazionale delle Ricerche, via Madonna del Piano 10, I-50019 Sesto Fiorentino (FI), Italy

Dipartimento di Fisica, Università di Firenze, Via G. Sansone 1, I-50019 Sesto Fiorentino (FI), Italy

INFN Sezione di Firenze, via G.Sansone 1, I-50019 Sesto Fiorentino (FI), Italy
e-mail: verrucchi@fi.infn.it

G.M. Nikolopoulos and I. Jex (eds.), *Quantum State Transfer and Network Engineering*, Quantum Science and Technology, DOI 10.1007/978-3-642-39937-4_1,

with minimal engineering, encoding and control. Next we present a couple of protocols for using nonequilibrium dynamics induced by quenches for establishing entanglement between well separated spins – these use the natural entanglement in a canonical condensed matter system, namely the Kondo system, but convert it to a useful form through the dynamics. Finally the possibility of usage of spin chains for quantum logic between remote registers is discussed along with a specific application to atomic systems.

## 1.1 Introduction: Motivations for Spin Chain Buses

For literally any type of computing hardware, data buses are an essential element. By linking a number of smaller processors together a larger effective processor is built. The same holds for quantum computing hardware where linking distinct quantum processors effectively amounts to being able to transfer qubits with high fidelity between the processors. Indeed this is regarded as an added DiVincenzo criteria for scalable quantum architecture [1] and a number of methods, namely, the physical movements of ions [2] and electrons [3], as well as mediation through optical qubits [4] are being actively pursued. Typically, a quantum computing hardware consists of entities such as spins in solid state systems or trapped ions or superconducting systems as qubits. These are essentially static entities (a notable exception is linear optics quantum computing where flying photons are used as qubits). It is thereby interesting to realize buses for quantum states which entirely rely on such static qubits, as opposed to physically moving the qubits or transferring their states to photons. The quantum state will be transferred from qubit to qubit down a chain solely due to the *interactions* and thereby there will be no necessity of moving entities. If we want a protocol which is minimally controlled, i.e., it does not require time control of *all* or *most* of the interactions along the chain of qubits through which we intend transfer the quantum state, then we end up with a line of qubits with permanent interactions (typically among the nearest neighbour qubits of the chain). Such a system of many permanently coupled qubits (or equivalently spin-1/2 systems) is an example of a spin chain. The central horizontal line of qubits in Fig. 1.1 where the dashed lines between qubits are the permanent interactions, is an example of a spin chain (in this chapter, we will often use the words qubits and spins interchangeably). Thereby, as an alternative to either physically moving static qubits or using hybrid technologies to interchange/correlate their states with photonic flying qubits, one may use a spin chain of the same static qubits to transport arbitrary quantum states (or equivalently quantum information) between one place and another [5, 6]. Particularly, the above strategy will have the appeal of enabling the fabrication of "all solid-state" chips containing only a single species of qubits for both information processing and transport. The question then is how well does this strategy work – or whether it works well at all enough to be a viable alternative to the other methods mentioned above. This is the central question that we will be addressing in this chapter and indeed show that there are quite a few clever but simple strategies to use a spin chain to affect a high quality quantum state transfer.

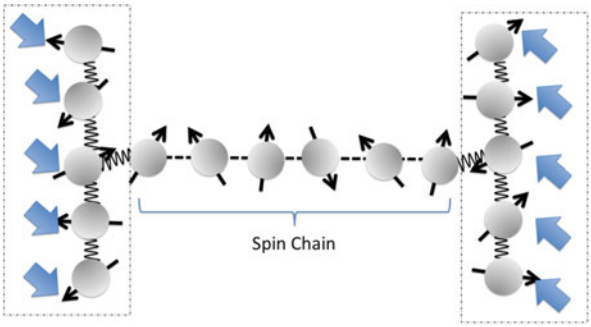


**Fig. 1.1** Two quantum registers (vertical arrays of qubits) with control fields (*block arrows*) on each qubit and fully switchable couplings (*wiggly lines*) being connected by a spin chain (horizontal array of qubits with permanent interactions shown as *dashed lines*)

Before moving over to discuss the strategies, let us point out a few other motivations. One of these is the fact that a quantum register is a highly controlled region with controls essentially going to each qubit and their interactions. Schematic examples of quantum registers are the two vertical rows of qubits shown in Fig. 1.1, where the block-arrows represent controls going to each qubit. However, controls are also required for interactions, so in principle, there should be even more block arrows than shown in the figure. Each of these block arrows depict, for example, electrodes or fiber tips or some such way of applying classical fields to the qubits. These are connected to distinct macroscopic controls in the end, which should typically be "keys or dials" accessible to a programmer/experimentalist and in this sense, much larger than the qubit (say a single spin) that it controls! So it will eventually be *necessary* for small collections of qubits (i.e., a quantum register) to be deliberately separated by spacers, so that there is enough space to accommodate all the macroscopic controls going into each register [7]. Naturally, these spacers have to be regions without controls, but they should still be able to transport states of qubits between registers. Thus if they are a line of qubits without controls, then, at least, the interactions between them must be permanent so that states can flow through them. In other words, they have to be spin chains, and it is this full scenario, i.e., two registers connected by a spin chain acting as both a spacer and an information bus, that is shown in Fig. 1.1. There might also be scenarios where *all* qubits of a given quantum processor have to be deliberately kept far apart from each other. This may arise because, in general, we want logic gates between "arbitrary pairs" of qubits for quantum computation. However, this flexibility is hard to achieve in a fixed array of static qubits (for example, for atomic qubits held in an optical lattice), which may notably interact only with their nearest neighbours. Thereby it may advisable to space them sufficiently apart so that no qubit interacts with any other qubit unless we want them to. When we want any two specific qubits to take part in a logic gate, we resort to some sort of a bus that mediates the desired quantum gate involving them. This bus can be a spin chain as demonstrated in Refs. [8,9] (this scenario will be discussed in Sect. 1.7).

Fundamentally, the interface of spin chains, or more generally quantum many-body systems and quantum information has been a widely studied field in recent

years. Notably, applications of many-body systems in quantum information processing already exist, such as in topological quantum computation [10] and in measurement based quantum computation [11]. These applications mainly concern stationary states, and do not go into many-body nonequilibrium dynamics (by which we mean nearly unitary dynamics, fast/non-adiabatic, for an extended duration of time), though this is now a widely studied field of condensed matter physics [12] and now possible to realize in many-body systems [13]. The idea of using a spin chain as a bus for communicating quantum states is an example of a minimal application of such dynamics to quantum information processing.

An alternative motivation stems from the fact that spin chains, as defined above as an array of permanently coupled qubits, are increasingly becoming feasible in varied systems. With the progress in maintaining the coherence of qubits for longer durations, their arrays are also likely to support near unitary dynamics for extended durations – if this is not the case, then it is unlikely that quantum computation will be possible with that type of qubit. Thus numerous candidates are on the way for affecting spin chain mediated quantum state transfer. The earliest proposals of implementations were given for chains of quantum dots [14] and superconducting qubits [15]. More recently with realizations of long time nonequilibrium dynamics [13] and existing spin chain proposals [16, 17], ultracold atoms in optical lattices are emerging as an interesting prospect and so are trapped ions [18, 19]. Recently a simulation of certain protocols have also been performed with coupled optical waveguides [20]. In actual spin systems, chains of electrons of nitrogen impurities in diamond have recently been considered as a potential connector for room temperature NV center quantum registers [21–24], spin chain simulations have been probed with NMR [25], solid state NMR [26,27] and phosphorous donor spin chains in silicon [28].

## 1.2 A Basic State Transfer Scheme

We first intend to illustrate the simple fact that a quantum state can indeed be transferred "over a distance" using the dynamics of a spin chain Hamiltonian. Here by "over a distance" we mean over a chain composed of several ($N$) spins. Note that there must be a quantification of the quality of the transfer, and for this we use a figure of merit called the fidelity. Suppose a pure state $|\psi_{in}\rangle$ evolves to a slightly different and possibly mixed state $\rho_{out}$ while passing through a communication channel (e.g., our spin chain), then the fidelity of the output state ($\rho_{out}$) relative to the input state ($|\psi_{in}\rangle$) is given by $\langle\psi_{in}|\rho_{out}|\psi_{in}\rangle$. The fact that this is a useful figure of merit can be made clear by observing that if the spin chain were to serve as a "perfect" channel, then $\rho_{out} = |\psi_{in}\rangle\langle\psi_{in}|$ and the fidelity is unity. Transferring the state of a qubit will be useful only when this fidelity is above a threshold, which is, for example, $\frac{2}{3}$ for qubits (if the fidelity of transmission is below $\frac{2}{3}$, then one need not have used a quantum channel such as a spin chain to transfer

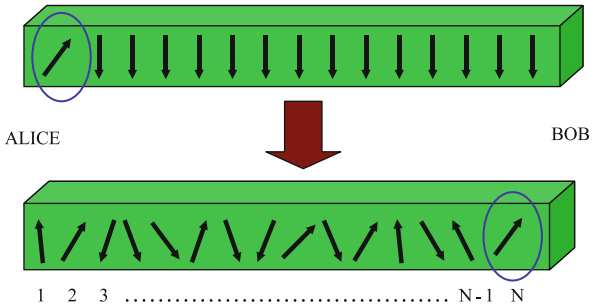


**Fig. 1.2** The simplest spin chain communication protocol. A spin-1/2 ferromagnetic spin chain with all spins facing down is the quantum channel. Alice simply places a quantum state at one end of the chain and Bob simply picks up a close approximation of this state from his end of the spin chain after waiting a while (This figure is adopted from Ref. [5])

the state and instead could simply have measured the state and sent the measurement data – the receiving party could reconstruct the state with a fidelity of $\frac{2}{3}$ from this measured data [29]).

With the above figure of merit in mind, we now examine one of the simplest spin chains and a most naive protocol for quantum communication through it. This is based on the scheme presented in Ref. [5], where the idea of using a spin chain as a communication channel was first explored. The scheme is not meant to optimize the usage of the spin chain as a channel, but just check how well it can transfer a state without any optimizations. We will use isotropic couplings in a spin chain (i.e, coupling between all components of spin being equal) so that its Hamiltonian is

$$\mathbf{H} = J \sum_{j=1}^{N} \boldsymbol{\sigma}_j . \boldsymbol{\sigma}_{j+1} = J \sum_{j} (\sigma_j^x \sigma_{j+1}^x + \sigma_j^y \sigma_{j+1}^y + \sigma_j^z \sigma_{j+1}^z). \tag{1.1}$$

We assume that the spin chain initialized to a very simple state, such as one in which all spins are in the state $|0\rangle$ (or pointing down). We will have to choose the couplings $J$ in Eq. (1.1) in such a manner that initialization of the spin chain to such a state is easy. Accordingly, we choose $J < 0$, i.e., the spin chain is *ferromagnetic*. The ground state of a ferromagnet in a magnetic field, however weak, is a *symmetry broken* state in which all spins align with the direction of the field. For communication, Alice places an arbitrary quantum state at one end of the spin chain in such an "all down" state. This is depicted in the upper part of Fig. 1.2, where Alice has placed an arbitrary state on the first spin of the chain, while all the other spins are still in the down state. Due to the natural evolution of the chain this state both disperses and propagates along the chain. As a result of this evolution, the state of the spin at Bob's end of the chain will vary with time. Bob now chooses an optimal moment of time in a long interval (as long as he can afford to wait!) to receive Alice's state. This moment of time is carefully chosen so that the state of the

spin at Bob's end of the chain is as close as possible to the one that Alice intended to transmit. At this optimum time, Bob simply picks up the spin at his end of the chain, to conclude the communication protocol.

Say there are $N$ spins in the chain and these are numbered $1, 2, \ldots, N$ as shown in Fig. 1.2. As mentioned above, we initialize the ferromagnet in its ground state $|\mathbf{0}\rangle = |000\ldots0\rangle$ where $|0\rangle$ denotes the spin down state of a spin (to be more specific, spins aligned along $-z$ direction). We will set the ground state energy $E_0 = 0$ (i.e., redefine $\mathbf{H}$ as $E_0 + \mathbf{H}$) for the rest of this section. We also introduce the class of states $|\mathbf{j}\rangle = |00\ldots010\ldots.0\rangle$ (where $\mathbf{j} = \mathbf{1}, \mathbf{2}, \ldots, \mathbf{N}$) in which the spin at the $j$th site has been flipped to the $|1\rangle$ state. We now assume that the state sender Alice is located closest to the first spin and the state receiver Bob is located closest to the $N$th spin. As mentioned before, to start the protocol, Alice simply places the state she wants to transmit to Bob on the first spin at time $t = 0$. Let this state be $|\psi_{in}\rangle = \cos(\theta/2)|0\rangle + e^{i\phi}\sin(\theta/2)|1\rangle$. We can then describe the state of the whole chain at this instant (time $t = 0$) as

$$|\Psi(0)\rangle = \cos\frac{\theta}{2}|\mathbf{0}\rangle + e^{i\phi}\sin\frac{\theta}{2}|\mathbf{1}\rangle. \tag{1.2}$$

Bob now waits for a specific time till the initial state $|\Psi(0)\rangle$ evolves to a final state which is as close as possible to $\cos\frac{\theta}{2}|\mathbf{0}\rangle + e^{i\phi}\sin\frac{\theta}{2}|\mathbf{N}\rangle$. As $[\mathbf{H}, \sum_{i=1}^{N}\sigma_z^i] = 0$, the state $|\mathbf{1}\rangle$ only evolves to states $|\mathbf{j}\rangle$ and the evolution of the spin chain (with $\hbar = 1$) is

$$|\Psi(t)\rangle = \cos\frac{\theta}{2}|\mathbf{0}\rangle + e^{i\phi}\sin\frac{\theta}{2}\sum_{\mathbf{j}=\mathbf{1}}^{\mathbf{N}}\langle\mathbf{j}|e^{-i\mathbf{H}t}|\mathbf{s}\rangle|\mathbf{j}\rangle. \tag{1.3}$$

The state of the $N$th spin will, in general, be a mixed state, and can be obtained by tracing off the states of all other spins from $|\Psi(t)\rangle$. This means that the density operator $\rho_{out}$ of the output state is obtained by $\mathrm{Tr}_{1,2,\ldots,N-1}(|\Psi(t)\rangle\langle\Psi(t)|)$, where $\mathrm{Tr}_{1,2,\ldots,N-1}$ means tracing over the states of the systems 1 to $N-1$. This evolves with time as

$$\rho_{out}(t) = P(t)|\psi_{out}(t)\rangle\langle\psi_{out}(t)| + (1 - P(t))|0\rangle\langle 0|, \tag{1.4}$$

with

$$|\psi_{out}(t)\rangle = \frac{1}{\sqrt{P(t)}}(\cos\frac{\theta}{2}|0\rangle + e^{i\phi}\sin\frac{\theta}{2}f_N(t)|1\rangle), \tag{1.5}$$

where $P(t) = \cos^2\frac{\theta}{2} + \sin^2\frac{\theta}{2}|f_N(t)|^2$ and $f_N(t) = \langle\mathbf{N}|\exp\{-i\mathbf{H}t\}|\mathbf{1}\rangle$. Note that $f_N(t)$ is just the transition amplitude of an excitation (the $|1\rangle$ state) from the first to the $N$th site of a graph of $N$ spins.

Now suppose it is decided that Bob will pick up the $N$th spin (and hence complete the communication protocol) at a predetermined time $t = t^*$. The fidelity

of quantum communication through the channel averaged over all pure input states $|\psi_{in}\rangle$ in the Bloch-sphere ($(1/4\pi)\int\langle\psi_{in}|\rho_{out}(t^*)|\psi_{in}\rangle d\Omega$) is then

$$F = \frac{|f_N(t^*)|\cos\gamma}{3} + \frac{|f_N(t^*)|^2}{6} + \frac{1}{2}, \tag{1.6}$$

where $\gamma = \arg\{f_N(t^*)\}$. To maximize the above average fidelity, we must choose the magnetic fields $B_i$ such that $\gamma$ is a multiple of $2\pi$. Assuming this special choice of magnetic field value (which can always be made for any given $t^*$) to be a part of our protocol, we can simply replace $f_N(t^*)$ by $|f_N(t^*)|$ in Eq. (1.5).

We now want to examine the performance of the spin chain described by the nearest neighbour isotropic Heisenberg Hamiltonian $\mathbf{H}$, as a quantum channel. In the subspace of states $|\mathbf{j}\rangle$, this Hamiltonian can be written as

$$\mathbf{H} = 2J\sum_{j=1}^{N-1}(|\mathbf{j}\rangle\langle\mathbf{j+1}| + |\mathbf{j+1}\rangle\langle\mathbf{j}|) + J(N-5)\sum_{j=2}^{N-1}|\mathbf{j}\rangle\langle\mathbf{j}| + J(N-3)(|\mathbf{1}\rangle\langle\mathbf{1}| + |\mathbf{N}\rangle\langle\mathbf{N}|). \tag{1.7}$$

The $N$ single excitation eigenstates relevant to our problem can then be identified by quasimomenta labels $k_n = \frac{(n-1)\pi}{N}$, where the symbol $k$ is used to denote momenta states, while the index $n = 1, \ldots, N$. The eigenstates can easily be verified to be

$$|k_n\rangle = a_n\sum_{j=1}^{N}\cos\left\{\frac{k_n}{2}(2j-1)\right\}|\mathbf{j}\rangle, \tag{1.8}$$

where $a_1 = 1/\sqrt{N}$ and $a_{n\neq 1} = \sqrt{2/N}$ with energy (on setting $E_0 = 0$) given by $E_n = 2J(1-\cos k_n)$. In this case, $f_N(t^*)$ is given by

$$f_N(t^*) = \sum_{n=1}^{N}\langle\mathbf{N}|k_n\rangle\langle k_n|\mathbf{1}\rangle e^{-iE_nt^*} = \mathscr{C}(v_n) \tag{1.9}$$

where, $v_n = a_n\cos\{\frac{k_n}{2}(2N-1)\}e^{-iE_nt^*}$ and

$$\mathscr{C}(v_n) = \sum_{n=1}^{N}a_nv_n\cos\frac{k_n}{2} \tag{1.10}$$

is the first element of the inverse discrete cosine transform of the vector $\{v_n\}$.

We are now in a position to list the performance of our protocol for various chain lengths $N$ (Alice and Bob at opposite ends of the chain as shown in Fig. 1.2). In general, Bob has to wait for different lengths of time $t^*$ for different chain lengths $N$, in order to obtain a high fidelity of quantum state transfer. Using Eqs. (1.6) and (1.9), we can numerically evaluate the maximum of $|f_N(t^*)|$ for

various chain lengths from $N = 2$ to $N = 80$ when Bob is allowed to choose $t_0$ within a finite (but long) time interval of length $T_{max} = 4{,}000/\mathrm{J}$. This evaluation is fast because Eq. (1.9) allows us to use numerical packages for the discrete cosine transform. Taking a finite $T_{max}$ is physically reasonable, as Bob cannot afford to wait indefinitely. It is to be understood that within $[0, T_{max}]$, the time $t^*$ at which optimal quantum communication occurs varies with $N$. Let us now briefly point out the interesting features of our protocol.

Firstly, there are quite a few finite size effects due to constructive interference of the various one excitation wavepackets propagating down the chain. In addition to the trivial case of $N = 2$, $N = 4$ gives perfect ($F = 1.000$) quantum state transfer to three decimal places and $N = 8$ gives near perfect ($F = 0.994$). The fidelity also exceeds 0.9 for $N = 7, 10, 11, 13$ and 14. We did not have a clear cut explanation of the above number dependent finite size effects for several years, though it obviously pointed to a link between number theory and constructive interference in a line. However, in this direction rigorous results were obtained quite recently in Ref. [30] where the notion of "pretty good state transfer" (PGST) was used (introduced in Ref. [31]) by relaxing the constraints on time $T_{max}$. The work of Ref. [30] imply that even for as simple protocol as stated above, near arbitrarily fidelity of state transfer is possible for chains of lengths $p, 2p$ and $2^m$, where $p$ is prime, as long as one is willing to wait for enough time for the state to arrive. This work also implies that spin chains used as above are a natural physical system whose dynamics enables the purely number theoretic task of *primality testing*. Note that in the above presentation of the scheme, though we took a finite (but large) $T_{max}$, we still obtained relatively high fidelities for $2, 4, 7, 8, 10, 11, 13$ and 14, all of which fall within the category of $p, 2p$ and $2^m$.

## 1.3 Entanglement Creation as an Alternative

Unfortunately, for the protocol of Fig. 1.2, the fidelity of quantum state transfer achieved in a reasonable time interval falls below $2/3$ when the chain length $N$ exceeds 80. Thus it is clear that the spin chain used as naively as stated above, while useful for chains of few spins, cannot transfer states with a high fidelity over longer distances. However, there is always another interesting alternative, namely the establishment of entanglement between two qubits in the two registers through the spin chain. If two qubits, $A$ in one register and $B$ in the other, can be prepared in a state very close to a singlet $|\psi^-\rangle_{AB} = \frac{1}{\sqrt{2}}(|0\rangle_A|1\rangle_B - |1\rangle_A|0\rangle_B)$, then one can transport an arbitrary quantum state $|\psi_{in}\rangle$ from one register to another with a very high fidelity by means of quantum teleportation [32]. It suffices even if the spin chain can only establish a noisy entangled state, say, $\eta_{1N} = p|\psi^-\rangle\langle\psi^-|_{1N} + (1-p)I_{1N}$, where $p$ is a probability and $I_{1N}$ is the identity (completely mixed) state of the end qubits 1 and $N$ of the chain, because of a process called entanglement distillation [33]. After generating one copy of $\eta_{1N}$ it is transferred to a pair of qubits in the

registers, the state of qubit 1 to some qubit in one register and the state of qubit $N$ to some qubit in the other register. This process is *repeated* (by using the spin chain channel repeatedly) to get several pairs of qubits in the state $\eta_{A_i B_i}$, with $A_i$ in one register and $B_i$ in the other. Then one can use entanglement distillation on the collection of states $\eta_{A_i,B_i}$ to produce a lower number of copies of a state with very high $p$, i.e., a state very close to $|\psi^-\rangle_{AB}$. Once that is established, teleportation can enable high fidelity state transfer.

There are actually two qualitatively different ways in which a spin chain may be used to establish a noisy entangled state such as $\eta_{AB}$ of qubits $A$ held in one register with a qubit $B$ held in another. Firstly, one can use quantum state transfer through the spin chain of qubits 1 to $N$ exactly as outlined in the previous section, but the state of qubit 1 is first prepared in the entangled state $|\psi^-\rangle_{A1}$ with qubit $A$. As the state of qubit 1 is transferred to qubit $N$ with some fidelity through the spin chain channel, the joint state of the qubits $A$ and $N$ evolve to an entangled state $\eta_{AN}$. By an operation in the second register, which maps the state of qubit $N$ to qubit $B$, we prepare $A$ and $B$ in the entangled state $\eta_{AB}$. Using this procedure, and using a certain measure of entanglement called concurrence [34], the entanglement that can be generated between qubits $A$ and $B$ is found to be

$$E_{AB}(t) = |f_N(t)|, \tag{1.11}$$

so that one can use certain approximations to prove that

$$E_{AB}\left(t \sim \frac{N}{J}\right) \sim \frac{1}{N^{\frac{1}{3}}}. \tag{1.12}$$

Obviously the above estimate of entanglement transfer is based on using the Hamiltonian $\mathbf{H}$ of Eq. (1.1) which can be called *uniformly coupled* in view of the couplings between each pair of neighbouring spins being exactly the same and on using the naive protocol discussed above. In general $|f_N(t)|$ can be improved by various clever tricks, which we will discuss in the next section, and, thereby the entanglement can be increased. Such entanglement transfer has also been studied employing spin-1 chains [35].

On the other hand, a spin chain is an interacting system of spins, and interactions between spins can generate entanglement when one initializes the spins in an appropriate state. In a spin chain matters are made complicated by the fact that each spin in the body of the chain has two neighbours to interact, and the entanglement generated might not be the type of entanglement useful for linking the registers, i.e., a type of state $\eta_{1N}$ with a large probability $p$ of $|\psi^-\rangle_{1N}$. However, it is very interesting to point out that if one initializes an Ising spin chain

$$\mathbf{H}_{\text{Ising}} = J \sum_{j=1}^{N-1} \sigma_j^z \sigma_{j+1}^z, \tag{1.13}$$

with $J > 0$ in its *Neel ordered* ground state $|010101\ldots01\rangle$, and suddenly globally quenches all the couplings to a *XY* Hamiltonian

$$\mathbf{H_{XY}} = J \sum_{j=1}^{N-1} (\sigma_j^x \sigma_{j+1}^x + \sigma_j^y \sigma_{j+1}^y), \tag{1.14}$$

then a large amount of entanglement, falling as $N^{-0.77}$ can be generated between its ends in a time $\sim \frac{N}{J}$ [36]. This type of a "quench" (sudden change of Hamiltonian) to generate entanglement in a spin chain system has been further investigated by some of the authors of this chapter in the context of Kondo spin chains [37, 38], a work that will be described in more detail in Sect. 1.6.

## 1.4 A Brief Overview of Some Schemes that Enable Nearly Perfect State Transfer

The transmission quality of almost uniform channels is generally expected to deteriorate as the length of the channel is increased [5,6,39] due to dispersion, which is integral to uniformly coupled spin chains. Although using an antiferromagnetic Heisenberg Hamiltonian ($\mathbf{H}$ with $J > 0$) and its rotationally symmetric ground state, some improvements are possible in entanglement transmission due to the different nature of noise and dispersion in this channel [40], the transmission still deteriorates with $N$. This deterioration of quality is exemplified by Fig. 1.3, which considers state transmission by the same protocol as described in Sect. 1.2, but with the usage of a uniform *XY* spin chain described by $\mathbf{H_{XY}}$ of Eq. (1.14) (here the sign of $J$ does not matter). On the other hand, modelling a scalable quantum-state transfer process whose quality depends as little as possible on the physical length of the channel is an essential issue to address, especially if solid-state implementations and/or experimental analysis are in order. Among the types of schemes to use a spin chain or other many-body system as a bus to connect quantum computers, there are varied methodologies. We now broadly classify these based upon their principal methodology and present them below under the broad headings.

### *1.4.1 Engineering of Interactions*

One method of enabling a perfect quantum state transfer through a spin chain is to engineer all its interactions [41–44]. For example, consider a *XY* chain

$$\mathbf{H_{XY}^{Engd}} = \sum_{j=1}^{N-1} J_{j,j+1} (\sigma_j^x \sigma_{j+1}^x + \sigma_j^y \sigma_{j+1}^y). \tag{1.15}$$

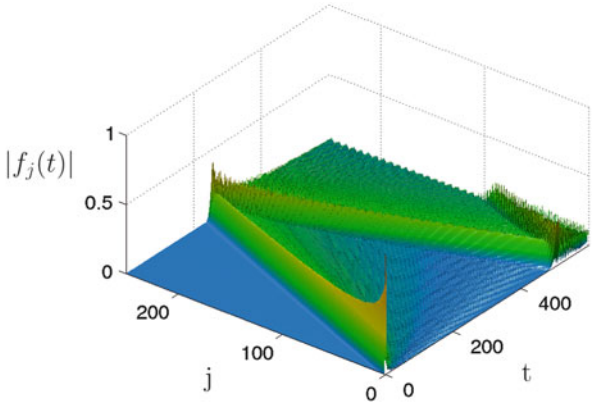


**Fig. 1.3** This figure illustrates the dynamics of quantum state transmission through a uniformly coupled *XY* spin chain which is initialized in the state $|000..00\rangle$ using the simple protocol described in Sect. 1.2. $|f_j|$ denotes the modulus of the amplitude for the state $|1\rangle$ to be in the site $j$ (for $j = N$, this is the $|f_N|$ which enters the formula Eq. (1.6) for the fidelity). This is plotted as a function of time $t$. The length of the chain $N$ here is 250, and the deterioration of the transfer quality, as signified by $|f_j|$, with increasing length of the chain is clear (This figure is adopted from Ref. [69])

If the couplings $J_{j,j+1}$ of the chain are symmetric about its centre, i.e., $J_{1,2} = J_{N-1,N}, J_{2,3} = J_{N-2,N-1}$, and so on (the chain is said to be mirror symmetric), then alternate eigenstates $|k_n\rangle$ have opposite parity i.e., $\langle k_n|\mathbf{N}\rangle = \langle k_n|\mathbf{1}\rangle e^{i\pi n}$, were $n$ is the integer label of the eigenstates [43]. The readers aware of basic quantum mechanics in 1D can consider the above mirror-symmetric couplings and the resulting alternating parity condition to be the discrete space analogues of $V(-x) = V(x)$ and $\psi_n(-x) = (-1)^n \psi_n(x)$ respectively, where $\psi_n(x)$ are the eigenfunctions of the potential $V(x)$ with the location $j$ of the excitation replacing position $x$. Due to alternate eigenstates having opposite parity, time evolution by $\mathbf{H}_{\mathbf{XY}}^{\mathrm{Engd}}$ implies

$$f_N(t) = \sum_n \rho(k_n) e^{i(\pi n - E_n t)} \quad , \quad \rho(k_n) = |\langle \mathbf{1}|k_n\rangle|^2, \tag{1.16}$$

where $E_n$ are the energies of the eigenstates $|k_n\rangle$. Moreover, if one engineers the interactions $J_{j,j+1}$ in a particular way [41, 42], it is possible to make its spectrum $E_n = \nu n$, where $\nu$ is a constant (again, the continuous variable analogue of this would be the potential $V(x)$ being a harmonic oscillator). Then

$$f_N(t) = \sum_n \rho(k_n)\, e^{i\pi n(1-\nu t/\pi)}\,, \tag{1.17}$$

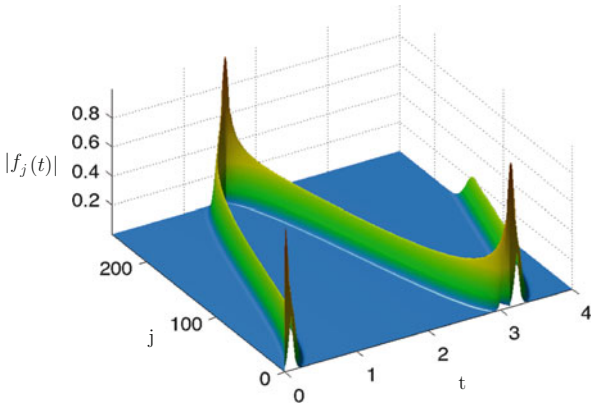


**Fig. 1.4** This figure illustrates the dynamics of quantum state transmission through an engineered *XY* spin chain, all whose couplings have been engineered. It is initialized in the state $|000..00\rangle$. $|f_j|$ denotes the modulus of the amplitude for the state $|1\rangle$ to be in the site $j$. This is plotted as a function of time $t$. The length of the chain $N$ here is 250, and the perfect nature of the transfer is visible by noting that $|f_N| = 1$ at an appropriate time (This figure is adopted from Ref. [69])

so that at an optimal time $t^*=\pi/\nu$, we get $|f_N(t^*)| = \sum_n \rho(k_n) = 1$, and thereby both fidelity and entanglement, which depend on $|f_N(t^*)|$ are arbitrarily close to unity. The dynamics of state transfer through such engineered spin chains is depicted in Fig. 1.4. Note that for models such as *XY* chain given by $\mathbf{H}_{\mathbf{XY}}^{\mathrm{Engd}}$, the quantity $|f_N(t^*)|$ is independent of the initialization of the spin chain channel [45]. Moreover, the idea of perfect state transfer has been extended to networks of varied topologies [46]. Although engineering a profile of couplings in a spin chain looks difficult at first glance, some promising ideas have been suggested recently [47].

### *1.4.2 Encodings of Information and/or Quantum Control*

Another possible approach for making $f_N$ arbitrarily close to unity stems from the idea of exploiting, in an almost uniform channel (say the Hamiltonian $\mathbf{H}$ of Eq. (1.1)), the ballistic state-transfer mechanism that allows perfect transmission of a wavepacket [48–50], in virtue of a perfectly coherent, non dispersive, dynamics. Here the initial state $|1\rangle$ is encoded in *multiple spins* as the gaussian wavepacket state $\sum_j \exp\{(j-j_0)^2/2\sigma^2\}\exp\{ik_{\mathrm{opt}}j\}|\mathbf{j}\rangle$, where the centre $j_0$ of the wavepacket is proximal to Alice (the sender of the information) and the width $\sim\sigma$ of the packet corresponds to a finite number of sites $j$. The state $|0\rangle$ is encoded as $|000\ldots0\rangle$ in $\sim\sigma$ sites. If the wavepacket momentum $k_{\mathrm{opt}}$ is optimally chosen [48], then the second order dispersion of the wavepacket can effectively be made to vanish. Near-perfect transfer of the state to Bob in another part of the chain then follows from a linear dispersion relation which implies that essentially the wavepacket propagates

unhindered. Moreover, if one chooses $\sigma \sim N^{1/3}$, then the wavepacket spreads only by a constant factor due to the third order dispersion. While what we have stated above holds strictly for spin-chains with closed boundary conditions (spin rings), it can be adapted to open spin chains [49]. Of course, the chief difficulty of the above approach is the encoding in several ($O(N^{1/3})$) spins, though this control in the "number" of spins can be converted to a "continuous time control" of very few spins at both Alice's and Bob's ends of the chain.

Alternatively, one could encode the state in only *two spins* – the first spins of two distinct spin chains $A$ and $B$ [51,52]. This is called the dual rail protocol. Alice encodes $|0\rangle$ as $|\mathbf{0}\rangle_A|\mathbf{1}\rangle_B$, which propagates through the dual chain intermediate states $|\mathbf{0}\rangle_A|\mathbf{j}\rangle_B$, while $|1\rangle$ is encoded as $|\mathbf{1}\rangle_A|\mathbf{0}\rangle_B$, which propagates through intermediate states $|\mathbf{j}\rangle_A|\mathbf{0}\rangle_B$. Bob does a two-qubit gate and a measurement on the two spins at his end of the chain so that the measurement result indicates either that "the state has not arrived at his end" (in which case Bob waits longer and repeats his measurement after an interval) or that "the state having arrived" in which case the original state $\alpha|0\rangle + \beta|1\rangle$ will be available in one of his spins [51]. This scheme can be continued for a longer time of the order of $O(N^{5/3}/J)$ to obtain the transmitted state perfectly with an arbitrarily high probability and is quite robust to disorders [52]. The encoding in these schemes can eventually be eliminated in exchange of several swap operations to a memory at the receiving end of the spin chain [53,54] – in this sense, again, encoding can be converted to time control. Last, but not the least, one can use global fields at regular time intervals (another example of time control) on a Ising Hamiltonian described by $\mathbf{H}_{\text{Ising}}$ to accomplish a perfect state transfer [55].

### *1.4.3 Weak Couplings to Gapped Systems*

Some of these alternative strategies are based on the idea of *substantially weakening* the coupling between the channel and the sender/receiver qubits, a solution that has been shown [21, 56–58, 60] to lead to a very high-quality state transfer. Say the couplings of the sending and receiving qubits with a spin/spins of the channel are $\epsilon J$, where the couplings between spins comprising the channel, which can be a uniform spin chain (and many other graphs) are $J$. Then, for sufficiently small, $\epsilon << 1$, one can ensure that only *one* of the modes of the channel would resonantly couple to the sending and receiving spins. Then the whole channel can be thought of as an effective qubit with the states $|0\rangle$ and $|1\rangle$ identified with the mode being unoccupied and occupied respectively. The three qubit system of the sending, channel and receiving qubits then reduce to a three spin $XY$ model described by $\mathbf{H}_{\mathbf{XY}}$ of Eq. (1.14) with $J$ replaced by $\epsilon J$ and $N = 3$. This transfers a state perfectly from the sending to the receiving qubits [59] in a time $O(1/\epsilon J)$ [21,56,57]. Clearly, this scheme yields very large transmission times – we will call it the quantum Rabi model to highlight that the state oscillates between the sending and the receiving qubits with a single frequency. The typical dynamics of state transfer through such

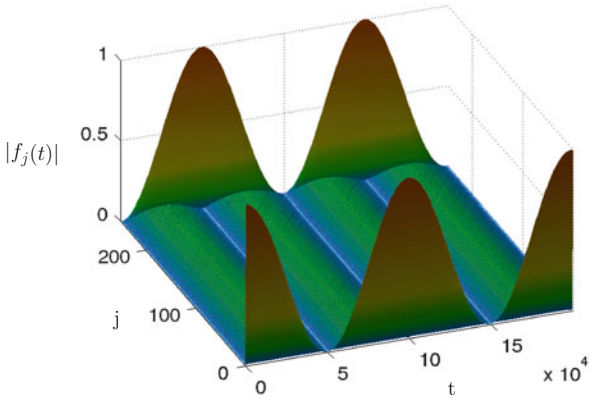


**Fig. 1.5** This figure illustrates the dynamics of quantum state transmission by coupling the input and output spins (1 and N respectively) weakly to a gapped spin chain. $|f_j|$ denotes the modulus of the amplitude for the state $|1\rangle$ to be in the site $j$. This is plotted as a function of time $t$. The length of the chain $N$ here is 250, and both the near perfect nature of the transfer, as well as the exceptionally large time needed is clear from the figure

chains is depicted in Fig. 1.5. Another alternative is to eliminate the central mode altogether by assuming that the channel is a gapped system with such a large gap $O(J)$ that no mode of the channel is ever occupied during the dynamics. This leads to an effective direct coupling of strength $\epsilon^2 J$ between the sending and the receiving spins leading to a state transfer over a time-scale $1/\epsilon^2 J$, which is even larger than the quantum Rabi model presented above. Despite the exceptionally large time-scales, which might be disadvantageous from the viewpoint of decoherence, these models do have a couple advantages: (a) a less precise choice of the time of retrieval of the state from the receiving spin does not change the state significantly and (b) it will work for a wide variety of initial states of the intervening bus [21], as well as for various random architectures of interacting spins [60].

### *1.4.4 Adiabatic Processes*

Another way to achieve high quality quantum state transfer is to adapt the adiabatic passage techniques of atomic physics [61] to spin chain settings. The idea is to use adiabatic processes starting from a two fold degenerate ground state (comprising of $|0\rangle_1|GS\rangle_{2,3,..,N}$ and $|1\rangle_1|GS\rangle_{2,3,..,N}$) of a spin chain. Initially all the proximal neighbour interactions between spins 2 to $N$ are switched on (say, of magnitude $\sim J$), so that $|GS\rangle_{2,3,..,N}$ can be the easily initializable ground state of these spins. The first spin, on the other hand, encodes the qubit and is uncoupled to anything else. Gradually (with a frequency much lower than any gap $O(J)$ in the system) the interactions between the spins 1 and 2 are switched on at the expense of turning

off the interaction between the spins $N-1$ and $N$. If the interactions are such that they do not have any matrix elements for a bit flip, then the above process evolves the state of the spin chain unitarily as: $|0\rangle_1|GS\rangle_{2,3,\ldots,N} \rightarrow |GS\rangle_{1,2,\ldots,N-1}|0\rangle_N$ and $|1\rangle_1|GS\rangle_{2,3,\ldots,N} \rightarrow |GS\rangle_{1,2,\ldots,N-1}|1\rangle_N$, whereby the state of the first spin has been transferred to the last spin. This approach, and its variants (such as cases were every alternate interaction in a nearest neighbour coupled spin chain are varied slowly with time), have been proposed with $XY$ spin chains [62], with spin-1 chains [63], with antiferromagnetic Heisenberg spin chains [64], or with the allied system of a chain of quantum dots [65] as the channel. While being very slow, the adiabatic state transfer schemes have the key advantage that at the end of the process the state has arrived in the receiving spin permanently and will not be lost back into the chain due to further dynamics.

## 1.5 A Minimal Engineering Scheme for High Fidelity Transfer Without Encoding

For enabling high fidelity (i.e., near perfect) state transfer under reasonable requirements, one is somehow squeezed between the seemingly incompatible criteria of avoiding too much a detailed engineering of the physical channel, or elaborate active control of the chain or encoding information and yet get a reasonably long channel characterized by a relatively convenient transfer time. However, a strategy for precisely achieving this has recently been proposed in Refs. [66, 67], where it has been shown that engineering all the interactions, so as to get a linear spectrum $E_n = \nu n$ (as in Sect. 1.4.1), is not actually necessary, as only the modes involved in the initial configuration of the overall system need to have a linear spectrum [66]. This realizes a coherent ballistic transmission in spite of the dispersion relation not being linear in the whole range, but only in the neighbourhood of the normal modes excited by the initialization of the state of the first qubit. Considering quasi-free models, such as the Hamiltonian $\mathbf{H_{XY}}$, these modes do not interact and the resulting transmission can be depicted in terms of a travelling wavepacket carrying the state of qubit $A$, which is eventually reconstructed at the opposite endpoint qubit $B$ thanks to the overall mirror symmetry. This approach works where the interactions between the spins of the bus are uniform, whereas the couplings $x$ between the boundaries of the bus and the external qubits $A$ and $B$ are different. This setting is very natural for connecting distant registers, as it is clear from Fig. 1.1. We assume that the distant registers are initially detached from the bus, and that the couplings $x$, can be switched on and set to a particularly tuned value. In the limit of very weak $x$ only one mode of the chain is involved in the dynamics, a mechanism which we called the Rabi model in Sect. 1.4.3, but as we discussed, the resulting transmission times are very long. Here we are going to consider values of $x$ which are not so small as to give the Rabi model, but considerably stronger or, in other words, *non-perturbative*.

As the system is almost translationally invariant in the limit of big $N$, one can consider the quasimomentum $k_n$ to become a continuous momentum $k$ and

energies $E_n = E(k)$, which can be interpreted as a dispersion relation, which is nonlinear over the whole range of $k_n$, but linear close to any inflection-point. In this momentum space, the centre of the wave-packet depicting the state transmission can be adjusted to be peaked at the inflection point (the centre of the linear zone) by controlling magnetic fields on spins 1 and $N$ only – however, for some cases, for example for $\mathbf{H_{XY}}$, even without any fields the centre is automatically at the inflection point. The width of this wavepacket increases for increasing $x$, as more modes come into play. A coherent ballistic evolution of the wave-packet is obtained by setting $x$ to the value that leads to the optimal width, by this meaning the width that corresponds to the best-quality state transmission, within the scheme. Notice that, at variance with the first approach of Sect. 1.4.2 where a gaussian wave-packet in real space encodes the initial state, here Alice and Bob control the width of the wave-packet in momentum space by adjusting only *one coupling*, namely $x$ to a fixed value, without requiring the control of multiple spins or elaborate time-control. The advantages of this strategy with hardly any demands on control is thus evident. Moreover, thanks to the non-perturbative couplings, the transmission times are fast. Finally, it has been shown [68] that the dynamics is also stable against static perturbations.

### *1.5.1 Mathematical Explanation of the Minimal Engineering Scheme*

We are now in the position of looking for the conditions leading to a dynamical evolution that corresponds to the best quality of the transmission processes through a spin chain with no encoding and control, and minimal engineering. Let us consider the transmission scheme of Fig. 1.2 where the state of the qubit has to be transferred from Alice's qubit 1 to Bob's qubit $N$ across a spin chain where all qubits, except for 1, face down. We consider here $\mathbf{H}_{\mathbf{XY}}^{\mathrm{Engd}}$ as described in Sect. 1.4.1. In the single excitation sector this corresponds to the Hamiltonian

$$\mathbf{H}_{\mathbf{XY,single}}^{\mathrm{Engd}} = 2\sum_{j=1}^{N} J_{j,j+1}\ (|\mathbf{j+1}\rangle\langle\mathbf{j}| + |\mathbf{j}\rangle\langle\mathbf{j+1}|)\ , \tag{1.18}$$

were states $|\mathbf{j}\rangle$ have been defined in Sect. 1.2. The above is a Hamiltonian with only nearest neighbour interactions, in which, following Refs. [66, 67], all couplings are uniform except for those of the extremal bonds, whose value is allowed to vary: $4J_{12} = 4J_{N-1,N} = x$, while $4J_{j,j+1} = 1$ for all other couplings (*minimally engineered*). In [66, 67] more general quasi-free models are considered, where many-body effects and different initial state of the chain are taken into account. From such analysis, it turns out that, when quasiperfect state transmission is considered, many-body effects due to initial states with many excitations only slightly perturb the process [67]; therefore, we here restrict the discussion to the

single-excitation subspace. As shown in Sect. 1.2 the transmission quality can be obtained from the transition amplitude $f_N(t)$. As noted in Sect. 1.4.1, thanks to the mirror-symmetry of the Hamiltonian, we have the alternating parity condition $\langle k_n|\mathbf{N}\rangle = \langle k_n|\mathbf{1}\rangle e^{i\pi n}$ on its eigenstates $|k_n\rangle$. Thus following Eqs. (1.16) and (1.17) if those modes that are predominantly populated, i.e., for which $\rho(k_n)$ is significant, satisfy $E_n \sim vn$, then $f_N(t^*) \sim 1$ can be obtained at an appropriate time $t^*$.

In practice, due to the uniformity of the interactions in the bulk, the energy eigenvalues can be written as

$$E_n = \cos k_n \,, \tag{1.19}$$

where the quasi-momenta, because of the different interactions $x$ at the boundaries, take the discrete values

$$k_n = \frac{\pi\, n + 2\varphi_{k_n}}{N+1} \,, \quad (n = 1, \ldots, N) \,, \tag{1.20}$$

with

$$\varphi_{k_n} = k_n - \cot^{-1}\Big(\frac{\cot k_n}{\Delta}\Big) \quad \in \big(-\tfrac{\pi}{2}, \tfrac{\pi}{2}\big) \,, \tag{1.21}$$

$$\Delta = \frac{x^2}{2 - x^2} \,, \tag{1.22}$$

From the above equations it follows that the $k_n$'s correspond to the equispaced values $\pi n/(N+1)$, slightly shifted towards $\pi/2$ of a quantity which is smaller than $\pi/(N+1)$. The density $\rho(k_n)$ in the transition amplitude expression (1.16) reads [67]:

$$\rho(k_n) = \frac{1}{N+1-2\varphi'_{k_n}} \, \frac{\Delta(1+\Delta)}{\Delta^2 + \cot^2 k_n} \,, \tag{1.23}$$

where $k_n$ is taken to be a continuous label (large $N$) to define the derivative $\varphi'_{k_n}$. Equation (1.23) implies that the distribution $\rho(k)$ is peaked at $k_n = \pi/2$ around which $E_n \sim vn$ holds to a good degree with $v = \pi/(N+1)$. Thus if the width of $\rho(k)$, characterized by the parameter $\Delta$ (the smaller $x$ the narrower $\rho(k)$) is appropriately chosen, Eq. (1.17) holds to a very good accuracy and perfect state transmission occurs at an optimal time of about $t^* \sim \pi/v = N + 1$.

### *1.5.2 The Parameter Regime for Ballistic Transfer*

The dependence of $\Delta$ upon $x$ reveals the possibility of identifying different dynamical regimes, characterized by a qualitatively different distribution $\rho(k)$ and

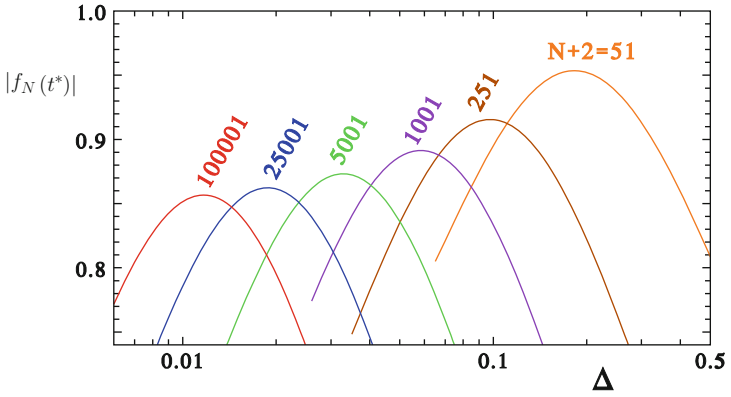


**Fig. 1.6** Value of $f_N(t^*, \Delta)$ as a function of $\Delta$, for different chain lengths $N$. $t^*$ is obtained numerically by maximizing (1.16) around $t \simeq N+1$ (This figure is adopted from Ref. [67])

hence, as for the transfer process, a different behaviour of the transition amplitude $f_N(t)$. For extremely small $x$ the distribution $\rho(k)$ can be so narrow that (for even $N$) only two opposite small eigenvalues come into play, say differing by $\delta\omega$, and perfect transmission will be attained at a large time $t = \pi(\delta\omega)^{-1}$. This is the Rabi-like regime discussed in Sect. 1.4.3. When $x$ is increased, and a few more eigenvalues come into play, an intermediate regime is observed, which can be easily shown [67] to be useless for the purpose of quantum communication. As $x$ further increases, the ballistic regime eventually manifests itself, and a more regular behaviour with short transmission time $t^* \sim N$ sets in. The ballistic regime is characterized by relatively large values of $f_N(t^*, \Delta)$, shown in Fig. 1.6 for increasing chain lengths. Each curve has a maximum for a particular optimal value of $\Delta = \Delta^{\text{opt}}(N)$ or, equivalently, of $x = x^{\text{opt}}(N)$: such maxima are remarkably stable for very high $N$ and yield very high transmission quality.

This last 'ballistic-transfer' regime is the one we are interested in, since it has three strong advantages: first, the transmission time $t^* \sim N$ is the shortest attainable; second, the maximum value $f_N(t^*, \Delta^{\text{opt}})$ of $f_N(t^*, \Delta)$ is such that one can achieve very good state transfer, e.g., the corresponding transmission fidelity is far beyond the classical threshold, even for very long chains; third, it is not necessary to fine-tune $x$ to $x^{\text{opt}}$ for example a 15 % mismatch in $x$ results in a loss of less than 2 % in the transition amplitude.

#### 1.5.2.1 Ballistic Regime and Optimal Values

From the above reasoning, since the modes contributing to the amplitude lie in a range of size $\Delta$ around $k_n = \pi/2$, in order to get high-quality transfer processes it is necessary that the corresponding frequencies be almost equally spaced, meaning

that $E_n$ is approximately linear in $n$. Actually, $E_n$ has an inflection point in $k_n = \pi/2$: its nonlinearity is of the third order in $k_n - \pi/2$ and the modes close to $k_n = \pi/2$ satisfy the required condition. However, from the phase shifts (1.21) a further cubic term arises, which depends on $\Delta$. As $\Delta$ varies with $x$, the latter can be chosen so as to eliminate the cubic terms, yielding a wide interval with almost constant frequency spacing. The latter can be expressed just as the derivative of $E_n$ with respect to $n$,

$$\partial_n E_n = \frac{\pi}{t^*}\left[1 + \left(2\,\frac{1-\Delta^2}{t^*\Delta^3} - \frac{1}{2}\right)\cos^2 k_n + (\cos^4 k_n)\right], \tag{1.24}$$

where $t^* = N + 1 + 2\,(1-\Delta)/\Delta$ is the exact arrival time (the $t^* \sim N + 1$ quoted in the previous section was more approximate). It follows that one can minimize the nonlinearity of $E_n$ by setting the width to the value $\Delta_0$ satisfying

$$\Delta_0 = \left[\frac{4}{t^*}\,(1-\Delta_0^2)\right]^{1/3} \underset{N\gg 1}{\longrightarrow} 2^{2/3} N^{-1/3}\,, \tag{1.25}$$

i.e., $x \simeq 2^{5/6} N^{-1/6}$ for large $N$. Therefore the main mechanism that produces an optimal ballistic transmission is that of varying the endpoint exchange parameter to the value $x$ that 'linearizes' the dispersion relation. Actually, if the corresponding $\Delta_0 = \Delta(x)$ is such that $\rho(k)$ exceeds the region of linearity, further gain arises by lowering $x$ so as to tighten the relevant modes towards $k_n = \pi/2$. However, at the same time $E_{k_n}$ becomes less linear and the trade-off between these two effects explains why a maximum is observed as $\Delta$ is varied in Fig. 1.6 [67].

### 1.5.3 *Quality of Information Transmission in the Minimally Engineered Scheme*

The best attainable information transfer quality (as quantified by either fidelity or entanglement) corresponds to the maximum amplitude $f_{N,\mathrm{opt}} \equiv f_N(t^*, \Delta^{\mathrm{opt}})$. In Fig. 1.7 we report these values together with the corresponding optimal $\Delta^{\mathrm{opt}}$ as a function of the chain length $N$ in a logarithmic scale; the inset shows that $\Delta^{\mathrm{opt}}$ obeys the same power-law behaviour predicted in (1.25) for $\Delta_0$. Figure 1.7 also shows that for larger and larger $N$ the maximal amplitude $f_{N,\mathrm{opt}}$ does not decrease towards zero, but it rather tends to a constant value of about 0.85, which is surprisingly high, as, e.g., it corresponds to an average fidelity $F(t^*) \gtrsim 0.9$.

In Table 1.1 we report some of the optimal values $\Delta^{\mathrm{opt}}(N)$ and $x^{\mathrm{opt}}(N)$ for a wide interval of chain lengths. Notice that in the minimally engineered scheme described here the bus initialization is not crucial, as different initial states with

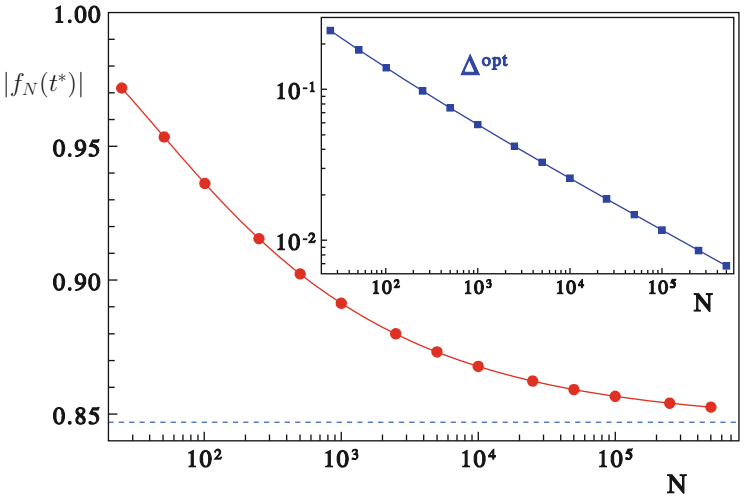


**Fig. 1.7** Behaviour of the maximum attainable amplitude $f_{N,\text{opt}}$ and (*inset*) of the corresponding optimal value of $\Delta^{\text{opt}}$ vs. logarithm of the chain length $N$. The *horizontal dashed line* is the infinite $N$ limit of $f_{N,\text{opt}}$ (This figure is adopted from Ref. [67])

**Table 1.1** Optimal values $\Delta^{\text{opt}}$ and the corresponding $x^{\text{opt}}$ and $f_N(t^*, \Delta^{\text{opt}})$ for different $N$ (This table is adopted from Ref. [67])

| $N$ | $\Delta^{\text{opt}}$ | $x^{\text{opt}}$ | $\lvert f_N(t^*, \Delta^{\text{opt}})\rvert$ |
|---|---|---|---|
| 25 | 0.243 | 0.625 | 0.968 |
| 51 | 0.181 | 0.554 | 0.949 |
| 101 | 0.138 | 0.493 | 0.932 |
| 251 | 0.098 | 0.422 | 0.913 |
| 501 | 0.075 | 0.374 | 0.900 |
| 1,001 | 0.058 | 0.332 | 0.890 |
| 2,501 | 0.042 | 0.284 | 0.879 |
| 5,001 | 0.033 | 0.252 | 0.873 |
| 10,001 | 0.026 | 0.224 | 0.868 |
| 25,001 | 0.0188 | 0.192 | 0.862 |
| 50,001 | 0.0148 | 0.171 | 0.859 |
| 100,001 | 0.0117 | 0.152 | 0.857 |
| 250,001 | 0.0086 | 0.1303 | 0.854 |
| 500,001 | 0.0068 | 0.1160 | 0.853 |

many excitations give rise to almost the same dynamics [67]. Lastly, but not the least, the quality of transmission in the scheme can be improved by engineering the first two couplings and the last two couplings of a spin chain [69]. The dynamics of the information transmission when following the minimally engineered scheme is depicted in Fig. 1.8.

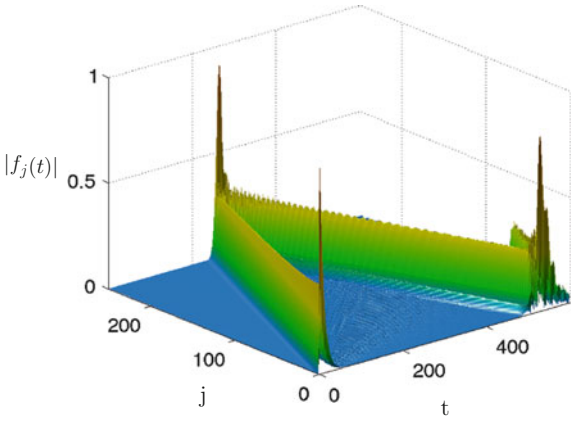


**Fig. 1.8** This figure illustrates the dynamics of quantum state transmission through a minimally engineered *XY* spin chain. Only two couplings at the very ends are engineered, while the rest of the chain has uniform couplings. $|f_j|$ denotes the modulus of the amplitude for the state $|1\rangle$ to be in the site $j$. This is plotted as a function of time $t$. The length of the chain $N$ here is 250, and both the near perfect nature of the transfer, as well as the short time taken by it are clear from the plot. The similarity of this figure with Fig. 1.4 implies that essentially engineering just two couplings is enough to adequately mimic the state transfer of more extensively engineered chains (This figure is adopted from Ref. [69])

## 1.6 Long Distance Entanglement & Routers from Quantum Quenches in Kondo Spin Chains

We are now going to describe a method for the preparation of a high amount of entanglement between distant spins by suddenly coupling the ends of two separate (long) spin chains as shown if Fig. 1.9. This is a scheme which converts the entanglement inherent in a many body ground state, which is usually not easily exploitable, to a useful entanglement between two individual spins. As we pointed out in Sect. 1.3, such entanglement is useful for connecting separated quantum registers through teleportation. Establishing a high amount of entanglement between distant spins is thus as good as achieving a high fidelity quantum state transfer across the same distance. It also facilitates the preparation of multi-particle entangled states for measurement based quantum computation. One could ask whether many-body systems can serve as mediums for entanglement between arbitrary distant qubits in a multi-site network. Though this is a most important question from an "applied" perspective, long range entanglement between individual spins is notoriously uncommon [70]. There are proposals exploiting weak couplings of distant spins to a spin chain so that these distant spins are entangled in the ground state [71–73], but these have either a limited thermal stability or a very long time-scale of entanglement generation. Alternatively, a global quench [36] may generate long distance entanglement, though this decays with the system size. Finally, there

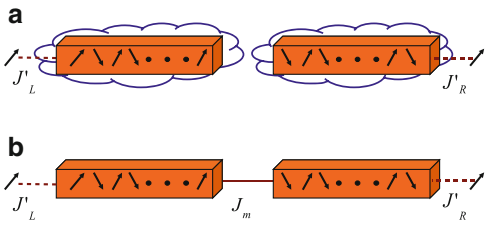


**Fig. 1.9** (**a**) The composite system made of two separate Kondo spin chains initialized in their ground states in the Kondo regime. The extension of the clouds is tuned by $J'_R$ and $J'_L$ so that $\xi_k = N_k - 1$ ($k = R, L$). (**b**) To induce dynamics, one switches on the interaction between the two chains by the amount $J_m$ (This figure is adopted from Ref. [38])

is a proposal [37] for distance independent entanglement through a local quench which, however, lacks the versatility of routing entanglement between multiple sites. We now describe a scheme which exploits a canonical many-body phenomenon for routing entanglement between multiple distant spins [38].

The many-body system we use here is paradigmatic system of condensed matter physics called the Kondo model. The original Kondo model [74, 75] describes a single impurity spin interacting with the conduction electrons in a metal; the ground state is a highly nontrivial many body state in which the impurity spin is screened by conduction electrons in a large orbital of size $\xi$ – the so called Kondo screening length. Many physical observables vary on the characteristic length scale $\xi$, which is a well defined function of the Kondo coupling [74]. The most relevant feature for the scheme reported here is that in Kondo systems, the impurity spin is believed to be maximally entangled [76] with a block of spins whose spatial extent may be varied at will by tuning $\xi$. This was, of course, merely an intuition which has recently been quantitatively verified with a genuine measure of entanglement [76].

Recently [77], it has been pointed out that the universal low energy long distance behavior of this simple Kondo model arises also in a spin chain when a magnetic impurity is coupled to the end of a gapless Heisenberg anti-ferromagnetic $J_1 - J_2$ spin 1/2 chain. The spin chain Kondo model [77] is defined by the Hamiltonian

$$H_I = J'(J_1 \sigma_1.\sigma_2 + J_2 \sigma_1.\sigma_3) + \sum_{i=2}^{N-1} J_1 \sigma_i.\sigma_{i+1} + J_2 \sum_{i=2}^{N-2} \sigma_i.\sigma_{i+2}, \qquad (1.26)$$

where $\sigma_i = (\sigma_i^x, \sigma_i^y, \sigma_i^z)$ is a vector of Pauli operators at site $i$, $N$ is the total length of the chain, $J_2$ is the next nearest neighbour coupling and the nearest neighbour coupling $J_1$ is normalized to 1. The impurity spin, located at one end of the chain, is accounted for by weaker couplings to the rest of the system; in the following, see Fig. 1.9a, both couplings $J_1$ and $J_2$ are weakened by the same factor $J'$, which quantifies then the impurity strength. For $0 \leq J_2 \leq J_2^c = 0.2412$, the spin system is gapless and it supports a Kondo regime [78, 79]. For $J_2 > J_2^c$, the system enters the gapped *dimer regime* which does not any more have the relevant entanglement of a block of spins with the impurity.

### 1.6.1 Long Distance Entanglement by Joining Kondo Spin Chains

We now describe a dynamical mechanism by which long range distance independent entanglement may be generated by suddenly switching on of a single coupling between two Kondo spin chains. We will subsequently show that this mechanism provides an efficient way to route entanglement between various distant parties. Indeed we show that, the key features of our mechanism are remarkably well described by a four spin system made of two singlets.

Let us first consider two spin singlets each formed by only two spins interacting with a Heisenberg interaction of strength $J_1'$ and $J_2'$, respectively. The ground state of the composite system is then given by $|gs\rangle = |\psi^-\rangle \otimes |\psi^-\rangle$ with $|\psi^-\rangle = (|01\rangle - |10\rangle)/\sqrt{2}$. In this simple setting, one may generate high entanglement between the boundary spins, 1 and 4 by merely turning on an interaction $J_m$ between the spins 2 and 3. After quenching, the evolution of the system is ruled by the Hamiltonian $H = J_1'\boldsymbol{\sigma}_1.\boldsymbol{\sigma}_2 + J_2'\boldsymbol{\sigma}_3.\boldsymbol{\sigma}_4 + J_m\boldsymbol{\sigma}_2.\boldsymbol{\sigma}_3$ and, since the initial state is a global singlet, time evolution allows for a nonzero overlap only with the singlet subspace of the spectrum of $H$ so that

$$|\psi(t)\rangle = e^{-iE_{S_1}t}|S_1\rangle\langle S_1|gs\rangle + e^{-iE_{S_2}t}|S_2\rangle\langle S_2|gs\rangle, \tag{1.27}$$

where, $|S_1\rangle$ and $|S_2\rangle$ are two singlet eigenvectors of $H$ with energy $E_{S_1} = -4J_m$ and $E_{S_2} = 0$ respectively. In order to get maximal entanglement between the boundary spins 1 and 4 – after a certain time $t^*$ – one has to choose $J_m = J_1' + J_2'$. Once this condition is satisfied the state of the system at time $t$, up to a global phase, is given by

$$\begin{aligned}|\psi(t)\rangle = & \frac{-i\,\sin(2J_m t)}{2}(|0011\rangle + |1100\rangle) \\ & - \frac{\cos(2J_m t)}{2}(|1001\rangle + |0110\rangle) + \frac{e^{i2J_m t}}{2}(|0101\rangle + |1010\rangle).\end{aligned} \tag{1.28}$$

Surprisingly, $|\psi(t)\rangle$ depends only on $J_m$ and, by tracing out the spins 2 and 3, one gets the density matrix $\rho_{14}(t)$ of the boundary spins. The entanglement between the spins 1 and 4 may be easily computed using concurrence [34] yielding

$$E = max\left\{0, \frac{1 - 3\cos(4J_m t)}{4}\right\}. \tag{1.29}$$

Equation (1.29) shows that $E$ oscillates with a period of $\frac{\pi}{2J_m}$ and that, at time $t^* = \frac{\pi}{4J_m}$, the spins 1 and 4 form a singlet state. In this simple setting one sees that: (i) the entanglement dynamics is determined only by two singlet eigenvectors of $H$; (ii) that maximal entanglement is achieved only when $J_m = J_1' + J_2'$; (iii) the entanglement dynamics is oscillatory with period $2t^*$, which is only a function of $J_m$ and, thus, does not depend on $J_1'$ and $J_2'$ separately.

**Table 1.2** Typical values of $J_k'$ to generate Kondo clouds of size $\xi_k$ as given in Eq. (1.31) (This table is adopted from Ref. [38])

| $N_k$ | 4 | 6 | 8 | 10 | 12 | 14 | 16 | 18 | 20 |
|---|---|---|---|---|---|---|---|---|---|
| $J_k'$ | 0.300 | 0.280 | 0.260 | 0.250 | 0.240 | 0.230 | 0.220 | 0.215 | 0.210 |
| $N_k$ | 22 | 24 | 26 | 28 | 30 | 32 | 34 | 36 | 38 |
| $J_k'$ | 0.205 | 0.202 | 0.198 | 0.195 | 0.190 | 0.187 | 0.184 | 0.180 | 0.175 |

We now show that the above simple dynamics and the resulting high entanglement between the boundary spins, may be reproduced even with many-body systems – for *arbitrary length scales* – using pertinent spin chains. For this purpose we consider two Kondo spin chains [78] in the Kondo regime, i.e. two chains of lengths $N_k$ described by

$$H_k = J_k'(J_1\boldsymbol{\sigma}_1^k.\boldsymbol{\sigma}_2^k + J_2\boldsymbol{\sigma}_1^k.\boldsymbol{\sigma}_3^k) + J_1\sum_{i=2}^{N_k}\boldsymbol{\sigma}_i^k.\boldsymbol{\sigma}_{i+1}^k + J_2\sum_{i=2}^{N_k-2}\boldsymbol{\sigma}_i^k.\boldsymbol{\sigma}_{i+2}^k,\quad k = R, L \tag{1.30}$$

where, $J_1$ and $J_2$ are nearest and next to nearest neighbour couplings, $k = R$ ($k = L$) labels the right (left) chain, $\boldsymbol{\sigma}_i^k$ is the vector of three Pauli operators at site $i$ for the chain $k$ and $J_R'$ ($J_L'$) is the impurity coupling of the right (left) hand side.

In the Kondo regime the Kondo screening length is uniquely determined by the impurity coupling [76, 78] and, for large chains, the explicit dependence is given by $\xi_k = e^{\alpha/\sqrt{J_k'}}$, where $\alpha$ is a constant; $\xi_k$ sets the size of a block of spins forming a singlet with the impurity [76]. In the following we shall fix the value of $J_R'$ and $J_L'$ so that

$$\xi_k = N_k - 1,\quad k = R, L. \tag{1.31}$$

We report in Table 1.2 the values of the impurity couplings – determined for chains of arbitrary lengths in Ref. [76] – as $N_k$ is increased. Equation (1.31) allows to build two macroscopic singlets (i.e., extended over a distance $\xi_k$ tuned by $J_k'$). The composite spin system is depicted in Fig. 1.9a; the two impurities sit at the opposite sides and may be regarded as the boundary spins of the composite system while, due to Eq. (1.31), the two Kondo clouds are tuned to take over each chain separately. Note that not only is this $J_k' \sim 1/Log^2 N_k$ much stronger than the weak couplings in Refs. [56, 57, 71–73], but also the chain is *gapless*, so it cannot lead to perturbative end-to-end effective Hamiltonians.

Initially, the two chains are separated and initialized in their ground states (see Fig. 1.9a) and the initial state of the composite chain is given by $|\psi(0)\rangle = \Pi_{k=R,L}|GS_k\rangle$ where $|GS_k\rangle$ is the ground state of the chain $k$. Then, we switch on

$$H_I = J_m(J_1\boldsymbol{\sigma}_{N_L}^L.\boldsymbol{\sigma}_{N_R}^R + J_2\boldsymbol{\sigma}_{N_L-1}^L.\boldsymbol{\sigma}_{N_R}^R + J_2\boldsymbol{\sigma}_{N_L}^L.\boldsymbol{\sigma}_{N_R-1}^R) \tag{1.32}$$

between the two chains (see Fig. 1.9b). The Hamiltonian of the composite system of length $N = N_L + N_R$ is given by $H = H_L + H_R + H_I$. Now the ground state evolves according to $|\psi(t)\rangle = e^{-iHt}|\psi(0)\rangle$. From knowing $|\psi(t)\rangle$ one obtains the reduced density matrix of the boundary spins at a generic time $t$ by tracing out all other spins from the state $|\psi(t)\rangle$ and evaluate the concurrence $E(t, J_m)$ between the boundary spins. The dynamics is now not analytically solvable and one has to resort to numerical simulations which, for $N > 20$, use the time dependent density matrix renormalization group (tDMRG) while, for $N < 20$, use exact diagonalization. For temperatures $T < 1/\xi \sim 2/N$, i.e. when the two constituent chains are in the Kondo ground state, we find that the evolution of the composite chain well reproduces all the relevant features exhibited by the simple dynamics of a four spin system made out of two singlets.

If the composite system built out of two extended Kondo singlets should reproduce the remarkable features of the simple example discussed above one should expect that, $E(t, J_m)$ oscillates with a period depending only on $J_m$ and that maximal entanglement between the boundary spins is reached at the half of the period provided that

$$J_m = \Phi(N)(J'_L + J'_R). \tag{1.33}$$

The function $\Phi(N)$ accounts for the effects arising due to the extended size of the Kondo singlets. Of course, for our dynamics to make sense at all one has to require that, as $N \to \infty$, $J_m$ should take a nonzero and finite limiting value $J$ (otherwise, one injects either zero or infinite energy). It is remarkable that this condition alone suffices to determine $\Phi(N)$. Indeed, if $N_L \approx N_R \to \infty$, one has

$$\Phi(N) \sim \frac{J}{\alpha^2} \log^2\left(\frac{N}{2}\right), \tag{1.34}$$

since, in the Kondo regime, one has that $\xi_k = e^{\alpha/\sqrt{J'_k}}$.

Here we will consider chains for which $N_L = N_R$ and so that $N = 2N_L$. In Fig. 1.10a we plot the evolution of the entanglement as a function of time for $J_m = 0.97J_1$ when $N = 32$ in the Kondo regime ($J_2 = 0$) of each chain. We see that entanglement dynamics is oscillatory with a period $2t^*$. Restricting only to the first period of oscillations one sees that, there is an optimal value of $J_m$ for which, at time $t^*$, the entanglement reaches its maximum $E_m$. In Fig. 1.10b we plot $E_m$ as a function of $N$. Though the entanglement decreases as $N$ increases for short chains, its value remains very high and becomes *distance independent* for very long chains. It is remarkable that this distance independent value seems to be 0.9 (e.g. for chains of length $N = 40$). To complete the picture of entanglement evolution in Fig. 1.10c we plot $t^*$ as a function of $N$. We see that the time needed to generate the entanglement between the boundary spins increases linearly with $N$ with a slope that is small enough to allow for fast dynamics. The results for $0 \leq J_2 \leq J_2^c$ are very similar, as the system supports a Kondo cloud in this whole domain, and these details

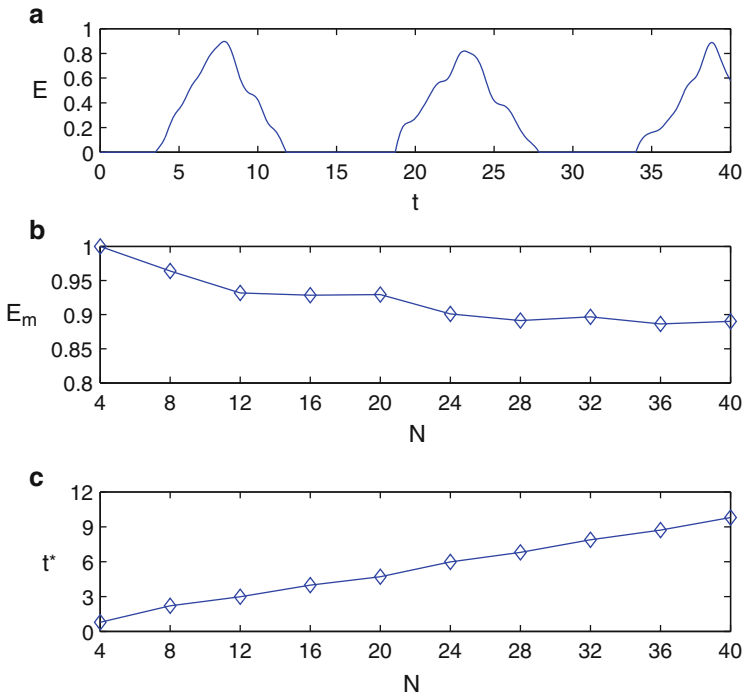


**Fig. 1.10** (**a**) The oscillatory dynamics of entanglement $E$ vs. time $t$ in the Kondo regime ($J_2 = 0$) for a composite system of $N = 32$ when $N_L = N_R$. (**b**) The maximal entanglement $E_m$ vs. $N$ at $t = t^*$ when $J_m$ has its optimal value. (**c**) $t^*$ vs. $N$. Very similar results hold for $0 \leq J_2 \leq J_2^c$ as reported in Ref. [38] (This figure is adopted from Ref. [38])

have been reported in Ref. [38]. The linear dependence of $t^*$ on $N$ implies that, for a system composed of two extended Kondo singlets, $t^*$ is related to $J_m$ by

$$t^* \sim N \sim \xi_k \sim e^{\alpha\sqrt{\frac{2\Phi(N)}{J_m}}}. \tag{1.35}$$

In Fig. 1.11a we have plotted the optimal value of $J_m$ as a function of $N$. One sees that, as $N$ increases, $J_m$ goes to 1 thus, confirming the assumption used in the derivation of $\Phi(N)$ (see Eq. (1.34)). In Fig. 1.11b we plot $\Phi(N)$ versus $\log^2(N/2)$. The linearity of the plot provides an independent numerical confirmation of the result obtained in Eq. (1.34).

The proposed mechanism for generating high entanglement between the boundary spins of a composite spin system relies heavily on Eq. (1.31) and, thus, on the fact that, for Kondo chains of arbitrary sizes $N_L$ and $N_R$, one can always tune the impurity couplings $J_L'$ and $J_R'$ so as to make the Kondo cloud comparable with the size of the chains. As a result, entanglement generation between the boundary spins should vanish for $\xi_k < N_k/2$ as well as when the constituent Kondo chains are in the dimer regime (i.e., $J_2 > J_2^c$) where the cloud does not exist at all. We computed

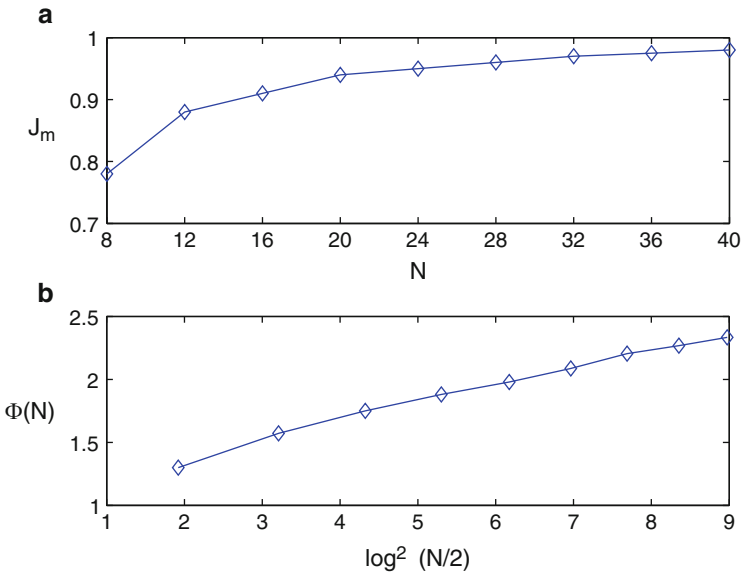


**Fig. 1.11** (**a**) Optimal $J_m$ vs. $N$ for $N_L = N_R$ in the Kondo regime. (**b**) The asymptotic behavior of $\Phi(N)$ vs. $\log^2(\frac{N}{2})$ (This figure is adopted from Ref. [38])

**Table 1.3** Comparison between $E_m$ and $t^*$ for a Kondo spin chain in the Kondo ($J_2 = 0$) and dimer regimes ($J_2 = 0.42$). In the table $K$ stands for Kondo and $D$ for dimer (This table is adopted from Ref. [38])

| $N$ | 8 | 12 | 16 | 20 | 24 | 28 | 32 | 36 | 40 |
|---|---|---|---|---|---|---|---|---|---|
| $E_m$(K) | 0.964 | 0.932 | 0.928 | 0.929 | 0.901 | 0.891 | 0.897 | 0.886 | 0.891 |
| $E_m$(D) | 0.957 | 0.903 | 0.841 | 0.783 | 0.696 | 0.581 | 0.468 | 0.330 | 0.160 |
| $t^*$(K) | 2.200 | 2.980 | 3.980 | 4.700 | 5.980 | 6.800 | 7.880 | 8.720 | 9.800 |
| $t^*$(D) | 3.780 | 7.290 | 10.32 | 13.41 | 16.89 | 20.43 | 24.51 | 27.12 | 35.01 |

numerically $E_m$ and $t^*$, for a chain composed of two Kondo spin chains in the dimer regime. The results are reported in Table 1.3 and compared with the results obtained for the same quantities when the two constituent chains are in the Kondo regime and Eq. (1.31) is satisfied. Table 1.3 shows that, as $N$ increases, entanglement $E_m$ (optimal time $t^*$) is very small (large): for instance, for $N = 40$, in the dimer regime, $E_m = 0.16$ and $t^* = 35.01$ while, in the Kondo regime, $E_m = 0.89$ and $t^* = 9.80$.

### *1.6.2 Entanglement Router*

Our analysis allows to engineer an efficient entanglement router dispatching entanglement between very distant qubits. A four-node entanglement router is sketched

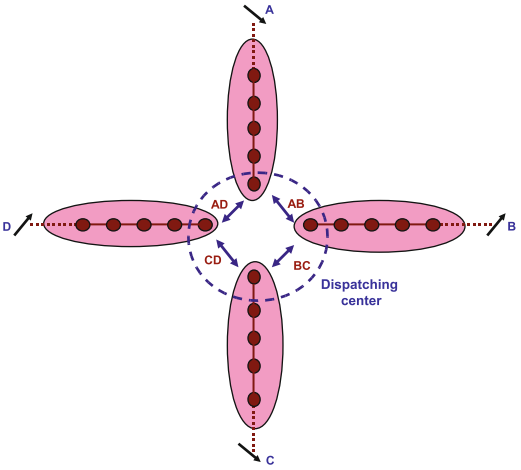


**Fig. 1.12** A four-node router in which each user controls one boundary spin. A dispatcher connects two chains to induce dynamics in a channel composed of two spin chains in order to generate entanglement between the boundary spins (This figure is adopted from Ref. [38])

in Fig. 1.12. Each node, say $A$, $B$, $C$ and $D$, has a boundary spin whose coupling to its adjacent chain is tuned so as to generate a Kondo cloud reaching the dispatch center (Fig. 1.12). The dispatcher can entangle the spins of two arbitrarily chosen nodes, say $A$ and $B$, by switching on a coupling $J_m$ between the chains $A$ and $B$ and, thus, induce the quench dynamics previously analyzed. At $t = t^*$, the entanglement may be taken out of the boundary spins by a fast swap to any memory qubits in nodes $A$ and $B$ for building resources for quantum computation. Note that exclusive pairs of nodes, e.g. $(A, B)$ and $(C, D)$, can be connected simultaneously.

## 1.7 Towards Scalable Quantum Information Processing: Long Distance Quantum Gates and a Physical Implementation

After having demonstrated state transfer and entanglement generation, we now describe a scalable, non-perturbative (i.e. not relying on weak couplings) dynamical scheme for achieving high-quality entangling gates between two arbitrarily distant qubits, suitable for subsequent uses without resetting. This scheme essentially combines the mirror inversion dynamics of certain spin chains, particularly that described in Sect. 1.5 with the fact that spins in $XY$ chains can be mapped to free fermions. The states $|0\rangle$ and $|1\rangle$ of a qubit encoded at an end site of the spin chain can be thought of as the absence and presence respectively of a fermion at that site. If two qubits are encoded, one at each end, with all the chain in the middle devoid of spin flips (in the state $|00\ldots\rangle$), then only the $|11\rangle$ state of the two qubits gets a phase due to the fermionic exchange accompanying a mirror inversion, while no such exchange takes place for the other logical states, which

are no-fermion and single fermion states. This essentially results in a gate that transforms $|00\rangle \rightarrow |00\rangle, |01\rangle \rightarrow |10\rangle, |10\rangle \rightarrow |01\rangle, |11\rangle \rightarrow -|11\rangle$. This gate can generate maximal entanglement, and its possibility in spin chains has been known for some time [43, 80–82]. However, in all of the earlier schemes, the mirror inversion was accomplished by the highly engineered chains described in Sect. 1.4. That these gates also work for the minimally engineered chains of Sect. 1.5, which also accomplishes mirror inversion, was not realized till the work of Ref. [83], which we will now describe. Note that the scheme also works when the spin chain is populated with spin flips other than those at the end spins, and this only results in some extra phase shifts which do not change the fundamental entangling nature of the gate. As a result of incorporating the types of spin chain buses described in Sect. 1.5, we do not demand encoding, engineering or weak couplings: we only need switchable couplings between qubits and the bus. Here we also describe an application, based on a combination of Near Field Fresnel Diffraction (NFFD) traps and optical lattices, which is robust against possible imperfections.

### 1.7.1 Schematic Description

Let us describe our bus as a chain of spin 1/2 particles interacting through

$$H_M = J \sum_{n=1}^{N-1} \left(\sigma_n^x \sigma_{n+1}^x + \sigma_n^y \sigma_{n+1}^y + \lambda\, \sigma_n^z \sigma_{n+1}^z\right), \tag{1.36}$$

where $\sigma_n^\alpha$ ($\alpha = x, y, z$) are Pauli operators acting on site $n$, $J$ is the exchange energy and $\lambda$ is the anisotropy. The qubits $A$ and $B$, on which the gate acts, sit at the opposite sides of the bus, labeled by site 0 and $N+1$ respectively. The interaction between the bus and the qubits is

$$H_Q = J_0 \sum_{n=0,N} \left(\sigma_n^x \sigma_{n+1}^x + \sigma_n^y \sigma_{n+1}^y + \lambda\, \sigma_n^z \sigma_{n+1}^z\right), \tag{1.37}$$

where the coupling $J_0$ can be switched on/off. To see the connection with the scheme of Sect. 1.5 note that here the whole chain is $N+2$ spins long, with spins 0 and $N+1$ being the qubits on which the logic gate acts, while the rest of the spins (1 to $N$) comprise the bus. For the moment the anisotropy $\lambda$ is set to zero. Initially the qubits are prepared in the states $|\psi_A\rangle$ and $|\psi_B\rangle$ and decoupled from the bus which is in the state $|\psi_M\rangle$, an eigenstate of $H_M$, for instance the ground state. Since $H_M$ commutes with the parity operator $\prod_{n=1}^{N}(-\sigma_n^z)$ and with the mirror inversion operator, the state $|\psi_M\rangle$ has a definite parity $(-1)^p$, for some integer $p$, and is mirror symmetric. At time $t = 0$ the coupling $J_0$ is switched on and the whole system evolves under the effect of the total Hamiltonian $H = H_M + H_Q$, i.e. $|\Psi(t)\rangle = e^{-iHt}|\psi_A\rangle|\psi_M\rangle|\psi_B\rangle$. From Sect. 1.5 we know that by tuning $J_0$ to an

optimal non-perturbative value $J_0^{\rm opt} \sim JN^{-1/6}$ the mirror-inversion condition [43] is nearly satisfied resulting in a fast high-quality transmission. In fact, when $|\psi_B\rangle$ is initialized in either $|0\rangle \equiv |\uparrow\rangle$ or $|1\rangle \equiv |\downarrow\rangle$ an arbitrary quantum state of $A$ is transmitted almost perfectly to $B$ after time $t^* \simeq (0.25N + 0.52N^{1/3})/J$.

The Hamiltonian $H$ is mapped to a free fermionic model by Jordan-Wigner transformation $c_n = \Pi_{k=0}^{n-1}(-\sigma_k^z)\sigma_n^-$ (where $\sigma_n^{\pm} = (\sigma_n^x \pm \sigma_n^y)/2$) followed by a unitary transformation $d_k = \sum_n g_{kn}c_n$. The total Hamiltonian finally reads $H = \sum_k \omega_k\, d_k^\dagger d_k$ where the explicit form of $g_{kn}$ and $\omega_k$ are given in [57]. The dynamics in the Heisenberg picture is given by $c_n(t) = \sum_m f_{nm}(t)c_m$ where $f_{nm}(t) = \sum_k g_{kn}g_{km}e^{-i\omega_k t}$. When the perfect transmission condition, i.e. $J_0 = J_0^{\rm opt}$, is satisfied we have $|f_{0,N+1}(t^*)|^2 \simeq 1$, and thus we set $f_{0,N+1}(t^*) = e^{i\alpha_N}$.

Notice that in any state transfer problem there always might be an overall phase which is irrelevant to the quality of the state transmission. However, exploiting this phase is the heart of our proposal for obtaining an entangling two-qubit gate between $A$ and $B$. We define $|\Psi_{ab}\rangle = |\Psi(0)\rangle$ with $|\psi_A\rangle = |a\rangle$ and $|\psi_B\rangle = |b\rangle$ where $a, b = 0, 1$. When $J_0$ is switched on the whole system evolves and at $t = t^*$ the states of $A$ and $B$ are swapped, while the bus takes its initial state $|\psi_M\rangle$, as a result of the mirror inverting dynamics. Therefore, an almost perfect transmission is achieved with an overall phase $\phi_{ab}$, namely $e^{-iHt^*}|\Psi_{ab}\rangle \approx e^{i\phi_{ab}}|\Psi_{ba}\rangle$. The explicit form of $\phi_{ab}$ follows from the dynamics depicted above with the freedom of setting $\phi_{00} = 0$. For instance to get $\phi_{10}$ we have

$$e^{-iHt^*}|\Psi_{10}\rangle = e^{-iHt^*}c_0\,|\Psi_{00}\rangle \simeq\ f_{0,N+1}(-t^*)\,c_{N+1}\,|\Psi_{00}\rangle = \\ = (-1)^{p+1}e^{-i\alpha_N}\,|\Psi_{01}\rangle \equiv e^{i\phi_{10}}\,|\Psi_{01}\rangle. \tag{1.38}$$

This defines $\phi_{10} = (p+1)\pi - \alpha_N$ while $\phi_{01} = \phi_{10}$ due to the symmetry of the system. With similar argument we get $\phi_{11} = \pi - 2\alpha_N$. Furthermore, the phase $\alpha_N$ is found to be equal to $\frac{\pi}{2}(N+1)$. Therefore, the ideal mirror-inverting dynamics defines a quantum gate $G$ between $A$ and $B$, which reads $G|ab\rangle = e^{i\phi_{ab}}|ba\rangle$ in the computational basis. Independent of the value of $\alpha_N$ when the pair $A, B$ is initially in the state of $|{+}{+}\rangle$, where $|+\rangle = (|0\rangle + |1\rangle)/\sqrt{2}$, the application of the gate $G$ results in a maximally entangled state between $A$ and $B$. For example, for odd $p$ and $\alpha_N = 2\pi m$ (were $m$ is an integer), the state generated is $\frac{1}{\sqrt{2}}(|0\rangle|+\rangle + |1\rangle|-\rangle)$.

Since the dynamics is not perfectly dispersionless, $|f_{0,N+1}(t^*)|$ is not exactly 1, gate $G$ is not a perfect unitary operator. In fact, the dynamics of the qubits is described by a completely positive map, $\rho_{0,N+1}(t) = \mathscr{E}_t\big[\rho_{0,N+1}(0)\big]$, which can be written in components as $\langle i|\rho_{0,N+1}(t)|j\rangle = \sum_{k,l}\mathscr{E}_{ij,kl}(t)\langle k|\rho_{0,N+1}(0)|l\rangle$. To quantify the quality of the gate we calculate average gate fidelity

$$\mathscr{F}_G(t) = \int d\psi\ \langle\psi|G^\dagger\mathscr{E}_t\big[|\psi\rangle\langle\psi|\big]G|\psi\rangle, \tag{1.39}$$

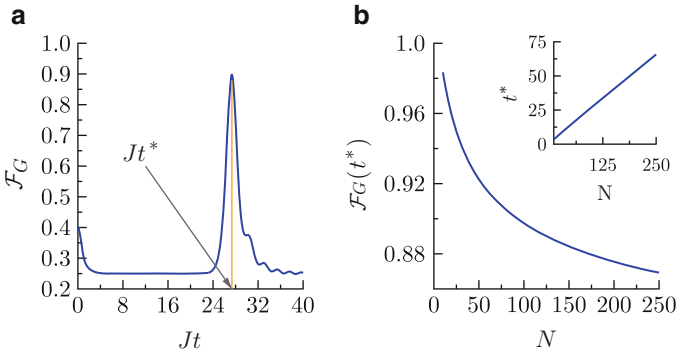


**Fig. 1.13** (**a**) Evolution of the average gate fidelity for a chain of $N = 100$ and $J_0 = 0.5\,J$. (**b**) $\mathscr{F}_G(t^*)$ as a function of $N$. Insets shows the optimal time versus $N$ (This figure is adopted from Ref. [9])

**Table 1.4** $\mathscr{F}_G(kt^*)$ and $F_M(kt^*)$ for up to eight subsequent uses of the bus of length $N = 8$ without resetting (This table is adopted from Ref. [9])

| $k$ | 1 | 2 | 3 | 4 | 5 | 6 | 7 | 8 |
|---|---|---|---|---|---|---|---|---|
| $\mathscr{F}_G(kt^*)$ | 0.984 | 0.961 | 0.939 | 0.918 | 0.898 | 0.879 | 0.861 | 0.844 |
| $F_M(kt^*)$ | 0.966 | 0.926 | 0.884 | 0.840 | 0.795 | 0.748 | 0.701 | 0.654 |

where the integration is over all possible two-qubit pure states. Using the results of [84, 85] we get

$$\mathscr{F}_G(t) = \frac{\sum_{i,j,k,l} G^*_{ik}\mathscr{E}_{ij,kl}(t)G_{jl} + 4}{20}, \tag{1.40}$$

where $\mathscr{E}_{ij,kl}(t) = \langle i|\mathscr{E}_t\big[|k\rangle\langle l|\big]|j\rangle$ are numerically evaluated.

In Fig. 1.13a we plot the time evolution of the average gate fidelity for a bus of length $N = 100$ initially in its ground state: $\mathscr{F}_G(t)$ displays a marked peak at $t = t^*$. To show the scaling of the gate fidelity we plot $\mathscr{F}_G(t^*)$ as a function of $N$ in Fig. 1.13b where we remarkably see that $\mathscr{F}_G(t^*)$ exceed 0.9 even for chains up to $N = 100$ and decays very slowly with $N$. Moreover, as shown in the inset of Fig. 1.13b and unlike the perturbative schemes proposed in [21, 57] our dynamics is fast.

Our dynamical gate works properly for arbitrary initial states of the bus with fixed parity. Ideally after each gate application the parity of the bus remains unchanged making it perfect for reusing. However, initialization in an eigenstate of $H_M$, besides automatically fixing the parity, has the advantage of simplicity for preparation. Let us initially set the bus in its ground state and define $F_M(t)$ as the fidelity between the ground state of $H_M$ and the density matrix of the bus at time $t$. To see how the quality of the gate operation is affected by $k$ subsequent uses of the bus, we compute $\mathscr{F}_G(kt^*)$ and $F_M(kt^*)$ which are shown in Table 1.4 for $k = 1, \ldots, 8$ subsequent uses.

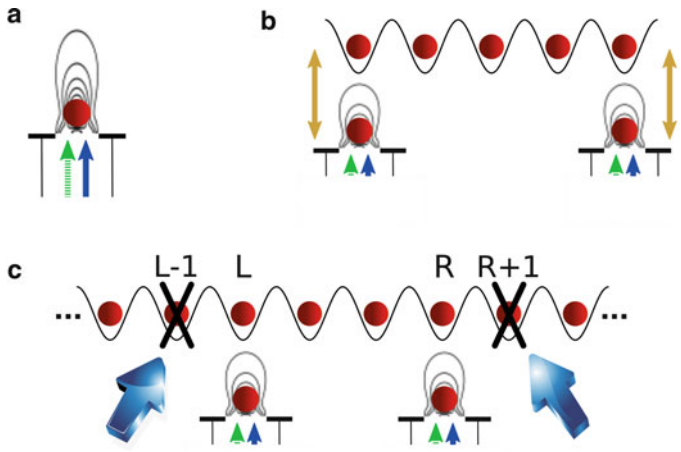


**Fig. 1.14** (**a**) Local NFFD trap with two optical fibers, one for trapping (*solid blue*) and one for unitary single qubit operations (*dashed green*). (**b**) Schematic interaction between qubits (local traps) and the ending sites of the bus (optical lattice). (**c**) Adiabatic cutting of the bus into three parts (This figure is adopted from Ref. [9])

### *1.7.2 Application*

Let us now propose an application of the above gate mechanism for a scalable neutral atom quantum computer with qubits held in static traps. We consider a network of qubits each encoded in two degenerate hyperfine levels of a neutral atom, cooled and localized in a separate NFFD trap [86]. In Fig. 1.14a we show a single atom confined in a NFFD trap. The position of the minimum of the trapping potential is controlled by varying the aperture radius [86] through micro electro mechanical system technology, as proposed in [87]. Local unitary operation on each qubit may be applied through an extra fiber, along with the NFFD trapping fiber [87], as shown in Fig. 1.14a. The qubits in the network are connected by a bus realized by cold atoms in an optical lattice , prepared in the Mott insulator regime [88]. The polarization and intensity of lasers are tuned so that one ends up [16] with an effective Hamiltonian of Eq. (1.36). For the moment we assume that the distance between the two qubits, on which we want to apply the gate, is equal to the length of the lattice such that the two qubits interact with the atoms in the ending sites of the lattice, as shown in Fig. 1.14b. To switch on the interaction $H_I$ between the qubits and the bus we have to move the minimum of NFFD trapping potential slightly higher such that the qubits move upwards and sit at a certain distance from the ends of the lattice. By controlling such distance one can tune the interaction coupling to be $J_0^{\text{opt}}$. In order to simultaneously obtain interactions effectively described by $H_M$ and $H_I$ we have to use the same spin dependent trapping laser beams in both NFFD traps and optical lattice.

Next we consider the situation in which the optical lattice size is larger than the distance between the qubits $A$ and $B$ (see Fig. 1.14c). In this case if we simply switch on the interaction between qubits and two intermediate sites $(L, R)$ of the optical lattice, shown in Fig. 1.14c, the two external parts of the lattice play the role of environment and deteriorate the quality of the gate. To preserve the gate quality we need to cut the lattice into three parts and separate the bus, extended from $L$ to $R$, from the rest of the optical lattice. This can be done by adiabatically shining a localized laser beam on the atoms sitting on sites $L-1$ and $R+1$ to drive them off resonance, as shown in Fig. 1.14c. In this case driving the atom effectively generates a Stark shift between the two degenerate ground state through a highly detuned classical laser beam with strength $\Omega$ and detuning $\Delta \gg \Omega$. This provides an energy shift $\delta E = \Omega^2/\Delta$ between the two degenerate ground states, which can be treated as a local magnetic field in the $z$ direction on sites $L-1$ and $R+1$. Keeping $\Omega/\Delta$ small one can control the strength $\Omega$ and detuning $\Delta$ such that $\delta E$ becomes larger than $J$. When $\delta E \gg J$ the bus is separated from the external parts of the optical lattice. Moreover, as $\delta E$ adiabatically increases, the bus moves into its ground state, meanwhile splitting up from the rest. Despite the gapless nature of Hamiltonian (1.36) there is always a gap $\propto J/N$ due to the finite size of the bus which guarantee the success of the adiabatic evolution. Once the bus been prepared in its ground state the gate operation can be accomplished as discussed above.

### *1.7.3 Time Scale*

We now give an estimation of $t^*$ in the *worst* case scenario where $A$ and $B$ sit on the boundary of the lattice, which typically consists of $N \simeq 100$. The typical values for $J$ in optical lattices are few hundred Hertz (e.g. $J = 360\,\mathrm{h\,Hz}$ in [89]). From the inset of Fig. 1.13b we get $Jt^* \simeq 30$ for $N = 100$ and thus $t^* \simeq 13\,\mathrm{ms}$ which is well below the typical decoherence time of the hyperfine levels ($\simeq$10 min [90]). Though there are some recent realizations of entangling gates [91, 92], faster than ours, they are much less versatile as they design a single, very specific, isolated gate and do not construct the gate as part of an extended system. Considering this latter kind of architecture, our mechanism is much faster than the perturbative methods [21, 57], and operates at the time scale of $\mathcal{O}(N/J)$ which is the best possible in any physical realization.

## 1.8 Concluding Remarks and Further Developments

In this chapter, we have first briefly introduced and reviewed various proposals for the usage of spin chains as buses for quantum information transfer. We recounted that a high quality of transfer usually comes at a price, perhaps requiring significant engineering of the couplings or encoding or time-control or the employment of slow

processes, such as schemes with very weak couplings or adiabatic processes. We then presented the more recent proposal of Refs. [66] and [67], which has a rather low price to pay while accomplishing a very high fidelity state transfer ($|f_{1N}(t^*)| \to 0.85$ as $N \to \infty$). The requirements for this scheme are surprisingly minimal – one merely has to engineer an optimal interaction $x \sim JN^{-1/6}$ between the qubits and a spin chain which has quasi-uniform nearest neighbour couplings. The time of transfer is $O(N/J)$ because the couplings $x$ are much stronger in comparison to the Rabi-like schemes which couple to a single mode of the bus. Here, instead, a number of modes are excited due to the non-perturbative value of $x$ and a high-quality transfer is obtained across very large distances by requiring that only the modes excited by the initialization of the first qubit have a linear dispersion. While certainly this scheme is promising, its extendability to models which do not map to free fermions, such as the isotropic Heisenberg models, is yet to be investigated.

We then moved on to describing how to establish entanglement between the two far ends of a spin chain through quench induced nonequilibrium dynamics [38]. Of course, as is well known for quite some time, entanglement can be also established between the terminal spins of a spin chain by using quantum state transfer, where one locally generates an entangled state of a pair of spins and transmits the state of one of these spins through the spin chain [5, 23, 40, 67]. This, of course, requires quite a bit of local control in the sense that a maximally entangled state first has to be generated locally before launching one part of it in a spin chain. This is qualitatively very different from the type of scheme we have presented here. The entanglement exploited here, is in a sense, already present naturally in the spin chain in its ground state, but not in a readily usable form. It is present as the entanglement between a spin at one end of a spin chain (which is called the impurity spin) and a block of spins in the chain (which is called the Kondo screening cloud) in a spin chain emulation of the Kondo system of solid state physics [77–79]. By suddenly coupling two such spin chains together at the ends farthest from the impurities, we can induce a dynamics that eventually entangles the well separated impurities in a time state $O(N/J)$. The long term dynamics could only be studied numerically and indicates a distance $(N)$ independent value nearing 0.9 [38]. While this scheme works for Heisenberg models, this, as well as other literature on quench induced entanglement [36, 37] are yet to be adapted to a realistic setting. As there has already been quite a few physical implementation proposals/demonstrations of quantum state transfer through spin chains (for example, Refs. [9, 15, 20–23, 25–27]), the adaptation of quench induced entanglement in similar systems would also be interesting.

In the end, we have described a scalable scheme for realizing a two-qubit entangling gate between arbitrary distant qubits. In our proposal, qubits are made of localized objects which makes single qubit gates affordable. The qubits interact dynamically via an extended unmodulated spin chain bus which does not need being specifically engineered and, besides embodying a quantum channel, actively serves to operate the entangling gate. Moreover, thanks to the non-perturbative interaction between the qubits and the bus our dynamics is fast ($O(N/J)$) which minimizes destructive decoherence effects. Our proposal is general and can be implemented in various physical realizations. Specifically we have proposed an application based

on neutral atom qubits in an array of separated NFFD traps connected by an optical lattice spin chain data bus, which both are accessible to the current technology.

**Acknowledgements** SB acknowledges the support of an ERC grant. Much of the reviewed work was supported, when it was done, by the EPSRC, the Royal Society and the Wolfson Foundation. LB and PV want to thank their collaborators in the work reported, namely, Tony John George Apollaro, Alessandro Cuccoli and Ruggero Vaia. PS thanks CNPq (Brazil) and the EC Seventh Framework Programme (FP7/2007–2013) under grant 295234-FP7-PEOPLE-2011-IRSES (project QICFT) for financial support. P.V. acknowledges financial support from the Consiglio Nazionale delle Ricerche, in the framework of the Short Term Mobility Program 2010.

## References

1. D.P. DiVincenzo, Fortschritte der Physik **48**, 771–783 (2000)
2. J.P. Home, D. Hanneke, J.D. Jost, J.M. Amini, D. Leibfried, D.J. Wineland, Science **325**, 1227 (2009)
3. S. Hermelin et al., Nature **477**, 435–438 (2011)
4. P. Maunz, S. Olmschenk, D. Hayes, D. Matsukevich, L.-M. Duan, C. Monroe, Phys. Rev. Lett. **102**, 250502 (2009)
5. S. Bose, Phys. Rev. Lett. **91**, 207901 (2003)
6. S. Bose, Contemp. Phys. **48**, 13 (2007)
7. I thank Daniel Burgarth for this additional and subtle motivational insight
8. L.-A. Wu, D.A. Lidar, M. Friesen, Phys. Rev. Lett. **93**, 030501 (2004)
9. L. Banchi, A. Bayat, P. Verrucchi, S. Bose, Phys. Rev. Lett. **106**, 140501 (2011)
10. A. Yu. Kitaev, Annals Phys. **303**, 2 (2003)
11. Y. Li, D.E. Browne, L.C. Kwek, R. Raussendorf, T.-C. Wei, Phys. Rev. Lett. **107**, 060501 (2011)
12. A. Dutta, U. Divakaran, D. Sen, B.K. Chakrabarti, T.F. Rosenbaum, G. Aeppli. arXiv:1012.0653
13. M. Cheneau, P. Barmettler, D. Poletti, M. Endres, P. Schauß, T. Fukuhara, C. Gross, I. Bloch, C. Kollath, S. Kuhr, Nature **481**, 484 (2012)
14. G.M. Nikolopoulos, D. Petrosyan, P. Lambropoulos, Europhys. Lett. **65**, 297 (2004)
15. A. Romito, R. Fazio, C. Bruder, Phys. Rev. B **71**, 100501(R) (2005); A.O. Lyakhov, C. Bruder, Phys. Rev. B **74**, 235303 (2006)
16. L.-M. Duan, E. Demler, M.D. Lukin, Phys. Rev. Lett. **91**, 090402 (2003)
17. M. Lubasch, V. Murg, U. Schneider, J.I. Cirac, M. Bañuls, Phys. Rev. Lett. **107**, 165301 (2011)
18. D. Porras, J.I. Cirac, Phys. Rev. Lett. **92**, 207901 (2004)
19. F. Mintert, C. Wunderlich, Phys. Rev. Lett. **87**, 257904 (2001)
20. M. Bellec, G.M. Nikolopoulos, S. Tzortzaki, Opt. Lett. **37**, 4504 (2012)
21. N.Y. Yao, L. Jiang, A.V. Gorshkov, Z.-X. Gong, A. Zhai, L.-M. Duan, M.D. Lukin, Phys. Rev. Lett. **106**, 040505 (2011)
22. N. Yao, L. Jiang, A. Gorshkov, P. Maurer, G. Giedke, J. Cirac, M. Lukin, Nat. Commun. **3**, 800 (2012)
23. Y. Ping, B.W. Lovett, S.C. Benjamin, E.M. Gauger, Phys. Rev. Lett. **110**, 100503 (2013)
24. C. Belthangady, N. Bar-Gill, L.M. Pham, K. Arai, D. Le Sage, P. Cappellaro, R.L. Walsworth, Phys. Rev. Lett. **110**, 157601 (2013)
25. J. Zhang et al., Phys. Rev. Lett. **80**, 012316 (2009)
26. P. Cappellaro, C. Ramanathan, D.G. Cory, Phys. Rev. A **76**, 032317 (2007)
27. C. Ramanathan, P. Cappellaro, L. Viola, D. Cory, New J. Phys. **13**, 103015 (2011)
28. A.D. Greentree, S.J. Devitt, L.C.L. Hollenberg, Phys. Rev. A **73**, 032319 (2006)

29. M Horodecki, P Horodecki, R Horodecki, Phys. Rev. A **60**, 1888 (1999)
30. C. Godsil, S. Kirkland, S. Severini, J. Smith, Phys. Rev. Lett. **109**, 050502 (2012)
31. C. Godsil, Discret. Math. **312**, 129 (2012)
32. C.H. Bennett, G. Brassard, C. Crépeau, R. Jozsa, A. Peres, W.K. Wootters, Phys. Rev. Lett. **70**, 1895 (1993)
33. C.H. Bennett, D.P. DiVincenzo, J.A. Smolin, W.K. Wootters, Phys. Rev. A **54**, 3824 (1996)
34. W.K. Wootters, Phys. Rev. Lett. **80**, 2245 (1998)
35. O. Romero-Isart, K. Eckert, A. Sanpera, Phys. Rev. A **75**, 050303(R) (2007)
36. H. Wichterich, S. Bose, Phys. Rev. A **79**, 060302(R) (2009)
37. P. Sodano, A. Bayat, S. Bose, Phys. Rev. B **81**, 100412(R) (2010)
38. A. Bayat, S. Bose, P. Sodano, Phys. Rev. Lett. **105**, 187204 (2010)
39. E.B. Fel'dman, E.I. Kuznetsova, A.I. Zenchuk, Phys. Rev. A **82**, 022332 (2010)
40. A. Bayat, S. Bose, Phys. Rev. A **81**, 012304 (2010)
41. G.M. Nikolopoulos, D. Petrosyan, P. Lambropoulos, J. Phys.: Condens. Matter **16**, 4991 (2004)
42. M. Christandl, N. Datta, A. Ekert, A.J. Landahl, Phys. Rev. Lett. **92**, 187902 (2004)
43. M.-H. Yung, S. Bose, Phys. Rev. A **71**, 032310 (2005)
44. P. Karbach, J. Stolze, Phys. Rev. A **72**, 030301 (2005)
45. C. Di Franco, M. Paternostro, M.S. Kim, Phys. Rev. Lett. **101**, 230502 (2008)
46. V. Kost'ak, G.M. Nikolopoulos, I. Jex, Phys. Rev. A **75**, 042319 (2007)
47. A. Ajoy, P. Cappellaro, Phys. Rev. Lett. **110**, 220503 (2013)
48. T.J. Osborne, N. Linden, Phys. Rev. A **69**, 052315 (2004)
49. H.L. Haselgrove, Phys. Rev. A **72**, 062326 (2005)
50. H. Yadsan-Appleby, T.J. Osborne, Phys. Rev. A **85**, 012310 (2012)
51. D. Burgarth, S. Bose, Phys. Rev. A **71**, 052315 (2005)
52. D. Burgarth, S. Bose, New J. Phys. **7**, 135 (2005)
53. V. Giovannetti, D. Burgarth, Phys. Rev. Lett. **96**, 030501 (2006)
54. D. Burgarth, V. Giovannetti, S. Bose, Phys. Rev. A **75**, 062327 (2007)
55. J. Fitzsimons, J. Twamley, Phys. Rev. A **72**, 050301(R) (2005)
56. M.B. Plenio, F.L. Semiao, New J. Phys. **7**, 73 (2005); M.J. Hartmann, M.E. Reuter, M.B. Plenio, New J. Phys. **8**, 94 (2006)
57. Y. Li, T. Shi, B. Chen, Z. Song, C.P. Sun, Phys. Rev. A **71**, 022301 (2005); A. Wójcik, T. Łuczak, P. Kurzyński, A. Grudka, T. Gdala, M. Bednarska, Phys. Rev. A **72**, 034303 (2005)
58. L.C. Venuti, C.D.E. Boschi, M. Roncaglia, Phys. Rev. Lett. **99**, 060401 (2007)
59. M.-H. Yung, D.W. Leung, S. Bose, Quan. Inf. Com. **4**, 174 (2003)
60. A. Ajoy, P. Cappellaro, Phys. Rev. B **87**, 064303 (2013)
61. J. Oreg, F.T. Hioe, J.H. Eberly, Phys. Rev. A **29**, 690 (1984); J.R. Kuklinski, U. Gaubatz, F.T. Hioe, K. Bergmann, Phys. Rev. A **40**, 6741 (1989); U. Gaubatz, P. Rudecki, S. Schiemann, K. Bergmann, J. Chem. Phys. **92**, 5363 (1990)
62. T. Ohshima, A. Ekert, D.K.L. Oi, D. Kaslizowski, L.C. Kwek. arXiv:quant-ph/0702019
63. K. Eckert, O. Romero-Isart, A. Sanpera, New J. Phys. **9**, 155 (2007)
64. N. Chancellor, S. Haas, New J. Phys. **14**, 095025 (2012)
65. D. Petrosyan, P. Lambropoulos, Opt. Commun. **264**, 419 (2006)
66. L. Banchi, T.J.G. Apollaro, A. Cuccoli, R. Vaia, P. Verrucchi, Phys. Rev. A **82**, 052321 (2010)
67. L. Banchi, T.J.G. Apollaro, A. Cuccoli, R. Vaia, P. Verrucchi, New J. Phys. **13**, 123006 (2011)
68. A. Zwick, O. Osenda, J. Phys. A **44**, 105302 (2011)
69. T.J.G. Apollaro, L. Banchi, A. Cuccoli, R. Vaia, P. Verrucchi, Phys. Rev. A **85**, 052319 (2012)
70. A. Osterloh et al., Nature **416**, 608 (2002); T.J. Osborne, M.A. Nielsen, Phys. Rev. A **66**, 032110 (2002)
71. L.C. Venuti, C.D.E. Boschi, M. Roncaglia, Phys. Rev. Lett. **96**, 247206 (2006)
72. L.C. Venuti, S.M. Giampaolo, F. Illuminati, P. Zanardi, Phys. Rev. A **76**, 052328 (2007); S.M. Giampaolo, F. Illuminati, New J. Phys. **12**, 025019 (2010); S.M. Giampaolo, F. Illuminati, Phys. Rev. A **80**, 050301 (2009); G. Gualdi, S.M. Giampaolo, F. Illuminati, Phys. Rev. Lett. **106**, 050501 (2011)
73. S.M. Giampaolo, F. Illuminati, Phys. Rev. A **80**, 050301(R) (2009)

74. I. Affleck, Lecture Notes, Les Houches (2008). arXiv:0809.3474
75. A. Hewson, *The Kondo Model to Heavy Fermions* (Cambridge University, Cambridge, 1997)
76. A. Bayat, P. Sodano, S. Bose, Phys. Rev. B **81**, 064429 (2010)
77. N. Laflorencie, E.S. Sorensen, I. Affleck, J. Stat. Mech. **2008**, P02007 (2008)
78. E.S. Sorensen, M.S. Chang, N. Laflorencie, N.I. Affleck, J. Stat. Mech. **2007**, P08003 (2007)
79. N. Laflorencie, E.S. Sorensen, M.S. Chang, I. Affleck, Phys. Rev. Lett. **96**, 100603 (2006)
80. S.R. Clark, C.M. Alves, D. Jaksch, New J. Phys. **7**, 124 (2005)
81. M.H. Yung, S.C. Benjamin, S. Bose, Phys. Rev. Lett. **96**, 220501 (2006)
82. R. Ronke, I. D'Amico, T.P. Spiller, Phys. Rev. A **84**, 032308 (2011)
83. A. Bayat, L. Banchi, S. Bose, P. Verrucchi, Phys. Rev. A **83**, 062328 (2011)
84. P. Zanardi, D.A. Lidar, Phys. Rev. A **70**, 012315 (2004)
85. M.A. Nielsen, Phys. Lett. A **303**, 249 (2002)
86. T.N. Bandi, V.G. Minogin, S.N. Chormaic, Phys. Rev. A **78**, 013410 (2008)
87. E.H. Lapasar, K. Kasamatsu, Y. Kondo, M. Nakahara, T. Ohmi, J. Phys. Soc. Jpn. **80**, 114003 (2011)
88. J.F. Sherson, C. Weitenberg, M. Endres, M. Cheneau, I. Bloch, S. Kuhr, Nature **467**, 68 (2010)
89. S. Trotzky et al., Phys. Rev. Lett. **105**, 265303 (2010)
90. J. Bollinger et al., IEEE Trans. Instrum. Meas. **40**, 126 (1991)
91. T. Wilk et al., Phys. Rev. Lett. **104**, 010502 (2010)
92. L. Isenhower et al., Phys. Rev. Lett. **104**, 010503 (2010)

# Chapter 2
# Communication in Engineered Quantum Networks

**Georgios M. Nikolopoulos, Thomas Brougham, Antonin Hoskovec, and Igor Jex**

**Abstract** We review the engineering of passive quantum networks for performing fundamental quantum communications tasks, such as the transfer, routing, and splitting of signals that are associated with quantum states. After an introduction to fundamental concepts and notions, the problem of quantum state transfer is discussed for networks of various physical and logical topologies. The discussion is cast in terms of a unified theoretical formalism, which is perfectly suited to addressing the problem in the context of various physical realizations.

## 2.1 Introduction

In this section we introduce the reader to fundamental concepts of quantum networks.

G.M. Nikolopoulos (✉)
Foundation for Research and Technology – Hellas, Institute of Electronic Structure and Laser, P.O. Box 1385, GR-711 10 Heraklion, Greece
e-mail: nikolg@iesl.forth.gr

T. Brougham
Department of Physics, University of Strathclyde, 107 Rottenrow, Glasgow, G4 0NG, Scotland, UK
e-mail: thomas.brougham@gmail.com

A. Hoskovec · I. Jex
Faculty of Nuclear Sciences and Physical Engineering, Department of Physics, Czech Technical University in Prague, Břehová 7, Praha 1, Staré Město, 115 19, Czech Republic
e-mail: a.hoskovec@gmail.com; igor.jex@fjfi.cvut.cz

G.M. Nikolopoulos and I. Jex (eds.), *Quantum State Transfer and Network Engineering*, Quantum Science and Technology, DOI 10.1007/978-3-642-39937-4_2,

### 2.1.1 Elements of Quantum Networks

A quantum network typically consists of a number of quantum objects (e.g., atoms, ions, quantum dots, cavities, etc.), to be referred to hereafter as the sites or the nodes of the network. In other words, quantum networks are discrete lattices of various geometric arrangements, and the interaction law underlying the coupling of the different sites depends on the details of the particular realization under consideration.

In the framework of quantum information processing (QIP), quantum networks may perform different communication tasks, such as transfer, routing, switching and splitting of quantum signals. The information to be communicated is encoded onto quantum states associated with excitations of the lattice. The elementary unit of quantum information is the quantum bit (qubit), which is represented by a physical system with well-defined characteristics allowing for meaningful separation and addressing of two orthogonal states making up the qubit basis, which can store the logical 0 and 1 as well as their arbitrary superpositions. In general, the encoding of a logical bit may involve one or more physical qubits (e.g., electrons, photons, atoms, ions, etc.). Theoretical studies have shown that the use of quantum states in various information-processing tasks may lead to remarkable qualitative as well as quantitative improvements [1].

Depending on whether external control is required for the transfer of the state (besides the initialization and the read-out processes which are always present), one can distinguish between active and passive networks. The operation of *active quantum networks* relies on some sort of external control. The most straightforward approach in this context pertains to a sequence of SWAP gates, which ensure the successive transfer of the state between neighbouring sites; an approach that requires the ability to modulate in time the strength and the nature of the interactions throughout the entire network. Another class of active networks relies on the encoding of information on wave-packet states that pertain to a large number of nodes and ensure low dispersion and transport at a definite group velocity. In either case, the operation of active networks relies on a judicious sequence of operations and/or measurements that are applied individually or collectively on the nodes. As a result, active networks are considered to be very susceptible to errors that accumulate in each operation applied during the transfer, as well as to decoherence and dissipation, since they have to be connected to the environment (e.g., to macroscopic devices), in order to allow for external control. Such a type of errors and problems can be avoided by resorting to networks with permanently coupled sites, the so-called *passive quantum networks*. These networks are engineered under the constraint of minimal external control, in the sense that they do not require any external control to perform their tasks (besides the initialization and read-out). Thus, they are also less susceptible to decoherence and dissipation, since they can be isolated from their environment to a large extent. The engineering typically pertains to the permanent adjustment of certain parameters across the network.

In the spirit of large-scale QIP, passive quantum networks may operate as black boxes that perform certain communication tasks, and they do not require

any external control, or prior knowledge on the information to be transferred. For instance, a passive quantum chain that ensures the faithful transfer of a quantum signal between its two ends, can be used to build a quantum chip by interconnecting different small components, such as processors and memories. Moreover, in this case there is no need for converting back and forth between different types of information carriers (e.g., photons and atoms), since passive quantum networks can be engineered with hardware that is fully compatible with the one used for the other components of the chip, including the information carriers.

In the following we focus on passive quantum networks, and the transfer of single- or multi-qubit states. Some of the results, however, are expected to be applicable to cases where the information is encoded in a higher-dimensional quantum system.[1]

### *2.1.2 Hamiltonians*

A physical implementation of a quantum network involves one way or another a discrete lattice, and there are different scenarios one may consider for the transfer of a state between two or more nodes. Schematic representations of two different scenarios are depicted in Fig. 2.1, for a one-dimensional (1D) network, and a single-qubit state. In the first scenario depicted in Fig. 2.1a, the transfer of the state is accompanied by the transfer of the physical qubit. The lattice is initially in its ground state (it could be also the vacuum), and the information is encoded onto the state of excess particle(s) that play the roles of information carriers. When the ground state is not the vacuum, but rather it pertains to a particular configuration of particles (not shown in Fig. 2.1a), it should remain frozen throughout the evolution of the system, so that only the excess information carrier(s) participate in the transfer. When the ground state is the vacuum, this condition is readily satisfied. In the second scenario depicted in Fig. 2.1b, each site of the network is occupied by a physical qubit, and the entire network is initially prepared in its ground state. The information is encoded in the state of some of the existing physical qubits, and this excitation (perturbation) propagates along the chain due to the presence of always-on couplings between adjacent qubits. In the following we refer to these two scenarios as A and B.

Whether a physical qubit is involved in the transfer of the state or not, the dynamics of the lattice can be analysed in the framework of second quantization. In general, each particle in the lattice, and thus the state of the network, is characterized by many degrees of freedom, such as its position on the lattice, the single-particle energy level (orbital) that it occupies, as well as additional internal degrees of freedom. Throughout this chapter we will focus on networks operating under the

[1] For a $d$-dimensional system the unit of quantum information is the qudit.

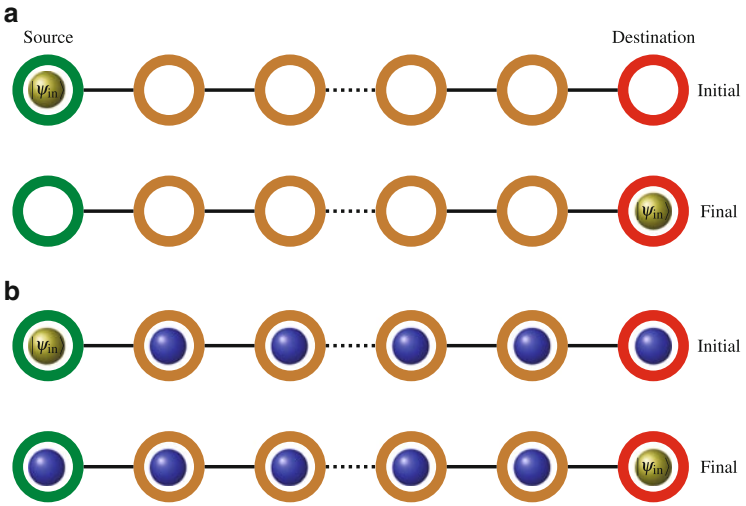


**Fig. 2.1** Two different schemes for transfer of quantum states on a 1D lattice. The sites of the network are represented by *open circles*, and the physical qubits by *filled circles* (different colours denote different qubit states). (**a**) Scenario A: The transfer of the input, in this case single-qubit state $|\psi_{\text{in}}\rangle$, from the first to the last site is accompanied by the transfer of the associated physical qubit. (**b**) Scenario B: All the sites are occupied by physical qubits, and the state is transferred via exchange interactions, without altering the initial qubit configuration (i.e., one physical qubit per site with the states of the outermost qubits exchanged)

tight-binding approximation, with the dynamics restricted to the lowest available orbitals.[2] The Hamiltonians of interest are of the form

$$\hat{\mathscr{H}}_Q = \sum_{i,\xi} \varepsilon_{i,\xi} \hat{n}_{i,\xi} + \frac{1}{2} \sum_{i,k} \sum_{\xi,\xi'} U_{i,\xi}^{k,\xi'} \hat{n}_{i,\xi} \left( \hat{n}_{k,\xi'} - \delta_{i,k} \delta_{\xi,\xi'} \right) + \sum_{i<k} \sum_{\xi} g_{i,k}^{(\xi)} (\hat{a}_{i,\xi}^{\dagger} \hat{a}_{k,\xi} + \hat{a}_{k,\xi}^{\dagger} \hat{a}_{i,\xi}), \tag{2.1}$$

where the fermionic/bosonic operator $\hat{a}_{j,\xi}^{\dagger}$ creates a particle at the lowest available orbital of the $j$th site and in state $|\xi\rangle$, which accounts for internal degrees of freedom (e.g., spin, angular momentum, etc.). The number operator is $\hat{n}_{i,\xi} = \hat{a}_{i,\xi}^{\dagger} \hat{a}_{i,\xi}$, while typically the single-particle energy can be expressed as

$$\varepsilon_{i,\xi} = \varepsilon_i + \varepsilon_{\xi}, \tag{2.2}$$

[2]The energy separation of successive orbitals in a node is assumed to be much larger than the coupling constants between adjacent nodes, as well as than the typical energy scales of various excitation mechanisms.

where $\varepsilon_i$ is associated with the occupied site and orbital, whereas $\varepsilon_\xi$ refers to the internal state of the particles. Thus the first term of (2.1) can be split into two parts as follows

$$\sum_{i,\xi} \varepsilon_{i,\xi} \hat{n}_{i,\xi} = \sum_i \varepsilon_i \hat{n}_i + \sum_\xi \varepsilon_\xi \hat{n}_\xi, \tag{2.3}$$

where $\hat{n}_\xi \equiv \sum_j \hat{n}_{j,\xi}$ and $\hat{n}_j \equiv \sum_\xi \hat{n}_{j,\xi}$. The operator $\hat{n}_j$ refers to the total number of particle at the lowest orbital of the $j$th site (irrespective of their internal state), and the operator $\hat{n}_\xi$ gives the total number of particles with internal state $|\xi\rangle$ for all the sites. Clearly, the operator $\hat{n} = \sum_\xi \hat{n}_\xi = \sum_j \hat{n}_j$ refers to total number of particles in the system.

The second term of the Hamiltonian describes repulsive ($U_{i,\xi}^{k,\xi'} > 0$) or attractive ($U_{i,\xi}^{k,\xi'} < 0$) inter-particle interactions, whose magnitude may depend on the position of the two particles in the network as well as on $\xi$. The dependence on $\xi$, however, is usually so weak that can be neglected. Finally, the last term of the Hamiltonian describes the hopping of particles between the lowest orbitals of adjacent sites in the network, with the corresponding set of coupling constants denoted by $\{g_{i,k}^{(\xi)}\}$, and may in general depend on $\xi$. Such types of Hamiltonians appear in the context of various physical realizations of lattices (e.g., photonic lattices, optical lattices, electrons confined in coupled quantum dots, etc.).

Henceforth, the variable $\xi$ will be associated with two orthogonal internal states that form our qubit basis

$$|\xi\rangle \in \{|u\rangle, |v\rangle\}. \tag{2.4}$$

In order for the states $\{|u\rangle, |v\rangle\}$ to form a qubit basis, they have to be well-separated, and thus the energy difference $|\varepsilon_{i,u} - \varepsilon_{i,v}|$ should be sufficiently large for all $i$.[3] Let us define here the operator $\hat{\Xi} = \hat{n}_u - \hat{n}_v$, which is the total $\xi$-imbalance i.e., the difference of the total populations in the two qubit basis states. One can readily confirm the following observation.

**Observation 1.** Hamiltonian (2.1) commutes with the operators $\hat{n}$, $\hat{n}_\xi$ and $\hat{\Xi}$. Thus, it preserves the total number of excitations, as well as the degrees of freedom $\xi$, and the system remains in the initially occupied sector of the Hilbert space.

By contrast to the conservation of degrees of freedom $\xi$, note that Hamiltonian (2.1) does not preserve the position of the excitations. Thus, it can be expressed in the form $\hat{\mathscr{H}} = \hat{\mathscr{H}}_0 + \hat{\mathscr{V}}$, where $\hat{\mathscr{H}}_0$ and $\hat{\mathscr{V}}$ are the unperturbed and the interaction parts of the Hamiltonian, with respect to the position degree of freedom.

[3] It should be sufficiently large with respect to decoherence mechanisms, but at the same time sufficiently small with respect to other system parameters e.g., the energy separation between successive orbitals, so that the dynamics are restricted to equivalent orbitals only.

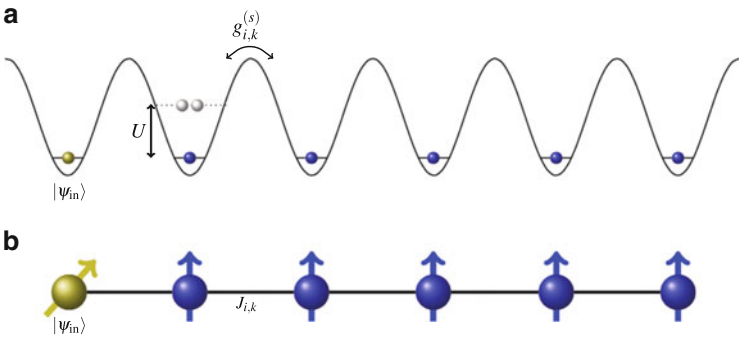


**Fig. 2.2** (**a**) Schematic representation of a 1D lattice where the lowest orbital of each site is occupied by a fermionic particle with two internal states (the related energy difference is not shown). The input state is encoded in the state of the first particle. Single-particle hopping is energetically expensive, and double occupancy is absent. Exchange of particles, however, is possible, thus allowing for the transfer of the state. (**b**) The spin-chain equivalent of (**a**). Each site is associated with a spin, and the spins interact via spin-exchange interactions

The vast majority of papers on the problem of quantum state transfer have been formulated in the framework of spin-chain Hamiltonians. In many physical realizations of lattices, however, spin-chain Hamiltonians arise as effective Hamiltonians describing adequately the dynamics of the lattice only for a specific regime of parameters, although the real system does actually involve many degrees of freedom. To illustrate this fact, consider a deep 1D lattice with identical sites and all the interactions restricted to nearest-neighbours only (see Fig. 2.2a). The lowest orbital of each site is occupied by a single fermionic particle with two relevant orthogonal internal states $\{|u\rangle, |v\rangle\}$. This is a realistic scenario that can be implemented e.g., in the context of optical lattices or chains of quantum dots. The dynamics of the system are described by the Hamiltonian (2.1), which in view of the Pauli principle can be simplified to

$$\hat{\mathscr{H}}_Q = \sum_{i,\xi} \varepsilon_{i,\xi} \hat{n}_{i,\xi} + \sum_i U_{i,u}^{i,v} \hat{n}_{i,u} \hat{n}_{i,v} + \sum_{\langle i,k \rangle} \sum_{\xi} g_{i,k}^{(\xi)} (\hat{a}_{i,\xi}^{\dagger} \hat{a}_{k,\xi} + \hat{a}_{k,\xi}^{\dagger} \hat{a}_{i,\xi}), \tag{2.5}$$

where $\langle i,k \rangle$ denotes nearest neighbour sites. For a lattice with identical sites, we also have $\varepsilon_{i,\xi} = \varepsilon + \varepsilon_{\xi}$ and $U_{i,u}^{i,v} \equiv U_{u,v}$.

In this case, for $g_{i,k}^{(\xi)} \ll U_{u,v}$, the initial configuration of the particles remains practically frozen, because single-particle jumps cost a lot of energy, since they result in changes of the total on-site population. As shown in [2, 3], in this regime Eq. (2.5) is equivalent to the following effective spin-chain Hamiltonian

$$\hat{\mathscr{H}}_S = \sum_k B_k \hat{\sigma}_k^z - \sum_{\langle i,k \rangle} \left[ J_{i,k} (\hat{\sigma}_i^x \hat{\sigma}_k^x + \hat{\sigma}_i^y \hat{\sigma}_k^y) + J'_{i,k} \hat{\sigma}_i^z \hat{\sigma}_k^z \right], \tag{2.6}$$

where $\hat{\sigma}_k^{x,y,z}$ are the Pauli spin operators at position $k$, $B_k$ determines the energy separation between the spin-up and spin-down states playing the role of the local "magnetic field", and $J_{i,k}$ is the nearest-neighbour spin-exchange interaction. This is the so-called anisotropic Heisenberg spin-chain Hamiltonian. One sees therefore that in this particular regime of parameters, the lattice with a single fermionic particle per site operates as a spin chain. Although single-particle jumps are practically absent, exchange of two particles in neighbouring sites is not so expensive energetically, and it can therefore take place. The Pauli operators can be expressed in terms of the annihilation/creation operators of (2.5) as follows,

$$\hat{\sigma}_k^z = \hat{n}_{k,u} - \hat{n}_{k,v}, \quad \hat{\sigma}_k^x = \hat{a}_{k,u}^\dagger \hat{a}_{k,v} + \hat{a}_{k,v}^\dagger \hat{a}_{k,u}, \quad \hat{\sigma}_k^y = -i(\hat{a}_{k,u}^\dagger \hat{a}_{k,v} - \hat{a}_{k,v}^\dagger \hat{a}_{k,u}). \tag{2.7}$$

Similarly, the parameters entering Hamiltonian (2.6) can be expressed in terms of $g_{i,k}^{(\xi)}$, $\varepsilon_{k,\xi}$ and $U_{u,v}$. Other effective spin-chain Hamiltonians can be also simulated in the framework of second quantization Hamiltonians e.g., by considering bosons instead of fermions, or by applying external fields (e.g., see [4]). In the spin-chain formalism the qubit basis states for the $k$th spin $\{|\uparrow\rangle, |\downarrow\rangle\}$, are typically represented by the eigenvectors of the operator $\hat{\sigma}_k^z$. In view of the correspondences (2.7), $\hat{\sigma}_k^z$ refers to the difference of populations of particles in states $|u\rangle$ and $|v\rangle$ at site $k$, and thus the eigenstate $|\uparrow\rangle$ with eigenvalue $+1$, corresponds to $|u\rangle$, while $|\downarrow\rangle$ with eigenvalue $-1$, corresponds to $|v\rangle$.

Finally, employing the Jordan-Wigner transformation [5], the spin-chain Hamiltonian (2.6) can be mapped to a Hubbard Hamiltonian for non-interacting *spinless fermions* (or hard-core bosons). For instance, when $J'_{i,k} = 0$ we find

$$\hat{\mathscr{H}}_Q' = 2\sum_k B_k \hat{c}_k^\dagger \hat{c}_k - 2\sum_{\langle i,k\rangle} J_{i,k}(\hat{c}_i^\dagger \hat{c}_k + \hat{c}_k^\dagger \hat{c}_i), \tag{2.8}$$

where

$$\hat{c}_k = \frac{1}{2}\left[\prod_{j<k} \hat{\sigma}_k^z\right](\hat{\sigma}_k^x - i\hat{\sigma}_k^y), \quad \hat{c}_k^\dagger = \frac{1}{2}\left[\prod_{j<k} \hat{\sigma}_k^z\right](\hat{\sigma}_k^x + i\hat{\sigma}_k^y), \tag{2.9}$$

and $\hat{c}_k^\dagger \hat{c}_k = (1+\hat{\sigma}_k^z)/2$. One should not confuse here the new operators $\{\hat{c}_k, \hat{c}_k^\dagger\}$, with $\{\hat{a}_{k,\xi}, \hat{a}_{k,\xi}^\dagger\}$ in Eq. (2.5). The latter refer to the annihilation/creation of real particles, whereas the new operators $\{\hat{c}_k, \hat{c}_k^\dagger\}$ refer to the excitations of the lattice. Indeed, from Eqs. (2.7) and (2.9) one sees that $\hat{c}_k \sim \hat{a}_{k,v}^\dagger \hat{a}_{k,u}$. The Hamiltonian (2.8) is still an effective one that is equivalent to (2.5) only when $g_{i,k}^{(\xi)} \ll U_{i,v}^{i,u}$. The eigenvectors of $\hat{c}_k^\dagger \hat{c}_k$ are $|0\rangle$ and $|1\rangle$, with eigenvalues 0 and 1, and they correspond to the spin states $|\downarrow\rangle$ and $|\uparrow\rangle$, respectively. Hence, the vacuum state of Hamiltonian (2.8) refers

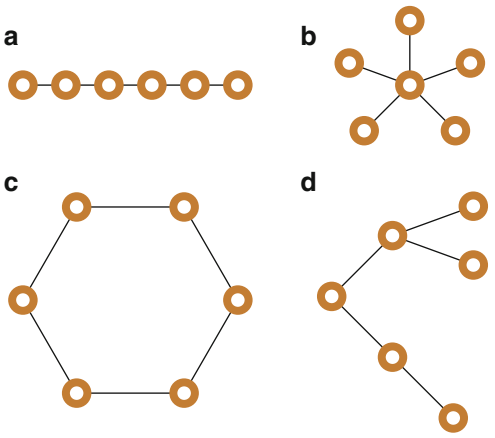


**Fig. 2.3** Various network topologies: (**a**) line; (**b**) star; (**c**) ring; and (**d**) tree or hierarchical. The *circles* show physical nodes, and the *lines* represent the links between them. Configurations with couplings beyond nearest-neighbours are also possible but are not shown here

to the ground state of the spin chain where excitations are absent, whereas in the vacuum state of Hamiltonian (2.5) there are no particles.

In closing this section, we keep in mind that discrete networks of various types can be described within the unified theoretical framework of second quantization. The state to be transferred is associated with excitations of the network, and is characterized by the position of the excitations on the lattice, and additional degrees of freedom $\xi$, that provide a good qubit basis for the encoding of information. The Hamiltonians under consideration preserve all the degrees of freedom, but the position of the excitations. Finally, it is worth emphasizing here that although all of the above Hamiltonians pertain to $\xi$-dependent coupling constants, the majority of the work on quantum networks and the faithful transfer of states has been performed in the framework of Hamiltonians with $\xi$-independent couplings.

### *2.1.3 Topologies*

In general, networks of different configurations and geometries can be considered, depending on the particular tasks and physical realizations one aims at. For instance, the geometries depicted in Fig. 2.3, or combinations thereof, have been discussed in the context of quantum networks.

Physical topology describes how different sites are coupled to each other, whereas logical topology refers to the flow of information between the various sites in a particular network. These definitions are inspired by conventional network topologies (e.g., see [6, 7]) although, due to the discreteness of quantum networks, the analogies are not always so clear. For instance, in a classical setting two nodes are connected via wires, whereas as we will see later on, in the context of quantum networks under consideration a wire is represented by a 1D discrete lattice. The logical topology focuses on the flow of information from the source

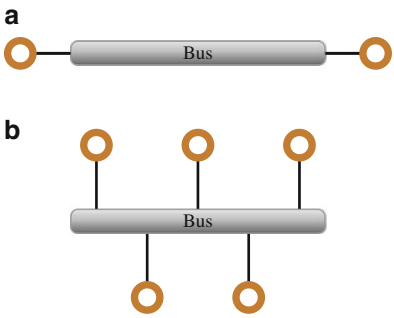


**Fig. 2.4** Point-to-point (**a**) and bus (**b**) logical topologies. The hosts (*open circles*) communicate via the bus that is provided by the remaining physical nodes

to the destination nodes in a particular configuration, and it is not necessarily the same as the physical topology. Furthermore, in a classical setting an outgoing signal originates from a particular source node, whereas in quantum networks the signal may involve many nodes in a superposition state. These are fundamental differences, which however, do not prevent us from defining logical topologies based on how signals move between the source and the destination nodes (also to be referred to hereafter as the *hosts*) [8]. *The set of hosts is thus a subset of the set of all the physical nodes in the network*. The nodes that are not hosts operate as gateways/routers, providing the channel (or the bus) for the communication. Throughout this chapter, the set of all the physical nodes will be denoted by $\mathbb{P}$, and the sets of source and the destination nodes by $\mathbb{S}$ and $\mathbb{D}$, respectively.

The simplest logical topology one may consider is the so-called *point-to-point (PP) topology* pertaining to two hosts. Irrespective of any intermediate physical connections between the source and the destination nodes, any message originating from the source is intended for the destination node only (see Fig. 2.4a). A direct generalization of the PP logical topology is the so called *bus topology*, which enables a larger number of hosts to communicate using the same shared media. Physically speaking, the various hosts are connected to a common wire, known as backbone or bus (see Fig. 2.4b), which is provided by the other nodes of the network. A transmitted message is visible and, in principle, accessible by all the hosts, although the intended recipient is actually the one that accepts and processes the message.[4] When the logical network encompasses the entire physical network (i.e., the sets of hosts and physical nodes coincide), we have the *universal bus topology*. Other types of logical topologies may also be defined in the same framework.

[4]In a classical setting, this can be achieved by means of the so-called internet-protocol (IP) addresses. As the message arrives at each node, the corresponding device checks the destination address contained in the message to see if it matches its own address. If the two addresses match the device processes the message, otherwise it does nothing. Clearly, no addressing is required in a PP topology since any data transmitted from one node is intended for the other node.

## 2.2 The Problem of Quantum State Transfer

Having introduced fundamental notions and concepts of quantum networks, in this section we define the problem of quantum state transfer (QST), which was introduced for the first time by Bose, in the framework of spin chains [9]. The present definitions and concepts, however, are provided in the general framework of quantum networks, without specifying any particular physical realization of the network.

The pure quantum state $|\psi_{\text{in}}\rangle$ to be transferred is initially prepared on one or more sites of the network, to be referred to hereafter as the *source* sites (or nodes). To this end, the quantum network has to be initially prepared in a state that remains invariant during the transfer, and this is usually taken to be the ground state of the network which, depending on the details of the system and the adopted theoretical formalism, may be the vacuum. Moreover, for the scenario of Fig. 2.1a, b, the encoding of the state requires the addition of excess physical qubits in the lattice, whereas this is not necessary for the setup of Fig. 2.1c, d. The preparation of the state in the source node(s) has to take place on a time scale much shorter than all the other characteristic time scales of the Hamiltonian. Hence, one typically assumes that the source nodes are initially decorrelated from the rest of the network i.e., the initial state of the entire network is

$$|\Psi(0)\rangle = |\psi_{\text{in}}\rangle_{\mathbb{S}} \otimes |\oslash\rangle_{\mathbb{R}}, \tag{2.10}$$

where the subscripts $\mathbb{S}$ and $\mathbb{R}$ refer to the source nodes and the rest of the network (i.e., $\mathbb{R} = \mathbb{P}\backslash\mathbb{S}$), whereas the ground state is denoted by $|\oslash\rangle$. This assumption allows for an unambiguous definition of the problem of QST. When $\mathbb{R}$ is not initially in a pure state, we have

$$\hat{\rho}(0) = \hat{\rho}^{(\mathbb{S})}(0) \otimes \hat{\rho}^{(\mathbb{R})}(0), \tag{2.11}$$

where $\hat{\rho}^{(\mathbb{S})}(0) = (|\psi_{\text{in}}\rangle\langle\psi_{\text{in}}|)_{\mathbb{S}}$, and $\hat{\rho}^{(\mathbb{R})}$ refers to the mixed state of the rest of the network.

An excitation created somewhere in a quantum network will unavoidably propagate in all possible directions and, after some time, various sites of the network will be excited; albeit with different probabilities. In other words, even in the absence of imperfections (such as disorder, dissipation and decoherence), we have a dispersion (spreading) of the initially well-localized quantum information, all over the network (e.g., see Figs. 2.5a and 2.7a). Given the finite size of a network, the excitation will appear after some time at the destination nodes with high probability, but we do not know in advance when this will happen. In general the number of source nodes need not be equal to the number of destination nodes.

The problem of QST, refers to the engineering of Hamiltonians that govern the evolution of a quantum network and guarantee the transfer of an input quantum state from the source to the destination nodes, in a deterministic manner and after a prescribed time.

The presence of imperfections in a particular realization of a network is inevitable, and is expected to affect the transfer in addition to the aforementioned dispersion problems. A quantum network may be useful in practise only if it can be designed with sufficiently small imperfections, so that the associated disturbances are weak perturbations to the operation of an otherwise perfect network.[5] In this spirit therefore dispersion (diffraction) effects are usually treated separately, by solving the problem of QST in the absence of any imperfections. One can thus derive Hamiltonians that ensure the faithful or even the perfect transfer of the state for the ideal scenario, and subsequently investigate their robustness against various types of imperfections in a particular physical realization. Moreover, a QST scheme is useful only if it operates reliably irrespective of the input qubit state. Hence, ideally we are interested in QST Hamiltonians $\hat{\mathscr{H}}$, for which the corresponding evolution operator

$$\hat{\mathscr{U}}(t) \equiv e^{-i\hat{\mathscr{H}}t/\hbar}, \tag{2.12}$$

is such that the state of the entire network at a prescribed time $\tau$ is the target state $|\Psi_{\text{target}}\rangle$ (or $\hat{\rho}_{\text{target}}$) i.e.,

$$\hat{\mathscr{U}}(\tau)|\Psi(0)\rangle = |\psi_{\text{in}}\rangle_{\mathbb{D}} \otimes |\diamond\rangle_{\mathbb{R}'} \equiv |\Psi_{\text{target}}\rangle, \tag{2.13}$$

or

$$\hat{\mathscr{U}}(\tau)\hat{\rho}(0)\hat{\mathscr{U}}^{\dagger}(\tau) = (|\psi_{\text{in}}\rangle\langle\psi_{\text{in}}|)_{\mathbb{D}} \otimes \hat{\rho}_{\mathbb{R}'}(\tau) = \hat{\rho}_{\text{target}}, \tag{2.14}$$

where $|\Psi(0)\rangle$ and $\hat{\rho}(0)$ are given by Eqs. (2.10) and (2.11), respectively. The subscript $\mathbb{D}$ refers to the destination nodes, while $\mathbb{R}'$ refers to the rest of the network (i.e., $\mathbb{R}' = \mathbb{P} \setminus \mathbb{D}$), with the corresponding pure state denoted by $|\diamond\rangle_{\mathbb{R}'}$. Note that we have allowed for arbitrary changes in the state of all the nodes, but the hosts, during the transfer i.e., the states of $\mathbb{R}$ and $\mathbb{R}'$ need not be the same. Our only requirement is that the input state has been transferred from the source to the destination nodes at time $\tau$, perhaps up to an unimportant global phase $\varphi$ that need not be considered here.

As soon as the state has been transferred to the destination nodes, it has to be read out and to this end, the destination nodes have to decouple from the rest of the network. Throughout this chapter we focus on the problem of QST and the engineering of related Hamiltonians, but it has to be emphasized that both the initialization and the read out processes are key components for the successful operation of a quantum network. In both cases, the coupling and decoupling of sites to the rest of the network have to be, on the one hand fast enough so that the state of the system remains practically frozen during the (de)coupling, and on the other hand adiabatic to prevent new non-resonant excitations. Keeping this in mind,

[5] For instance, if the network is viewed as part of a larger fault-tolerant quantum-information processor, the probability of errors at the end of the transfer must be below $\approx 10^{-4}$ [1].

from now on we focus on the engineering of time-independent QST Hamiltonians, and we begin with a necessary and sufficient condition for a Hamiltonian to satisfy Eqs. (2.13) and (2.14).

**Theorem 1.** *A Hamiltonian satisfies Eqs. (2.13) and (2.14) for given $\tau$, if and only if its eigenenergies $\lambda_j$ and eigenstates $|\lambda_j\rangle$ satisfy*

$$e^{-i\lambda_j\tau/\hbar}\langle\lambda_j|\Psi(0)\rangle = \langle\lambda_j|\Psi_{\text{target}}\rangle \tag{2.15}$$

*and*

$$e^{-i(\lambda_j-\lambda_k)\tau/\hbar}\langle\lambda_j|\hat{\rho}(0)|\lambda_k\rangle = \langle\lambda_j|\hat{\rho}_{\text{target}}|\lambda_k\rangle, \tag{2.16}$$

*respectively.*

*Proof.* Condition (2.15) is a special case of (2.16), and working along the lines of [10], we will prove the latter. Assume that a Hamiltonian $\hat{\mathscr{H}}$ has a spectral decomposition

$$\hat{\mathscr{H}} = \sum_{\lambda_j}\lambda_j|\lambda_j\rangle\langle\lambda_j|, \tag{2.17}$$

and satisfies

$$\hat{\mathscr{U}}(\tau)\hat{\rho}(0)\hat{\mathscr{U}}^{\dagger}(\tau) = \hat{\rho}_{\text{target}}. \tag{2.18}$$

Then condition (2.16) is readily obtained if we take the overlap with any two eigenstates. On the other hand, if condition (2.16) is satisfied, then using the spectral decomposition of the Hamiltonian we have

$$\begin{aligned}\hat{\mathscr{U}}(\tau)\hat{\rho}(0)\hat{\mathscr{U}}^{\dagger}(\tau) &= \sum_{\lambda_j,\lambda_k} e^{-i(\lambda_j-\lambda_k)\tau/\hbar}|\lambda_j\rangle\langle\lambda_j|\hat{\rho}(0)|\lambda_k\rangle\langle\lambda_k| \\ &= \sum_{\lambda_j,\lambda_k}|\lambda_j\rangle\langle\lambda_j|\hat{\rho}_{\text{target}}|\lambda_k\rangle\langle\lambda_k| = \hat{\rho}_{\text{target}}.\end{aligned} \tag{2.19}$$

□

The necessary and sufficient conditions of Theorem 1 can be also expressed in terms of the moduli and the phases of the overlaps.

Finally, in closing this section, we should emphasize that, in general, faithful transfer of excitation probabilities does not necessarily imply faithful transfer of the associated quantum state. The quality of the state transfer can be quantified by the fidelity

$$F = \langle\psi_{\text{in}}|\hat{\rho}^{(\mathbb{D})}(\tau)|\psi_{\text{in}}\rangle, \tag{2.20}$$

where $\hat{\rho}^{(\mathbb{D})}$ is the reduced density matrix describing the state of the destination nodes at the end of the transfer, and $|\psi_{\text{in}}\rangle$ is the input state. The reason is that the excitation probabilities do not carry any phase information, which is inherently present in a quantum state. Thus, even when the excitation has been transferred perfectly from the source to the destination nodes, the relative phase between the various components of the associated state may have changed, yielding thus small overlap with the input state $|\psi_{\text{in}}\rangle$. In general, dephasing is expected to be present, irrespective of the presence or the absence of imperfections. When imperfections are present, the dephasing will be random and the reduction of the fidelity is inevitable. On the contrary, in the absence of imperfections, which is the focus of the present chapter, the dephasing pertains to a fixed and known off-set of the phase and, in principle, it can be corrected. In this sense, the transfer of excitation probabilities does imply faithful transfer of the associated quantum state, assuming that we can always compensate for any known and fixed dephasing.

This point can be made clearer, if we recall here that the Hamiltonian under consideration can be written as $\hat{\mathscr{H}} = \hat{\mathscr{H}}_0 + \hat{\mathscr{V}}$, with $\hat{\mathscr{V}}$ affecting the position of the excitations while preserving $\xi$. Typically the computational basis states are chosen according to the eigenstates of the unperturbed Hamiltonian $\hat{\mathscr{H}}_0$. For Hamiltonians of the form (2.1), a good orthonormal basis for expressing the state of the network consists of the vectors

$$|\mathbf{n}\rangle \equiv |n_{1,u}, n_{1,v}; n_{2,u}, n_{2,v}; \ldots\rangle \equiv \bigotimes_{j,\xi} |n_{j,\xi}\rangle, \tag{2.21}$$

where $|n_{r,\xi}\rangle$ denotes the number of excitations or particles (depending on the scenario under consideration) in the $r$th site of the network and in state $|\xi\rangle$, while

$$\hat{\mathscr{H}}_0|\mathbf{n}\rangle = E(\mathbf{n})|\mathbf{n}\rangle. \tag{2.22}$$

When the state of $\mathbb{R}$ is pure, the initial state of the network can be written as

$$|\Psi(0)\rangle = \left[\sum_{\mathbf{n}} A_{\mathbf{n}}(0)|\mathbf{n}\rangle_{\mathbb{S}}\right] \otimes \left[\sum_{\mathbf{m}} B_{\mathbf{m}}(0)|\mathbf{m}\rangle_{\mathbb{R}},\right] \tag{2.23}$$

for some complex amplitudes $A_{\mathbf{n}}$ and $B_{\mathbf{n}}$, whereas for a mixed state we have

$$\hat{\rho}(0) = \left[\sum_{\mathbf{n},\mathbf{n}'} \rho^{(\mathbb{S})}_{\mathbf{n},\mathbf{n}'}(0)|\mathbf{n}\rangle\langle\mathbf{n}'|\right] \otimes \left[\sum_{\mathbf{m},\mathbf{m}'} \rho^{(\mathbb{R})}_{\mathbf{m},\mathbf{m}'}(0)|\mathbf{m}\rangle\langle\mathbf{m}'|\right]. \tag{2.24}$$

In both cases, the first term in the tensor product refers to the pure state of the source, and the second term to the remaining sites.

In view of Eq. (2.22), different components in Eqs. (2.23) and (2.24) will, in general, experience different phase shifts even under the influence of the unperturbed Hamiltonian only, since

$$e^{-i\hat{\mathscr{H}}_0 t/\hbar}|\mathbf{n}\rangle_X|\mathbf{m}\rangle_Y = e^{-iE(\mathbf{n},\mathbf{m})t/\hbar}|\mathbf{n}\rangle_X|\mathbf{m}\rangle_Y, \tag{2.25}$$

where

$$\hat{\mathscr{H}}_0|\mathbf{k}\rangle_X \otimes |\mathbf{q}\rangle_Y = E(\mathbf{k},\mathbf{q})|\mathbf{k}\rangle_X \otimes |\mathbf{q}\rangle_Y.$$

The perturbation $\hat{\mathscr{V}}$ is also expected, in general, to add additional relative phases. In principle, one can compensate for such phases when they are known and fixed (i.e., in the ideal scenario); a task that may require involved unitary rotations on the entire system, or individual subsystems. However, in the presence of imperfections that randomize the parameters entering $\hat{\mathscr{H}}$ (e.g., diagonal and off-diagonal disorder), there is no way to correct entirely the phases since they become random. In this case, one has to investigate the robustness of the scheme relative to different types and levels of imperfections. The reader may also refer to [11] for a thorough discussion on the quantification of state transfer by means of various measures.

## 2.3 Engineering of Quantum Networks

The design of a quantum network begins with the specification of the class of QST Hamiltonians that we are interested in, as well as the identification of all the relevant basis states [8, 12–14]. In most cases, the input state, the form of the Hamiltonians, and perhaps additional physical constraints, enable us to restrict the problem to a particular sector of the Hilbert space. Clearly, the initial state of the network, as well as the final state we are aiming at, have to belong to the same working subspace, and our task is the estimation of judicious parameters (energies and couplings) so that QST from the source to the destination nodes takes place in a deterministic manner, at a prescribed time $\tau$. In this section we will discuss a particular approach to the design of QST Hamiltonians. Consider for the time being that the sets of source and destination nodes have the same cardinality (i.e., $|\mathbb{S}| = |\mathbb{D}|$), although the performance of certain QIP tasks may require relaxation of this constraint.

Let us consider first the case of a network initially prepared in any basis state

$$|\mathbf{n}\rangle_{\mathbb{S}} \otimes |\mathbf{m}\rangle_{\mathbb{R}} \equiv |n_{s_1,u}, n_{s_1,v}; n_{s_2,u}, n_{s_2,v}; \ldots\rangle_{\mathbb{S}} \otimes |m_{r_1,u}, m_{r_1,v}; m_{r_2,u}, m_{r_2,v}; \ldots\rangle_{\mathbb{R}} \tag{2.26}$$

where $s_j \in \mathbb{S}$, $r_j \in \mathbb{R}$, and $\mathbb{R} \equiv \mathbb{P} \setminus \mathbb{S}$. The problem of QST pertains to the quest for Hamiltonians, which perform the transformation

$$|\mathbf{n}\rangle_{\mathbb{S}} \otimes |\mathbf{m}\rangle_{\mathbb{R}} \to |\mathbf{n}\rangle_{\mathbb{D}} \otimes |\mathbf{m}'\rangle_{\mathbb{R}'} \tag{2.27}$$

where $|\mathbf{m}'\rangle_{\mathbb{R}'} = |m'_{r'_1,u}, m'_{r'_1,v}; m'_{r'_2,u}, m'_{r'_2,v}; \ldots\rangle$, $r'_j \in \mathbb{R}'$ and $\mathbb{R}' \equiv \mathbb{P} \setminus \mathbb{D}$.

One way to achieve this transformation is to ask for the evolution operator to be a permutation on the basis states at time $\tau$ i.e., the evolution operator satisfies

$$\hat{\mathscr{U}}(\tau) = \hat{\mathscr{P}}, \tag{2.28}$$

where

$$\hat{\mathscr{P}} = \sum_{\mathbf{n}} |\bar{n}_{\mathscr{P}(1)}; \bar{n}_{\mathscr{P}(2)}; \bar{n}_{\mathscr{P}(3)}; \ldots\rangle\langle \bar{n}_1; \bar{n}_2; \bar{n}_3; \ldots|, \tag{2.29}$$

and $\mathbf{n} \equiv |\bar{n}_1; \bar{n}_2; \bar{n}_3; \ldots\rangle$. For the sake of simplicity in Eq. (2.29) we have set $|\bar{n}_j\rangle \equiv |n_{j,u}, n_{j,v}\rangle$, and the action of the unitary on the nodes is determined by[6]

$$\hat{\mathscr{P}} = \begin{pmatrix} 1 & 2 & \ldots\, \mathbb{S}\, \ldots & \mathbb{D} & \ldots \\ \mathscr{P}(1) & \mathscr{P}(2) & \ldots\, \mathbb{D}\, \ldots & \mathscr{P}(\mathbb{D}) & \ldots \end{pmatrix}. \tag{2.30}$$

The only restriction imposed in these equations is that the permutation should map the set of source nodes to the set of destination nodes i.e., $\hat{\mathscr{P}} : \mathbb{S} \to \mathbb{D}$, which means that for each element $s_j \in \mathbb{S}$, we have $\mathscr{P}(s_j) = d_j$ with $d_j \in \mathbb{D}$. In view of the permutation, this mapping has to be one-to-one.[7] Then, Eqs. (2.28)–(2.30) ensure that the initial state of the sources appears at the destination nodes at time $\tau$. Indeed, we have

$$\hat{\mathscr{U}}(\tau)|\mathbf{n}\rangle_{\mathbb{S}} \otimes |\mathbf{m}\rangle_{\mathbb{R}} = \hat{\mathscr{P}}|\mathbf{n}\rangle_{\mathbb{S}} \otimes |\mathbf{m}\rangle_{\mathbb{R}} = |\mathbf{n}\rangle_{\mathbb{D}} \otimes |\mathbf{m}\rangle_{\mathbb{R}'}. \tag{2.31}$$

Using Eq. (2.31) in Eqs. (2.13) and (2.14), with $|\Psi(0)\rangle$ and $\hat{\rho}(0)$ given by Eqs. (2.23) and (2.24), one sees immediately what happens if the source nodes are initially prepared in a pure state $|\psi_{\text{in}}\rangle$, and the rest of the network is prepared in an arbitrary pure or mixed state. For instance, we find

$$|\Psi(\tau)\rangle = \left[\sum_{\mathbf{n}} A_{\mathbf{n}}(0)|\mathbf{n}\rangle_{\mathbb{D}}\right] \otimes \left[\sum_{\mathbf{m}} B_{\mathbf{m}}(0)|\mathbf{m}\rangle_{\mathbb{R}'}\right], \tag{2.32}$$

The evolution operator (2.28) has transferred the excitation from the source to the destination nodes, mixing up the state of the remaining nodes. An analogous result is obtained if the initial state of $\mathbb{R}$ is a mixed state, which shows that our approach works efficiently irrespective of the actual state of $\mathbb{R}$.

[6] For the sake of simplicity in Eq. (2.30) we assume that the labels of the source and the destination nodes are successive. This is not important for the present formalism, but in general one can always relabel the sites in a given network so that the permutation is of the form (2.30).

[7] For more general mappings, one has to relax the constraint of the evolution operator being a permutation (e.g., see [13]).

Recall here that the information is encoded in the state $\xi$, which is preserved throughout the evolution of the system, whereas $\hat{\mathscr{V}}$ is responsible for the change of the position and thus for the transfer of the state. Asking for Hamiltonians that satisfy Eq. (2.28) one essentially engineers the network with respect to all of the degrees of freedom, ensuring thus that all of the components of the wavefunction (see the previous section) will experience the same phase shifts, so that there are no additional relative phases at the end of the transfer. This, however, may imply conditions on the parameters entering the Hamiltonian, which are hard to fulfil in practise. Hence, the majority of related work in the literature allows for relative phase shifts that are fixed and known and originate from $\hat{\mathscr{H}}_0$ and perhaps $\hat{\mathscr{V}}$ when the coupling constants are $\xi$-dependent. In this spirit, if various degrees of freedom can be separated in the Hamiltonian, we can exclude $\xi$ from the engineering. The aforementioned engineering technique can be then applied on the part of the Hamiltonian that pertains to the orbital, position, and other degrees of freedom. A related example will be presented in the following section.

For a set of $M$ basis states, there are $(M-1)!$ different permutations, because one column and one row of the permutation are fixed by the imposed constraint $\mathscr{P}(s_j) = d_j$. The particular choice of the permutation is usually determined by additional physical constraints imposed e.g., by the geometry and the topology of the network. This will become clearer in the examples to follow. We turn now to discuss how one can obtain QST Hamiltonians that are of a particular form (e.g., tridiagonal, block-diagonal, etc.) and at the same time consistent with requirements (2.28)–(2.30).

In general, $\hat{\mathscr{P}}$ can be decomposed into disjoint cycles $\hat{\mathscr{P}}_j$, i.e., $\hat{\mathscr{P}} = \sum_j \hat{\mathscr{P}}_j$, and let $\mathbb{B}_j$ denote the set of basis states permuted by $\hat{\mathscr{P}}_j$.[8] The sets $\{\mathbb{B}_j\}$ are disjoint, while the dimensions of the support of each cycle $\hat{\mathscr{P}}_j$ is the cardinality of the corresponding set denoted by $|\mathbb{B}_j|$. The spectrum of each cycle $\hat{\mathscr{P}}_j$ is nondegenerate, with eigenvectors $|w_j^{(\lambda_n)}\rangle$ and corresponding eigenvalues $\lambda_n$, where $\hat{\mathscr{P}}_j|w_j^{(\lambda_n)}\rangle = \lambda_n|w_j^{(\lambda_n)}\rangle$, with

$$|w_j^{(\lambda_n)}\rangle = \frac{1}{\sqrt{|\mathbb{B}_j|}} \sum_{|b\rangle \in \mathbb{B}_j} \lambda_n^{\zeta_b} |b\rangle, \tag{2.33}$$

and

$$\lambda_n = \exp\left(i 2\pi \frac{n}{|\mathbb{B}_j|}\right) \quad \text{for} \quad n \in \mathbb{Z}_{|\mathbb{B}_j|} \equiv \{0, 1, \ldots, |\mathbb{B}_j| - 1\}. \tag{2.34}$$

[8] A closed cycle is a permutation or sub-permutation, which cannot be decomposed further.

A label $\zeta_b \in \mathbb{Z}_{|\mathbb{B}_j|}$ can be assigned to every basis state $|b\rangle \in \mathbb{B}_j$, and thus the elements of $\mathbb{B}_j$ are considered to be arranged in ascending order, with respect to their labels.[9] Hence, for the permutation $\hat{\mathscr{P}}$ the eigenvalue $\lambda_n$ corresponds to $\eta_{\lambda_n}$ distinct eigenvectors $\{|w_j^{(\lambda_n)}\rangle\}$, with $j$ running only on the various cycles having $\lambda_n$ in common.

A class of Hamiltonians that satisfy Eq. (2.28) is of the form

$$\hat{\mathscr{H}}_{\mathbf{x}} = \frac{\hbar}{\tau} \sum_{\lambda_n} \sum_{a=1}^{\eta_{\lambda_n}} f_{\lambda_n}^{(a)} |y_{\lambda_n}^{(a)}\rangle\langle y_{\lambda_n}^{(a)}|, \tag{2.35}$$

where

$$f_{\lambda_n}^{(a)} = -\arg(\lambda_n) + 2\pi x_{\lambda_n}^{(a)} \tag{2.36}$$

and

$$\mathbf{x} \in \mathbb{Z}^d \equiv \{(x_{\lambda_0}^{(1)}, \ldots, x_{\lambda_0}^{(\eta_{\lambda_0})}; x_{\lambda_1}^{(1)}, \ldots, x_{\lambda_1}^{(\eta_{\lambda_1})}; \ldots) \mid x_{\lambda_n}^{(a)} \in \mathbb{Z}\}.$$

Note here that $f_{\lambda_n}^{(a)}$ are associated with the eigenenergies of the Hamiltonian. They are basically equal to the phase of the eigenvalues $\lambda_n$ of the chosen permutation, shifted by an arbitrary integer multiple of $2\pi$.

For a given eigenvalue $\lambda_n$, the $\eta_{\lambda_n}$ distinct vectors $\{|y_{\lambda_n}^{(a)}\rangle\}$ form an orthonormal basis for the corresponding subspace and are of the form

$$|y_{\lambda_n}^{(a)}\rangle = \sum_i \beta_{a,i}^{(\lambda_n)} |w_i^{(\lambda_n)}\rangle, \tag{2.37}$$

with $\beta_{a,j}^{(\lambda_n)} \in \mathbb{C}$ and $\sum_j \beta_{a,j}^{(\lambda_n)*} \beta_{a',j}^{(\lambda_n)} = \delta_{a,a'}$. In other words, the rows of the matrix $\tilde{B}_{\lambda_n}$ with elements $\beta_{a,j}^{\lambda_n}$ are orthonormal, which implies unitarity of $\tilde{B}_{\lambda_n}$ and thus orthonormality of its columns as well, i.e.,

$$\sum_a \beta_{a,j}^{(\lambda_n)} \beta_{a,j'}^{(\lambda_n)*} = \delta_{j,j'}. \tag{2.38}$$

So, starting from a particular permutation $\hat{\mathscr{P}}$, we have derived a class of Hamiltonians that is parametrized by the integer vector $\mathbf{x}$, and permutes the basis

[9] Clearly, the labelling of the basis states in $\mathbb{B}_j$ is to some extent ambiguous. One may consider any ordering for which Eq. (2.33) yields a complete set of eigenstates of $\hat{\mathscr{P}}_j$. In this case, the ambiguity is unimportant, and does not affect our approach.

states at the prescribed time $\tau$, as determined by the chosen $\hat{\mathscr{P}}$. Indeed, for any chosen $\mathbf{x}$, the evolution operator for the corresponding member of the class reads

$$\hat{\mathscr{U}}_{\mathbf{x}}(t) \equiv e^{-i\hat{\mathscr{H}}_{\mathbf{x}}t/\hbar} = \sum_{\lambda_n}\sum_{a=1}^{\eta_{\lambda_n}} \exp\left(-if_{\lambda_n}^{(a)}t/\tau\right)|y_{\lambda_n}^{(a)}\rangle\langle y_{\lambda_n}^{(a)}|, \tag{2.39}$$

with $f_{\lambda_n}^{(a)}$ and $|y_{\lambda_n}^{(a)}\rangle$ given by Eqs. (2.36) and (2.37), respectively. Hence, at $t = \tau$, this evolution operator reduces to (2.28), for the particular permutation under consideration.

The key point here is that the Hamiltonians (2.35) are diagonal in the eigenbasis of the permutation. This is possible only for Hamiltonians $\hat{\mathscr{H}}$ that commute with the chosen permutation i.e., for

$$[\hat{\mathscr{P}}, \hat{\mathscr{H}}] = 0. \tag{2.40}$$

This condition restricts our quest to QST Hamiltonians that have a particular form in the computation basis, so that they are compatible with the permutation. Finally, after expressing the eigenvectors of the permutation in terms of the computational basis states by means of Eqs. (2.33) and (2.37), one can estimate all of the open parameters entering the Hamiltonian, by solving a system of (non)linear equations.

In the following we apply the above design technique in the framework of networks of various topologies. Before this, however, it is worth emphasizing here that condition (2.28) is rather restrictive since, in general, one may derive QST Hamiltonians which do not lead to permutations at time $\tau$, but rather to other unitary operations. Actually, there are tasks that cannot be described in the framework of permutations. For instance, this is the case of mapping different basis states onto the same basis state. Such a mapping requires inevitably, the extension of the present formalism to unitary transformations (e.g., see [13]).

Despite any weaknesses, it has been demonstrated that the present theoretical framework is suitable for engineering of passive networks [8, 12, 13], and actually many known perfect QST Hamiltonians satisfy condition (2.28). The present formalism has the advantage of being applicable to networks of various topologies, and it is perfectly suited to addressing the problem of QST in the context of various physical realizations, allowing for the inclusion of non-trivial interactions. Infinitely many QST Hamiltonians can be specified within the present theoretical framework, and this enables us to find the most suitable Hamiltonian for a given physical realization and topology. Finally, we have seen that there is no requirement for the initial overall state of the network (minus the source nodes) to have a specific form. It is crucial, however, for the source nodes to be initially decorrelated from the rest of the network, which can be prepared in any state.

## 2.4 Quantum State Transfer in the Single Excitation Subspace

The vast majority of papers on the problem on QST has been focused on the single-excitation subspace. For instance, in the first scenario discussed in Sect. 2.1.2, the excitation may correspond to the addition of a single excess particle in a network that is initially in the vacuum state, whereas for the second scenario the excitation refers to the perturbation of a single physical qubit in the initial ground state. We will demonstrate here how one can design perfect QST Hamiltonians that operate in the single-excitation subspace, by utilizing the above design technique. As showed in Sect. 2.3, the design works for any states but, for the sake of simplicity, in the following we assume that all the nodes, but the source, are initially in vacuum.

Based on the approach discussed in Sect. 2.2, we focus on the engineering of quantum networks that suppress (and if possible minimize) the dispersion (diffraction) effects, neglecting the effects of imperfections pertaining to disorder, decoherence, and dissipation mechanisms. The form of the QST Hamiltonians that we are interested in is

$$\hat{\mathscr{H}} = \sum_{i=1}^{N} \sum_{\xi} \varepsilon_{i,\xi} \hat{n}_{i,\xi} + \sum_{\substack{i,k=1 \\ i<k}}^{N} \sum_{\xi} g_{i,k} (\hat{a}^{\dagger}_{i,\xi} \hat{a}_{k,\xi} + \hat{a}^{\dagger}_{k,\xi} \hat{a}_{i,\xi}), \tag{2.41}$$

where the energies and the real couplings are open parameters to be determined, and $N$ is the number of nodes in the network. Such Hamiltonians preserve the input state $|\psi_{\text{in}}\rangle$ and affect only its position on the network, ensuring thus the transfer irrespective of the details of the input state. If one neglects the variable $\xi$ dropping the related summations in (2.41), then Hamiltonian (2.41) is of the form (2.8), with the corresponding spin-chain Hamiltonian given by Eq. (2.6) for $J'_{i,k} = 0$. In this case, we essentially focus on the transfer of the excitation, leaving aside the accompanied information encoded in the $\xi$ degree of freedom.

Hamiltonian (2.41) preserves the total number of excitations in the network, which means that our theoretical analysis can be restricted to the single excitation sector only, spanned by the states $\{|j : \xi\rangle\}$, where for the sake of simplicity $|j : \xi\rangle \equiv a^{\dagger}_{j,\xi}|\mathbf{0}\rangle$ and $|\mathbf{0}\rangle$ denotes the vacuum state. In this representation, the single excitation is in the state $|\xi\rangle \in \{|u\rangle, |v\rangle\}$, and occupies the $j$th site. The initial state of the network is $|\Psi(0)\rangle = |\psi_{\text{in}}\rangle$, where

$$|\psi_{\text{in}}\rangle = \alpha|1 : u\rangle + \beta|1 : v\rangle = |1\rangle \otimes (\alpha|u\rangle + \beta|v\rangle), \tag{2.42}$$

and our task is to define $\{\varepsilon_{i,\xi}, g_{i,k}\}$ in (2.41), so that at time $\tau$ we have $|\Psi(\tau)\rangle = \alpha|N : u\rangle + \beta|N : v\rangle = |N\rangle \otimes (\alpha|u\rangle + \beta|v\rangle)$ i.e., the excitation is transferred to the $N$th site. One can follow the approach outlined in the previous section, to engineer Hamiltonians in the $2N$-dimensional space spanned by the states $|j : \xi\rangle$. However, noting that the Hamiltonian preserves $\xi$, and affects only the position of

the excitation, we can restrict the engineering to smaller subspaces of the single-excitation sector.

The single excitation sector can be also decomposed into two subspaces $\mathbb{V}_\xi = \text{Span}\{|j\rangle : \xi\rangle\}$, with $\xi \in \{u, v\}$. The full single-excitation subspace will just be $\mathbb{V}_u \oplus \mathbb{V}_v$. Let $\hat{\Pi}_\xi$ be the projector onto the subspace $\mathbb{V}_\xi$. The Hamiltonian (2.41) contains no terms that would couple basis states with different internal degrees of freedom $\xi$, and thus the subspaces $\mathbb{V}_\xi$ are invariant i.e., $[\hat{\Pi}_\xi, \hat{\mathscr{H}}] = 0$. One may thus express the Hamiltonian formally as $\hat{\mathscr{H}} = \sum_\xi \hat{\Pi}_\xi \hat{\mathscr{H}} \hat{\Pi}_\xi$, where the dynamics in the subspace $\mathbb{V}_\xi$ are governed by the Hamiltonian $\hat{\Pi}_\xi \hat{\mathscr{H}} \hat{\Pi}_\xi$. All the invariant subspaces $\mathbb{V}_\xi$ are equivalent, and the engineering of Hamiltonians can be restricted to anyone of them.

Alternatively, the problem can be solved in the $N$-dimensional subspace spanned by the positions $|j\rangle$ only. Using Eqs. (2.2) and (2.3), the Hamiltonian (2.41) can be written as

$$\hat{\mathscr{H}} = \hat{h}_{\text{pos}} \otimes \hat{\mathbf{1}}_\xi + \hat{\mathbf{1}}_{\text{pos}} \otimes \hat{h}_\xi, \tag{2.43a}$$

where

$$\hat{h}_{\text{pos}} = \sum_{i=1}^{N} \varepsilon_i |i\rangle\langle i| + \sum_{\substack{i,k=1 \\ i<k}}^{N} g_{i,k} (|i\rangle\langle k| + |k\rangle\langle i|), \tag{2.43b}$$

$$\hat{h}_\xi = \sum_\xi \varepsilon_\xi |\xi\rangle\langle\xi|, \tag{2.43c}$$

and the identity operators $\hat{\mathbf{1}}_{\text{pos}}$ and $\hat{\mathbf{1}}_\xi$ act on the subspaces spanned by $\{|j\rangle\}$ and $\{|\xi\rangle\}$. The engineering can be now restricted to $\hat{h}_{\text{pos}}$ only and begins with the choice of a permutation of the form

$$\hat{\mathscr{P}} = |N\rangle\langle 1| + \hat{\mathscr{Q}} \tag{2.44}$$

where $\hat{\mathscr{Q}}$ acts on the nodes $2, 3, \ldots, N$. There are $(N-1)!$ different permutations of this form, and our choice is dictated by the topology of the network under consideration, and thus by the form of the Hamiltonians that we are interested in. For instance, it turns out that a mirror-symmetric chain is compatible only with an antidiagonal permutation of the form

$$\hat{\mathscr{P}} = \sum_{j=1}^{N} |N+1-j\rangle\langle j|. \tag{2.45}$$

Indeed, from Eq. (2.40), we find that the Hamiltonians that are compatible with the permutation (2.45) satisfy

$$g_{i,k} = g_{N+1-i,N+1-k}, \quad \text{and} \quad \varepsilon_i = \varepsilon_{N+1-i}, \tag{2.46}$$

which refer to a centro-symmetric (or else mirror-symmetric) network. In the following we will outline the design of Hamiltonians in two special cases, by means of two examples.

### 2.4.1 Networks with Nearest-Neighbour Interactions

Assume that we are interested in QST Hamiltonians with nearest-neighbour (NN) interactions that operate on a 4-node centrosymmetric chain, and ensure the perfect transfer of a qubit state between its two ends [12]. In view of the previous discussion, we begin with the permutation

$$\mathscr{P} = \begin{pmatrix} 0\,0\,0\,1 \\ 0\,0\,1\,0 \\ 0\,1\,0\,0 \\ 1\,0\,0\,0 \end{pmatrix}. \tag{2.47}$$

This permutation involves two cycles of dimension two namely, $\mathscr{P}_1 = (1,4)$ and $\mathscr{P}_2 = (2,3)$.[10] Hence, we have two eigenvalues $\lambda_0 = e^{\mathrm{i}0} = +1$ and $\lambda_1 = e^{\mathrm{i}\pi} = -1$. Both eigenvalues $\pm 1$ are doubly degenerate (i.e., $\eta_\pm = 2$) and the corresponding eigenvectors are given by $|w_\pm^{(1)}\rangle = (|1\rangle \pm |4\rangle)/\sqrt{2}$ and $|w_\pm^{(2)}\rangle = (|2\rangle \pm |3\rangle)/\sqrt{2}$, for cycles $\mathscr{P}_1$ and $\mathscr{P}_2$, respectively. Accordingly, the corresponding subspaces are

$$\Lambda_\pm = \left\{ |w_\pm^{(1)}\rangle, |w_\pm^{(2)}\rangle \right\}.$$

Having defined the permutation matrix, the construction of perfect QST Hamiltonians now proceeds in two steps.

#### 2.4.1.1 Parameterisation

For each one of the subspaces we can choose an orthonormal basis in many different ways. For example, we may choose for the two subspaces[11]

[10] Thereby the notation $(2,3)$ means that starting from the original site ordering of the sites $\{1,2,3,4\}$, the second site is replaced by the third and the third site by the second.

[11] We have simplified the notation relative to the previous section, but the overall approach remains the same.

$$\Lambda_+ : \begin{cases} |y_+^{(1)}\rangle = a_+^{(1)}|w_+^{(1)}\rangle + b_+^{(1)}|w_+^{(2)}\rangle \\ \\ |y_+^{(2)}\rangle = a_+^{(2)}|w_+^{(1)}\rangle + b_+^{(2)}|w_+^{(2)}\rangle, \end{cases} \tag{2.48}$$

and

$$\Lambda_- : \begin{cases} |y_-^{(1)}\rangle = a_-^{(1)}|w_-^{(1)}\rangle + b_-^{(1)}|w_-^{(2)}\rangle \\ \\ |y_-^{(2)}\rangle = a_-^{(2)}|w_-^{(1)}\rangle + b_-^{(2)}|w_-^{(2)}\rangle. \end{cases} \tag{2.49}$$

Thereby, $a_\pm^{(i)}, b_\pm^{(i)} \in \mathbb{C}$ with

$$|a_\pm^{(i)}|^2 + |b_\pm^{(i)}|^2 = 1, \quad i = 1, 2 \tag{2.50}$$

$$a_\pm^{(1)} a_\pm^{(2)*} + b_\pm^{(1)} b_\pm^{(2)*} = 0, \tag{2.51}$$

so that $|y_\pm^{(i)}\rangle$ are orthonormal.

According to the theory of the previous section, the corresponding eigenenergies can be chosen as

$$\Lambda_+ : \begin{cases} f_+^{(1)} = 0 + 2\pi x_+^{(1)} \\ \\ f_+^{(2)} = 0 + 2\pi x_+^{(2)}, \end{cases} \tag{2.52}$$

and

$$\Lambda_- : \begin{cases} f_-^{(1)} = \pi + 2\pi x_-^{(1)} \\ \\ f_-^{(2)} = \pi + 2\pi x_-^{(2)}, \end{cases} \tag{2.53}$$

for $x_j^{(k)} \in \mathbb{Z}$. Thereby, note that the eigenvalues of subspace $\Lambda_+$ ($\Lambda_-$) are even (odd) integer multiples of $\pi$.

Thus, the whole class of perfect QST Hamiltonians (2.35) reads

$$\hat{h}(\mathbf{x}) = \frac{\hbar}{\tau}\Big[ f_+^{(1)}|y_+^{(1)}\rangle\langle y_+^{(1)}| + f_+^{(2)}|y_+^{(2)}\rangle\langle y_+^{(2)}| \ + f_-^{(1)}|y_-^{(1)}\rangle\langle y_-^{(1)}| + f_-^{(2)}|y_-^{(2)}\rangle\langle y_-^{(2)}| \Big], \tag{2.54}$$

with open parameters the spectrum $\{f_+^{(1)}, f_+^{(2)}, f_-^{(1)}, f_-^{(2)}\}$ (or equivalently the integers $x_\pm^{(1,2)}$) and two independent complex numbers (due to normalisation). As we discuss in the following subsection, all these parameters can be specified by imposing additional constraints on the form of the resulting Hamiltonian.

#### 2.4.1.2 Parameter Estimation

Assume now that we are interested in the whole class of NN-type Hamiltonians leading to the antidiagonal permutation matrix (2.47) and are of the form

$$\hat{h}_{\rm pos} = \begin{pmatrix} \varepsilon_1 & g_{1,2} & 0 & 0 \\ g_{1,2} & \varepsilon_2 & g_{2,3} & 0 \\ 0 & g_{2,3} & \varepsilon_2 & g_{1,2} \\ 0 & 0 & g_{1,2} & \varepsilon_1 \end{pmatrix}. \tag{2.55}$$

Since the class (2.54) has been derived within a rather general framework (limited only by the particular form of the permutation), our task reduces to the application of specific constraints on the parameters entering $\hat{h}(\mathbf{x})$, so that it acquires the form of Eq. (2.55).[12] In view of the symmetries in (2.55), we have the following constraints

$$\begin{gathered} \langle 1|\hat{h}_{\mathbf{x}}|1\rangle = \varepsilon_1, \quad \langle 2|\hat{h}_{\mathbf{x}}|2\rangle = \varepsilon_2, \\ \langle 1|\hat{h}_{\mathbf{x}}|2\rangle = g_{1,2}, \quad \langle 2|\hat{h}_{\mathbf{x}}|3\rangle = g_{2,3}, \\ \langle 1|\hat{h}_{\mathbf{x}}|3\rangle = 0, \quad \langle 1|\hat{h}_{\mathbf{x}}|4\rangle = 0, \quad \langle 2|\hat{h}_{\mathbf{x}}|4\rangle = 0 \end{gathered}$$

which together with the 6 orthonormality conditions form a set of 13 equations that have to be solved simultaneously with respect to the 12 variables $\{\varepsilon_j, g_{i,j}, a_{\pm}^{(1,2)}, b_{\pm}^{(1,2)}\}$, for a particular fixed choice of $f_{\pm}^{(i)}$ or equivalently of the integer string $\mathbf{x}$. In general, changing $\mathbf{x}$ one obtains new solutions for the 12 variables.

A solution that has been discussed thoroughly in the literature and can be obtained within the current theoretical approach, pertains to equidistant eigenenergies, and is of the form

$$\varepsilon_j = -\tilde{\varepsilon}(N-1), \quad \text{and} \quad g_{j,j+1} = \tilde{\varepsilon}\sqrt{j(N-j)} \tag{2.56}$$

with $j = 1, 2, \ldots, N-1$ and the constant $\tilde{\varepsilon} = \hbar\pi/(2\tau)$, determined by the time at which the transfer has to take place. This solution involves resonant nodes and engineered couplings between nearest neighbours. It ensures the perfect transfer of the excitation from the $j$th to the $(N+1-j)$th node at time $\tau$ (see Fig. 2.5). The total Hamiltonian is given by Eqs. (2.43) and (2.55), and the evolution operator reads

$$\hat{\mathscr{U}}(\tau) = \exp[-i(\hat{h}_{\rm pos} \otimes \hat{\mathbf{1}}_{\xi} + \hat{\mathbf{1}}_{\rm pos} \otimes \hat{h}_{\xi})\tau/\hbar] = \hat{\mathscr{P}} \otimes e^{-i\hat{h}_{\xi}\tau/\hbar}, \tag{2.57}$$

[12] We focus on the case of Hamiltonians with non-degenerate spectrum. The case of degenerate spectrum can be treated similarly and leads to NN-type Hamiltonians with vanishing couplings i.e., to a broken network and thus QST from the first to the last site is impossible.

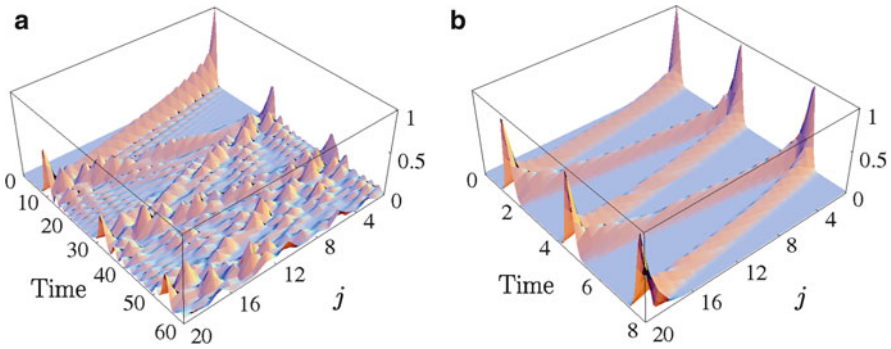


**Fig. 2.5** Evolution of a single excitation in a chain of 20 resonant sites ($\varepsilon_j = 0$), in the absence of losses and disorder. The probability for the excitation to occupy the $j$th site is plotted as a function of time for (**a**) uniform couplings ($g_{j,j+1} = \tilde{\varepsilon}$) and (**b**) judiciously engineered couplings ($g_{j,j+1} = \tilde{\varepsilon}\sqrt{j(N-j)}$). Initially the excitation occupies the first site. Time is in units of $\tilde{\varepsilon}^{-1}$ (Adapted from [15])

where we have used the fact that, by construction, $e^{-i\hat{h}_{\text{pos}}\tau/\hbar} = \mathscr{P}$. Thus, for the input state (2.42) the output state at time $\tau$, will be

$$|\Psi(\tau)\rangle = \alpha|N:u\rangle + e^{i\Delta_{u,v}\tau}\beta|N:v\rangle, \tag{2.58}$$

where $\Delta_{u,v} = \varepsilon_{j,u} - \varepsilon_{j,v}$, for all $j = 1,\ldots,N$. As mentioned before, in the absence of disorder and imperfections, this relative phase is fixed and known, and therefore can be amended. It is worth noting here that perfect QST from the $j$th to the $(N+1-j)$th site at time $\tau$ also occurs for $\varepsilon_j = \tilde{\varepsilon}$ in Eq. (2.56). In this case, one has

$$\hat{\mathscr{U}}(\tau) = e^{-i(\tilde{\varepsilon}\tau/\hbar)}(-i)^{N-1}\hat{\mathscr{P}},$$

i.e., condition (2.28) is satisfied up to an unimportant global phase. As depicted in Fig. 2.5b a chain with the couplings of Eq. (2.56) behaves as a two-level system i.e., the excitation oscillates back and forth between its two ends. Dispersion phenomena have been minimized as opposed to the case of a uniform chain (see Fig. 2.5a).

Surprisingly enough, the solution (2.56) has been known since the 1970s, albeit in a different context, namely the coherent dynamics of $N$-level atoms [16–18]. As shown in [17], the Hamiltonian (2.43b) with the parameters given by (2.56), is isomorphic to a Hamiltonian describing the rotation of a spin-system $J = (N-1)/2$, around a fixed axis. In 2004, the scheme (2.56) was proposed almost simultaneously and independently, as a solution to the QST problem between the two ends of a mirror-symmetric chain, in four different works [15, 19–21]. Christandl et al., addressed the problem in the framework of spin chains and their formalism was based on graphs, whereas Plenio et al. considered entanglement dynamics in a system of coupled harmonic oscillators. The work of Nikolopoulos

et al., and Gordon on the other hand pertained to specific realizations of chains based on coupled quantum dots and coupled waveguides, respectively. Furthermore, Nikolopoulos et al. applied the scheme of Eqs. (2.41) and (2.56) to the transfer of states associated with two physical qubits and the controlled generation of entanglement between them [22], while they also studied its robustness against static disorder and dissipation [15]. It has been also demonstrated that, based on the coupling configuration (2.56), one can design networks where unitary rotations are performed while a qubit state is transferred, and build beam splitters and intereferometric setups [23, 24]. Such networks, however, may require complex couplings between different sites and their realization in the context of many physical platforms is a rather difficult (if not impossible) task. Finally, the solution (2.56) has been also discussed in connection with state amplification [25] as well as with quantum walks [26, 27].

Besides solution (2.56), other perfect QST Hamiltonians have been also discussed in the literature, mainly in the context of mirror-symmetric chains, and most of them can be derived within the present theoretical framework. The commensurate spectrum seems to play a pivotal role in such perfect QST Hamiltonians, and this led other scientists to engineer perfect QST Hamiltonians starting from a specific spectrum and solving the inverse eigenvalue problem [10, 28–31]. The spectrum of Hamiltonian (2.43b) with the parameters given by (2.56) is integer, and other coupling schemes with commensurate spectra have been presented in the literature [19, 29, 32–34]. In many cases, however, the scheme of Eqs. (2.41) and (2.56), seems to be rather robust relative to other perfect QST schemes under various types of imperfections, whereas it seems to be the optimal coupling configuration with respect to quantum speed limit [31, 35]. For more information on the perfect QST scheme (2.56), the reader may refer to the review article by Kay [10].

Finally, although for the sake of simplicity throughout this section we have focused on networks with nearest-neighbour couplings, it is worth emphasizing that the present approach to network engineering has been shown capable of providing solutions even when interactions beyond nearest neighbours are present [12]. In the following we turn to review some of the main results on the design of networks with logical bus topology.

### *2.4.2 Networks of Logical Bus Topology*

The problem of QST in networks of logical bus topologies, has been addressed by Brougham et al. [8], in the framework of the theoretical approach presented above. In the classical theory of networks [6, 7] one often assumes that the hosts have an equivalence property that is, no matter which host the signal starts at, it will be transferred around the predetermined hosts. Similarly, throughout this chapter we focus on passive quantum networks with equivalent hosts, and thus the QST (flow of information) is restricted within the predetermined hosts, irrespective of the source of the state. The authors in [8] have explored the conditions under which multiple PP

QST links are compatible (in the sense to be defined below) and can thus be used as building blocks for the design of passive networks with more involved logical topologies pertaining to a prescribed set of hosts. The following rather general theorem was proved.

**Theorem 2.** *The unitary operators of a given set* $\{\hat{\mathscr{U}}_j \mid \hat{\mathscr{U}}_j \neq \hat{\mathscr{U}}_{j'} \text{ for } j \neq j' \text{ and } j, j' \in \mathbb{N}\}$ *are compatible iff any pair of these operators satisfy the following conditions*

*(i) There exist* $\tau_j, \tau_i \in (0,\infty) : \hat{\mathscr{U}}_i^{\tau_j} = \hat{\mathscr{U}}_j^{\tau_i}$ *for* $\tau_i \neq \tau_j$, *and for all* $t \in (0,\infty)$ $\hat{\mathscr{U}}_i^t \neq \hat{\mathscr{U}}_j^t$.

*(ii) The two unitary operators commute, i.e.* $[\hat{\mathscr{U}}_1, \hat{\mathscr{U}}_2] = 0$.

If the compatibility conditions of Theorem 2 are satisfied, there exists a single Hamiltonian to implement the unitary operators $\{\hat{\mathscr{U}}_j\}$ at well-defined distinct times $\{\tau_j \in (0,\infty) \mid \tau_j > \tau_{j'} \text{ for } j > j'\}$. Theorem 2 is very general and applicable to various kinds of PP perfect QST links, including the schemes of Refs. [15,19,21,29–31,33]. If, however, one of the unitaries is a permutation one can show that *perfect transfer of a single excitation at several different destination nodes at different times, is possible only if all of these hosts belong to the same cycle of* $\hat{\mathscr{P}}$ *[8]*. The choice of hosts thus places a restriction on our choice of $\hat{\mathscr{P}}$, and vice-versa. This in turn imposes physical constraints on the type of Hamiltonians that one can derive. From another point of view, we cannot achieve perfect QST between hosts that belong to different cycles of $\hat{\mathscr{P}}$. Hence, for the design of a *universal bus*, which transfers a single excitation successively to every node of the network within a well-defined time $\tau$, $\hat{\mathscr{P}}$ must be a one-cycle permutation [8].

The design of quantum networks of logical bus topology always leads to Hamiltonians with complex couplings. In fact one can prove the following theorem.

**Theorem 3.** *Quantum networks of logical bus topology cannot be described by real perfect QST Hamiltonians.*

*Proof.* Working along the lines of the corresponding proof for a single excitation [10], we will provide here a more general proof pertaining to arbitrary numbers of source and destination nodes, as well as to multiple excitations. More precisely, the input state pertains to a set of source nodes $S$, and there are two different sets of destination nodes $D_1$ and $D_2$.

Consider first the evolution operator corresponding to a *real* Hamiltonian

$$e^{-i\hat{\mathscr{H}}t/\hbar} = \hat{\mathscr{U}}(t). \tag{2.59}$$

Hermiticity of $\hat{\mathscr{H}}$ implies that

$$\langle \mathbf{k}|\hat{\mathscr{H}}(t)|\mathbf{l}\rangle = \langle \mathbf{l}|\hat{\mathscr{H}}(t)|\mathbf{k}\rangle^* = \langle \mathbf{l}|\hat{\mathscr{H}}(t)|\mathbf{k}\rangle,$$

for any two basis states $|\mathbf{k}\rangle$ and $|\mathbf{l}\rangle$, where for the last equality we have used the fact that $\hat{\mathscr{H}}$ is real. Thus one has that $\hat{\mathscr{H}}$ is symmetric, and by taking the Taylor

expansion in Eq. (2.59), one has that $\hat{\mathscr{U}}(t)$ is also symmetric. This means that $\hat{\mathscr{U}}(t) = [\hat{\mathscr{U}}(t)]^T$ and thus

$$[\hat{\mathscr{U}}(t)]^\dagger = [\hat{\mathscr{U}}(t)]^*. \tag{2.60}$$

Note here that this result applies to the evolution operator of any real Hamiltonian.

Now, assume that $\hat{\mathscr{H}}$ is a real perfect QST Hamiltonian, and let $\tau_2$ be the *shortest time* for which one can achieve perfect QST between the set of source nodes $S$ and a set of destination nodes $D_2$. This means that $\hat{\mathscr{U}}(\tau_2)$ transforms the basis states[13] as follows

$$\hat{\mathscr{U}}(\tau_2)|\mathbf{n}\rangle_S \otimes |\mathbf{m}\rangle_R = e^{i\theta_2}|\mathbf{n}\rangle_{D_2} \otimes |\mathbf{m}\rangle_{R_2}, \tag{2.61}$$

for some angle $\theta_2 \in [0, 2\pi]$, where $R = P \setminus S$ and $R_2 = P \setminus D_2$. Let us assume further that there exists $\tau_1 < \tau_2$, such that perfect QST is achieved between $S$ and another set of destination nodes $D_1$, with $D_1 \neq D_2$. That is, we have

$$\hat{\mathscr{U}}(\tau_1)|\mathbf{n}\rangle_S \otimes |\mathbf{m}\rangle_R = e^{i\theta_1}|\mathbf{n}\rangle_{D_1} \otimes |\mathbf{m}\rangle_{R_1}, \tag{2.62}$$

where $\theta_1 \in [0, 2\pi]$ and $R_1 = P \setminus D_1$.

Acting with $\hat{\mathscr{U}}(\tau_1)$ on Eq. (2.62), and using Eqs. (2.62) and (2.60), we obtain

$$[\hat{\mathscr{U}}(\tau_1)]^2|\mathbf{n}\rangle_S \otimes |\mathbf{m}\rangle_R = e^{i2\theta_1}|\mathbf{n}\rangle_S \otimes |\mathbf{m}\rangle_R.$$

Using Eqs. (2.61) and (2.60), we can express the $|\mathbf{n}\rangle_S \otimes |\mathbf{m}\rangle_R$ in terms of $|\mathbf{n}\rangle_{D_2} \otimes |\mathbf{m}\rangle_{R_2}$ obtaining

$$[\hat{\mathscr{U}}(\tau_1)]^2[\hat{\mathscr{U}}(\tau_2)]^*|\mathbf{n}\rangle_{D_2} \otimes |\mathbf{m}\rangle_{R_2} = e^{i(2\theta_1-\theta_2)}|\mathbf{n}\rangle_S \otimes |\mathbf{m}\rangle_R,$$

or equivalently, using Eq. (2.60),

$$\hat{\mathscr{U}}(2\tau_1 - \tau_2)|\mathbf{n}\rangle_S \otimes |\mathbf{m}\rangle_R = e^{i(2\theta_1-\theta_2)}|\mathbf{n}\rangle_{D_2} \otimes |\mathbf{m}\rangle_{R_2}.$$

This last equation shows that we can transfer between $S$ and $D_2$, at time $2\tau_1 - \tau_2 < \tau_2$, which contradicts our initial assumption that $\tau_2$ is the shortest possible time at which perfect QST between these two particular sets of nodes can be achieved for the real perfect QST Hamiltonian $\hat{\mathscr{H}}$. Hence, we conclude that it is not possible to construct quantum networks with a logical bus topology that operate under real perfect QST Hamiltonians. □

[13] Recall here that, in view of the previous discussion, it is sufficient to consider the transformation of the basis states for our purposes.

## 2.5 Perfect Transfer of States in Higher Excitation Subspaces

In the case of multiple excitations, one may consider various scenarios that cannot be described in the framework of Hamiltonians that have been derived in the single-excitation sector. As far as the problem of QST is concerned, when the state to be transferred pertains to a single quantum particle and no other particles are present, the particular character of the information carrier (boson or fermion) does not play any role, and is not reflected in the solutions one may derive. The situation, however, becomes substantially different when the state to be transferred is encoded on two or more particles. In this case, the bosonic or fermionic nature of the information carriers is expected to reveal itself, and together with interparticle interactions, will impose additional constraints on the physically acceptable solutions. Furthermore, one may also ask for more general solutions that cannot be described within the single-excitation formalism, such as the transfer of two or more excitations, from different nodes, onto the same node. As has been shown in [13], the approach presented in Sect. 2.3 is also applicable to the engineering of quantum networks for the transfer of states that involve multiple excitations.

For the sake of clarity, let us focus only on the case of two excitations; this will considerably simplify our notation. As shown before, the formalism of Sect. 2.3 is applicable to arbitrary states of the network. To keep the present formalism as simple as possible, we will consider a network that is initially in its vacuum state, and the information to be transferred is encoded in the state of two excess particles. The two-excitation Hilbert space $\mathbb{H}_2$ is spanned by the states $\{|i,\xi_1;j,\xi_2\rangle\}$, with $\xi_1,\xi_2 \in \{u,v\}$, where we have set $|i,\xi_1;j,\xi_2\rangle := |0,\ldots,0,1_{i,\xi_1},0,\ldots,0,1_{j,\xi_2},0,\ldots,0\rangle$. We can thus define three different subspaces of $\mathbb{H}_2$, with respect to the initial ordering, that is

$$\mathbb{H}_2^{(<)}, \quad \text{spanned by } \{|i,\xi_1;j,\xi_2\rangle \ : \ i<j\}, \tag{2.63a}$$

$$\mathbb{H}_2^{(=)}, \quad \text{spanned by } \{|i,\xi_1;j,\xi_2\rangle \ : \ i=j\}, \tag{2.63b}$$

$$\mathbb{H}_2^{(>)}, \quad \text{spanned by } \{|i,\xi_1;j,\xi_2\rangle \ : \ i>j\}. \tag{2.63c}$$

The state to be transferred is, in general, a superposition of all the basis states $\{|i,\xi_1;j,\xi_2\rangle\}$ but, as discussed in Sect. 2.3, for our purposes it is sufficient to consider one of the basis states i.e., $|\Psi(0)\rangle = |s_1,\xi_1;s_2,\xi_2\rangle$, which automatically specifies a particular ordering of the states $\{\xi_1,\xi_2\}$, with respect to their position in the network. When the subspaces are decoupled, the system is restricted within the subspace that is specified by $|s_1,\xi_1;s_2,\xi_2\rangle$. Hence, the problem of QST is simplified further, as it can be solved separately within each subspace. In particular, one can consider permutations of the block-diagonal form depicted in Fig. 2.6. The block $\hat{\mathscr{P}}^{(\cdot)}$ is a permutation that permutes all the basis states of the corresponding subspace $\mathbb{H}_2^{(\cdot)}$. For networks with couplings that are insensitive to $\xi$, the subspaces $\mathbb{H}_2^{(<)}$ and $\mathbb{H}_2^{(>)}$ are basically equivalent and thus $\hat{\mathscr{P}}^{(<)} = \hat{\mathscr{P}}^{(>)}$. Starting from

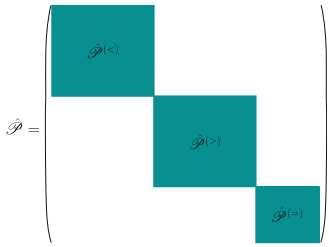

**Fig. 2.6** A permutation of block diagonal form (Adapted from [13])

the eigenvalues of $\hat{\mathscr{P}}^{(\cdot)}$, one can work backwards along the lines of the Sect. 2.3, to design Hamiltonians that generate this permutation at time $\tau$, i.e., they satisfy Eq. (2.28) with $\hat{\mathscr{P}} = \hat{\mathscr{P}}^{(\cdot)}$. In the most general scenarios, however, the subspaces are not decoupled and cannot be treated separately. In these cases, one may also have transfer between states that belong to different subspaces, and the QST problem is more involved.

Using the above methodology, one can design QST Hamiltonians in the case of two or more interacting as well as non-interacting excitations, which can be either bosons or fermions. In the following section we will demonstrate, using some simple examples, how various constraints regarding the nature of the excitations can be incorporated in the formalism. We restrict ourselves to networks with couplings that are insensitive to different values of $\xi \in \{u, v\}$, and their evolution is governed by time-independent Hamiltonians, that preserve the total number of excitations, as well as the initial choice of $(\xi_1, \xi_2)$ on the time scales of interest, and are of the form (2.1) with $g_{i,k}^{(\xi)} = g_{i,k}$.

In the case of noninteracting excitations, the basis state $|i, \xi_1; j, \xi_2\rangle$ is characterized by the energy,

$$E_{i,\xi_1}^{j,\xi_2} = \varepsilon_{i,\xi_1} + \varepsilon_{j,\xi_2}.$$

In the case of interacting particles, however, one has

$$\tilde{E}_{i,\xi_1}^{j,\xi_2} = E_{i,\xi_1}^{j,\xi_2} + U_{i,\xi_1}^{j,\xi_2}.$$

The additional energy $U_{i,\xi_1}^{j,\xi_2}$, accounts for repulsive ($U_{i,\xi_1}^{j,\xi_2} > 0$) or attractive ($U_{i,\xi_1}^{j,\xi_2} < 0$) interactions, whose magnitude may depend on the position of the two excitations in the network, as well as on other degrees of freedom. When the excitations are associated with fermions and occupy the same site, the Pauli principle requires that $\xi_1 \neq \xi_2$, i.e., the excitations must pertain to different states. For instance, the ground state of a two-electron quantum dot in zero magnetic field is the spin singlet state, where the two electrons occupy the lowest orbital and they have antiparallel spins [36]. By contrast, in the case of bosons, there are no such restrictions, and both excitations can be in the same state, while occupying the same site. This is, for instance, the case of the so-called dimers, trimers, etc., in optical lattices [37–39]. Besides onsite interactions which pertain to particles occupying

the same site, one may also have inter-site interactions when the two interacting excitations occupy different sites, but their spatial separation is sufficiently small for interactions to occur. Certain implementations offer unprecedented controllability on both of these types of interactions (quantum dots, optical lattices, etc.), allowing thus for various scenarios.

### 2.5.1 Decoupled Subspaces

In various realistic scenarios, the onsite interaction $U_{j,\xi_1}^{j,\xi_2}$ is much larger (in absolute value) than any other energy scale in the system.[14] In such cases, the energy gap between the basis states $\{|i,\xi_1;j,\xi_2\rangle\}$ and $\{|j,\xi_1;j,\xi_2\rangle\}$ is of the order of $U_{j,\xi_1}^{j,\xi_2}$. Assuming further $\xi$-independent nearest-neighbour (NN) couplings in Eq. (2.1) (i.e., $g_{i,k}^{(\xi)} = g_{i,k} \neq 0$ for $i = k \pm 1$), transitions between states $\{|i,\xi_1;j,\xi_2\rangle\}$ with $i < j$ and $i > j$ are only possible via doubly occupied states. In the limit of $U_{j,\xi_1}^{j,\xi_2} \gg g_{i,k}$ double occupancy is practically forbidden throughout the evolution of the system. Reordering of the excitations is thus a second-order process, which may occur when neighbouring sites are occupied. E.g., consider the state $|j-1,\xi_1;j,\xi_2\rangle$ which is coupled to $\{|j,\xi_1;j-1,\xi_2\rangle, |j+1,\xi_1;j,\xi_2\rangle, |j-1,\xi_1;,j-2,\xi_2\rangle\}$ via the doubly occupied states $|j,\xi_1;j,\xi_2\rangle$ and $|j-1,\xi_2;j-1,\xi_2\rangle$. Such a transition can be neglected if the time scale over which perfect QST is achieved, is sufficiently short relative to the time scales over which these second-order processes take place. Then, the subspaces of Eq. (2.63) can be considered, to a good approximation, decoupled throughout the evolution of the system.

Suppose that the system is initially prepared in the state $|\Psi(0)\rangle = |s_1,\xi_1;s_2,\xi_2\rangle$, with $s_1 < s_2$.[15] Given that the system is restricted within the subspace $\mathbb{H}_2^{(<)}$ throughout its evolution, the initial ordering of $\{\xi_1,\xi_2\}$ will be preserved, whereas the states of the other subspaces, are practically forbidden. We will thus focus on the subspace $\mathbb{H}_2^{(<)}$, and onsite interparticle interactions can be neglected in Hamiltonian (2.1). The corresponding sub-permutation, $\hat{\mathscr{P}}^{(<)}$, will be determined by the definition of the destination nodes $(d_1,d_2)$ as well as any additional physical restrictions imposed on the system. For instance, if one is interested in QST Hamiltonians with mirror symmetry, the permutation $\hat{\mathscr{P}}^{(<)}$ has to have the antidiagonal form

$$\hat{\mathscr{P}}^{(<)} = \sum_{i=1}^{N} \sum_{j>i} |i,\xi_1;j,\xi_2\rangle\langle(N+1-j),\xi_1;(N+1-i),\xi_2|, \tag{2.64}$$

[14] In the same fashion (i.e., by setting $U_{j,\xi}^{j,\xi} \to \infty$) one can formally describe the Pauli principle, which does not allow two electrons with the same state, to occupy the same site.

[15] As long as we are interested in networks that are insensitive to different degrees of freedom, the subspaces $\mathbb{H}_2^{(<)}$ and $\mathbb{H}_2^{(>)}$ are equivalent, and the case of $s_1 > s_2$ is covered by the present discussion on the case $s_1 < s_2$.

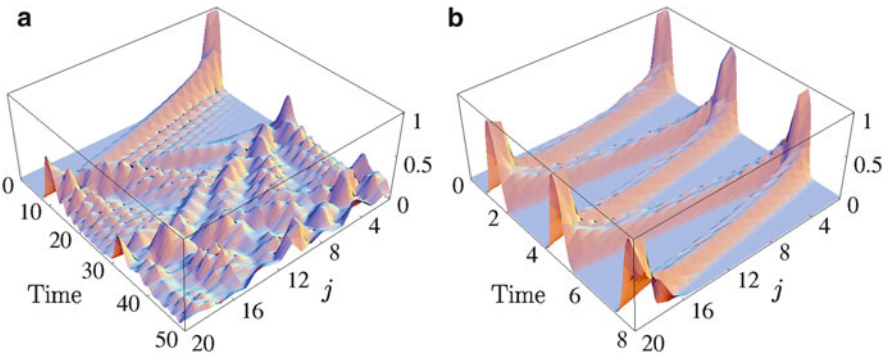


**Fig. 2.7** As in Fig. 2.5, for two excitations initially occupying the first and the second site (Adapted from [15])

where $i, j \in \{1, 2, \ldots, N\}$. Working along the lines of the Sect. 2.3, one may determine the parameters entering Hamiltonian (2.1), so that Eq. (2.28) is satisfied within the subspace $\mathbb{H}_2^{(<)}$.

In order for the Hamiltonian (2.1) to be compatible with the permutation (2.64), one has to ask for

$$[\hat{\mathscr{P}}^{(<)}, \hat{\mathscr{H}}] = 0, \tag{2.65}$$

within the subspace of interest spanned by the states $\{|i, \xi_1; j, \xi_2\rangle \mid i < j\}$. This requirement for real $\xi$-independent couplings imposes the first constraints on the choices of $\varepsilon_{i,\xi}$, $g_{i,k}$, and $U_{i,\xi}^{j,\xi'}$ namely,

$$g_{i,k} = g_{N+1-k,N+1-i}, \tag{2.66a}$$

$$\tilde{E}_{i,\xi_1}^{k,\xi_2} = \tilde{E}_{N+1-k,\xi_1}^{N+1-i,\xi_2}. \tag{2.66b}$$

Additional constraints, depend on the details of the network one is interested in.

In the absence of any intersite repulsive (or attractive) interactions (i.e., $U_{i,\xi}^{k,\xi'} = 0$ for $i \neq k$), within the subspace $\mathbb{H}_2^{(<)}$ the Hamiltonian (2.1) basically reduces to Eq. (2.43), and allows for the separation of different degrees of freedom. Given that $\xi$ is preserved, in analogy to Sect. 2.4 one can restrict the engineering on the part of the Hamiltonian that acts on the position of the excitations. As depicted in Fig. 2.7, one of the solutions is given by Eq. (2.56). This was to be expected, since within $\mathbb{H}_2^{(<)}$ we essentially work with non-interacting particles that remain distinct as they never occupy the same site. This result has been also predicted in [15], and its robustness against various types of imperfections has been analysed [15, 40]. We should emphasize, however, that this is only one of the infinitely many solutions that one may obtain within the present theoretical framework, for the particular choice of $\hat{\mathscr{P}}^{(<)}$.

Relaxing the constraint $U_{i,\xi}^{k,\xi'} = 0$ for $i \neq k$, allows one to take account of repulsive(attractive) interactions between excitations. In this case, the derivation of analytic expressions is far from trivial, but one can always resort to numerical solutions. The allowed solutions are basically determined by the magnitude of the various $U_{i,\xi}^{k,\xi'}$ relative to the various couplings $g_{i,k}$ (e.g., see [13] for related examples).

### 2.5.2 Transitions Between Subspaces

Our examples up to now were for perfect QST Hamiltonians with NN couplings only. There are, however, realistic situations where the effects of couplings beyond NN cannot be ignored. Formally speaking, the presence of non-vanishing couplings beyond NN in Eq. (2.1), automatically enables transitions between different subspaces, and thus the permutations one may consider cannot be expressed in the block diagonal form of Fig. 2.6. The engineering of Hamiltonians proceeds along the lines of Sect. 2.3, and related examples can be found in [13].

From the perspective of quantum control a useful and important task would be to perfectly transfer two excitations that are in different sites onto the same site and vice-versa (i.e., $|i, \xi_1; j, \xi_2\rangle \leftrightarrow |j, \xi_1; j, \xi_2\rangle$), coupling thus the subspaces $\mathbb{H}_2^{(<)}$ and $\mathbb{H}_2^{(>)}$ to $\mathbb{H}_2^{(=)}$. This would allow one to perform simple logical operations within the quantum network. Such a class of problems cannot be described with the framework of permutations, since by definition they provide only a one-to-one mapping between the basis states. As discussed in [13], however, one can still work along the lines of Sect. 2.3, but starting from a judiciously chosen unitary rather than a permutation.

In closing, we would like to point out that in this section the formalism of Sect. 2.3 was used for the derivation of effective Hamiltonians, which act on a subspace of near-resonant states. An effective Hamiltonian is basically an approximation of the original Hamiltonian, and the state transfer is thus not perfect, but rather occurs with high fidelity. How large the fidelity can be made depends on to what extent the system remains in the particular subspace throughout its evolution on the time scale of interest. Ideally, for a network whose components allow for arbitrary adjustment of all the related parameters (such as couplings, detunings, interactions, etc.), the actual evolution of the system can be brought arbitrarily close to the effective one, and thus the fidelity can be arbitrarily close to 1 (in the absence of disorder and dissipation). In this direction, quantum dots, optical and photonic lattices, have been shown to offer unprecedented controllability in many respects, although deviations from the ideal case are to be expected.

## 2.6 The Quantum Directional Coupler (QDC)

A dual-channel directional coupler (DC) is a passive device with two input and two output ports. The ports are the ends of two waveguides, the so-called source and drain channels, which are brought in close proximity over a certain region. The division of a signal between the outputs of the two channels is achieved by varying a control parameter. DCs have many applications in (opto)electronics [41–44]. For instance, directional couplers (DCs) may perform a number of useful functions in thin-film devices such as power division, switching, frequency selection, and (de)multiplexing.

In 2008, a dual-channel DC for quantum computing and communication purposes was proposed [45]. In analogy to conventional DCs, a dual-channel quantum DC (QDC) can be defined as a device which allows the selective transfer of quantum signals between two adjacent quantum channels, and it is thus expected to be the key element for various useful quantum information processing tasks, such as quantum switching, (de)multiplexing, etc.

The main problem addressed in [45] was the following. Given two perfect quantum channels, is it possible to define inter-channel interactions, for which the entire system operates as a dual-channel QDC? Focusing on single-qubit states prepared initially in the first site of one of the channels, inter-channel interactions should allow for the transfer of the state to the last site of either of the two channels, in a controlled and deterministic manner. In the spirit of passive quantum networks, this study was focused on configurations with minimal external control, i.e., without elaborate sequences of time-dependent pulses and measurements, and here we will review the main results of this work.

### *2.6.1 Formalism*

The dual-channel QDC under consideration involves two nearly identical channels, the source (s) and the drain (d). Each channel consists of $N > 2$ nearly identical sites denoted by $\mathbf{r} = (i, j)$, with $i \in \{\mathrm{s}, \mathrm{d}\}$ and $1 \leq j \leq N$. Accordingly, the computational basis of the system can be chosen as $\{|\mathbf{r} : \xi\rangle\}$, with $|\mathbf{r} : \xi\rangle \equiv a^{\dagger}_{\mathbf{r},\xi}|\mathbf{0}\rangle$ denoting an excitation on the $\mathbf{r}$th site in state $|\xi\rangle$. The first two sites of the chains $\{(\mathrm{s}, 1); (\mathrm{d}, 1)\}$ play the role of the two input ports, whereas the output ports are represented by the last sites $\{(\mathrm{s}, N); (\mathrm{d}, N)\}$.

In the following we assume that the source and the drain chains have been independently engineered to allow for the perfect transfer of a qubit state between their two ends. Their dynamics are described by a perfect QST Hamiltonian of the form (2.43) with the parameters given in Eq. (2.56). Recall here Observation 1, together with the fact that the interaction part of the Hamiltonian that governs each channel cannot distinguish between different states $|\xi\rangle$. Without modifying all of these properties, our task is to define interactions between the channels so that an

excitation initially occupying one of the input ports, can be transferred to either of the two output ports in a controlled and deterministic way.[16] More precisely, consider that the entire configuration is initially in the vacuum state, and the qubit state is prepared on the first site of the source channel. The initial state of the entire network is

$$|\Psi_{\mathrm{C}}(0)\rangle = |\mathrm{s}, 1 : \psi(\xi)\rangle, \tag{2.67}$$

where $|\psi(\xi)\rangle$ is the qubit state to be transferred.

In analogy to the previous sections, we will solve the problem in the ideal scenario first, i.e., in the absence of imperfections. Hence, it is sufficient to focus on the transfer of the excitation, ignoring degrees of freedom $\xi$. A dual-channel QDC, should be able to perform perfectly the following transformations

$$|\mathrm{s}, 1\rangle \rightarrow |\mathrm{s}, N\rangle, \tag{2.68a}$$

$$|\mathrm{s}, 1\rangle \rightarrow |\mathrm{d}, N\rangle, \tag{2.68b}$$

at well defined time instants, and irrespective of $|\xi\rangle$. The dynamics of the excitation in either of the two chains is governed by

$$\hat{\mathscr{H}}_{\mathrm{QST}}^{(i)} = \sum_{j=1}^{N} \varepsilon_j |i, j\rangle\langle i, j| + \sum_{j=1}^{N-1} g_{j,j+1}(|i, j\rangle\langle i, j+1| + |i, j+1\rangle\langle i, j|), \tag{2.69}$$

with $i \in \{\mathrm{s}, \mathrm{d}\}$, $\varepsilon_j = -\tilde{\varepsilon}(N-1)$ and $g_{j,j+1} = \tilde{\varepsilon}\sqrt{j(N-j)}$.

### 2.6.2 Mathematical Analogy

Let us employee the mathematical analogy between Hamiltonian (2.69) and the rotation of a spin system around a fixed axis [16–18]. We introduce two angular-momentum operators $\hat{\mathbf{J}}_1$ and $\hat{\mathbf{J}}_2$ acting on different subspaces, with

$$J_1 = (M-1)/2, \quad m_1 = i - (M+1)/2; \tag{2.70a}$$

$$J_2 = (N-1)/2, \quad m_2 = j - (N+1)/2, \tag{2.70b}$$

[16] By contrast to passive networks of logical bus topology where the state is transferred successively to different destination nodes, here the transfer pertains to one of the two available output nodes, and the choice is performed in a controlled manner.

for a positive integer $M \geq 2$. An orthonormal basis for the state space of the spin-$J_k$ system can be chosen as $\{|J_k, m_k\rangle\}$, where $|J_k, m_k\rangle$ are degenerate eigenvectors of the operator $\hat{J}_k^2$. The basis states of the composite system are $\{|J_1, m_1; J_2, m_2\rangle\}$, where $|J_1, m_1; J_2, m_2\rangle \equiv |J_1, m_1\rangle \otimes |J_2, m_2\rangle$.

The dynamics of the excitation in either of the two nearly identical channels (source or drain) are described by the spin-$J_2$ system. Using Eqs. (2.70b) one may define a one-to-one correspondence between the basis states $\{|j\rangle\}$ and $\{|J_2, m_2\rangle\}$ for fixed channel parameters $\{N, \tilde{\varepsilon}\}$ i.e., we have

$$|J_2, m_2\rangle \equiv |j\rangle. \tag{2.71a}$$

The spin-$J_1$ system describes the inter-channel dynamics, with the only convention being

$$|J_1, -J_1\rangle \equiv |\mathrm{s}\rangle, \quad |J_1, J_1\rangle \equiv |\mathrm{d}\rangle. \tag{2.71b}$$

Given the distinct roles of the two spin systems, in the angular-momentum representation the dynamics of a single excitation in a dual-channel QDC are described by a Hamiltonian of the form

$$\hat{\mathscr{H}} = \hat{\mathscr{H}}_1 + \hat{\mathscr{H}}_2, \tag{2.72}$$

where $\hat{\mathscr{H}}_k \equiv \hat{\mathscr{H}}_k^{(0)} + \hat{\mathscr{V}}_k$ refers to the spin-$J_k$ system only. The basis states $\{|J_k, m_k\rangle\}$ are degenerate eigenstates of the corresponding unperturbed Hamiltonian $\hat{\mathscr{H}}_k^{(0)} \equiv \varepsilon_k \hat{J}_k^2$, while $\hat{\mathscr{V}}_k$ is the coupling between various states $\{|J_k, m_k\rangle\}$.

The part of the initial condition (2.67) pertaining to the position of the quantum state reads in angular-momentum representation

$$|\Psi_{\mathrm{AM}}(0)\rangle = |J_1, -J_1; J_2, -J_2\rangle, \tag{2.73}$$

whereas for transformations (2.68) we have

$$|J_1, -J_1; J_2, -J_2\rangle \to |J_1, -J_1; J_2, J_2\rangle, \tag{2.74a}$$

$$|J_1, -J_1; J_2, -J_2\rangle \to |J_1, J_1; J_2, J_2\rangle. \tag{2.74b}$$

It is sufficient for our purposes therefore, to specify forms of the Hamiltonian (2.72) for which transformations (2.74) take place at well defined time instants, while one may switch between them in a controlled manner.

Transformation (2.74a) pertains to the evolution of the spin-$J_2$ system only, and is thus expected to be implementable by Hamiltonian (2.72) for $\hat{\mathscr{V}}_1 = 0$ (no inter-channel coupling). Recall now that the dynamics of the spin-$J_2$ system have to describe accurately the evolution of the excitation in either of the two identical channels. Given that both channels are described by a perfect QST Hamiltonian

of the form (2.69), with fixed parameters $\{N, \tilde{\varepsilon}\}$, using the correspondences (2.70b) we find

$$\hat{\mathscr{H}}_2 = \hat{\mathbf{1}}_1 \otimes (\varepsilon_2 \hat{J}_2^2 + 2\tilde{\varepsilon}\hat{J}_{2,x}/\hbar), \tag{2.75}$$

where $\varepsilon_2 = -\tilde{\varepsilon}/[\hbar^2 J_2(J_2+1)]$ and $\hat{J}_{2,x}$ is the $x$-component of the vector $\hat{\mathbf{J}}_2$. According to (2.75), the initial state of the isolated spin-$J_2$ system undergoes a rotation by an angle $\varphi_2 = 2\tilde{\varepsilon}t/\hbar$ around the $x$-axis, at time $t$. Hence, for the initial condition (2.73), the transformation (2.74a) takes place at time

$$\tau = \hbar\pi/(2\tilde{\varepsilon}).$$

### 2.6.3 A QDC Scheme Based on the Rotation of Independent Spins

We have to determine the inter-channel interaction $\hat{\mathscr{V}}_1$, for which transformation (2.74b) takes place at a well defined time instant. The transformation (2.74b) involves a simultaneous rotation of both spins. This leads us to introduce the total angular momentum $\hat{\mathbf{J}} = \hat{\mathbf{J}}_1 + \hat{\mathbf{J}}_2$, with $|J_1 - J_2| \leq J \leq J_1 + J_2$ and $|m| \leq J$, while the corresponding basis states $\{|J,m\rangle\}$ can be expanded on the basis $\{|J_1,m_1;J_2,m_2\rangle\}$ as follows

$$|J,m\rangle = \sum_{\substack{m_1,m_2 \\ m=m_1+m_2}} C^J_{m_1,m_2} |J_1,m_1;J_2,m_2\rangle,$$

with $|m_k| \leq J_k$. Using the properties of the Clebsch-Gordan coefficients $C^J_{m_1,m_2}$, initial condition (2.73) reads in the basis $\{|J,m\rangle\}$, $|\Psi_{\mathrm{AM}}(0)\rangle = |J,-J\rangle$, while for the transformation (2.74b) we have

$$|J,-J\rangle \to |J,J\rangle. \tag{2.76}$$

This transformation, however, is similar to transformation (2.74a) which, as discussed earlier, can be achieved if the evolution of the corresponding spin system is governed by a Hamiltonian of the form (2.75). Hence, to perform transformation (2.76) it suffices to define the inter-channel coupling (which is represented by the Hamiltonian $\hat{\mathscr{H}}_1$), so that the total Hamiltonian (2.72) is of the form $\hat{\mathscr{H}} \sim \hat{J}_x$. Clearly, for fixed $\hat{\mathscr{H}}_2$ given by Eq. (2.75) and for $\hat{\mathscr{H}}_1^{(0)} = \varepsilon_1 \hat{J}_1^2$, this is possible only if we define interactions $\hat{\mathscr{V}}_1 \propto \hat{J}_{1,x}$, between the states $\{|J_1,m_1\rangle\}$. For instance, setting $\hat{\mathscr{V}}_1 = 2K\hat{J}_{1,x} \otimes \hat{\mathbf{1}}_2/\hbar$, with $K$ denoting the inter-channel coupling strength, the total Hamiltonian (2.72) reads

$$\hat{\mathscr{H}} = (\varepsilon_1 \hat{J}_1^2 + 2K\hat{J}_{1,x}/\hbar) \otimes \hat{\mathbf{1}}_2 + \hat{\mathbf{1}}_1 \otimes (\varepsilon_2 \hat{J}_2^2 + 2\tilde{\varepsilon}\hat{J}_{2,x}/\hbar), \tag{2.77}$$

with $\varepsilon_1 = -K/[\hbar^2 J_1(J_1+1)]$. This Hamiltonian acquires the desired form for $K = \tilde{\varepsilon}$ i.e., we obtain $\hat{\mathscr{H}} = \varepsilon_1 \hat{J}_1^2 \otimes \hat{\mathbf{1}}_2 + \varepsilon_2 \hat{\mathbf{1}}_1 \otimes \hat{J}_2^2 + 2\tilde{\varepsilon}\hat{J}_x/\hbar$.

The Hamiltonian (2.77) describes the operation of a perfect dual-channel QDC in an angular-momentum representation. The corresponding evolution operator reads

$$\hat{\mathscr{U}}(t) = \left[e^{-i\varepsilon_1 \hat{J}_1^2 t/\hbar} \hat{\mathscr{R}}_1^{(x)}(\varphi_1)\right] \otimes \left[e^{-i\varepsilon_2 \hat{J}_2^2 t/\hbar} \hat{\mathscr{R}}_2^{(x)}(\varphi_2)\right] \tag{2.78}$$

where we have introduced the rotation operator $\hat{\mathscr{R}}_k^{(x)}(\varphi_k) = e^{-i\hat{J}_{k,x}\varphi_k/\hbar}$, with $\varphi_1(t) = 2Kt/\hbar$ and $\varphi_2(t) = 2\tilde{\varepsilon}t/\hbar$. According to Eq. (2.78) the two spins are rotated independently around the $x$ axis, and after time $t$ the initial state of the spin-$J_k$ system has been rotated by an angle $\varphi_k$. Hence, the spin-$J_k$ system is in a superposition state of the form $|\chi_k(t)\rangle = e^{i\varphi_k/2} \sum_{m_k} A_{m_k}^{(k)}(t)|J_k, m_k\rangle$, with $A_{m_k}^{(k)}(t) = \langle J_k, m_k|\hat{\mathscr{R}}_k^{(x)}(\varphi_k)|J_k, -J_k\rangle$. These amplitudes can be obtained from the expansion of the rotation operator, as follows $\hat{\mathscr{R}}_k^{(x)}(\varphi_k) = \sum_{l=0}^{2J_k} D_{k,l}(\varphi_k)\hat{J}_{k,x}^{\,l}$. For fixed $\hat{J}_k$, i.e., for fixed channels and coupler, the coefficients $D_{k,l}(\varphi_k)$ are expressed in closed form, in terms of trigonometric functions [46], which also determine the relative amplitudes in the superpositions $|\chi_k(t)\rangle$. We see therefore that for $t > 0$ the state of the composite spin system is, in general, a superposition of all the basis states $\{|J_1, m_1; J_2, m_2\rangle\}$. In the computational basis this situation corresponds to a completely delocalized excitation, distributed among all of the sites of both channels and the coupler.

Of particular interest, however, is the state of the system at time $t = \tau$, when the rotation angles of the two spins read: $\varphi_2(\tau) = \pi$; $\varphi_1(\tau) = \pi\mu$, with $\mu = K/\tilde{\varepsilon}$. Hence, with the system initially prepared in the state (2.73), the following transformation has occurred at $t = \tau$:

$$|J_1, -J_1; J_2, -J_2\rangle \to e^{i\mu\pi/2} \sum_{m_1=-J_1}^{J_1} A_{m_1}^{(1)}(\tau)|J_1, m_1; J_2, J_2\rangle. \tag{2.79}$$

The superposition state in this transformation involves only the spin-$J_1$ system, and can be controlled by adjusting the corresponding rotation angle $\varphi_1(\tau)$, by means of the ratio $\mu$. Clearly, the transformations (2.74a) and (2.74b) are performed for $\mu = 0$ and $\mu = 1$, respectively.

A quantum network involving a number of coupled sites, may operate as a QDC if the Hamiltonian of the entire system in an angular momentum representation acquires the form (2.77). For instance, one can readily show, using Eqs. (2.70), that Hamiltonian (2.77) reduces to a Hamiltonian for an $M \times N$ grid of the form

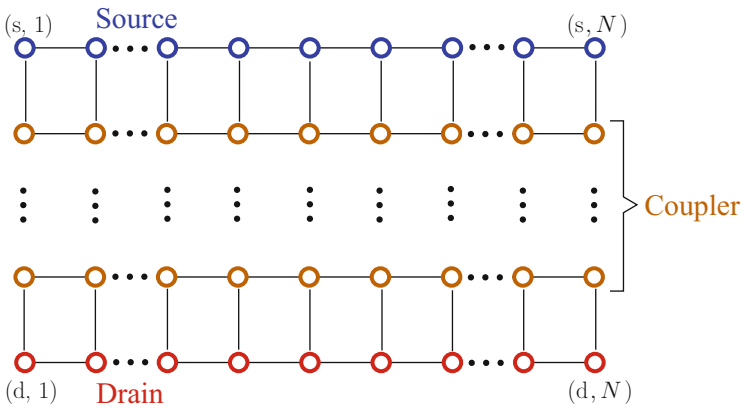


**Fig. 2.8** A grid of $M \times N$ nodes operating as a dual-channel QDC with the source and drain channels represented by the two outermost chains, and the intermediate chains providing the coupling between them. The *horizontal* and the *vertical* couplings are modulated according to $\propto \sqrt{l(Z-l)}$, where $1 \leq l < Z$ and $Z \in \{N, M\}$

$$\begin{aligned}\hat{\mathscr{H}}_{M\times N} = & -\sum_{i=1}^{M}\sum_{j=1}^{N}[K(M-1)+\tilde{\varepsilon}(N-1)]\hat{a}_{i,j}^{\dagger}\hat{a}_{i,j} \\ & +\sum_{i=1}^{M}\sum_{j=1}^{N-1}G_{i,j}^{i,j+1}(\hat{a}_{i,j}^{\dagger}\hat{a}_{i,j+1}+\hat{a}_{i,j+1}^{\dagger}\hat{a}_{i,j}) \\ & +\sum_{i=1}^{M-1}\sum_{j=1}^{N}G_{i,j}^{i+1,j}(\hat{a}_{i,j}^{\dagger}\hat{a}_{i+1,j}+\hat{a}_{i+1,j}^{\dagger}\hat{a}_{i,j}),\end{aligned} \tag{2.80}$$

where adjacent sites are coupled with strengths $G_{i,j}^{i,j+1} = \tilde{\varepsilon}\sqrt{j(N-j)}$ and $G_{i,j}^{i+1,j} = K\sqrt{i(M-i)}$ (see Fig. 2.8). The operator $\hat{a}_{i,j}^{\dagger}$ creates an excitation on the $j$th site of the $i$th row, while the coupling strength between two different sites $(i, j)$ and $(i', j')$, is denoted by $G_{i,j}^{i',j'}$. In this formalism, the two outermost chains represent the source and the drain channels (i.e., $\mathrm{s} \equiv 1$ and $\mathrm{d} \equiv M \geq 2$), while any intermediate sites $(i, j)$ with $i \neq \{1, M\}$ pertain to the coupler. This 2D coupling configuration has also been investigated in [47], albeit in a different context. The present chapter, however, reveals another aspect of such a structure, namely its use as a QDC with source and drain channels the two outermost chains. In particular, a qubit state can be transferred selectively from the input port $(\mathrm{s}, 1)$, to either of the two output ports $\{(\mathrm{s}, N), (\mathrm{d}, N)\}$ at time $t = \tau$ for $K = \{0, \tilde{\varepsilon}\}$, respectively. Moreover, we have seen the mathematical analogy between the 2D lattice Hamiltonian (2.80), and the rotation of independent spins.

The simplest configuration one may consider in the context of Hamiltonian (2.80), is a $2 \times N$ grid pertaining to two directly coupled quantum channels.

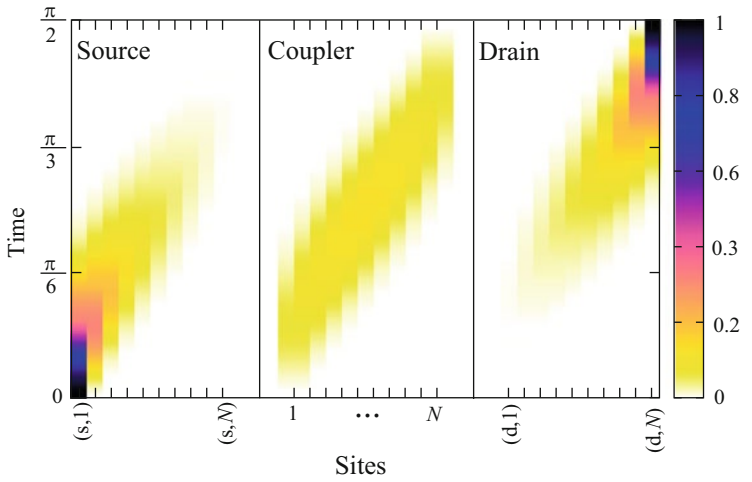


**Fig. 2.9** Time evolution of an excitation in a dual-channel QDC, consisting of $M = 3$ nearly identical arrays, with $N = 10$ sites each. Setting the coupling strength to the coupler $K = \tilde{\varepsilon}$, an excitation initially occupying the input port of the source channel (s, 1), is transferred to the output port of the drain channel (d, $N$) at $\tau = \hbar\pi/(2\tilde{\varepsilon})$. The time is in units of $\tilde{\varepsilon}$

This system can be easily analysed in the angular-momentum representation (with $J_1 = 1/2$), obtaining an analytic expression for its wavefunction at any time $t > 0$. At time $\tau$, the right-hand side of transformation (2.79) reads

$$e^{i\mu\pi/2}\left[\cos(\mu\pi/2)\,|\frac{1}{2},-\frac{1}{2}\rangle - i\,\sin(\mu\pi/2)\,|\frac{1}{2},\frac{1}{2}\rangle\right]|J_2,J_2\rangle. \tag{2.81}$$

In the computational basis, this is equivalent to

$$e^{i\mu\pi/2}\left[\cos(\mu\pi/2)|\mathrm{s};N\rangle - i\,\sin(\mu\pi/2)|\mathrm{d};N\rangle\right].$$

So, in general, both output ports can be excited at $t = \tau$, with probabilities determined by $\mu$; the structure operates as a splitter. The transformations (2.68a) and (2.68b) are performed for $\mu = 0$ (i.e., decoupled chains) and $\mu = 1$ (i.e., $K = \tilde{\varepsilon}$), respectively. For the sake of illustration, in Fig. 2.9 we present results pertaining to directional coupling in a larger grid, which have been obtained through the solution of the Schrödinger equation in the computational basis. The depicted behaviour is in perfect agreement with the previous discussion.

### *2.6.4 A QDC Scheme Based on Coupled Spins*

In the configuration depicted in Fig. 2.8, all the sites of the source channel have to be coupled (directly or indirectly) to the corresponding sites of the drain channel via

nearest-neighbour interactions. A question is whether one can achieve directional coupling between two chains by defining inter-channel interactions for a certain number of sites only.

This question has been addressed in [45], where it was shown that one of the solutions pertains to the coupling between a spin $J_1 = 1/2$ and an angular momentum $J_2 = 1$, such that the interaction part of the Hamiltonian (2.72) is of the form ($\hbar = 1$)[17]

$$\hat{\mathscr{V}} = \hat{\mathscr{V}}_1 + \hat{\mathscr{V}}_2 = 2\tilde{\varepsilon}\hat{\mathbf{1}}_1 \otimes \hat{J}_{2,x} + K\hat{J}_{1,y}\hat{J}_{2,y}, \tag{2.82}$$

and the transformation (2.74a) can be achieved for $K = 0$, when only the vector $\hat{\mathbf{J}}_2$ is rotated around the $x$-axis. Turning on the inter-channel interaction, i.e., setting $K \neq 0$, both vectors $\hat{\mathbf{J}}_1$ and $\hat{\mathbf{J}}_2$ can be rotated simultaneously around the $y$-axis. By contrast to Hamiltonian (2.77), we have two distinct evolution routes that may interfere either constructively or destructively, and the transformation (2.74b) can be achieved by choosing judiciously the ratio $\mu$. Indeed, for the initial condition (2.73), one can show that the transformation (2.74b) occurs at $t = \tau/\sqrt{2}$ for $K = -4\tilde{\varepsilon}$.

The Hamiltonian (2.82), can be implemented in the $2 \times 3$ grid depicted in Fig. 2.10a, for $g = \sqrt{2}\tilde{\varepsilon}$ and $\kappa = K/(2\sqrt{2})$. This arrangement requires the adjustment of geometric phases which is possible e.g., by looping around magnetic or electric fields, depending on the nature of information carriers, while for optical networks one may use phase shifters. More interestingly, a configuration similar to Fig. 2.10a can be used as a coupler for selective transfer of an excitation between two chains involving an arbitrary number of sites $N > 3$ (see [45] for more information). For the sake of illustration, in Fig. 2.11 we present numerical results pertaining to the transfer of a single excitation between two chains of $N = 7$ sites each.

In closing we would like to emphasize that the directional coupling of quantum states between two lattices that operate as wires, is a rather difficult task. We have discussed the problem in the framework of a mathematical analogy between a particular perfect QST Hamiltonian and angular momenta rotations around a fixed axis. This analogy enabled us to find two solutions, which are by no means unique. Most probably there exist other schemes which are more efficient and flexible than the ones presented here. In any case, the performance of such schemes has to be investigated under realistic conditions, and perhaps in the framework of specific realizations.

[17] As we have seen, the main effect of the unperturbed Hamiltonians $\hat{\mathscr{H}}_k^{(0)}$ is the introduction of an accumulated phase at the end of the transfer which, however, is fixed and known in the absence of disorder and other imperfections. Hence, for the time being we focus on the interaction part of the Hamiltonian.

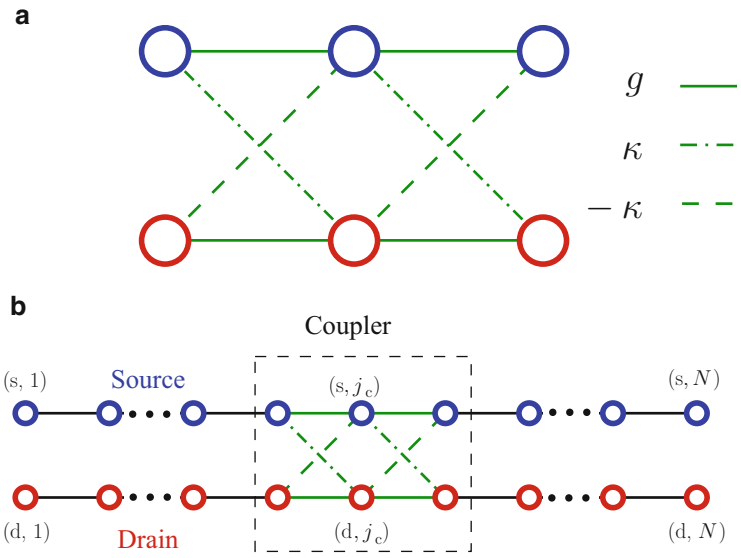


**Fig. 2.10** **(a)** A QDC consisting of six sites, with inter-channel coupling constant $\kappa = -g$. (**b**) The coupler integrated in a dual-channel system (Adapted from [45])

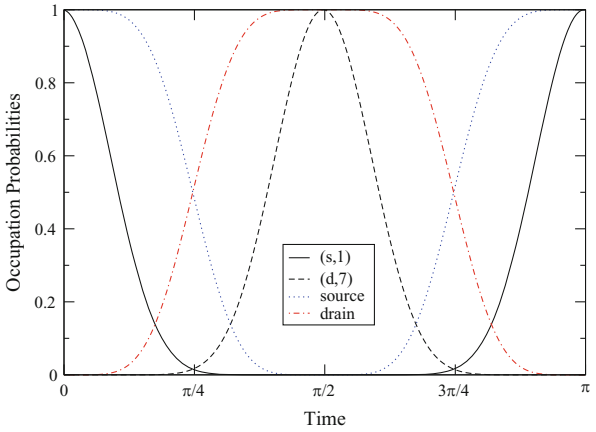


**Fig. 2.11** Time evolution of an excitation in the QDC of Fig. 2.10b, with $N = 7$. The excitation is transferred from the input port (s, 1), to the output port of the drain channel (d, $N$) at $t = \tau$. The time is in units of $\widetilde{\varepsilon}$ (Adapted from [45])

## 2.7 Effects of Bending in 2D and 3D Quantum Networks

In analogy to conventional networks [41], large-scale QIP and networking, irrespective of the physical platform, require efficient complex signal manipulations (such as routing, splitting, switching, etc.), which are possible only in higher-dimensional

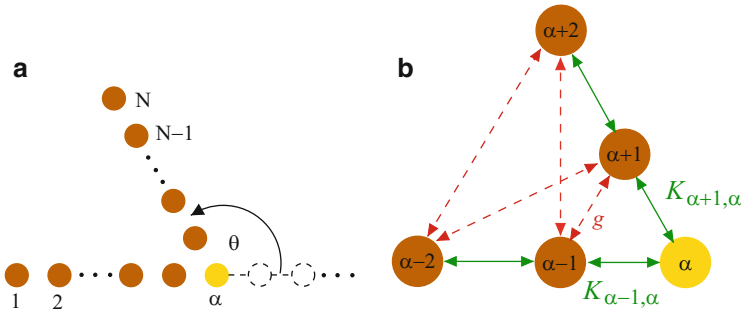


**Fig. 2.12** (**a**) A bent quantum chain of $N$ sites. (**b**) A closeup of the bend. *Green* (*solid*) *arrows* denote NN interactions of strength $K_{l,m}$. *Red* (*dashed*) *arrows* denote interactions beyond NNs, with the strongest one (of strength $g$) corresponding to the first neighbours of the corner site $\alpha$ (Adapted from [55])

geometric arrangements. This necessity has motivated studies on state transfer in various 2D arrangements [21, 23, 24, 45, 47–54], most of which rely on nearest-neighbour (NN) Hamiltonians. Bends are expected to be at the core of any 2D or 3D configuration, and their effects have been analysed recently by Nikolopoulos et al. [55]. Here we review some of the main results of [55].

### 2.7.1 Formalism

The 2D arrangement of [55] pertains to $N$ identical sites and is depicted in Fig. 2.12. Assuming that the configuration is initially prepared in vacuum and the qubit state to be transferred is prepared on the first site, we work in the ideal scenario (i.e., in the absence of imperfections) for the reasons discussed above. We focus on the position of the state in the configuration, assuming that the remaining degrees of freedom $\xi$ are preserved throughout the evolution of the system. The dynamics of the excitation in the bent chain is described by a Hamiltonian of the form ($\hbar = 1$)

$$\hat{\mathscr{H}} = \hat{\mathscr{H}}_0 + \hat{\mathscr{V}}(\theta), \tag{2.83a}$$

where

$$\hat{\mathscr{H}}_0 = \sum_{j=1}^{N} \varepsilon_j \hat{a}_j^\dagger \hat{a}_j + \sum_{j=1}^{N-1} K_{j,j+1}(\hat{a}_j^\dagger \hat{a}_{j+1} + \hat{a}_{j+1}^\dagger \hat{a}_j), \tag{2.83b}$$

is the unperturbed Hamiltonian corresponding to the unbent wire i.e., to $\theta = 0$, and $\hat{\mathscr{V}}(\theta)$ is the perturbation associated with the bending. We consider two different centrosymmetric faithful state-transfer Hamiltonians with NN interactions, which

ensure the faithful transfer of information between the two ends of the unbent chain, and we discuss their performance as we bend the chain.

*Protocol 1.* The first Hamiltonian was presented by Banchi et al. [56,57]. It involves $\varepsilon_j = \varepsilon$, $K_{j,j+1} = K_0 \; \forall j \neq 1, N-1$, and $K_{1,2} = K_{N-1,N} = K$. For a given $N$, the ratio $K/K_0$ is optimized so that faithful transfer of information between the two ends of the chain occurs at time $T_1^{(0)}$.

*Protocol 2.* The second Hamiltonian has been discussed in Sect. 2.4. Again, all the sites are on resonance, while the couplings along the entire chain are engineered according to $K_{j,j+1} = K_0\sqrt{(N-j)\,j}$. In contrast to Protocol 1, this scheme promises ideally perfect transfer at time $T_2^{(0)} = \pi/(2K_0)$.

Both of these protocols are designed for chains with NN couplings. In many physical realizations of quantum networks, the coupling between two adjacent sites is directly related to their spatial separation (e.g., see [8, 12, 31, 58–62]). Hence, interactions beyond NNs are expected to get enhanced in the neighbourhood of bends (see Fig. 2.12), disturbing the communication. For not too sharp bends, the perturbation is dominated by the coupling between the first-order neighbours of the corner site $\alpha$, and the perturbation in Eq. (2.83a) can be chosen as

$$\hat{\mathscr{V}}(\theta) = g(\theta)(\hat{a}_{\alpha-1}^{\dagger}\hat{a}_{\alpha+1} + \hat{a}_{\alpha+1}^{\dagger}\hat{a}_{\alpha-1}). \tag{2.83c}$$

In general, the dynamics of the chain are expected to be determined by the strength of the perturbation $g$, relative to the NN couplings around the corner, rather than the actual origin of the perturbation. Hence, for the following analysis we introduce the ratio $\kappa = g/K_{\max}$, where $K_{\max} \equiv \max\{K_{l,m}\}$.

The Hamiltonian (2.83) preserves the number of excitations and thus, the system is restricted to the one-excitation sector of the Hilbert space throughout its evolution. The computational basis can be chosen as $\{|j\rangle\}$, where $|j\rangle$ is the state with one excitation on the $j$th site. Initially $|\Psi(0)\rangle = |1\rangle$, and the probability for the excitation to occupy the $N$th site at time $t$ when protocol $i$ is used, is given by $|P_i(t)|^2 = |\langle N|\hat{\mathscr{U}}(t)|\Psi(0)\rangle|^2$, with $\hat{\mathscr{U}}(t) = e^{-i\hat{\mathscr{H}}t}$. The corresponding probabilities for the unbent chains are denoted by $P_i^{(0)}(t)$.

### 2.7.2 Analysis and Minimization of Bending Losses

The analysis of [55] pertained to $\kappa \in [0, 1]$ for various values of $\alpha$, and focused on the ratios $Q_i \equiv P_i/P_i^{(0)}$ and $S_i \equiv T_i/T_i^{(0)}$.

The performance of Protocol 2 in the presence of a bend is summarized in Fig. 2.13. As depicted in the histograms, the ratio $Q_i$ is close to 1 for relatively weak perturbations (up to $\kappa \approx 0.2$), and drops as we increase the strength of the perturbation, following a Gaussian law. The effect of the bend on the time of

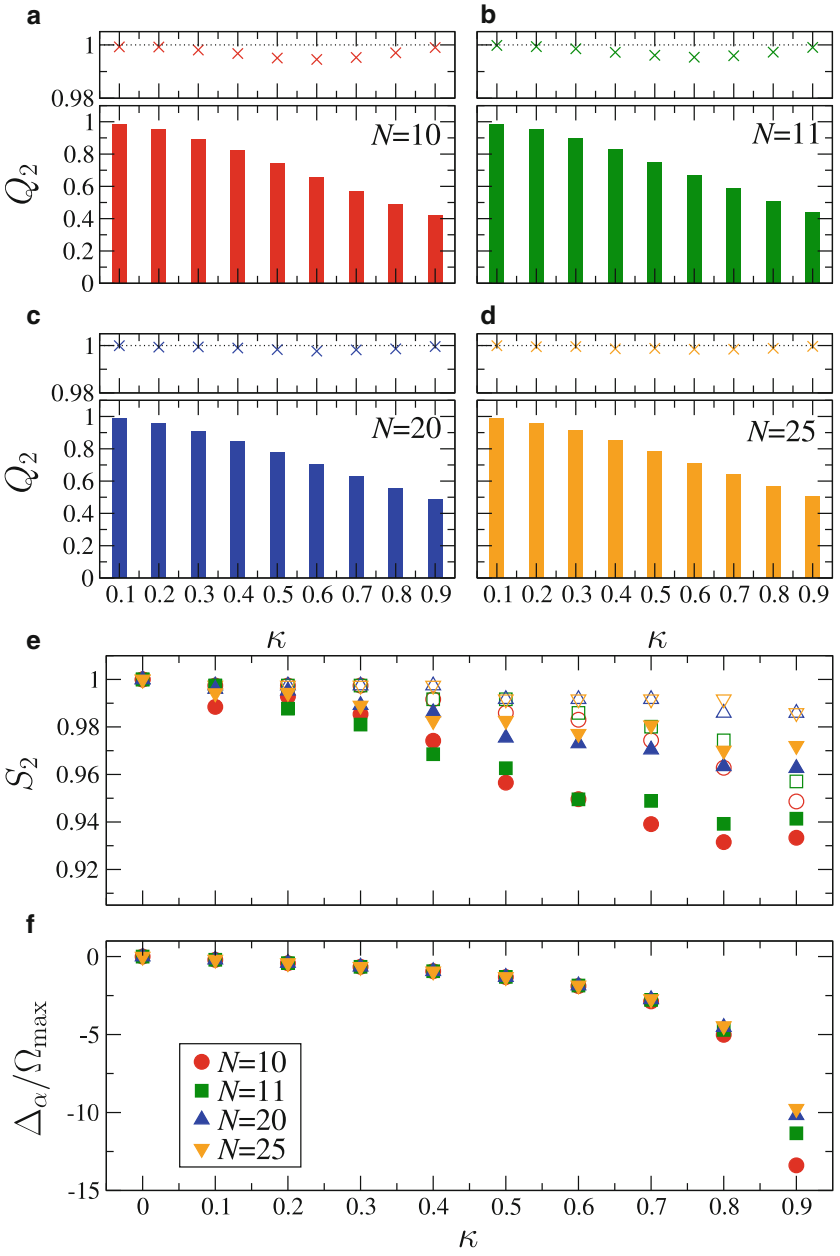


**Fig. 2.13** Performance of the bent chain for protocol 2 and various $N$. (**a**-**d**) The normalized probability of transfer $Q_i$, for the bent chain without (*bars*), and with (×) corner defect. Corner sites: (**a**,**b**) $\alpha = 6$; (**c**) $\alpha = 11$; (**d**) $\alpha = 13$. (**e**) Time of transfer through the bent chain without (*open symbols*) and with (*filled symbols*) corner defect. (**f**) Optimal detunings of the defect corner site relative to the other sites (Adapted from [55])

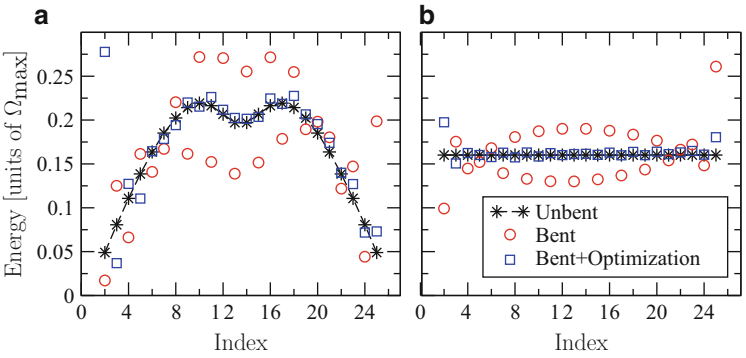


**Fig. 2.14** Difference between successive eigenenergies of the Hamiltonians for $N = 25$ and $\alpha = 12$. (**a**) Protocol 1, $\kappa = 0.5$; (**b**) Protocol 2, $\kappa = 0.3$ (Adapted from [55])

transfer is not as disastrous as on the fidelity (see open symbols in Fig. 2.13e). The transfer is accelerated relative to the unbent chains, since the couplings around the corner increase whereas, as a result of the finite spatial extension of the perturbation, the acceleration becomes less pronounced as we increase $N$. The performance of Protocol 1 is very close to the performance of Protocol 2 and is not shown here (the reader may refer to [55] for detailed results).

In [55] it was shown that bending losses can be minimized, without deviating significantly from the protocol under consideration, as long as one has external control on the energy of the corner site only. The detuning $\Delta_\alpha$ of the corner site relative to the others can be optimized so that the transfer from the first to the last site is maximized for a given strength of the perturbation $\kappa$ and for times $t \in [0, T_i^{(0)}]$. As depicted in Fig. 2.13, for given $N$, $\kappa$ and $\alpha$, there is an optimal value of $\Delta_\alpha$ for which the probability of transfer is above 99 % of the corresponding probability for the unbent chain. The results are analogous for Protocol 1 and in fact, detunings of the same order are required for the minimization of losses in the two protocols against the same disturbance $\kappa$. The optimization procedure works efficiently irrespective of the position of the bend on the chain for both protocols.

The role of the bends and the minimization of the associated losses, can be understood in the framework of the spectrum of the Hamiltonians (one-excitation sector). The operation of many QST Hamiltonians (including the ones discussed here), relies on the details of the spectrum, and the overlap of the initial state $|\Psi(0)\rangle$ with the corresponding eigenvectors. As shown in Fig. 2.14 the presence of the bend tends to distort the commensurate spectrum of the unperturbed QST Hamiltonians, leading thus to the observed decrease of the probability of transfer. When the detuning of the corner site is optimized, however, the initial distribution is restored to a large extent, minimizing thus the losses.

In summary, the above analysis shows that the transfer of signals through bent chains that operate under NN QST Hamiltonians, is distorted significantly by interactions beyond nearest-neighbours that originate from the bend. The limited

spatial extent of such perturbations, allows one to minimize efficiently the associated losses by controlling the energy of the corner site. Bends play a pivotal role in the reliable and efficient navigation of quantum signals in higher-dimensional networks, which are essential for large-scale QIP. The present results shed light on the role of bends facilitating the engineering of reliable quantum networks in higher dimensions, including various 2D geometric arrangements that have been discussed in the literature [15, 19, 21, 23, 24, 45, 47–54, 56, 57].

## 2.8 Conclusions

We have reviewed many aspects of the problem of quantum state transfer in engineered quantum networks. The problem has been defined in a rather general theoretical framework, while fundamental aspects of quantum networks such as the form of the underlying Hamiltonians and the various topologies have been introduced. We have demonstrated a rather general and efficient theoretical framework that allows for the engineering of passive quantum networks of arbitrary topology and dimensionality, which perform various communication tasks (point-to-point transfer, routing, etc.) for states that involve multiple interacting or non-interacting excitations. The robustness of some of the state-transfer Hamiltonians discussed here, against various types of imperfections is discussed in the chapter by Stolze et al.

We have also reviewed the problem of the quantum directional coupler, which pertains to the directional coupling of a quantum state between two identical quantum chains. Such structures are expected to be of great importance for large-scale quantum-information processing, since they can perform a number of useful functions such as signal division, switching, (de) multiplexing, etc. To this end, however, one has to consider two-dimensional or even three-dimensional configurations, where the presence of bends is inevitable. We have discussed the effects of bends on known and rather promising state-transfer Hamiltonians, showing that they can be easily minimized by the inclusion of small defects.

Recently [62], one of the state-transfer Hamiltonians discussed here, has been demonstrated in the framework of photonic lattices, which offer a rather versatile tool for testing models that rely on tight-binding Hamiltonians (see the chapter by Bellec et al.). In view of these new developments, the ideas discussed in the present chapter, promise the systematic engineering of photonic architectures that operate in the linear regime and perform various communication tasks. On the other hand, for the realization of quantum state transfer in real spin chains, there are various candidates ranging from liquid- and solid-state NMR systems, to Nitrogen-Vacancy centers in diamond (see the chapter by Cappellaro). However, some of these systems do not allow for the degree of engineering that certain QST protocols require, not to speak about more complicated communication tasks. Hence, the field is certainly open to new challenging developments.

**Acknowledgements** I. J. received funding from MSM 6840770039, RVO 68407700 and GACR 13-33906S. A. H. was supported by the Grant Agency of the Czech Technical University in Prague, grant No. SGS13/217/OHK4/3T/14.

## References

1. M.A. Nielsen, I.L. Chuang, *Quantum Computation and Quantum Information* (Cambridge University Press, Cambridge, 2000)
2. A.B. Kuklov, B.V. Svistunov, Phys. Rev. Lett. **90**, 100401 (2003)
3. L.M. Duan, E. Demler, M.D. Lukin, Phys. Rev. Lett. **91**, 090402 (2003)
4. S.R. Clark, C.M. Alves, D. Jaksch, New J. Phys. **7**, 124 (2005)
5. S. Sachdev, *Quantum Phase Transitions* (Cambridge University Press, Cambridge, UK, 1999)
6. P. Ciccarelli, P. Faulkner, *Networking Foundations: Technology Fundamentals for IT Success* (Sybex, San Francisco, 2004)
7. S. Steinke, *Network Tutorial* (CMP Books, San Francisco, 2003)
8. T. Brougham, G.M. Nikolopoulos, I. Jex, Phys. Rev. A **80**, 052325 (2009)
9. S. Bose, Phys. Rev. Lett. **91**, 207901 (2003)
10. A. Kay, Phys. Rev. A **84**, 022337 (2011)
11. G.M. Nikolopoulos, Phys. Rev. A **87**, 042311 (2013)
12. V. Kostak, G.M. Nikolopoulos, I. Jex, Phys. Rev. A **75**, 042319 (2007)
13. T. Brougham, G.M. Nikolopoulos, I. Jex, Phys. Rev. A **83**, 022323 (2011)
14. P. Törmä, S. Stenholm, I. Jex, Phys. Rev. A **52**, 4853 (1995)
15. G.M. Nikolopoulos, D. Petrosyan, P. Lambropoulos, J. Phys.: Condens. Matter **16**, 4991 (2004)
16. Z. Bialynicka-Birula, I. Bialynicka-Birula, J.H. Eberly, B.W. Shore, Phys. Rev. A **16**, 2048 (1977)
17. R.J. Cook, B.W. Shore, Phys. Rev. A **20**, 539 (1979)
18. J.H. Eberly, B.W. Shore, Z. Bialynicka-Birula, I. Bialynicka-Birula, Phys. Rev. A **16**, 2038 (1977)
19. M. Christandl, N. Datta, A. Ekert, A.J. Landahl, Phys. Rev. Lett. **92**, 187902 (2004)
20. R. Gordon, Opt. Lett. **29**, 2752 (2004)
21. M.B. Plenio, J. Hartley, J. Eisert, New J. Phys. **6**(1), 36 (2004)
22. G.M. Nikolopoulos, D. Petrosyan, P. Lambropoulos, Europhys. Lett. **65**, 297 (2004)
23. A. Kay, M. Ericsson, New J. Phys. **7**, 143 (2005)
24. S. Yang, Z. Song, C. Sun, Eur. Phys. J. B **52**, 377 (2006)
25. A. Kay, Phys. Rev. Lett. **98**, 010501 (2007)
26. H.L. Haselgrove, Phys. Rev. A **72**, 062326 (2005)
27. P. Kurzyński, A. Wójcik, Phys. Rev. A **83**, 062315 (2011)
28. S. Bose, Contemp Phys. **48**, 13 (2007)
29. M.H. Yung, S. Bose, Phys. Rev. A **71**, 032310 (2005)
30. P. Karbach, J. Stolze, Phys. Rev. A **72**, 030301 (2005)
31. A. Kay, Phys. Rev. A **73**, 032306 (2006)
32. C. Albanese, M. Christands, N. Datta, A. Ekert, Phys. Rev. Lett. **93**, 230502 (2004)
33. T. Shi, Y. Li, Z. Song, C.P. Sun, Phys. Rev. A **71**, 032309 (2005)
34. X.Q. Xi, J.B. Gong, T. Zhang, R.H. Yue, W.M. Liu, Eur. Phys. J. D **50**, 193 (2008)
35. M.H. Yung, Phys. Rev. A **74**, 030303(R) (2006)
36. R. Hanson, L.P. Kouwenhoven, J.R. Petta, S. Tarucha, L.M.K. Vandersypen, Rev. Mod. Phys. **79**, 1217 (2007)
37. D. Petrosyan, B. Schmidt, J.R. Anglin, M. Fleischhauer, Phys. Rev. A **76**, 033606 (2007)
38. A.J. Daley, A. Kantian, H.P. Büchler, P. Zoller, K. Winkler, G. Thalhammer, F. Lang, R. Grimm, J.H. Denschlag, in *AIP Conference Proceedings*, vol. 869, ed. by C. Roos, H. Häffner, R. Blatt (2006), vol. 869, p. 212

39. J.H. Denschlag, A.J. Daley, in *Proceedings of the International School of Physics "Enrico Fermi"*, vol. 164, ed. by M. Inguscio, W. Ketterle, C. Salomon (2007), vol. 164, p. 677
40. D. Petrosyan, G.M. Nikolopoulos, P. Lambropoulos, Phys. Rev. A **81**, 042307 (2010)
41. A. Yariv, P. Yue, *Photonics: Optical Electronics in Modern Communications* (Oxford University, New York, 2006)
42. N. Dagli, G. Snider, J. Waldman, E. Hu, J. Appl. Phys. **69**, 1047 (1991)
43. J.A. del Alamo, C.C. Eugster, Appl. Phys. Lett. **56**, 78 (1990)
44. S. Fan, P.R. Villeneuve, J.D. Joannopoulos, H.A. Haus, Phys. Rev. Lett. **80**, 960 (1998)
45. G.M. Nikolopoulos, Phys. Rev. Lett. **101**, 200502 (2008)
46. B.W. Shore, *The Theory of Coherent Atomic Excitation* (Wiley, New York, 1990)
47. Y. Li, Z. Song, C.P. Sun, Commun. Theor. Phys. **48**, 445 (2007)
48. P.J. Pemberton-Ross, A. Kay, Phys. Rev. Lett. **106**, 020503 (2011)
49. I. D'Amico, B.W. Lovett, T.P. Spiller, Phys. Rev. A **76**, 030302(R) (2007)
50. D. Zueco, F. Galve, S. Kohler, P. Hänggi, Phys. Rev. A **80**, 042303 (2009)
51. M.I. Makin, J.H. Cole, C.D. Hill, A.D. Greentree, Phys. Rev. Lett. **108**, 017207 (2012)
52. T. Tufarelli, V. Giovannetti, Phys. Rev. A **79**(2), 022313 (2009)
53. V. Karimipour, M.S. Rad, M. Asoudeh, Phys. Rev. A **85**, 010302 (2012)
54. F.A.A. El-Orany, M.R.B. Wahiddin, Journal of Physics B: Atomic Mol Opt Phys **43**, 085502 (2010)
55. G.M. Nikolopoulos, A. Hoskovec, I. Jex, Phys. Rev. A **85**, 062319 (2012)
56. L. Banchi, T.J.G. Apollaro, A. Cuccoli, R. Vaia, P. Verrucchi, Phys. Rev. A **82**, 052321 (2010)
57. L. Banchi, A. Bayat, P. Verrucchi, S. Bose, Phys. Rev. Lett. **106**, 140501 (2011)
58. M. Avellino, A.J. Fisher, S. Bose, Phys. Rev. A **74**, 012321 (2006)
59. G. Gualdi, V. Kostak, I. Marzoli, P. Tombesi, Phys. Rev. A **78**, 022325 (2008)
60. G. Burkard, D. Loss, D.P. DiVincenzo, Phys. Rev. B **59**, 2070 (1999)
61. S. Longhi, Phys. Rev. B **82**, 041106 (2010)
62. M. Bellec, G.M. Nikolopoulos, S. Tzortzakis, Opt. Lett. **37**, 4504 (2012)

# Chapter 3
# Dual- and Multi-rail Encoding

**Daniel Klaus Burgarth and Vittorio Giovannetti**

**Abstract** We review the dual-rail encoding (Burgarth and Bose, Phys Rev A 71:052315, 2005) which demonstrates how the problem of dispersion in quantum state transfer in spin chain communication can be attacked and overcome through performing measurements at the receiver side. We discuss the performance of the dual-rail technique in detail with respect to noise, disorder in the chain couplings (Burgarth and Bose, New J Phys 7:135, 2005) and deviations from a strict one-dimensionality. We then show how the dual-rail method can be made more efficient by using multiple channels (Burgarth et al., Int J Quant Inf 4:405, 2006; J Phys A Math Gen 38:6793, 2005). We provide a convergence theorem which shows that any nearest-neighbor excitation preserving chain is capable of efficient and perfect state transfer using a multi-rail encoding.

## 3.1 Introduction

The role of measurement in quantum information theory has become more active recently. Measurements are not only essential to obtain information about some state or for preparation, but also, instead of gates, can be used for performing quantum computation [1]. In the context of quantum state transfer however, it seems at first glance that measurements would spoil the coherence of the system inhibiting the efficiency of the protocol. In this chapter we show that this is not necessarily

D.K. Burgarth (✉)
Institute of Mathematics and Physics, Aberystwyth University, Physical Sciences Building, Penglais Campus, SY23 3BZ Aberystwyth, UK
e-mail: dkb3@aber.ac.uk

V. Giovannetti
NEST, Scuola Normale Superiore and Istituto Nanoscienze-CNR, piazza dei Cavalieri 7, I-56126 Pisa, Italy
e-mail: vittorio.giovannetti@sns.it

G.M. Nikolopoulos and I. Jex (eds.), *Quantum State Transfer and Network Engineering*, Quantum Science and Technology, DOI 10.1007/978-3-642-39937-4_3,

the case by exhibiting explicit architectures where the dispersion of quantum information along arrays of coupled qubits (spin chains in brief) is compensated via measurements performed at the receiving end of the communication line.

A properly initialized spin chain whose Hamiltonian preserves the total number of excitations in the system is known to provide a primitive for quantum state transfer [2]. In this model the sender of the state (Alice) *writes* her message into the spin located at one of the ends of the chain (say the leftmost) while, after a sufficiently long time has elapsed, the receiver (Bob) *reads* it from the rightmost chain element. Unfortunately, even in the absence of external noise sources, the efficiency of the scheme is typically affected by dispersion that tends to spread Alice's messages along the chain. As a matter of fact, apart from very special, highly symmetric, arrangements of the spin couplings (e.g. see [3] and references therein), the input-output relations of the scheme can be effectively described as an amplitude damping channel with low transmission efficiency. Standard channel coding and quantum error correction techniques [4] can be employed to improve the information transmission. However, excluding those scenarios where prior entanglement is explicitly allowed between the communicating parties [2], these techniques are essentially ineffective as they require that most part of Alice's wave-packets should be able to reach the receiver [5] (this being a consequence of the non-cloning theorem). In this context it is clear that better performances can be achieved only by envisioning new ways of exploiting the dynamics of the spin chain, beyond the simple *write*, *wait* & *read* paradigm depicted above.

In terms of access to the system, we take the same "restricted control" approach of [2]: along the chain, we let the system evolve coherently without control, and allow no design of the spin-spin couplings; merely we assume the possibility of having access to multiple copies (two at least) of the same chain and identify proper measurement procedures which, when performed on the receiving end by Bob, *help* the transferring of Alice's messages [6–9]. As mentioned previously, the main disadvantage of the encoding used in basic state transfer protocols [2] is that once the information dispersed, there is no way of finding out *where* it is without destroying it. A dual-rail encoding [10] as used in quantum optics on the other hand allows us to perform parity type measurements that do *not* spoil the coherence of the state that is sent. The outcome of the measurement tells us if the state has arrived at the end (corresponding to a perfect state transfer) or not. We call this *conclusively perfect state transfer*. Moreover, by performing repetitive measurements, the probability of success can be made arbitrarily close to unity. As an example of such an *amplitude delaying channel*, we show how two parallel Heisenberg spin chains can be used as quantum wires. Perfect state transfer with a probability of failure lower than $P$ in a Heisenberg chain of $N$ qubits can be achieved in a time-scale of the order of $0.33\,\mathrm{J}^{-1}N^{1.7}|\ln P|$.

The content is organised as follows. In Sect. 3.2, we review a scheme for quantum communication using two parallel spin chains of the most natural type (namely those with constant couplings). It requires modest encodings (or gates) and measurements only at the ends of the chains. The state transfer is *conclusive*, which means that it is possible to tell by the outcome of a quantum measurement, without

destroying the state, if the transfer took place or not. If it did, then the transfer was *perfect*. The transmission time for conclusive transfer is not longer than for single spin chains. In Sect. 3.2.1, we demonstrate that the scheme offers even more: if the transfer was not successful, then we can wait for some time and just repeat the measurement, without having to resend the state. By performing sufficiently many measurements, the probability for perfect transfer approaches unity. Hence the transfer is *arbitrarily perfect*. We will show in Sect. 3.2.2 that the time needed to transfer a state with a given probability scales in a reasonable way with the length of the chain. Furthermore we show that the encoding to parallel chains and the conclusiveness also makes the protocol more robust to decoherence non-optimal timing than any scheme using single spin chains.

Section 3.3 analyzes how the scheme of Sect. 3.2 behaves when imperfections are present in the chain design. Here we will show that it performs well for both spatially correlated and uncorrelated fluctuations if they are relatively weak (say 5 %). Furthermore, we show that given a quite arbitrary pair of quantum chains, one can check whether it is capable of perfect transfer by only local operations at the ends of the chains, and the system in the middle being a *black box*. We argue that unless some specific symmetries are present in the system, it *will* be capable of perfect transfer when used with dual-rail encoding. In fact, the main idea can even be generalized to coupled chains and some spin networks (Sect. 3.3.4). Therefore the scheme puts minimal demand not only on the control of the chains when using them, but also on the design when building them.

A natural generalisation of the such an encoding on two chains is to use many parallel chains. Such a multi-rail encoding will be discussed in 3.4. It makes more efficient use of resources but one has to analyze the scaling of the success fidelity carefully (Sect. 3.4.1). In Sect. 3.4.2 we prove a theorem which provides us with a sufficient condition for achieving efficient and perfect state transfer in quantum chains using multiple chains for encoding. Finally, we compare the performance with two-chain encoding (Sect. 3.4.4) and conclude (Sect. 3.5).

## 3.2 Dual-Rail Scheme

Consider the scenario sketched in Fig. 3.1 where two communicating parties (Alice and Bob) are connected through two identical and uncoupled spin-1/2-chains 1 and 2 of length $N$, described by the global Hamiltonian

$$H^{(1,2)} = H^{(1)} \otimes I^{(2)} + I^{(1)} \otimes H^{(2)}. \tag{3.1}$$

Here for $i = 1, 2$, $I^{(i)}$ stands for the identity operator on the chain $i$, while $H^{(1)}$ and $H^{(2)}$ represent the same single chain Hamiltonian $H$ apart from the label of the Hilbert space they act on. We assume that the ground state of $H^{(i)}$ is a ferromagnetic ground state (which we indicate with the symbol $|\mathbf{0}\rangle_i$), and that the

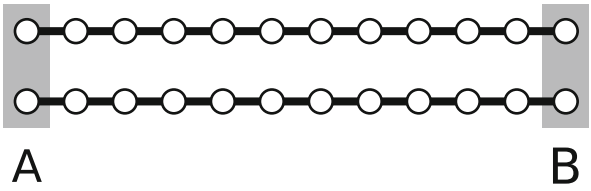


**Fig. 3.1** Two quantum chains interconnecting $A$ and $B$. Control of the systems is only possible at the two qubits of either end

subspace spanned by the single spin excitation states $\{|\boldsymbol{n}\rangle_i ; n = 1, 2, \cdots, N\}$ is invariant under the action of $H^{(i)}$ (later, we exemplify this by identifying $H^{(i)}$ with the Heisenberg Hamiltonian).[1]

In this configuration the sender of the message Alice is allowed to address the leftmost element of both chains (indicated by the gray area $A$ in the figure) in a coherent fashion, and the receiver Bob is given complete free access to the rightmost elements (gray area $B$). While these assumptions might pose some technical problem in terms of experimental implementations (see however the following paragraphs), the requirement of having two chains instead of just one as in other proposals [2, 3] is not a real issue, since in many experimental realisations of spin chains, it is much easier to produce a whole bunch of parallel uncoupled [11, 12] chains than just a single one.

Suppose then that, starting from the ground state of the two chains $|\mathbf{0}\rangle_1 \otimes |\mathbf{0}\rangle_2$, Alice "loads" into the system the qubit state she wishes to send to Bob, by encoding it in the first spin of the first chain, transforming $|\mathbf{0}\rangle_1$ into

$$|\boldsymbol{\psi}_A\rangle_1 \equiv \alpha\, |\mathbf{0}\rangle_1 + \beta\, |\mathbf{1}\rangle_1 . \tag{3.2}$$

The aim of the protocol is to transfer such superposition from the first to the $N$th qubit of the chain, i.e.

$$|\boldsymbol{\psi}_A\rangle_1 \to |\boldsymbol{\psi}_B\rangle_1 \equiv \alpha\, |\mathbf{0}\rangle_1 + \beta\, |\boldsymbol{N}\rangle_1 . \tag{3.3}$$

We achieve this by exploiting Alice's coherent control on the $A$ region of Fig. 3.1: the first step (see also Fig. 3.2) is to map the input qubit in a *dual-rail* encoding [10] by applying a NOT gate on the first qubit of system 2 controlled by the first qubit of system 1 being zero. The result is a superposition in which Alice's input is delocalized in the two chains, i.e.

$$|\boldsymbol{s}(0)\rangle = \alpha\, |\mathbf{0}, \mathbf{1}\rangle + \beta\, |\mathbf{1}, \mathbf{0}\rangle , \tag{3.4}$$

[1] Specifically, we identify the vector $|\mathbf{0}\rangle_i$ with the factorized state where all the qubits of the chain are initialized in $|0\rangle$, while $|\boldsymbol{n}\rangle_i$ with the factorized state where all the qubits of the chain are in zero apart from the $n$-th one which is in $|1\rangle$.

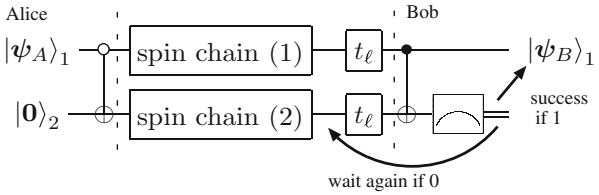


**Fig. 3.2** Quantum circuit representation of conclusive and arbitrarily perfect state transfer. The first gate at Alice's qubits represents a NOT gate applied to the second qubit controlled by the first qubit being zero (whereas the gate on Bob's side is a standard CNOT gate). The qubit $|\boldsymbol{\psi}_A\rangle_1$ on the left hand side represents an arbitrary input state at Alice's site, and the qubit $|\boldsymbol{\psi}_B\rangle_1$ represents the same state, successfully transferred to Bob's site. The $t_\ell$-gate represents the unitary evolution of the spin chains for a time interval of $t_\ell$

where we have introduced the short notation $|\boldsymbol{n},\boldsymbol{m}\rangle \equiv |\boldsymbol{n}\rangle_1 \otimes |\boldsymbol{m}\rangle_2$. The mapping from (3.2) to (3.4) is assumed to take place in a much shorter time-scale than the system dynamics. Even though a 2-qubit gate in solid state systems is difficult, such a gate for charge qubits has been reported [13]. For the same qubits, Josephson arrays have been proposed as single spin chains for quantum communication [14]. For this system, both requisites of the scheme are thus available. In fact, the demand that Alice and Bob can do measurements and apply gates to their local qubits (i.e. the ends of the chains) will be naturally fulfilled in practice since we are suggesting a scheme to transfer information between quantum computers.

Under the system Hamiltonian, the excitation in Eq. (3.4) will travel along the two systems. The state after the time $t_1$ can be written as

$$|\boldsymbol{\phi}(t_1)\rangle = \sum_{n=1}^{N} f_{n,1}(t_1)\,|\boldsymbol{s}(n)\rangle\,, \tag{3.5}$$

where $|\boldsymbol{s}(n)\rangle = \alpha\,|\mathbf{0},\boldsymbol{n}\rangle + \beta\,|\boldsymbol{n},\mathbf{0}\rangle$ and the complex amplitudes $f_{n,1}(t_1)$ are given by the time evolution operator of the system through

$$f_{n,m}(t) \equiv \langle \boldsymbol{n}|e^{-iHt}|\boldsymbol{m}\rangle.$$

In the above and for the remainder of the chapter, we set $\hbar = 1$. We can *decode* the qubit by applying a CNOT gate at Bob's site. Assuming that this happens on a time-scale much shorter than the evolution of the chain, the resulting state is given by

$$\sum_{n=1}^{N-1} f_{n,1}(t_1)\,|\boldsymbol{s}(n)\rangle + f_{N,1}(t_1)\,|\boldsymbol{\psi}_B\rangle_1 \otimes |\boldsymbol{N}\rangle_2\,. \tag{3.6}$$

Bob can now perform a measurement on his qubit of system 2. If the outcome of this measurement is 1, he can conclude that the state has been successfully transferred

to him. This happens with success probability $|f_{N,1}(t_1)|^2$. If the outcome is 0, the system is in the state

$$\frac{1}{\sqrt{P(1)}} \sum_{n=1}^{N-1} f_{n,1}(t_1) \, |s(n)\rangle \, , \tag{3.7}$$

where $P(1) = 1 - |f_{N,1}(t_1)|^2$ is the probability of *failure* for the first measurement. If the protocol stopped here, and Bob would just assume his state as the transferred one, the channel could be described as an *amplitude damping channel* [5], with exactly the same fidelity as the single chain scheme discussed in [2]. Note that here, opposed to basic state transfer schemes, the encoding is symmetric with respect to $\alpha$ and $\beta$, so the minimal fidelity is the same as the averaged one.

Success probability is more valuable than fidelity: Bob has gained knowledge about his state, and may reject it and ask Alice to retransmit (this is known as a *quantum erasure channel* [15]). Of course in general the state that Alice sends is the unknown result of some quantum computation and cannot be sent again easily. This can be overcome in the following way: Alice sends one e-bit on the dual-rail first. If Bob finds that the transfer was successful, he tells Alice, and they both start to teleport the unknown state. Otherwise, they reset the chains and start again. Since the joint probability of failure converges exponentially fast to zero this is quite efficient. This can be seen as a very simple entanglement distillation procedure, achieving a rate of $|f_{N,1}(t)|^2/2$. However the chain needs to be reset between each transmission, and Alice and Bob require classical communication. We will show in the next section that the reuse of the chain(s) is not necessary, as arbitrarily perfect state transfer can already achieved in the first transmission.

### 3.2.1 From Conclusive to Arbitrarily Perfect State Transfer

Because Bob's measurement has not revealed anything about the input state (the success probability is independent of the input state), the information is still residing in the chain. By letting the state (3.7) evolve for another time $t_2$ and applying the CNOT gate again, Bob has another chance of receiving the input state. The state before performing the second measurement is easily seen to be

$$\frac{1}{\sqrt{P(1)}} \sum_{n=1}^{N} \{ f_{n,1}(t_2 + t_1) - f_{n,N}(t_2) \, f_{N,1}(t_1) \} \, |s(n)\rangle \, . \tag{3.8}$$

Hence the probability to receive the qubit at Bobs site at the second measurement is

$$\frac{1}{P(1)} \, |f_{N,1}(t_2 + t_1) - f_{N,N}(t_2) \, f_{N,1}(t_1)|^2 \, . \tag{3.9}$$

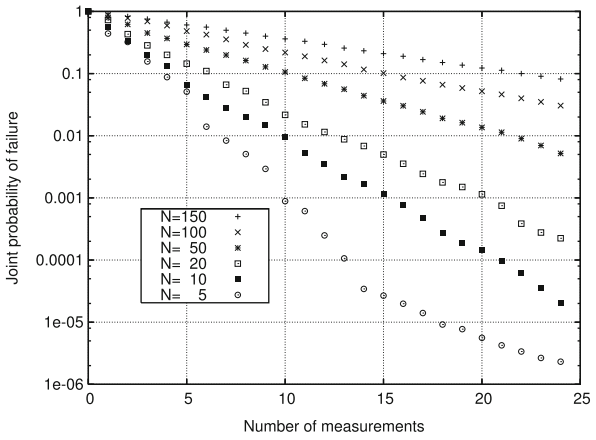


**Fig. 3.3** Semilogarithmic plot of the joint probability of failure $P(\ell)$ computed as detailed in Sect. 3.2.1, as a function of the number of measurements $\ell$. The results refer to the case of Heisenberg spin-1/2-chains (3.10) with different lengths $N$. The times between measurements $t_\ell$ have been optimized numerically

If the transfer was still unsuccessful, this strategy can be repeated over and over. Each time Bob has a probability of failed state transfer that can be obtained from the generalisation of Eq. (3.8) to an arbitrary number of iterations. The joint probability that Bob fails to receive the state all the time is just the product of these probabilities. We denote the joint probability of failure for having done $\ell$ unsuccessful measurements as $P(\ell)$. This probability depends on the time intervals $t_\ell$ between the $(\ell-1)$th and $\ell$th measurement, and we are interested in the case where the $t_\ell$ are chosen such that the transfer is fast. It is possible to write a simple algorithm that computes $P(\ell)$ for any transition amplitude $f_{r,s}(t)$. Figure 3.3 shows some results obtained by choosing as the single chain $H^{(i)}$ terms of Eq. (3.1) the Heisenberg Hamiltonian given by

$$H_{\text{Heisenberg}} = J \sum_{n=1}^{N-1} (X_n X_{n+1} + Y_n Y_{n+1} + Z_n Z_{n,n+1}), \tag{3.10}$$

(here for $n = 1, \cdots, N$, $X_n$, $Y_n$ and $Z_n$ stand for the Pauli matrices of the $n$-th spin of the chain, while $J$ is a coupling parameter which set the time scale of the model).

An interesting question is whether the joint probability of failure can be made arbitrarily small with a large number of measurements. In fact, the times $t_\ell$ can be chosen such that the transfer becomes arbitrarily perfect. We will prove this in Sect. 3.4, where a generalisation of the dual-rail scheme and a much wider class of Hamiltonians is considered. In the limit of large number of measurements, the spin channel will not damp the initial amplitude, but only *delay* it.

### 3.2.2 Estimation of the Time-Scale the Transfer

The achievable fidelity is an important, but not the only criterion of a state transfer protocol. In this Section, we give an heuristic approach to estimate the time that it needs to achieve a certain fidelity in a Heisenberg spin chain. The comparison with numeric examples is confirming this approach.

Let us first describe the dynamic of the chain in a very qualitative way. Once Alice has initialised the system, an excitation wave packet will travel along the chain. As shown in [2], for the Heisenberg Hamiltonian of Eq. (3.10), it will reach Bob at a time of the order of

$$t_{\text{peak}} \approx \frac{N}{2J}, \tag{3.11}$$

with an amplitude of

$$\left| f_{N,1}(t_{\text{peak}}) \right|^2 \approx 1.82 N^{-2/3}. \tag{3.12}$$

It is then reflected and travels back and forth along the chain. Since the wave packet is also dispersing, it starts interfering with its tail, and after a couple of reflections the wave packet is spread over the whole chain. This effect becomes even stronger due to Bobs measurements, which change the dynamics by projecting away parts of the wave packet. We now assume that $2t_{\text{peak}}$ (the time it takes for a wave packet to travel twice along the chain) remains a good estimate of the time-scale in which significant probability amplitude peaks at Bobs site occur, and that Eq. (3.12) remains a good estimate of the amplitude of these peaks.[2] Therefore, the joint probability of failure is expected to scale as

$$P(\ell) \approx \left(1 - 1.82 N^{-2/3}\right)^{\ell} \tag{3.13}$$

in a time of the order of

$$t(\ell) \approx 2 t_{max} \ell = J^{-1} N \ell. \tag{3.14}$$

If we combine Eqs. (3.13) and (3.14) and solve for the time $t(P)$ needed to reach a certain probability of failure $P$, we get for $N \gg 1$

$$t(P) \approx 0.55 J^{-1} N^{5/3} \left| \ln P \right|. \tag{3.15}$$

[2] This is not a strong assumption. If the excitation was fully randomly distributed, the probability would scale as $N^{-1}$. By searching for good arrival times, this can be slightly increased to $N^{-2/3}$.

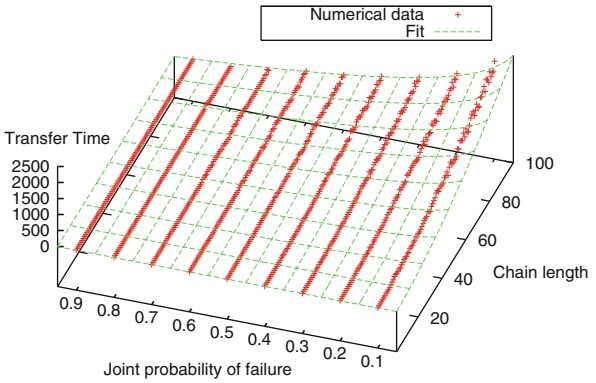


**Fig. 3.4** Time $t$ needed to transfer the state (3.4) with a given joint probability of failure $P$ across a chain of length $N$. The points denote exact numerical data obtained by solving the propagation of the system for the Heisenberg chain (3.10), and the fit is given by Eq. (3.16)

We compare this rough estimate with exact numerical results in Fig. 3.4. The best fit for the range shown in the figure is given by

$$t(P) = 0.33 J^{-1} N^{5/3} \left|\ln P\right| . \tag{3.16}$$

We can conclude that the transmission time for arbitrarily perfect transfer is scaling not much worse with the length $N$ of the chains than the single spin chain schemes. Despite of the logarithmic dependence on $P$, the time it takes to achieve high fidelity is still reasonable. For example, a system with $N = 100$ and $J = 20\,\mathrm{K}$ (expressed in units of the Boltzmann constant $k_B$) will take approximately 1.3 ns to achieve a fidelity of 99 %.

In many systems, decoherence is completely negligible within the time-scale associated with (3.16). For example, some Josephson junction systems [16] have a decoherence time of $T_\phi \approx 500\,\mathrm{ns}$, while trapped ions have even larger decoherence times. Nonetheless it is clear that if the coupling $J$ between the spins is very small, or the chains are very long, the transmission time (3.16) may no longer be negligible with respect to the decoherence time. It is interesting to note that also in these cases, the dual-rail encoding offers some significant general advantages over single chain schemes. Since we are suggesting a system-independent scheme, we will not study the effects of specific environments on the protocol, but just qualitatively point out its general advantages.

At least theoretically, it is always possible to cool the system down or to apply a strong magnetic field so that the environment is not causing further excitations. For example in flux qubit systems, the system is cooled to $\approx$25 mK to ensure that the energy splitting between qubit states $\Delta \gg k_B T$ [17]. Then, there are two remaining types of quantum noise that will occur: phase noise and amplitude damping. Phase noise is a serious problem and arises here *only* when an environment can distinguish

between spin flips on the first chain and spin flips on the second chain. It is therefore important that the environment cannot resolve their difference. In this case, the environment will only couple with the total $z$-component

$$Z_n^{(1)} + Z_n^{(2)} \tag{3.17}$$

of the spins of both chains at each position $n$. This has been discussed for spin-boson models in [18, 19] but also holds for spin environments as long as the chains are close enough. The qubit is encoded in a decoherence-free subspace [20] and the scheme is fully robust to phase noise. Even though this may not be true for all implementations of dual-rail encoding, it is worthwhile noticing it because such an opportunity does not exist *at all* for single chain schemes, where the coherence between two states with different total z-component of the spin has to be preserved. Having shown one way of avoiding phase noise, at least in some systems, we now proceed to analyze the effect of amplitude damping noise.

The evolution of the system in presence of amplitude damping of a rate $\Gamma$ can be easily derived using a quantum-jump approach [21]. This is based on a quantum master equation approach, which is valid in the Born-Markov approximation [22] (i.e. it holds for weakly coupled environments without memory effects). Similarly to phase noise, it is necessary that the environment acts symmetrically on the chains. The dynamics is then given by an effective non-Hermitian Hamiltonian

$$H_{\mathit{eff}} = H + i\Gamma \sum_n \left(Z_n^{(1)} + Z_n^{(2)} + 2\right)/2 \tag{3.18}$$

if no jump occurs. If a jump occurs, the system is back in the ground state $|\mathbf{0}\rangle$. The state of the system before the first measurement conditioned on no jump is given by

$$e^{-\Gamma t} \sum_{n=1}^{N} f_{n,1}(t)\, |\boldsymbol{s}(n)\rangle\,, \tag{3.19}$$

and this happens with the probability of $e^{-2\Gamma t}$ (the norm of the above state). If a jump occurs, the system will be in the ground state

$$\sqrt{1 - e^{-2\Gamma t}}\, |\mathbf{0}, \mathbf{0}\rangle\,. \tag{3.20}$$

The density matrix at the time $t$ is given by a mixture of (3.19) and (3.20). In case of (3.20), the quantum information is completely lost and Bob will always measure an unsuccessful state transfer. If Bob however measures a success, it is clear that no jump has occurred and he has the perfectly transferred state. Therefore the protocol *remains conclusive*, but the success probability is lowered by $e^{-2\Gamma t}$. This result is still valid for multiple measurements, which leave the state (3.20) unaltered. The probability of a successful transfer at each particular measurement $\ell$ will decrease by $e^{-2\Gamma t(\ell)}$, where $t(\ell)$ is the time at which the measurement takes place. After a certain number of measurements, the *joint* probability of failure will no longer

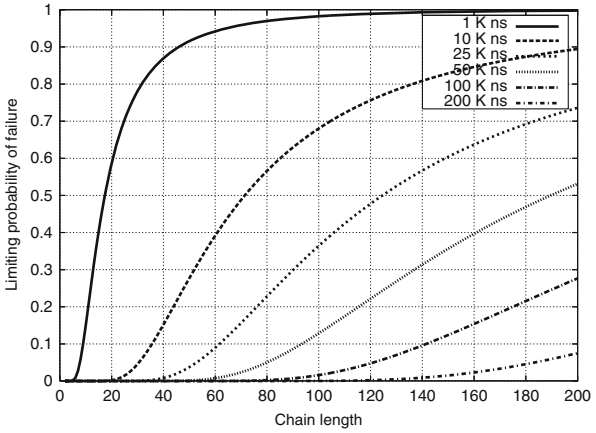


**Fig. 3.5** The minimal joint probability of failure $P(\ell)$ for chains with length $N$ in the presence of amplitude damping. The parameter $J/\Gamma$ of the curves is the coupling of the chain (in Kelvin) divided by the decay rate ($\mathrm{ns}^{-1}$)

decrease. Thus the transfer will no longer be *arbitrarily* perfect, but can still reach a very high fidelity. Some numerical examples of the minimal joint probability of failure that can be achieved,

$$\lim_{\ell\to\infty} P(\ell) \approx \prod_{\ell=1}^{\infty} \left(1 - 1.35N^{-2/3} e^{-\frac{2\Gamma N}{J}\ell}\right) \tag{3.21}$$

are given in Fig. 3.5. For $J/\Gamma = 50\,\mathrm{K\,ns}$ ($J$ being expressed in Kelvin) nearly perfect transfer is still possible for chains up to a length of $N \approx 40$.

Even if the amplitude damping is not symmetric, its effect is weaker than in single spin schemes. This is because it can be split in a symmetric and asymmetric part. The symmetric part can be overcome with the above strategies. For example, if the amplitude damping on the chains is $\Gamma_1$ and $\Gamma_2$ with $\Gamma_1 > \Gamma_2$, the state (3.19) will be

$$\sum_{n=1}^{N} f_{n,1}(t) \left\{\alpha e^{-\Gamma_2 t} \left|\mathbf{0}, \boldsymbol{n}\right\rangle + \beta e^{-\Gamma_1 t} \left|\boldsymbol{n}, \mathbf{0}\right\rangle\right\} \approx e^{-\Gamma_2 t} \sum_{n=1}^{N} f_{n,1}(t) \left|\boldsymbol{s}(n)\right\rangle \tag{3.22}$$

provided that $t \ll (\Gamma_1 - \Gamma_2)^{-1}$. Using a chain of length $N = 20$ with $J = 20\,\mathrm{K}$ and $\Gamma_1^{-1} = 4\,\mathrm{ns}$, $\Gamma_2^{-1} = 4.2\,\mathrm{ns}$ we would have to fulfil $t \ll 164\,\mathrm{ns}$. We could perform approximately 10 measurements (cf. Eq. (3.14)) without deviating too much from the state (3.22). In this time, we can use the protocol in the normal way. The resulting success probability given by the finite version of Eq. (3.21) would be 75 %. A similar reasoning is valid for phase noise, where the environment can be split into common and separate parts. If the chains are close, the common part will dominate and the separate parts can be neglected for short times.

## 3.3 Dual-Rail with Disordered and Coupled Chains

The main requirement for perfect transfer with dual-rail encoding presented in the previous sections is that two *identical* and *non-interacting* quantum chains have to be designed. While this is not so much a theoretical problem, for possible experimental realizations of the scheme [14] the question arises naturally how to cope with slight asymmetries of the channels or with small interactions which couple them. We are now going to demonstrate that in many cases, arbitrary perfect state transfer with dual-rail encoding is still possible even in these cases.

By doing so, we also offer a solution to another and perhaps more general problem: if one implements *any* of the schemes for quantum state transfer, the Hamiltonians will always be different from the theoretical ones by some random perturbation. This will lead to a decrease of fidelity in particular where specific energy levels were assumed (see [23, 24] for an analysis of fluctuations affecting chains with engineered Hamiltonians). This problem can be avoided using the scheme described below. Static disorder can lead to Anderson localisation [25–27] of the eigenstates, and therefore to low fidelity transport of quantum information. In this section however this is not relevant, as we consider only short chains ($N < 100$) and small disorder ($\approx 10\,\%$ of the coupling strength), and the localisation length is much longer then the length of the chain. We will show numerically that the dual rail scheme can still achieve arbitrarily perfect transfer for a uniformly coupled Heisenberg Hamiltonian with disordered coupling strengths (both for the case of spatially correlated and uncorrelated disorder). Moreover, for any two quantum chains, we show that Bob and Alice can check whether their system is capable of dual-rail transfer without directly measuring their Hamiltonians or local properties of the system along the chains but by only measuring *their* part of the system.

### *3.3.1 Transfer in the Presence of Disorder*

To address the effect of disorder, in contrast to the scenario described in Sect. 3.2, we now consider the case where the spin chains Hamiltonian $H^{(1)}$ and $H^{(2)}$ entering Eq. (3.1) are not identical. All other assumptions remain as before: in particular both chains are supposed to have the same length $N$ (but it will become clear in Sect. 3.3.2 that this requirement can be dropped) and Alice is asked to encodes her messages in the superpositions (3.4). The associated evolved state after a time $t$ can then be expressed as

$$\sum_{n=1}^{N} \left[\alpha g_{n,1}(t)\,|\mathbf{0},\boldsymbol{n}\rangle + \beta f_{n,1}(t)\,|\boldsymbol{n},\mathbf{0}\rangle\right], \tag{3.23}$$

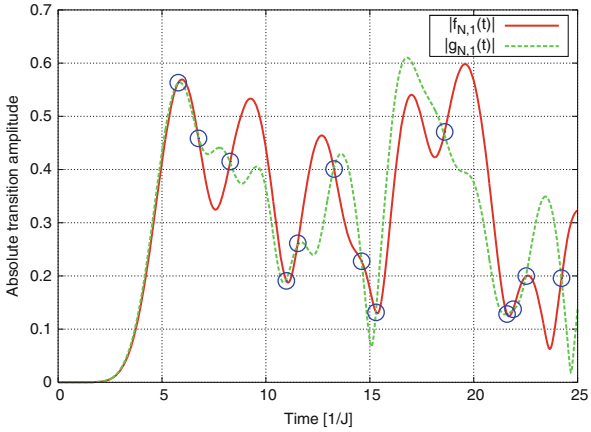


**Fig. 3.6** The absolute values of the transition amplitudes $f_{N,1}(t)$ and $g_{N,1}(t)$ for two Heisenberg chains of length $N = 10$. The couplings strengths of both chains were chosen randomly from the interval $[0.8J, 1.2J]$. The *circles* show times where Bob can perform measurements without gaining information on $\alpha$ and $\beta$

where now,

$$f_{n,1}(t) \equiv {}_1\langle \boldsymbol{n}| \exp[-iH^{(1)}t]|\mathbf{1}\rangle_1 \tag{3.24}$$

$$g_{n,1}(t) \equiv {}_2\langle \boldsymbol{n}| \exp[-iH^{(2)}t]|\mathbf{1}\rangle_2. \tag{3.25}$$

In Sect. 3.2 these functions were identical: this was a key feature which, leading to the identity (3.5), prevented Bob's subsequent operations from spoiling the coherence of Alice's input by hiding it into the vectors $|\boldsymbol{s}(n)\rangle$. For differing chains this is no longer the case. We may, however, find some special time $t_1$ such that the modulus of $f_{n,1}(t_1)$ and $g_{n,1}(t_1)$ for $n = N$ (i.e. on the last spins of the chains) are the same (see Fig. 3.6),

$$g_{N,1}(t_1) = e^{i\phi_1} f_{N,1}(t_1). \tag{3.26}$$

When this happens the state (3.23) can be written as

$$\sum_{n=1}^{N-1} \{\alpha g_{n,1}(t_1)\,|\mathbf{0}, \boldsymbol{n}\rangle + \beta f_{n,1}(t_1)\,|\boldsymbol{n}, \mathbf{0}\rangle\} + f_{N,1}(t_1)\left\{e^{i\phi_1}\alpha\,|\mathbf{0}, \boldsymbol{N}\rangle + \beta\,|\boldsymbol{N}, \mathbf{0}\rangle\right\}. \tag{3.27}$$

Therefore Bob can decode the state by applying a CNOT gate on his two qubits, with the first qubit as the control bit (same operation described in Sect. 3.2). The state thereafter is

$$\sum_{n=1}^{N-1} \{\alpha g_{n,1}(t_1)\,|\mathbf{0}, \boldsymbol{n}\rangle + \beta f_{n,1}(t_1)\,|\boldsymbol{n}, \mathbf{0}\rangle\} + f_{N,1}(t_1)\left\{e^{i\phi_1}\alpha\,|\mathbf{0}\rangle^{(1)} + \beta\,|\boldsymbol{N}\rangle^{(1)}\right\} \otimes |\boldsymbol{N}\rangle^{(2)}. \tag{3.28}$$

Bob then measures his second qubit. Depending on the outcome of this measurement, the system will either be in the state

$$\frac{1}{\sqrt{p_1}} \sum_{n=1}^{N-1} \{\alpha g_{n,1}(t_1) \, |\mathbf{0}, \boldsymbol{n}\rangle + \beta f_{n,1}(t_1) \, |\boldsymbol{n}, \mathbf{0}\rangle\} \tag{3.29}$$

or in

$$\left\{e^{i\phi_1}\alpha \, |\mathbf{0}\rangle^{(1)} + \beta \, |\boldsymbol{N}\rangle^{(1)}\right\} \otimes |\boldsymbol{N}\rangle^{(2)} , \tag{3.30}$$

where $p_1 = 1 - |f_{N,1}(t_1)|^2 = 1 - |g_{N,1}(t_1)|^2$ is the probability that Bob has *not* received the state. The state (3.30) corresponds to the correctly transferred state with a *known* phase error (which can be corrected by Bob using a simple phase gate). If Bob finds the system in the state (3.29), the transfer has been unsuccessful, but the information is still in the chain. We thus see that conclusive transfer is still possible with randomly coupled chains as long as the requirement (3.26) is met.

Arbitrarily perfect transfer can also be achieved. Indeed similarly to the ordered case discussed in Sect. 3.2.1, if after the first measurement the transfer was unsuccessful, the system, projected into the state (3.29), will evolve further, offering Bob further opportunities to receive Alice's message. For identical quantum chains, such strategy leads to a success for any reasonable Hamiltonian (Sect. 3.4.3). For differing chains, this is not necessarily the case, because measurements are only allowed at times where the probability amplitudes at the end of the chains are equal, and there may be systems where this is never the case. Still it is possible to provide a simple criterion that generalizes Eq. (3.26) and allows to check numerically whether a given system is capable of arbitrarily perfect state transfer. The quantity of interest for constructing such criterion is the joint probability $P(\ell)$ that after having checked $\ell$ times, Bob still has not received the proper state at his end of the chains. Optimally, this should approach zero if $\ell$ tends to infinity. In order to derive an expression for $P(\ell)$, let us assume that the transfer has been unsuccessful for $\ell - 1$ times with time intervals $t_\ell$ between the $\ell$th and the $(\ell - 1)$th measurement, and calculate the probability of failure at the $\ell$th measurement. In a similar manner, we assume that all the $\ell - 1$ measurements have met the requirement of conclusive transfer (that is, Bob's measurements are unbiased with respect to $\alpha$ and $\beta$) and derive the requirement for the $\ell$th measurement.

To calculate the probability of failure for the $\ell$th measurement, we need to take into account that Bob's measurements disturb the unitary dynamics of the chain. If the state before a measurement with the outcome "failure" is $|\psi\rangle$ , the state after the measurement will be

$$\frac{1}{\sqrt{p_\ell}} Q \, |\psi\rangle , \tag{3.31}$$

where $Q$ is the projector

$$Q = I - |\mathbf{0}, \boldsymbol{N}\rangle \langle \mathbf{0}, \boldsymbol{N}| - |\boldsymbol{N}, \mathbf{0}\rangle \langle \boldsymbol{N}, \mathbf{0}|, \tag{3.32}$$

and $p_\ell$ is the probability of failure at the $\ell$th measurement. The dynamics of the chain is alternating between unitary and projective, such that the state before the $\ell$th measurement can be expressed as

$$\frac{1}{\sqrt{P(\ell-1)}} \prod_{k=1}^{\ell} \{U(t_k)Q\} \{\alpha |\mathbf{1}, \mathbf{0}\rangle + \beta |\mathbf{0}, \mathbf{1}\rangle\}, \tag{3.33}$$

where

$$P(\ell-1) = \prod_{k=1}^{\ell-1} p_k. \tag{3.34}$$

Note that the operators in (3.33) do not commute and that the time ordering of the product (the index $k$ increases from right to left) is important. The probability that there is an excitation at the $N$th site of either chain is given by

$$\frac{1}{P(\ell-1)} \left\{ |\alpha|^2 |F(\ell)|^2 + |\beta|^2 |G(\ell)|^2 \right\}, \tag{3.35}$$

with

$$F(\ell) \equiv \langle \boldsymbol{N}, \mathbf{0}| \prod_{k=1}^{\ell} \{U(t_k)Q\} |\mathbf{1}, \mathbf{0}\rangle, \tag{3.36}$$

and

$$G(\ell) \equiv \langle \mathbf{0}, \boldsymbol{N}| \prod_{k=1}^{\ell} \{U(t_k)Q\} |\mathbf{0}, \mathbf{1}\rangle. \tag{3.37}$$

Bob's measurements are therefore unbiased with respect to $\alpha$ and $\beta$ if and only if

$$|F(\ell)| = |G(\ell)| \quad \forall \ell. \tag{3.38}$$

In this case, the state can still be transferred conclusively (up to a known phase), the probability of failure at the $\ell$th measurement being

$$p_\ell = 1 - \frac{|F(\ell)|^2}{P(\ell-1)}. \tag{3.39}$$

It is easy (but not very enlightening) to show [7] that the condition (3.38) is equivalent to

$$\left\| \prod_{k=1}^{\ell} \{U(t_k)Q\} \, |\mathbf{1},\mathbf{0}\rangle \right\| = \left\| \prod_{k=1}^{\ell} \{U(t_k)Q\} \, |\mathbf{0},\mathbf{1}\rangle \right\} \quad \forall \ell, \tag{3.40}$$

and that the joint probability of failure – if at each measurement the above condition is fulfilled – is simply given by

$$P(\ell) = \left\| \prod_{k=1}^{\ell+1} \{U(t_k)Q\} \, |\mathbf{1},\mathbf{0}\rangle \right\|^2 . \tag{3.41}$$

It may look as if Eq. (3.40) was a complicated multi-time condition for the measuring times $t_\ell$, that becomes increasingly difficult to fulfil with a growing number of measurements. This is not the case. If proper measuring times have been found for the first $\ell - 1$ measurements, a trivial time $t_\ell$ that fulfils Eq. (3.40) is $t_\ell = 0$. In this case, Bob measures immediately after the $(\ell - 1)$th measurement and the probability amplitudes on his ends of the chains will be equal – and zero (a useless measurement). But since the left and right hand side of Eq. (3.40) when seen as functions of $t_\ell$ are both almost-periodic functions with initial value zero, it is likely that they intersect many times, unless the system has some specific symmetry. Note that we do not claim at this point that any pair of chains will be capable of arbitrary perfect transfer. We will discuss in the next section how one can check this for a given system by performing some simple experimental tests.

### 3.3.2 Tomography

Suppose someone gives you two different experimentally designed spin chains. It may seem from the above that knowledge of the full Hamiltonian of both chains is necessary to check how well the system can be used for state transfer. This would be a very difficult task, because we would need access to all the spins along the channel to measure all the parameters of the Hamiltonian. In fact by expanding the projectors in Eq. (3.40) one can easily see that the only matrix elements of the evolution operator which are relevant for conclusive transfer are

$$f_{N,1}(t) = \langle \boldsymbol{N},\mathbf{0}| \, U(t) \, |\mathbf{1},\mathbf{0}\rangle \tag{3.42}$$

$$f_{N,N}(t) = \langle \boldsymbol{N},\mathbf{0}| \, U(t) \, |\boldsymbol{N},\mathbf{0}\rangle \tag{3.43}$$

$$g_{N,1}(t) = \langle \mathbf{0},\boldsymbol{N}| \, U(t) \, |\mathbf{0},\mathbf{1}\rangle \tag{3.44}$$

$$g_{N,N}(t) = \langle \mathbf{0},\boldsymbol{N}| \, U(t) \, |\mathbf{0},\boldsymbol{N}\rangle \, . \tag{3.45}$$

Physically, this means that the only relevant properties of the system are the transition amplitudes to *arrive* at Bob's ends and to *stay* there. The modulus of

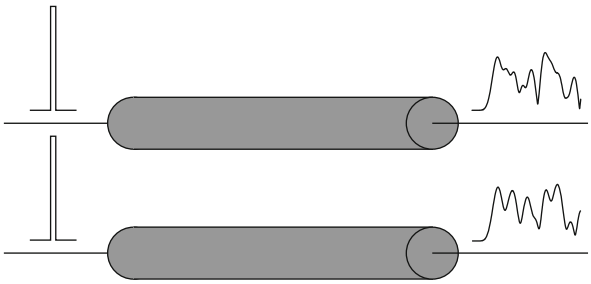

**Fig. 3.7** The relevant properties for conclusive transfer can be determined by measuring the response of the two systems at their ends only

$f_{N,1}(t)$ and $f_{N,N}(t)$ can be measured by initialising the system in the states $|\mathbf{1},\mathbf{0}\rangle$ and $|\boldsymbol{N},\mathbf{0}\rangle$ and then performing a density matrix tomography at Bob's site at different times $t$, and the complex phase of these functions is obtained by initialising the system in $(|\mathbf{0},\mathbf{0}\rangle + |\mathbf{1},\mathbf{0}\rangle)/\sqrt{2}$ and $(|\mathbf{0},\mathbf{0}\rangle + |\boldsymbol{N},\mathbf{0}\rangle)/\sqrt{2}$ instead. In the same way, $g_{N,1}(t)$ and $g_{N,N}(t)$ are obtained. All this can be done in the spirit of *minimal control* at the sending and receiving ends of the chain only, and needs to be done only once. It is interesting to note that the dynamics in the middle part of the chain is not relevant at all. It is a *black box* (see Fig. 3.7) that may involve even completely different interactions, number of spins, etc., as long as the total number of excitations is conserved. Once the transition amplitudes (Eqs. (3.42)–(3.45)) are known, one can search numerically for optimised measurement times $t_\ell$ using Eq. (3.41) and the condition from Eq. (3.40).

One weakness of the scheme described here is that the times at which Bob measures have to be very precise, because otherwise the measurements will not be unbiased with respect to $\alpha$ and $\beta$. This demand can be relaxed by measuring at times where not only the probability amplitudes are similar, but also their *slope* (see Fig. 3.6). In such a case small imperfections in the measurement timing should not matter. The computation of these optimal timings for a given system may be complicated, but it only needs to be done once. We also point out recent results that show that in one dimension, perhaps surprisingly, the mere knowledge of $f_{N,N}(t)$ and $g_{N,N}(t)$ implies knowledge of the system's Hamiltonian [28].

### 3.3.3 Numerical Examples

In this section, we show some numerical examples for two chains with Heisenberg couplings $J$ which are fluctuating. The Hamiltonians of the chains $i = 1, 2$ are given by

$$H^{(i)} = \sum_{n=1}^{N-1} J(1+\delta_n^{(i)}) \left( X_n^{(i)} X_{n+1}^{(i)} + Y_n^{(i)} Y_{n+1}^{(i)} + Z_n^{(i)} Z_{n+1}^{(i)} \right), \qquad (3.46)$$

**Table 3.1** The total time $t$ and the number of measurements $M$ needed to achieve a probability of success of 99 % for different fluctuation strengths $\Delta$ (uncorrelated case). Given is the statistical mean and the standard deviation. The length of the chain is $N = 20$ and the number of random samples is 10. For strong fluctuations $\Delta = 0.1$, we also found particular samples where the success probability could not be achieved within the time range searched by the algorithm

| | $\Delta = 0$ | $\Delta = 0.01$ | $\Delta = 0.03$ | $\Delta = 0.05$ | $\Delta = 0.1$ |
|---|---|---|---|---|---|
| $Jt$ | 377 | $524 \pm 27$ | $694 \pm 32$ | $775 \pm 40$ | $1{,}106 \pm 248$ |
| $M$ | 28 | $43 \pm 3$ | $58 \pm 3$ | $65 \pm 4$ | $110 \pm 25$ |

where $\delta_n^{(i)}$ are uniformly distributed random numbers from the interval $[-\Delta, \Delta]$. We have considered two different cases: in the first case, the $\delta_n^{(i)}$ are completely uncorrelated (i.e. independent for both chains and all sites along the chain). In the second case, we have taken into account a spatial correlation of the signs of the $\delta_n^{(i)}$ along each of the chains, while still keeping the two chains uncorrelated. Such correlations are relevant for Josephson junction chains [23]. For both cases, we find that arbitrarily perfect transfer remains possible except for some very rare realisations of the $\delta_n^{(i)}$.

Because measurements must only be taken at times which fulfil the condition (3.40), and these times usually do not coincide with the optimal probability of finding an excitation at the ends of the chains, it is clear that the probability of failure at each measurement will on average be higher than for chains without fluctuations. Therefore, more measurements have to be performed in order to achieve the same probability of success. The price for noisy couplings is thus a longer transmission time and a higher number of gating operations at the receiving end of the chains. Some averaged values are given in Table 3.1 for the Heisenberg chain with uncorrelated coupling fluctuations.

For the case where the signs of the $\delta_n^{(i)}$ are correlated, we have used the same model as in [23], introducing the parameter $c$ such that

$$\delta_n^{(i)} \delta_{n-1}^{(i)} > 0 \qquad \text{with propability } c, \tag{3.47}$$

and

$$\delta_n^{(i)} \delta_{n-1}^{(i)} < 0 \qquad \text{with propability } 1 - c. \tag{3.48}$$

For $c = 1$ ($c = 0$) this corresponds to the case where the signs of the couplings are completely correlated (anti-correlated). For $c = 0.5$ one recovers the case of uncorrelated couplings. We can see from the numerical results in Table 3.2 that arbitrarily perfect transfer is possible for the whole range of $c$.

For $\Delta = 0$, we know from Sect. 3.2.2 that the time to transfer a state with probability of failure $P$ scales as

$$t(P) = 0.33\, J^{-1} N^{1.6} \left| \ln P \right| . \tag{3.49}$$

**Table 3.2** The total time $t$ and the number of measurements $M$ needed to achieve a probability of success of 99 % for different correlations $c$ between the couplings (see Eqs. (3.47) and (3.48)). Given is the statistical mean and the standard deviation for a fluctuation strength of $\Delta = 0.05$. The length of the chain is $N = 20$ and the number of random samples is 20

| | $c = 0$ | $c = 0.1$ | $c = 0.3$ | $c = 0.7$ | $c = 0.9$ | $c = 1$ |
|---|---|---|---|---|---|---|
| $Jt$ | $666 \pm 20$ | $725 \pm 32$ | $755 \pm 41$ | $797 \pm 35$ | $882 \pm 83$ | $714 \pm 41$ |
| $M$ | $256 \pm 2$ | $62 \pm 3$ | $65 \pm 4$ | $67 \pm 4$ | $77 \pm 7$ | $60 \pm 4$ |

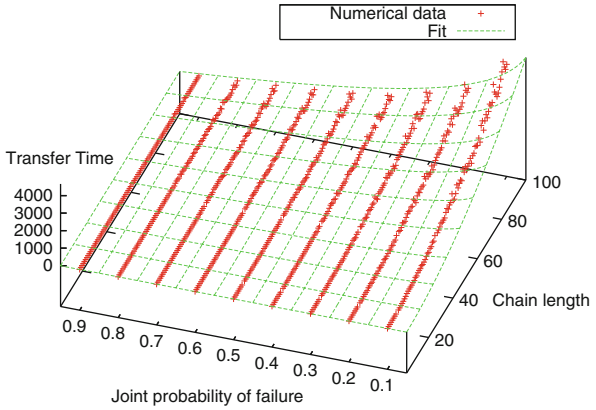


**Fig. 3.8** Time $t$ needed to transfer a state with a given joint probability of failure $P$ across a chain of length $N$ with uncorrelated fluctuations of $\Delta = 0.05$. The points denote numerical data averaged over 100 realisations, and the fit is given by Eq. (3.50). This figure should be compared with Fig. 3.4 where $\Delta = 0$

If we want to obtain a similar formula in the presence of noise, we can perform a fit to the exact numerical data. For uncorrelated fluctuations of $\Delta = 0.05$, this is shown in Fig. 3.8. The best fit is given by

$$t(P) = 0.2\, J^{-1} N^{1.9} |\ln P| \,. \tag{3.50}$$

We conclude that weak fluctuations (say up to 5 %) in the coupling strengths do not deteriorate the performance of the scheme much for the chain lengths considered. Both the transmission time and the number of measurements raise, but still in a reasonable way (cf. Table 3.1 and Fig. 3.8). For larger fluctuations, the scheme is still applicable in principle, but the amount of junk (i.e. chains not capable of arbitrary perfect transfer) may get too large.

Note that we have considered the case where the fluctuations $\delta_n^{(i)}$ are constant in time. This is a reasonable assumption if the dynamic fluctuations (e.g. those arising from thermal noise) can be neglected with respect to the constant fluctuations (e.g. those arising from manufacturing errors). If the fluctuations were varying with time, the tomography measurements in Sect. 3.3.2 would involve a time-average, and Bob


**Fig. 3.9** Most general setting for conclusive transfer: A *black box* with two inputs and two outputs, acting on states as defined by Eqs. (3.51) and (3.52)

would not measure exactly at the correct times. The transferred state (3.30) would then be affected by both phase and amplitude noise.

### *3.3.4 Coupled Chains*

We conclude the section by considering the case of chains which are mutually interacting. To address this configuration it is worth to look at the condition for conclusive transfer in the more general scenario indicated by Fig. 3.9: Alice and Bob have a black box acting as an amplitude damping channel in the following way. It has two inputs and two outputs. If Alice puts in state in the dual-rail,

$$|\psi\rangle = \alpha|01\rangle + \beta|10\rangle, \tag{3.51}$$

where $\alpha$ and $\beta$ are *arbitrary and unknown* normalised amplitudes, then the output at Bob is given by

$$p|\phi\rangle\langle\phi| + (1-p)\,|00\rangle\langle 00|, \tag{3.52}$$

with a normalised "success" state

$$|\phi\rangle = \frac{1}{\sqrt{p}}\Big[\alpha f|01\rangle + \beta g|10\rangle + \alpha\tilde{f}|10\rangle + \beta\tilde{g}|01\rangle\Big]. \tag{3.53}$$

This black box describes the behaviour of an arbitrarily coupled qubit system that conserves the number of excitations and that is initialised in the all zero state, including parallel uncoupled chains, and coupled chains (in fact, arbitrary networks). The parameters $f, g, \tilde{f}, \tilde{g}$ correspond to probability amplitudes which describe the transfer of spin excitations in the system.

From the normalisation of $|\phi\rangle$ it follows that

$$p = p(\alpha,\beta) = |\alpha f + \beta\tilde{g}|^2 + \left|\beta g + \alpha\tilde{f}\right|^2. \tag{3.54}$$

We are interested in conclusive transfer: by measuring the observable $|00\rangle\langle 00|$ Bob can project the output onto either the failure state $|00\rangle$ or $|\phi\rangle$. This is clearly possible,

but the question is if the output $|\phi\rangle$ and the input $|\psi\rangle$ are related by a *unitary* operation.

If Bob is able to recover the full information that Alice sent, then $p(\alpha, \beta)$ must be *independent of* $\alpha$ *and* $\beta$ (otherwise, some information on these amplitudes could be obtained by the measurement already, which contradicts the non-cloning theorem [4]). This implies that $p(1, 0) = p(0, 1)$, i.e.

$$|f|^2 + \left|\tilde{f}\right|^2 = |\tilde{g}|^2 + |g|^2 . \tag{3.55}$$

Because

$$p\left(\frac{1}{\sqrt{2}}, \frac{1}{\sqrt{2}}\right) = \frac{1}{2}|f + \tilde{g}|^2 + \frac{1}{2}\left|g + \tilde{f}\right|^2 \tag{3.56}$$

$$= p(1, 0) + \mathrm{Re}\left\{f^* \tilde{g} + g\tilde{f}^*\right\} \tag{3.57}$$

it also implies that

$$\mathrm{Re}\left\{f^* \tilde{g} + g\tilde{f}^*\right\} = 0. \tag{3.58}$$

Using the same trick for $p\left(\frac{1}{\sqrt{2}}, \frac{i}{\sqrt{2}}\right)$ we get that $\mathrm{Im}\left\{f^* \tilde{g} + g\tilde{f}^*\right\} = 0$ and therefore

$$f^* \tilde{g} + g\tilde{f}^* = 0. \tag{3.59}$$

If we write $|\psi\rangle = U|\phi\rangle$ we get

$$U = \frac{1}{\sqrt{p}} \begin{pmatrix} f & \tilde{f} \\ \tilde{g} & g \end{pmatrix}, \tag{3.60}$$

which is a unitary operator if Eqs. (3.55) and (3.59) hold. We thus come to the conclusion that conclusive transfer with the black box defined above is possible if and only if the probability $p$ is independent of $\alpha$ and $\beta$. It is interesting to note that a vertical mirror symmetry of the system does not guarantee this. A counterexample is sketched in Fig. 3.10: clearly the initial ("dark") state $|01\rangle - |10\rangle$ does not evolve, whereas $|01\rangle + |10\rangle$ *does*. Hence the probability must depend on $\alpha$ and $\beta$. A trivial case where conclusive transfer works is given by two uncoupled chains, at times where $|f|^2 = |g|^2$ (this is the case discussed in Sect. 3.2). A non-trivial example is given by the coupled system sketched in Fig. 3.11. This can be seen by splitting the Hamiltonian in a horizontal and vertical component,

$$H = H_v + H_z. \tag{3.61}$$

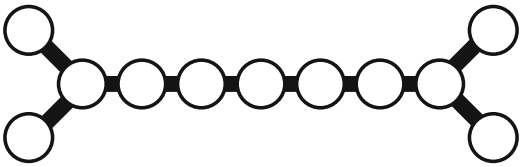

**Fig. 3.10** A simple counterexample for a vertically symmetric system where conclusive transfer is not possible. The *black lines* represent exchange couplings

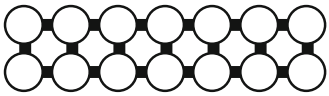

**Fig. 3.11** An example for a vertically symmetric system where conclusive transfer is possible. The *black lines* represent exchange couplings *of equal strength*

By applying $H_v H_z$ and $H_z H_v$ on single-excitation states it is easily checked that they commute in the first excitation sector (this is not longer true in higher sectors). Since the probability is independent of $\alpha$ and $\beta$ in the uncoupled case it must also be true in the coupled case (a rotation in the subspace $\{|01\rangle, |10\rangle\}$ does not harm). It is an interesting open question for which positions of the sender/receiver in a general network of spins these types of encoding are possible.

A final remark on dual-rail encoding – as Alice and Bob only deal with the states $\{|00\rangle, |10\rangle, |01\rangle\}$ it is obvious that the encoding used in this section is really living on *qutrits*. In some sense it would be more natural to consider permanently coupled systems of qutrits, such as SU(3) chains [6, 29–31]. The first level of the qutrit $|0\rangle$ is then used as a marker for "no information here", whereas the information is encoded in the states $|1\rangle$ and $|2\rangle$. One would have to ensure that there is no transition between $|0\rangle$ and $|1\rangle, |2\rangle$, and that the system is initialised in the all-zero state.

## 3.4 Multi-rail Encoding

In quantum information theory the rate $R$ of transferred qubits per channel is an important efficiency parameter [32]. In the dual-rail protocol of the last section, two chains were used for transferring one qubit, corresponding to a rate of $R = 1/2$. Therefore one question that naturally arises is whether or not there is any special meaning in the $1/2$ value. We will show now that this is not the case, because there is a way of bringing $R$ arbitrarily close to 1 by considering multi-rail encodings. Furthermore, in Sect. 3.2.1 it was still left open for which Hamiltonians the probability of success can be made arbitrarily close to 1. Here, we give a sufficient and easily attainable condition for achieving this goal.

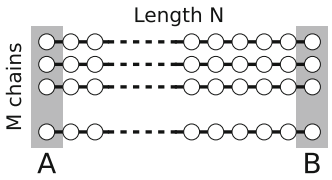


**Fig. 3.12** Schematic of the system: Alice and Bob operate $M$ chains, each containing $N$ spins. The spins belonging to the same chain interact through the Hamiltonian $H$ which accounts for the transmission of the signal in the system. Spins of different chains do not interact. Alice encodes the information in the first spins of the chains by applying unitary transformations to her qubits. Bob recovers the message in the last spins of the chains by performing joint measurements

Assume that the two communicating parties operate on $M$ independent (i.e. non interacting) copies of the chain. This is quite a common attitude in quantum information theory [32] where successive uses of a memoryless channel are formally described by introducing many parallel copies of the channel (see [5] for a discussion on the possibility of applying this formal description to quantum chain models). Moreover for the case at hand the assumption of Alice and Bob dealing with "real" parallel chains seems reasonable also from a practical point of view [11, 12]. The idea is to use these copies to improve the overall fidelity of the communication. As usual, we assume Alice and Bob to control respectively the first and last qubit of each chain (see Fig. 3.12). By preparing any superposition of her spins Alice can in principle transfer up to $M$ logical qubits. However, in order to improve the communication fidelity the two parties will find it more convenient to redundantly encode only a small number (say $Q(M) \leq M$) of logical qubits in the $M$ spins. By adopting these strategies Alice and Bob are effectively sacrificing the efficiency $R(M) \equiv Q(M)/M$ of their communication line in order to increase its fidelity. This is typical of any communication scheme and it is analogous to what happens in quantum error correction theory, where a single logical qubit is stored in many physical qubits. In the previous sections we have seen that for $M = 2$ it is possible to achieve perfect state transfer of a single logical qubit with an efficiency equal to $1/2$. Here we will generalise such result by proving that there exists an optimal encoding-decoding strategy which asymptotically allows to achieve perfect state transfer *and* optimal efficiency, i.e.

$$\lim_{M\to\infty} R(M) = 1 \,. \tag{3.62}$$

Our strategy requires Alice to prepare superpositions of the $M$ chains where $\sim M/2$ of them have a single excitation in the first location while the remaining are in $|\mathbf{0}\rangle$. Since in the limit $M \gg 1$ the number of qubit transmitted is $\log \binom{M}{M/2} \approx M$, this architecture guarantees optimal efficiency (3.62). On the other hand, the protocol requires Bob to perform collective measurements on his spins to determine if all the $\sim M/2$ excitations Alice is transmitting arrived at his location. We will prove that

by repeating these detections many times, Bob is able to recover the messages with asymptotically perfect fidelity.

Before beginning the analysis let us introduce some notation. The following definitions *look* more complicated than they really *are*; unfortunately we need them to carefully define the states that Alice uses for encoding the information. In order to distinguish the $M$ different chains we introduce the label $m = 1, \cdots, M$: in this formalism $|\boldsymbol{n}\rangle_m$ represents the state of $m$-th chain with a single excitation in the $n$-th spin. In the following we will be interested in those configurations of the whole system where $K$ chains have a single excitation while the remaining $M - K$ are in $|\mathbf{0}\rangle$, as in the case

$$|\mathbf{1}\rangle_1 \otimes |\mathbf{1}\rangle_2 \cdots \otimes |\mathbf{1}\rangle_K \otimes |\mathbf{0}\rangle_{K+1} \cdots \otimes |\mathbf{0}\rangle_M , \tag{3.63}$$

where for instance the first $K$ chains have an excitation in the first chain location. Another example is given in Fig. 3.13. The complete characterisation of these vectors is obtained by specifying *(i) which* chains possess a single excitation and *(ii) where* these excitations are located horizontally along the chains. In answering to the point *(i)* we introduce the $K$-element subsets $S_\ell$, composed by the labels of those chains that contain an excitation. Each of these subsets $S_\ell$ corresponds to a subspace of the Hilbert space $\mathscr{H}(S_\ell)$ with a dimension $N^K$. The total number of such subsets is equal to the binomial coefficient $\binom{M}{K}$, which counts the number of possibilities in which $K$ objects (excitations) can be distributed among $M$ parties (parallel chains). In particular for any $\ell = 1, \cdots, \binom{M}{K}$ the $\ell$-th subset $S_\ell$ will be specified by assigning its $K$ elements, i.e. $S_\ell \equiv \{m_1^{(\ell)}, \cdots, m_K^{(\ell)}\}$ with $m_j^{(\ell)} \in \{1, \cdots, M\}$ and $m_j^{(\ell)} < m_{j+1}^{(\ell)}$ for all $j = 1, \cdots, K$. To characterise the location of the excitations, point *(ii)*, we will introduce instead the $K$-dimensional vectors $\mathbf{n} \equiv (n_1, \cdots, n_K)$ where $n_j \in \{1, \cdots, N\}$. We can then define

$$|\mathbf{n}; \ell\rangle\rangle \equiv \bigotimes_{j=1}^{K} |\boldsymbol{n_j}\rangle_{m_j^{(\ell)}} \bigotimes_{m' \in \overline{S}_\ell} |\mathbf{0}\rangle_{m'} , \tag{3.64}$$

where $\overline{S}_\ell$ is the complementary of $S_\ell$ to the whole set of chains.

The state (3.64) represents a configuration where the $j$-th chain of the subset $S_\ell$ is in $|\boldsymbol{n_j}\rangle$ while the chains that do not belong to $S_\ell$ are in $|\mathbf{0}\rangle$ (see Fig. 3.13 for an explicit example). The kets $|\mathbf{n}; \ell\rangle\rangle$ are a natural generalisation of the states $|\boldsymbol{n}\rangle_1 \otimes |\mathbf{0}\rangle_2$ and $|\mathbf{0}\rangle_1 \otimes |\boldsymbol{n}\rangle_2$ which were used for the dual-rail encoding. They are useful for our purposes because they are mutually orthogonal, i.e.

$$\langle\langle \mathbf{n}; \ell | \mathbf{n'}; \ell' \rangle\rangle = \delta_{\ell\ell'} \, \delta_{\mathbf{n}\mathbf{n}'} , \tag{3.65}$$

and their time evolution under the Hamiltonian does not depend on $\ell$. Among the vectors (3.64) those where all the $K$ excitations are located at the beginning of the

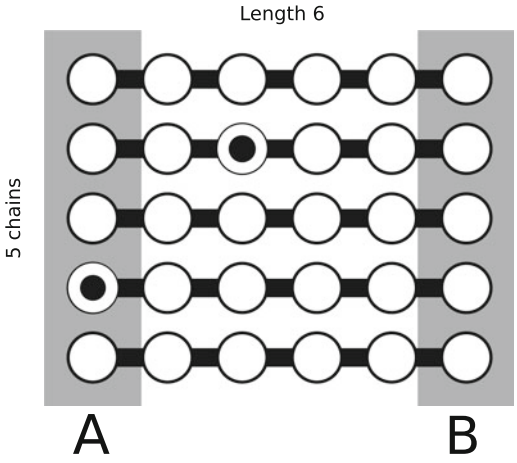


**Fig. 3.13** Example of our notation for $M = 5$ chains of length $N = 6$ with $K = 2$ excitations. The state above, given by $|\mathbf{0}\rangle_1 \otimes |\mathbf{3}\rangle_2 \otimes |\mathbf{0}\rangle_3 \otimes |\mathbf{1}\rangle_4 \otimes |\mathbf{0}\rangle_5$, has excitations in the chains $m_1 = 2$ and $m_2 = 4$ at the horizontal position $n_1 = 3$ and $n_2 = 1$. It is in the Hilbert space $\mathscr{H}(S_6)$ corresponding to the subset $S_6 = \{2, 4\}$ (assuming that the sets $S_\ell$ are ordered in a canonical way, i.e. $S_1 = \{1, 2\}$, $S_2 = \{1, 3\}$ and so on) and will be written as $|(3, 1); 6\rangle\rangle$. There are $\binom{5}{2} = 10$ different sets $S_\ell$ and the number of qubits one can transfer using these states is $\log_2 10 \approx 3$. The efficiency is thus given by $R \approx 3/5$ which is already bigger than in the dual-rail scheme

$S_\ell$ chains play an important role in our analysis. Here $\mathbf{n} = \mathbf{1} \equiv (1, \cdots, 1)$ and we can write

$$|\mathbf{1}; \ell\rangle\rangle \equiv \bigotimes_{m \in S_\ell} |\mathbf{1}\rangle_m \bigotimes_{m' \in \overline{S}_\ell} |\mathbf{0}\rangle_{m'} \,. \tag{3.66}$$

According to Eq. (3.65), for $\ell = 1, \cdots, \binom{M}{K}$ these states form orthonormal set of $\binom{M}{K}$ elements. Analogously by choosing $\mathbf{n} = \mathbf{N} \equiv (N, \cdots, N)$ we obtain the orthonormal set of $\binom{M}{K}$ vectors

$$|\mathbf{N}; \ell\rangle\rangle \equiv \bigotimes_{m \in S_\ell} |N\rangle_m \bigotimes_{m' \in \overline{S}_\ell} |\mathbf{0}\rangle_{m'}, \tag{3.67}$$

where all the $K$ excitations are located at the end of the chains.

If all the $M$ chains of the system are originally in $|\mathbf{0}\rangle$, the vectors (3.66) can be prepared by Alice by locally operating on her spins. Moreover since these vectors span a $\binom{M}{K}$ dimensional subspace, Alice can encode in the chain $Q(M, K) = \log_2 \binom{M}{K}$ qubits of logical information by preparing the superpositions,

$$|\Phi\rangle\rangle = \sum_\ell A_\ell \, |\mathbf{1}; \ell\rangle\rangle \,, \tag{3.68}$$

with $A_\ell$ complex coefficients. The efficiency of such encoding is hence $R(M,K) = \frac{\log_2 \binom{M}{K}}{M}$, which when maximised with respect to $K$ gives

$$R(M) = \frac{1}{M} \begin{cases} \log_2 \binom{M}{M/2} & \text{for } M \text{ even} \\ \log_2 \binom{M}{(M-1)/2} & \text{for } M \text{ odd} . \end{cases} \tag{3.69}$$

The Stirling approximation can then be used to prove that this encoding is asymptotically efficient (3.62) in the limit of large $M$, e.g.

$$\log_2 \binom{M}{M/2} \approx \log_2 \frac{M^M}{(M/2)^M} = M. \tag{3.70}$$

Note that already for $M = 5$ the encoding is more efficient (cf. Fig. 3.13) than in the dual-rail encoding. In the next section we show that the encoding (3.68) provides perfect state transfer by allowing Bob to perform joint measurements at his end of the chains.

### 3.4.1 Perfect State Transfer

Since the $M$ chains do not interact with each other and possess the same free Hamiltonian $H$, the unitary evolution of the whole system is described by $U(t) \equiv \otimes_m u_m(t)$, with $u_m(t)$ being the operator acting on the $m$-th chain. The time evolution of the input $|\mathbf{1};\ell\rangle\rangle$ of Eq. (3.66) is thus equal to

$$U(t)|\mathbf{1};\ell\rangle\rangle = \sum_{\mathbf{n}} F[\mathbf{n},\mathbf{1};t]\ |\mathbf{n};\ell\rangle\rangle\ , \tag{3.71}$$

where the sum is performed for all $n_j = 1,\cdots,N$ and

$$F[\mathbf{n},\mathbf{n'};t] \equiv f_{n_1,n'_1}(t)\cdots f_{n_K,n'_K}(t)\ , \tag{3.72}$$

is a quantity which does *not* depend on $\ell$. In Eq. (3.71) the term $\mathbf{n} = \mathbf{N}$ corresponds to having all the $K$ excitations in the last locations of the chains. We can split the summation into two components as

$$U(t)|\mathbf{1};\ell\rangle\rangle = \gamma_1(t)|\mathbf{N};\ell\rangle\rangle + \sqrt{1-|\gamma_1(t)|^2}\ |\boldsymbol{\xi}(t);\ell\rangle\rangle\ , \tag{3.73}$$

where

$$\gamma_1(t) \equiv \langle\langle \mathbf{N};\ell|U(t)|\mathbf{1};\ell\rangle\rangle = F[\mathbf{N},\mathbf{1};t] \tag{3.74}$$

is the probability amplitude that all the $K$ excitation of $|\mathbf{1};\ell\rangle\rangle$ arrive at the end of the chains, and

$$|\boldsymbol{\xi}(t);\ell\rangle\rangle \equiv \sum_{\mathbf{n}\neq\mathbf{N}} F_1[\mathbf{n},\mathbf{1};t]\ |\mathbf{n};\ell\rangle\rangle\ , \tag{3.75}$$

with

$$F_1[\mathbf{n},\mathbf{1};t] \equiv \frac{F[\mathbf{n},\mathbf{1};t]}{\sqrt{1-|\gamma_1(t)|^2}}, \tag{3.76}$$

is a superposition of terms where the number of excitations arrived to the end of the communication line is strictly less then $K$. It is worth noticing that Eq. (3.65) yields the following relations,

$$\langle\langle\mathbf{N};\ell|\boldsymbol{\xi}(t);\ell'\rangle\rangle = 0, \quad \langle\langle\boldsymbol{\xi}(t);\ell|\boldsymbol{\xi}(t);\ell'\rangle\rangle = \delta_{\ell\ell'}\ , \tag{3.77}$$

which shows that $\{||\boldsymbol{\xi}(t);\ell\rangle\rangle\}$ is an orthonormal set of vectors which spans a subspace orthogonal to the states $|\mathbf{N};\ell\rangle\rangle$. The time evolution of the input state (3.68) follows by linearity from Eq. (3.73), i.e.

$$|\Phi(t)\rangle\rangle = \gamma_1(t)\ |\Psi\rangle\rangle + \sqrt{1-|\gamma_1(t)|^2}\ |\overline{\Psi}(t)\rangle\rangle\ , \tag{3.78}$$

with

$$\begin{aligned} |\overline{\Psi}(t)\rangle\rangle &\equiv \sum_{\ell} A_\ell\ |\boldsymbol{\xi}(t);\ell\rangle\rangle\ , \\ |\Psi\rangle\rangle &\equiv \sum_{\ell} A_\ell\ |\mathbf{N};\ell\rangle\rangle\ . \end{aligned} \tag{3.79}$$

The vectors $|\Psi\rangle\rangle$ and $|\overline{\Psi}(t)\rangle\rangle$ are unitary transformations of the input message (3.68) where the orthonormal set $\{|\mathbf{1};\ell\rangle\rangle\}$ has been rotated into $\{|\mathbf{N};\ell\rangle\rangle\}$ and $\{|\boldsymbol{\xi}(t);\ell\rangle\rangle\}$ respectively. Moreover $|\Psi\rangle\rangle$ is the configuration we need to have for perfect state transfer at the end of the chain. In fact it is obtained from the input message (3.68) by replacing the components $|\mathbf{1}\rangle$ (excitation in the first spin) with $|N\rangle$ (excitation in the last spin). From Eq. (3.77) we know that $|\Psi\rangle\rangle$ and $|\overline{\Psi}(t)\rangle\rangle$ are orthogonal. This property helps Bob to recover the message $|\Psi\rangle\rangle$ from $|\Phi(t)\rangle\rangle$: he only needs to perform a collective measurement on the $M$ spins he is controlling to establish if there are $K$ or less excitations in those locations. The above is clearly a projective measurement that can be performed without destroying the quantum coherence associated with the coefficients $A_\ell$. Formally this can described by introducing the observable

$$\Theta \equiv I - \sum_{\ell} |\mathbf{N};\ell\rangle\rangle\langle\langle\mathbf{N};\ell|\ . \tag{3.80}$$

A single measurement of $\Theta$ on $|\Phi(t_1)\rangle\!\rangle$ yields the outcome 0 with probability $p_1 \equiv |\gamma_1(t_1)|^2$, and the outcome $+1$ with probability $1 - p_1$. In the first case the system will be projected in $|\Psi\rangle\!\rangle$ and Bob will get the message. In the second case instead the state of the system will become $|\overline{\Psi}(t_1)\rangle\!\rangle$. Already at this stage the two communicating parties have a success probability equal to $p_1$. Moreover, as in the dual-rail protocol, the channels have been transformed into a quantum erasure channel [15] where the receiver knows if the transfer was successful. Just like the dual-rail encoding, this encoding can be used as a simple entanglement purification method in quantum chain transfer (see end of Sect. 3.2). The rate of entanglement that can be distilled is given by

$$R(M)\,|F[\mathbf{N},\mathbf{1};t]|^2 = R(M)\,p(t)^{\lfloor M/2\rfloor}, \tag{3.81}$$

where we used Eq. (3.72) and $p(t) \equiv |f_{N,1}(t)|^2$. As we can see, increasing $M$ on one hand increases $R(M)$, but on the other hand decreases the factor $p(t)^{\lfloor M/2\rfloor}$. Its maximum with respect to $M$ gives us a lower bound of the entanglement of distillation for a single spin chain. We can also see that it becomes worth encoding on more than *three* chains for conclusive transfer only when $p(t) > 0.8$.

Consider now what happens when Bob fails to get the right answer from the measurement. The state of the chains is projected onto

$$|\overline{\Psi}(t_1)\rangle\!\rangle = \sum_{\mathbf{n}\neq\mathbf{N}} F_1[\mathbf{n},\mathbf{1};t_1] \sum_{\ell} A_\ell |\mathbf{n};\ell\rangle\!\rangle\ . \tag{3.82}$$

Let us now consider the evolution of this state for another time interval $t_2$. By repeating the same analysis given above we obtain an expression similar to (3.78), i.e.

$$|\Phi(t_2,t_1)\rangle\!\rangle = \gamma_2\,|\Psi\rangle\!\rangle + \sqrt{1-|\gamma_2|^2}\,|\overline{\Psi}(t_2,t_1)\rangle\!\rangle\ , \tag{3.83}$$

where now the probability amplitude of getting all excitation in the $N$-th locations is described by

$$\gamma_2 \equiv \sum_{\mathbf{n}\neq\mathbf{N}} F[\mathbf{N},\mathbf{n};t_2]\ F_1[\mathbf{n},\mathbf{1};t_1]. \tag{3.84}$$

In this case $|\overline{\Psi}(t)\rangle\!\rangle$ is replaced by

$$|\overline{\Psi}(t_2,t_1)\rangle\!\rangle = \sum_{\ell} A_\ell\ |\boldsymbol{\xi}(t_2,t_1);\ell\rangle\!\rangle\ , \tag{3.85}$$

with

$$|\boldsymbol{\xi}(t_2,t_1);\ell\rangle\!\rangle = \sum_{\mathbf{n}\neq\mathbf{N}} F_2[\mathbf{n},\mathbf{1};t_2,t_1]|\mathbf{n};\ell\rangle\!\rangle, \tag{3.86}$$

and $F_2$ defined as in Eq. (3.88) (see below). In other words, the state $|\Phi(t_2, t_1)\rangle\rangle$ can be obtained from Eq. (3.78) by replacing $\gamma_1$ and $F_1$ with $\gamma_2$ and $F_2$. Bob can hence try to use the same strategy he used at time $t_1$: i.e. he will check whether or not his $M$ qubits contain $K$ excitations. With (conditional) probability $p_2 \equiv |\gamma_2|^2$ he will get a positive answer and his quantum register will be projected in the state $|\Psi\rangle\rangle$ of Eq. (3.79). Otherwise he will let the system evolve for another time interval $t_3$ and repeat the protocol. By reiterating the above analysis it is possible to give a recursive expression for the conditional probability of success $p_q \equiv |\gamma_q|^2$ after $q-1$ successive unsuccessful steps. The quantity $\gamma_q$ is the analogue of $\gamma_2$ and $\gamma_1$ of Eqs. (3.74) and (3.83). It is given by

$$\gamma_q \equiv \sum_{\mathbf{n}\neq\mathbf{N}} F[\mathbf{N}, \mathbf{n}; t_q]\ F_{q-1}[\mathbf{n}, \mathbf{1}, t_{q-1}, \cdots, t_1]\ , \tag{3.87}$$

where

$$\begin{aligned} &F_{q-1}[\mathbf{n}, \mathbf{1}; t_{q-1}, \cdots, t_1] \\ &\equiv \sum_{\mathbf{n}'\neq\mathbf{N}} \frac{F[\mathbf{N}, \mathbf{n}'; t_{q-1}]}{\sqrt{1-|\gamma_{q-1}|^2}} F_{q-2}[\mathbf{n}', \mathbf{1}; t_{q-2}, \cdots, t_1] \end{aligned} \tag{3.88}$$

and $F_1[\mathbf{n}, \mathbf{1}, t]$ is given by Eq. (3.76). In these equations $t_q, \cdots, t_1$ are the *time-intervals* that occurred between the various protocol steps. Analogously the conditional probability of failure at the step $q$ is equal to $1 - p_q$. The probability of having $j-1$ failures and a success at the step $j$-th can thus be expressed as

$$\pi(j) = p_j(1-p_{j-1})(1-p_{j-2})\cdots(1-p_1)\ , \tag{3.89}$$

while the total probability of success after $q$ steps is obtained by the sum of $\pi(j)$ for all $j = 1, \cdots, q$, i.e.

$$P_q = \sum_{j=1}^{q} \pi(j)\ . \tag{3.90}$$

Since $p_j \geq 0$, Eq. (3.90) is a monotonic function of $q$. As a matter of fact in the next section we prove that under a very general hypothesis on the system Hamiltonian, the probability of success $P_q$ converges to 1 in the limit of $q \to \infty$. This means that by repeating many times the collective measure described by $\Theta$ Bob is guaranteed to get, sooner or later, the answer 0 and hence the message Alice sent to him. In other words the protocol allows perfect state transfer in the limit of repetitive collective measures. Notice that the above analysis applies for all classes of subsets $S_\ell$. The only difference between different choices of $K$ is in the velocity of the convergence of $P_q \to 1$. In any case, by choosing $K \sim M/2$ Alice and Bob can achieve perfect fidelity *and* optimal efficiency.

### 3.4.2 Convergence Theorem

**Theorem 1 (Arbitrarly perfect transfer).** *If there is no eigenvector* $|e_m\rangle$ *of the quantum chain Hamiltonian* $H$ *which is orthogonal to* $|\boldsymbol{N}\rangle$*, then there is a choice of the times intervals* $t_q, t_{q-1}, \cdots, t_1$ *such that the fidelity converges to* 1 *as* $q \to \infty$.

Before proving this Theorem, let us give an intuitive reasoning for the convergence. The unitary evolution can be thought of a *rotation* in some abstract space, while the measurement corresponds to a *projection.* The dynamics of the system is then represented by alternating rotations and projections. In general this will decrease the norm of each vector to null, unless the rotation axis is *the same* as the projection axis.

*Proof.* The state of the system at a time interval of $t_q$ after the $(q-1)$-th failure can be expressed in compact form as follows

$$|\Phi(t_q, \cdots, t_1)\rangle\!\rangle = \frac{U(t_q)\Theta U(t_{q-1})\Theta \cdots U(t_1)\Theta|\Phi\rangle\!\rangle}{\sqrt{(1-p_{q-1})\cdots(1-p_1)}} \tag{3.91}$$

with $U(t)$ the unitary time evolution generated by the system Hamiltonian, and with $\Theta$ the projection defined in Eq. (3.80). One can verify for instance that for $q = 2$, the above equation coincides with Eq. (3.83). (For $q = 1$ this is just (3.78) evaluated at time $t_1$.) By definition the conditional probability of success at step $q$-th is equal to

$$p_q \equiv |\langle\!\langle \Psi|\Phi(t_q, \cdots, t_1)\rangle\!\rangle|^2. \tag{3.92}$$

Therefore, Eq. (3.89) yields

$$\begin{aligned} \pi(q) &= |\langle\!\langle \Psi|U(t_q)\Theta U(t_{q-1})\Theta \cdots U(t_1)\Theta|\Phi\rangle\!\rangle|^2 \\ &= |\langle\!\langle \mathbf{N};\ell|U(t_q)\Theta U(t_{q-1})\Theta \cdots U(t_1)\Theta|\mathbf{1};\ell\rangle\!\rangle|^2 \,, \end{aligned} \tag{3.93}$$

where the second identity stems from the fact that, according to Eq. (3.65), $U(t)\Theta$ preserves the orthogonality relation among states $|\mathbf{n};\ell\rangle\!\rangle$ with distinct values of $\ell$. In analogy to the cases of Eqs. (3.72) and (3.74), the second identity of (3.93) establishes that $\pi(q)$ can be computed by considering the transfer of the input $|\mathbf{1};\ell\rangle\!\rangle$ for *arbitrary* $\ell$. The expression (3.93) can be further simplified by noticing that for a given $\ell$ the chains of the subset $\overline{S}_\ell$ contribute with a unitary factor to $\pi(q)$ and can be thus neglected (according to (3.66) they are prepared in $|\mathbf{0}\rangle$ and do not evolve under $U(t)\Theta$). Identify $|\mathbf{1}\rangle\!\rangle_\ell$ and $|\mathbf{N}\rangle\!\rangle_\ell$ with the components of $|\mathbf{1};\ell\rangle\!\rangle$ and $|\mathbf{N};\ell\rangle\!\rangle$ relative to the chains belonging to the subset $S_\ell$. In this notation we can rewrite Eq. (3.93) as

$$\pi(q) = |{}_\ell\langle\!\langle \mathbf{N}|U_\ell(t_q)\Theta_\ell \ \cdots U_\ell(t_1)\Theta_\ell|\mathbf{1}\rangle\!\rangle_\ell|^2 \,, \tag{3.94}$$

where $\Theta_\ell = 1 - |\mathbf{N}\rangle\!\rangle_\ell \langle\!\langle \mathbf{N}|$ and $U_\ell(t)$ is the unitary operator $\otimes_{m\in S_\ell} u_m(t)$ which describes the time evolution of the chains of $S_\ell$. To prove that there exist suitable choices of $t_\ell$ such that the series (3.90) converges to 1 it is sufficient to consider the case $t_\ell = t > 0$ for all $j = 1, \cdots, q$: this is equivalent to selecting decoding protocols with constant measuring intervals. By introducing the operator $T_\ell \equiv U_\ell(t)\Theta_\ell$, Eq. (3.94) becomes thus

$$\begin{aligned} \pi(q) &= |_\ell\langle\!\langle \mathbf{N}|\ (T_\ell)^q\, |\mathbf{1}\rangle\!\rangle_\ell|^2 \\ &=_\ell\langle\!\langle \mathbf{1}|(T_\ell^\dagger)^q\, |\mathbf{N}\rangle\!\rangle_\ell \langle\!\langle \mathbf{N}|\ (T_\ell)^q\, |\mathbf{1}\rangle\!\rangle_\ell = w(q) - w(q+1)\ , \end{aligned} \tag{3.95}$$

where

$$w(j) \equiv_\ell \langle\!\langle \mathbf{1}|(T_\ell^\dagger)^j\ (T_\ell)^j\, |\mathbf{1}\rangle\!\rangle_\ell = \|(T_\ell)^j\, |\mathbf{1}\rangle\!\rangle_\ell\|^2\ , \tag{3.96}$$

is the norm of the vector $(T_\ell)^j\, |\mathbf{1}\rangle\!\rangle_\ell$. Substituting Eq. (3.95) in Eq. (3.90) yields

$$P_q = \sum_{j=1}^{q} [w(j) - w(j+1)] = 1 - w(q+1) \tag{3.97}$$

where the property $w(1) = {}_\ell\langle\!\langle \mathbf{1}|\Theta_\ell|\mathbf{1}\rangle\!\rangle_\ell = 1$ was employed. Proving the thesis is hence equivalent to prove that for $q \to \infty$ the succession $w(q)$ nullifies. This last relation can be studied using properties of power bounded matrices [33]. In fact, by introducing the norm of the operator $(T_\ell)^q$ we have,

$$w(q) = \|(T_\ell)^q\, |\mathbf{1}\rangle\!\rangle_\ell\|^2 \leq \|(T_\ell)^q\|^2 \leq c \left(\frac{1+\rho(T_\ell)}{2}\right)^{2q} \tag{3.98}$$

where $c$ is a positive constant which does not depend on $q$ (if $S$ is the similarity transformation that puts $T_\ell$ into the Jordan canonical form, i.e. $J = S^{-1} T_\ell S$, then $c$ is given explicitly by $c = \|S\|\ \|S^{-1}\|$) and where $\rho(T_\ell)$ is the spectral radius of $T_\ell$, i.e. the eigenvalue of $T_\ell$ with maximum absolute value (N.B. even when $T_\ell$ is not diagonalisable this is a well defined quantity). Equation (3.98) shows that $\rho(T_\ell) < 1$ is a sufficient condition for $w(q) \to 0$. In our case we note that, given any normalised eigenvector $|\lambda\rangle\!\rangle_\ell$ of $T_\ell$ with eigenvalue $\lambda$ we have

$$|\lambda| = \|T_\ell |\lambda\rangle\!\rangle_\ell\| = \|\Theta_\ell |\lambda\rangle\!\rangle_\ell\| \leq 1\ , \tag{3.99}$$

where the inequality follows from the fact that $\Theta_\ell$ is a projector. Notice that in Eq. (3.99) the identity holds only if $|\lambda\rangle\!\rangle$ is also an eigenvector of $\Theta_\ell$ with eigenvalue $+1$, i.e. only if $|\lambda\rangle\!\rangle_\ell$ is orthogonal to $|\mathbf{N}\rangle\!\rangle_\ell$. By definition $|\lambda\rangle\!\rangle_\ell$ is eigenvector $T_\ell = U_\ell(t)\Theta_\ell$: therefore the only possibility to have the equality in Eq. (3.99) is that *(i)*

$|\lambda\rangle\!\rangle_\ell$ is an eigenvector of $U_\ell(t)$ (i.e. an eigenvector of the Hamiltonian[3] $H_\ell^{\rm tot}$ of the chain subset $S_\ell$) and *(ii)* it is orthogonal to $|\mathbf{N}\rangle\!\rangle_\ell$. By negating the above statement we get a sufficient condition for the thesis. Namely, if all the eigenvectors $|\mathbf{E}\rangle\!\rangle_\ell$ of $H_\ell^{\rm tot}$ are not orthogonal to $|\mathbf{N}\rangle\!\rangle_\ell$ than the absolute values of the eigenvalues $\lambda$ of $T_\ell$ are strictly smaller than 1 which implies $\rho(T_\ell) < 1$ and hence the thesis. Since the $S_\ell$ channels are identical and do not interact, the eigenvectors $|\mathbf{E}\rangle\!\rangle_\ell \equiv \bigotimes_{m\in S_\ell} |e_m\rangle_m$ are tensor product of eigenvectors $|e_m\rangle$ of the single chain Hamiltonians $H$. Therefore the sufficient condition becomes

$$ {}_\ell\langle\!\langle \mathbf{E}|\mathbf{N}\rangle\!\rangle_\ell = \prod_{m\in S_\ell} {}_m\langle \boldsymbol{N}|e_m\rangle_m \neq 0 \,, \tag{3.100} $$

which can be satisfied only if $\langle \boldsymbol{N}|e_m\rangle \neq 0$ for all eigenvectors $|e_m\rangle$ of the single chain Hamiltonian $H$.

*Remark 1.* While we have proven here that for equal time intervals the probability of success is converging to unity, in practice one may use *optimal* measuring time intervals $t_i$ for a faster transfer (see also Sect. 3.2.2). We also point out that timing errors may delay the transfer, but will not decrease its fidelity.

### 3.4.3 Quantum Chains with Nearest-Neighbour Interactions

It is worth noticing that Eq. (3.100) is a very weak condition, because eigenstates of Hamiltonians are typically entangled. For instance, it holds for open chains with nearest neighbour-interactions.

**Theorem 2 (Multi-rail protocol).** *Let $H$ be the Hamiltonian of an open nearest-neighbour quantum chain that conserves the number of excitations. If there is a time $t$ such that $f_{1,N}(t) \neq 0$ (i.e. the Hamiltonian is capable of at least partially transferring excitations from Alice to Bob) then the state transfer can be made arbitrarily perfect by using the multi-rail protocol.*

*Proof.* We show by contradiction that the criterion of Theorem 1 is fulfilled. Assume there exists a normalised eigenvector $|e\rangle$ of the single chain Hamiltonian $H$ such that

$$ \langle \boldsymbol{N}|e\rangle = 0. \tag{3.101} $$

[3]Notice that strictly speaking the eigenvectors of the Hamiltonian are not the same as those of the time evolution operators. The latter still can have evolution times at which additional degeneracy can increase the set of eigenstates. A trivial example is given for $t = 0$ where *all* states become eigenstates. But it is always possible to find times $t$ at which the eigenstates of $U(t)$ coincide with those of $H$.

Because $|e\rangle$ is an eigenstate, we can conclude that also

$$\langle e\,|H|\,\boldsymbol{N}\rangle = 0. \tag{3.102}$$

If we act with the Hamiltonian on the ket in Eq. (3.102) we may get some term proportional to $\langle e|\boldsymbol{N}\rangle$ (corresponding to an Ising-like interaction) and some part proportional to $\langle e|\boldsymbol{N-1}\rangle$ (corresponding to a hopping term). Since there are only nearest neighbor interactions, there cannot be any other terms, and we get

$$a\,\langle e|\boldsymbol{N}\rangle + b\langle e|\boldsymbol{N-1}\rangle = 0. \tag{3.103}$$

for some coefficients $a, b$. Moreover, $b \neq 0$: if this term did not exist, then clearly $f_{1,N}(t) = 0$ for all times, contrary to the assumptions of the theorem. We can thus conclude that

$$\langle e|\boldsymbol{N-1}\rangle = 0. \tag{3.104}$$

Note that for a closed chain, e.g. a ring, this need not be the case, because then also a term proportional to $\langle e|\boldsymbol{N+1}\rangle = \langle e|\boldsymbol{1}\rangle$ would occur. If we insert the Hamiltonian into Eq. (3.104) again, we can use the same reasoning to see that

$$\langle e|\boldsymbol{N-2}\rangle = \cdots = \langle e|\boldsymbol{1}\rangle = 0 \tag{3.105}$$

and hence $|e\rangle = 0$, which is a contradiction to $|e\rangle$ being normalised.

### 3.4.4 Comparison with Dual-Rail

As we have seen above, the multi-rail protocol allows us in principle to reach in principle a rate arbitrarily close to one. However for a fair comparison with the dual-rail protocol, we should also take into account the time-scale of the transfer. For the conclusive transfer of entanglement, we have seen in Sect. 3.4.1 that only for chains which have a success probability higher than $p(t) = 0.8$ it is worth encoding on more than three rails. The reason is that if the probability of success for a single excitation is $p$, then the probability of success for $\lfloor M/2 \rfloor$ excitations on $M$ parallel chains is lowered to $p^{\lfloor M/2 \rfloor}$. The protocol for three rails is always more efficient than on two, as still only one excitation is being used, but three complex amplitudes can be transferred per usage.

For arbitrarily perfect transfer, the situation is slightly more complicated as the optimal choice of $M$ also depends on the joint probability of failure that one plans to achieve. Let us assume that at each step of the protocol, the success probability on a single chain is $p$. Then the number of steps to achieve a given probability of failure $P$ using $M$ chains is given by

$$\ell(P, M) = \max\left\{\frac{\ln P}{\ln(1 - p^{\lfloor M/2 \rfloor})}, 1\right\}. \tag{3.106}$$

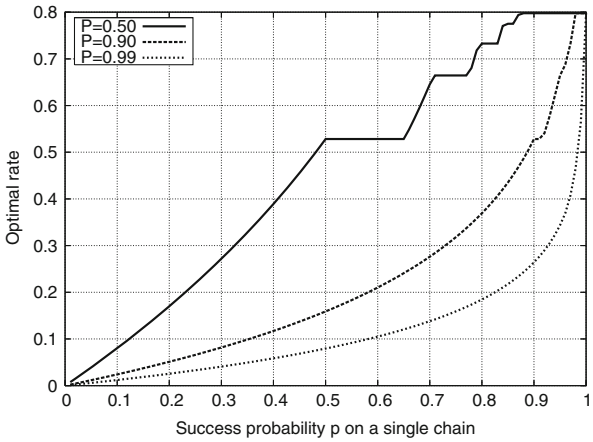


**Fig. 3.14** Optimal rates (maximisation of Eq. (3.107) with respect to $M$) for the multi-rail protocol. Shown are three curves corresponding to different values of the joint probability of failure $P$ one plans to achieve

If we assume that the total time-scale of the transfer is proportional to the number of steps, then the number of qubits that can be transferred per time interval is given by

$$v(P, M) \propto R(M)/\ell(P, M). \tag{3.107}$$

Optimising this rate with respect to $M$ we find three different regimes of the joint probability of failure (see Fig. 3.14). If one is happy with a large $P$, then the multi-rail protocol becomes superior to the dual-rail for medium $p$. For intermediate $P$, the threshold is comparable to the threshold of $p = 0.8$ for conclusive transfer of entanglement. Finally for very low $P$ the multi-rail only becomes useful for $p$ very close to one. In all three cases the threshold is higher than the $p(t)$ that can usually achieved with unmodulated Heisenberg chains. We can thus conclude that the multi-rail protocol only becomes useful for chains which already have a very good performance.

## 3.5 Conclusion

In conclusion, we have presented a simple scheme for conclusive and arbitrarily perfect quantum state transfer. To achieve this, two parallel spin chains (individually amplitude damping channels) have been used as one *amplitude delaying channel*. We have shown that the scheme is more robust to decoherence and imperfect timing than the single chain schemes. We have also shown that the scheme is applicable to disordered and coupled chains. The scheme can be used as a way of improving any of the other schemes from the introduction. For instance, one may try to engineer the couplings to have a very high probability of success already at the first measurement, and use further measurements to compensate the errors of implementing the correct values for the couplings. We remark that the dual-rail protocol is unrelated to error

filtration [34] where parallel channels are used for filtering out environmental effects on flying qubits, whereas the purpose of the dual-rail protocol is to ensure the *arrival* of the qubit. Indeed one could combine both protocols to send a qubit on say four rails to ensure the arrival *and* filter errors. We note that in [35] it was shown that the encoding can be used to perform quantum gates while the state is transferred, and that it can increase the convergence speed if one performs measurements at intermediate positions [36, 37].

Moving on to a multi-rail encoding, we have shown that any nearest-neighbour Hamiltonian that can transfer quantum information with nonzero fidelity (including the Heisenberg chains analysed above) is capable of efficient *and* perfect transfer when used in the context of parallel chains. Hamiltonians with non-nearest neighbour interactions [38, 39] can also be used as long as the criterion of Theorem 1 is fulfilled.

## References


1. R. Raussendorf, H.J. Briegel, Phys. Rev. Lett. **86**, 5188 (2001)
2. S. Bose, Phys. Rev. Lett. **91**, 207901 (2003)
3. M. Christandl, N. Datta, T.C. Dorlas, A. Ekert, A. Kay, A.J. Landahl, Phys. Rev. A **71**, 032312 (2005)
4. M.A. Nielsen, I.L. Chuang, *Quantum Computation and Quantum Information* (Cambridge University Press, Cambridge, 2000)
5. V. Giovannetti, R. Fazio, Phys. Rev. A **71**, 032314 (2005)
6. D. Burgarth, S. Bose, Phys. Rev. A **71**, 052315 (2005)
7. D. Burgarth, S. Bose, New. J. Phys. **7**, 135 (2005)
8. D. Burgarth, S. Bose, V. Giovannetti, Int. J. Quant. Inf. **4**, 405 (2006)
9. D. Burgarth, V. Giovannetti, S. Bose, J. Phys. A: Math. Gen. **38**, 6793 (2005)
10. I.L. Chuang, Y. Yamamoto, Phys. Rev. Lett. **76**, 4281 (1996)
11. N. Motoyama, H. Eisaki, S. Uchida, Phys. Rev. Lett. **76**, 3212 (1996)
12. P. Gambardella, A. Dallmeyer, K. Maiti, M.C. Malagoli, W. Eberdardt, K. Kern, C. Carbone, Nature **416**, 301 (2002)
13. T. Yamamoto, Y.A. Pashkin, O. Astafiev, Y. Nakamura, J.S. Tsai, Nature **425**, 941 (2003)
14. A. Romito, R. Fazio, C. Bruder, Phys. Rev. B **71**, 100501(R) (2005)
15. C.H. Bennett, D.P. DiVincenzo, J.A. Smolin, Phys. Rev. Lett. **78**, 3217 (1997)
16. D. Vion, A. Aassime, A. Cottet, P. Joyez, H. Pothier, C. Urbina, D. Esteve, M.H. Devoret, Science **296**, 886 (2002)
17. I. Chiorescu, Y. Nakamura, C.J.P.M. Harmans, J.E. Mooij, Science **299**, 1869 (2003)
18. G.M. Palma, K.A. Suominen, A.K. Ekert, Proc. R. Soc. Lond. A **452**, 567 (1996)
19. W.Y. Hwang, H. Lee, D.D. Ahn, S.W. Hwang, Phys. Rev. A **62**, 062305 (2000)
20. A. Beige, D. Braun, P. Knight, New J. Phys. **2**, 22 (2000)
21. M. Plenio, P. Knight, Rev. Mod. Phys. **70**, 101 (1998)
22. H.P. Breuer, F. Petruccione, *The Theory of Open Quantum Systems* (Oxford University Press, Oxford, 2002)
23. G.D. Chiara, D. Rossini, S. Montangero, R. Fazio, Phys. Rev. A **72**, 012323 (2005)
24. L. Dan, Z. Jing-Fu, Chin. Phys. **15**, 272 (2006)
25. P.W. Anderson, Phys. Rev. **109**, 1492 (1958)
26. J.P. Keating, N. Linden, J.C.F. Matthews, A. Winter Phys. Rev. A **75**, 012315 (2007)
27. T.J.G. Apollaro, F. Plastina, Phys. Rev. A **74**, 062316 (2006)

28. D. Burgarth, K. Maruyama, F. Nori, Phys. Rev. A **79**, 020305*R* (2009)
29. B. Sutherland, Phys. Rev. B **12**, 3795 (1975)
30. C. Hadley, A. Serafini, S. Bose, Phys. Rev. A **72**, 052333 (2005)
31. A. Bayat, V. Karimipour, Phys. Rev. A **75**, 022321 (2007)
32. C.H. Bennett, P.W. Shor, IEEE Trans. Inf. Theory **44**, 2724 (1998)
33. J.R. Schott, *Matrix Analysis for Statistics* (Wiley-Interscience, Hoboken, 1996)
34. N. Gisin, N. Linden, S. Massar, S. Popescu, Phys. Rev. A **72**, 012338 (2005)
35. A. Kay, M. Ericsson, New. J. Phys. **7**, 143 (2005)
36. B. Vaucher, D. Burgarth, S. Bose, J. Opt. B: Quantum Semiclass. Opt. **7**, S356 (2005)
37. B. Vaucher, Quantum communication of spin-qubits using a collaborative approach. Master's thesis, Ecole Polytechnique Federale de Lausanne (2005)
38. M. Avellino, A.J. Fisher, S. Bose, Phys. Rev. A **74**, 012321 (2006)
39. A. Kay, Phys. Rev. A **73**, 032306 (2006)

# Chapter 4
# Quantum State Transfer with Limited Resources

**Carlo Di Franco, Mauro Paternostro, and M.S. Kim**

**Abstract** In the quest for the achievement of realistic quantum state transfer protocols, relaxing the required conditions is a fundamental step. The use of multi-particle systems for the purpose of quantum information processing is made hard by a number of technical difficulties, related in particular to the lack of addressability of their single elements. We have thus to research novel ways to bypass these problems. Even if investigating the whole evolution of a quantum system is surely interesting, considering the behaviour of a few characteristic features could help us to find striking strategies in the context outlined above. This is exactly the idea at the basis of the method presented in this chapter, which we name *information flux approach*. Through it, we can design protocols for quantum state transfer in limited-control scenarios. In particular, we focus our interest in finding a way to avoid the initialisation of the spin chain. Different cases are described throughout the chapter.

## 4.1 Information Flux Approach

The concept of information flux in a quantum many-body system can be understood in terms of the influences that the dynamics of a specific element receives from other elements [1]. By quantifying the fluxes between the different parts during the performance of a protocol, one can design the most appropriate initial state of the total system and the distribution of coupling strengths among its elements. When analytic expressions cannot be obtained, the method can be easily adapted

C. Di Franco (✉) · M. Paternostro
Centre for Theoretical Atomic, Molecular and Optical Physics, School of Mathematics and Physics, Queen's University Belfast, BT7 1NN Belfast, UK
e-mail: c.difranco@qub.ac.uk; m.paternostro@qub.ac.uk

M.S. Kim
QOLS, Blackett Laboratory, Imperial College London, London SW7 2AZ, UK
e-mail: m.kim@imperial.ac.uk

G.M. Nikolopoulos and I. Jex (eds.), *Quantum State Transfer and Network Engineering*, Quantum Science and Technology, DOI 10.1007/978-3-642-39937-4_4,

for manageable numerical investigations. The intuitive nature of this tool and its flexibility are greatly useful in the study of interacting many-body systems such as quantum spin chains, showing remarkable advantages. Being performed in the Heisenberg picture, it is particularly suitable for the analysis of dynamical properties of many-body systems under the action of a specific Hamiltonian. This investigation has a fundamental impact on the understanding of quantum processes in general.

Let us consider a system of $N$ interacting spins (throughout the chapter, the word "spin" is used with the broader meaning of any possible two-level quantum system, i.e. a qubit) coupled via a Hamiltonian $\hat{\mathscr{H}}_{\{g\}}(t)$, depending on a set of parameters $g_i$ and a generalised time parameter $t$. For instance, $g_i$'s can represent the coupling strengths between the elements of the system. From now on, we use the following notation:

$$\hat{O}_j = \otimes_{k=1}^{j-1} \hat{\mathbb{1}}_k \otimes \hat{\sigma}_{O_j} \otimes_{l=j+1}^{N} \hat{\mathbb{1}}_l \qquad (O = X, Y, Z, I) \tag{4.1}$$

is the operator that applies the $\hat{\sigma}_O$ Pauli matrix only to the $j$-th qubit, with $\hat{\sigma}_I \equiv \hat{\mathbb{1}}$. Unless otherwise specified, the analysis is performed in the Heisenberg picture, where time-evolved operators satisfy

$$\frac{d\,\hat{\mathscr{O}}_j(t)}{dt} = i\,[\hat{\mathscr{H}}_{\{g\}}(t), \hat{\mathscr{O}}_j(t)] \tag{4.2}$$

and are indicated as

$$\hat{\mathscr{O}}_j(t) = \hat{\mathscr{U}}^\dagger \hat{O}_j\, \hat{\mathscr{U}} \tag{4.3}$$

with

$$\hat{\mathscr{U}}(t) = \hat{\mathrm{T}} e^{-i \int \hat{\mathscr{H}}_{\{g\}}(t')dt'} \tag{4.4}$$

the time evolution operator of the system. Physical units are chosen so that $\hbar = 1$ throughout this chapter. *Information is extractable from qubit $j$ at time $t$* whenever there is at least one $O$ (obviously excluding the identity) for which $\langle \hat{\mathscr{O}}_j(t) \rangle \neq 0$. Here the expectation value is calculated over the initial state of the register $|\Psi_0\rangle_{1\ldots N}$ (for the sake of simplicity we take such state as pure. The generalisation to the mixed case is in fact straightforward).

In order to give a clear idea of the approach, the following schematic description of a computation or communication process is adopted: let us assume that access is restricted to a selected qubit of a multi-particle system. This qubit can be considered as the input terminal of the black box given by the rest of the elements of the system and their mutual couplings. A detection stage can be attached to a suitable output port, connected to one of the qubits in the black box. A sketch of the scheme is given in Fig. 4.1. In this formalism, the initial state of a quantum system is described by the vector

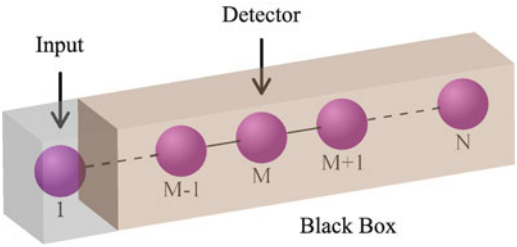


**Fig. 4.1** A computation or communication step is interpreted as a black box, whose operation depends on the coupling scheme within a multi-particle system, with movable input and detection terminals (Adapted from Phys. Rev. A **76**, 042316 (2007))

$$|\Psi_0\rangle_{1\ldots N} = |\phi_0\rangle_1 |\psi_0\rangle_{2\ldots N}. \tag{4.5}$$

The first qubit is initialised in a generic unknown *input* state, separable with respect to the rest of the system. The other qubits are prepared in an arbitrary pure state $|\psi_0\rangle_{2\ldots N}$ considered, for the moment, to be known. The assumption of knowing $|\psi_0\rangle_{2\ldots N}$ is physically motivated as it corresponds to the situation studied for many quantum information processing (QIP) protocols. However, we will drop it later on, so as to make the results independent of the initial state. A quantum process can be interpreted as the *flux* of appropriately processed information from the input qubit to the remaining components of the system. Such a flux is witnessed by any explicit dependence in the dynamics of the $i$-th qubit on the operators associated with the input one. Therefore, in order to find if qubit $i$ has developed any extractable information at time $t$ as a result of an information flux from the input qubit, we need to study the dependence of $\langle\Psi_0|\hat{\mathcal{O}}_i(t)|\Psi_0\rangle$'s on at least one of $\langle\Psi_0|\hat{O}'_1|\Psi_0\rangle$'s $(O, O' = X, Y, Z)$.

Each operator $\hat{\mathcal{O}}_i(t)$ can be decomposed over the basis built out of all the possible tensor products of single-qubit operators acting on the elements of the system $\{1, \ldots, N\}$. Such a basis has dimension $4^N$ and its elements can be partitioned in four disjoint groups, each of dimension $4^{N-1}$. Each group contains operators having the form $\hat{\sigma}_{O_1} \otimes \hat{\mathcal{G}}_{k,2\ldots N}$ $(k = 1, \ldots, 4^{N-1})$ with $\hat{\mathcal{G}}_{k,2\ldots N}$ one of the tensor products of single-qubit operators acting on the elements of the system $\{2, \ldots, N\}$ (there are $4^{N-1}$ possible products). It is thus possible to write $\hat{\mathcal{O}}_i(t)$ as

$$\hat{\mathcal{O}}_i(t) = \sum_{O'=X,Y,Z,I} \sum_{k=1}^{4^{N-1}} \alpha_{ik}^{OO'}(t)\, \hat{\sigma}_{O'_1} \otimes \hat{\mathcal{G}}_{k,2\ldots N}. \tag{4.6}$$

As stated above, we assume at the moment the initial state of the register $\{2, \ldots, N\}$ as known. One can thus introduce the vector $\boldsymbol{\chi}$, with components

$$\chi_k = {}_{2\ldots N}\langle\psi_0|\hat{\mathcal{G}}_{k,2\ldots N}|\psi_0\rangle_{2\ldots N} \tag{4.7}$$

in such a way that

$$\langle\Psi_0|\hat{\mathcal{O}}_i(t)|\Psi_0\rangle = \sum_{O'=X,Y,Z,I}\sum_{k=1}^{4^N-1}\alpha_{ik}^{OO'}(t)\chi_k\ {}_1\langle\phi_0|\hat{\sigma}_{O'_1}|\phi_0\rangle_1. \tag{4.8}$$

The matrix $\boldsymbol{\alpha}^{OO'}(t)$ incorporates the details of the time-evolved multi-qubit operators and is determined once $\hat{\mathscr{H}}_{\{g\}}(t)$ is assigned. The coefficient

$$\mathscr{I}_i^{OO'}(t) = \sum_{k=1}^{4^N-1}\alpha_{ik}^{OO'}(t)\chi_k \tag{4.9}$$

defines and quantifies the flux of extractable information (or, shortly, the *information flux*) from $\hat{O}'_1$ to $\hat{O}_i$ at time $t$. The formal definition of the information flux highlights the dual nature of the control that can be operated over the dynamics of the multi-particle system. Indeed, besides the dynamical part of $\mathscr{I}_i^{OO'}(t)$, there is a time-independent part that incorporates information about the initial state of the system, input qubit apart. This represents an additional control over the dynamics at hand. The flux of information towards a specific element of the register can be suppressed or enhanced by properly preparing qubits $\{2,\ldots,N\}$ in such a way that the $\chi_k$'s are properly engineered. The intrinsic dependence of the Hamiltonian on the set of interaction strengths $\{g\}$ makes the information flux implicitly dependent on the coupling scheme being chosen. Obviously, by choosing a different partition for the four groups of operators in which the basis has been divided, Eq. (4.8) can be straightforwardly modified so as to make the information flux from $\hat{O}'_j$ to $\hat{O}_i$ explicit. In the black-box model of Fig. 4.1, this corresponds to a change in the position of the input terminal. The dual control discussed above can be fully utilised for the preparation of a multi-particle device in the most appropriate configuration (of couplings and initial state) for a given QIP task.

## 4.2 Information Flux Approach to the Analysis of Quantum State Transfer in Spin Chains

Quantum state transfer in spin chains is a scenario where the information flux viewpoint is particularly useful. Such a change of perspective with respect to the standard approach to this problem [2] allows the study of the process even when there is no control or knowledge on the initial state of part of the medium, as shown later on. In general, a decomposition over the basis built out of all the possible tensor products of single-qubit operators acting on the elements of the system $\{1,\ldots,N\}$ (required for the analysis described above) can be demanding, especially for a large number of qubits. Indeed, the dimension of this basis is $4^N$. In some cases, in virtue of the symmetries of the interaction model, the evolution of an operator $\hat{O}_j$

involves only few elements of the basis. A simple method to estimate which terms are included in this evolution is presented here. For a time-independent Hamiltonian, the time-evolved form of an operator $\hat{O}_j$ is $\hat{\mathscr{O}}_j(t) = e^{i\hat{\mathscr{H}}t}\,\hat{O}_j\,e^{-i\hat{\mathscr{H}}t}$. The operator expansion formula gives

$$\hat{\mathscr{O}}_j(t) = \hat{O}_j + it[\hat{\mathscr{H}}, \hat{O}_j] + \frac{1}{2!}(it)^2[\hat{\mathscr{H}}, [\hat{\mathscr{H}}, \hat{O}_j]] + \ldots \tag{4.10}$$

If the Hamiltonian $\hat{\mathscr{H}}$ is expressed in terms of operators $\hat{O}_k'$'s, the contributions to the evolved form of $\hat{O}_j$ can be easily cast into an oriented graph. Let us consider, for instance, the open 5-qubit XX model

$$\hat{\mathscr{H}} = \sum_{i=1}^{4} J_i(\hat{X}_i\hat{X}_{i+1} + \hat{Y}_i\hat{Y}_{i+1}). \tag{4.11}$$

In order to analyse the information flux from the first to the last qubit, we need to study the evolution of the operators acting on the latter. Focusing on $\hat{X}_5$, the first commutators are

$$\begin{aligned}
&[\hat{\mathscr{H}}, \hat{X}_5] = -2i\ J_4\,\hat{Y}_4\hat{Z}_5,\\
&[\hat{\mathscr{H}}, \hat{Y}_4\hat{Z}_5] = 2i\ J_3\,\hat{X}_3\hat{Z}_4\hat{Z}_5 + 2i\ J_4\,\hat{X}_5,\\
&[\hat{\mathscr{H}}, \hat{X}_3\hat{Z}_4\hat{Z}_5] = -2i\ J_2\,\hat{Y}_2\hat{Z}_3\hat{Z}_4\hat{Z}_5 - 2i\ J_3\,\hat{Y}_4\hat{Z}_5,\\
&[\hat{\mathscr{H}}, \hat{Y}_2\hat{Z}_3\hat{Z}_4\hat{Z}_5] = 2i\ J_1\,\hat{X}_1\hat{Z}_2\hat{Z}_3\hat{Z}_4\hat{Z}_5 + 2i\ J_2\,\hat{X}_3\hat{Z}_4\hat{Z}_5,\\
&[\hat{\mathscr{H}}, \hat{X}_1\hat{Z}_2\hat{Z}_3\hat{Z}_4\hat{Z}_5] = -2i\ J_1\,\hat{Y}_2\hat{Z}_3\hat{Z}_4\hat{Z}_5.
\end{aligned} \tag{4.12}$$

The only operators involved in this iterative sequence are $\hat{X}_5$, $\hat{Y}_4\hat{Z}_5$, $\hat{X}_3\hat{Z}_4\hat{Z}_5$, $\hat{Y}_2\hat{Z}_3\hat{Z}_4\hat{Z}_5$, and $\hat{X}_1\hat{Z}_2\hat{Z}_3\hat{Z}_4\hat{Z}_5$. Therefore, it is possible to write the evolved operator $\hat{\mathscr{X}}_5(t)$ as

$$\begin{aligned}
\hat{\mathscr{X}}_5(t) = {}&\gamma_1(t)\hat{X}_1\hat{Z}_2\hat{Z}_3\hat{Z}_4\hat{Z}_5 + \gamma_2(t)\hat{Y}_2\hat{Z}_3\hat{Z}_4\hat{Z}_5\\
&+ \gamma_3(t)\hat{X}_3\hat{Z}_4\hat{Z}_5 + \gamma_4(t)\hat{Y}_4\hat{Z}_5 + \gamma_5(t)\hat{X}_5.
\end{aligned} \tag{4.13}$$

Here, we have introduced the time-dependent parameters

$$\gamma_j(t) = \sum_{l=0}^{\infty} \frac{(2t)^l}{l!}\gamma_j^{(l)}. \tag{4.14}$$


**Fig. 4.2** Oriented graph representing the recurrence formulas needed to obtain the $\hat{\mathscr{X}}_5(t)$ operator decomposition for a 5-qubit chain, whose Hamiltonian reads $\hat{\mathscr{H}} = \sum_{i=1}^{4} J_i(\hat{X}_i\hat{X}_{i+1} + \hat{Y}_i\hat{Y}_{i+1})$ (Adapted from Int. J. Quant. Inf. **6**, Supp. 1, 659 (2008))

For the Hamiltonian at hand, it is straightforward to prove that

$$\begin{aligned}
\gamma_1^{(l)} &= -J_1\gamma_2^{(l-1)}, & \gamma_2^{(l)} &= J_1\gamma_1^{(l-1)} + J_2\gamma_3^{(l-1)},\\
\gamma_3^{(l)} &= -J_2\gamma_2^{(l-1)} - J_3\gamma_4^{(l-1)}, & \gamma_4^{(l)} &= J_3\gamma_3^{(l-1)} + J_4\gamma_5^{(l-1)},\\
\gamma_5^{(l)} &= -J_4\gamma_4^{(l-1)}
\end{aligned} \tag{4.15}$$

with $\gamma_j^{(0)} = 0$ (1) for $j \neq 5$ ($j = 5$). When the parameters $\gamma_j(t)$'s cannot be analytically evaluated due to the difficulty of summing the series, it is possible to approximate them as

$$\gamma_j(t) \sim \sum_{l=0}^{m} \frac{(2t)^l}{l!}\gamma_j^{(l)}, \tag{4.16}$$

where $m$ is a proper cut-off. This analysis can be summarised in the oriented graph of Fig. 4.2, whose construction for a generic Hamiltonian is straightforward. Each node corresponds to an operator involved in the decomposition. If we concentrate on the evolution of $\hat{O}_j$, we have to put it in the first node of the graph. We should then add other linked nodes embodying all the operators resulting from the commutator of $\hat{O}_j$ with the Hamiltonian. In turn, each of them is connected to the operators resulting from its commutator with the Hamiltonian. The process ends when no new operator is created upon commutation. The edges connect thus a node to all the operators resulting from its commutator with the Hamiltonian. The corresponding numerical coefficients arising from such calculations, which are necessary to evaluate the information flux, are the weights of the edges. An outgoing (incoming) edge corresponds to a $+$ ($-$) sign. The factor $2i$ in front of each coefficient has been omitted for the sake of simplicity. The recurrence formulas can be easily derived from this graph. In the case of Eq. (4.11), taking

$$J_k = J\sqrt{k(5-k)}, \tag{4.17}$$

the spin chain becomes the one in Ref. [3] and the recurrence formulas give

$$\begin{aligned}
\gamma_1(t) &= \sin^4(2Jt), & \gamma_2(t) &= -2\cos(2Jt)\sin^3(2Jt),\\
\gamma_3(t) &= -\sqrt{(3/8)}\sin^2(4Jt), & \gamma_4(t) &= 2\cos^3(2t)\sin(2Jt),\\
\gamma_5(t) &= \cos^4(2Jt).
\end{aligned} \tag{4.18}$$

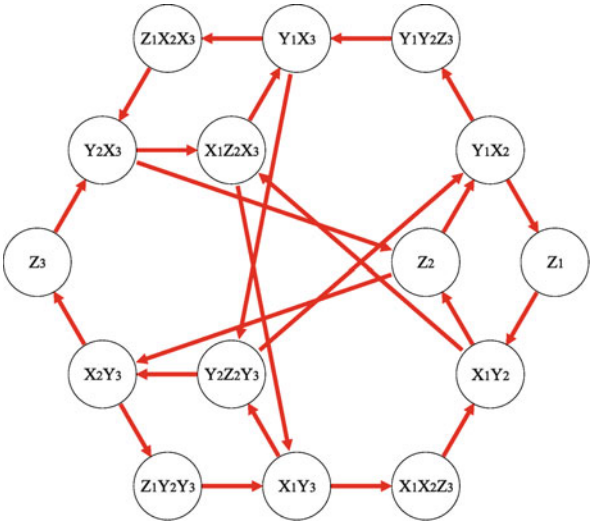


**Fig. 4.3** Oriented graph for $\hat{\mathscr{Z}}_3$ in a 3-qubit chain with an isotropic and homogeneous Heisenberg interaction (Eq. (4.19)). The coefficient $J$ above all the edges has been omitted for the sake of simplicity (Adapted from Int. J. Quant. Inf. **6**, Supp. 1, 659 (2008))

At $t^* = \pi/(4J)$[1] these imply $\gamma_1(t^*) = 1$ and $\gamma_j(t^*) = 0$ $(j = 2, \ldots, 5)$. Therefore, $\mathscr{I}_5^{XX}(t^*)$ (the information flux from $X_1$ to $X_5$ at time $t^* = \pi/(4J)$) for the initial state of qubits $\{2, \ldots, 5\}$ equal to $|0 \ldots 0\rangle_{2,\ldots,5}$ (so as to have ${}_{2\ldots5}\langle 0 \ldots 0|\hat{Z}_2\hat{Z}_3\hat{Z}_4\hat{Z}_5|0 \ldots 0\rangle_{2\ldots5} = 1$) is equal to 1. By means of a similar analysis, one can find the same result for the fluxes from $Y_1$ to $Y_5$ and from $Z_1$ to $Z_5$. *A perfect state transfer corresponds to information fluxes between homonymous operators equal to 1*, so the evolution of a spin chain under the action of the Hamiltonian in Eq. (4.11) with coefficients given by Eq. (4.17) results in perfect state transfer at time $t^* = \pi/(4J)$, as expected [3].

Needless to say, not every spin chain has associated graphs with linear structure. For example, in Fig. 4.3 we show the graph corresponding to $\hat{\mathscr{Z}}_3$ for the open three-qubit Heisenberg model

$$\hat{\mathscr{H}} = \sum_{i=1}^{2} J(\hat{X}_i\hat{X}_{i+1} + \hat{Y}_i\hat{Y}_{i+1} + \hat{Z}_i\hat{Z}_{i+1}). \tag{4.19}$$

The decomposition of $\hat{\mathscr{Z}}_3$ involves three elements where $\hat{Z}_1$ is present ($\hat{Z}_1$, $\hat{Z}_1\hat{X}_2\hat{X}_3$ and $\hat{Z}_1\hat{Y}_2\hat{Y}_3$). Let us consider $|\psi_0\rangle_{23} = |00\rangle_{23}$ as the initial state of qubits 2 and 3. The information flux from $\hat{Z}_1$ to $\hat{Z}_3$ is

[1]Throughout this chapter, the XX model has been taken as $\sum_{i=1}^{N-1} J_i(\hat{X}_i\hat{X}_{i+1} + \hat{Y}_i\hat{Y}_{i+1})$. For this reason, when the parameters follow the pattern $J_i = J\sqrt{i(N-i)}$, the time corresponding to perfect state transfer is $t = \pi/(4J)$.

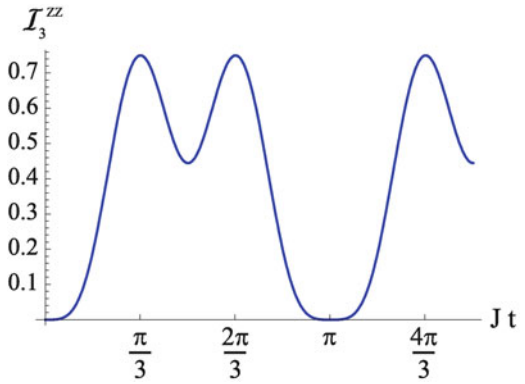


**Fig. 4.4** Evaluation of $\mathcal{I}_3^{ZZ}(t)$ for Eq. (4.19) with the initial state $|00\rangle_{23}$, by means of the recurrence formulas (Adapted from Int. J. Quant. Inf. **6**, Supp. 1, 659 (2008))

$$\begin{aligned}\mathcal{I}_3^{ZZ}(t) &= \delta_1(t)\,{}_{23}\langle 00|\hat{I}_2\hat{I}_3|00\rangle_{23} + \delta_2(t)\,{}_{23}\langle 00|\hat{X}_2\hat{X}_3|00\rangle_{23} \\ &+ \delta_3(t)\,{}_{23}\langle 00|\hat{Y}_2\hat{Y}_3|00\rangle_{23} = \delta_1(t),\end{aligned} \tag{4.20}$$

where $\delta_1(t)$, $\delta_2(t)$ and $\delta_3(t)$ are the coefficients of $\hat{Z}_1$, $\hat{Z}_1\hat{X}_2\hat{X}_3$ and $\hat{Z}_1\hat{Y}_2\hat{Y}_3$ in the decomposition of $\hat{\mathcal{I}}_3(t)$, respectively. A plot of $\mathcal{I}_3^{ZZ}(t)$, evaluated by means of the recurrence formulas, is presented in Fig. 4.4 (due to the choice of the initial state, only $\delta_1(t)$ has to be considered). In this case, $\mathcal{I}_3^{ZZ}(t)$ never reaches 1 [4]. The state fidelity $\mathcal{F} = \langle 1|\rho_3(t)|1\rangle$ (with $\rho_3(t)$ the density matrix describing the state of qubit 3) for the transmission of the initial state $|1\rangle$ has exactly the same value of the information flux $\mathcal{I}_3^{ZZ}(t)$.

## 4.3 Perfect State Transfer in a Chain with a Spin-Non-Preserving Interaction

When two Hamiltonian models reveal similarities in the behaviour of information fluxes, one can map some of the results known for one to the other. As a striking example, we compare a spin-non-preserving interaction with the Hamiltonian already analysed in Ref. [3]. In this way, the main result obtained for the latter, i.e. the possibility to achieve perfect state transfer, is shown to be valid also for the former model. In the analysis of spin chain systems, spin-preserving Hamiltonian models (for which the interaction commutes with $\sum_{i=1}^{n} Z_i$, so the number of spin excitations is conserved) have been frequently studied, applying usual techniques to find the exact spectrum [5]. When, however, the Hamiltonian does not preserve the total number of excited spins, an investigation from an information flux viewpoint shows the full potential of the method in tackling the evolution of the system [6]. This is possible because our method does not rely on the explicit analysis of the chain's spectrum and enables us to gather an intuitive picture of the dynamics at hand. The system considered here is the open $N$-qubit Ising model

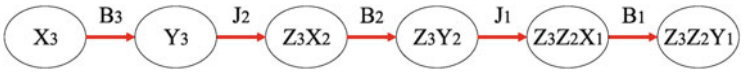


**Fig. 4.5** Oriented graph describing how the operators $\hat{\mathscr{X}}_N(t)$ and $\hat{\mathscr{Y}}_N(t)$ evolve under the action of $\hat{\mathscr{H}}_C$ in Eq. (4.22), with $N = 3$ (Adapted from [6])

$$\hat{\mathscr{H}} = \sum_{i=1}^{N-1} J_i \hat{Z}_i \hat{Z}_{i+1} + \sum_{i=1}^{N} B_i \hat{X}_i, \tag{4.21}$$

an instance of a spin-non-preserving interaction. The model in Eq. (4.21) describes, for example, a chain of interacting superconducting qubits, each at its degeneracy point [7]. Here, we keep the discussion as general as possible and free from a specific setup, so $\hat{\mathscr{H}}$ is interpreted as a generic spin chain model.

It is useful to consider first the Hamiltonian

$$\hat{\mathscr{H}}_C = \sum_{i=1}^{N-1} J_i \hat{X}_i \hat{X}_{i+1} + \sum_{i=1}^{N} B_i \hat{Z}_i. \tag{4.22}$$

By analysing the time evolution of $\hat{X}_N$ and $\hat{Y}_N$ under the action of $\hat{\mathscr{H}}_C$, we can write $\hat{\mathscr{X}}_N(t)$ and $\hat{\mathscr{Y}}_N(t)$ as

$$\begin{aligned}
\hat{\mathscr{X}}_N(t) &= \mu_1(t)\hat{X}_N + \mu_2(t)\hat{Y}_N + \mu_3(t)\hat{X}_{N-1}\hat{Z}_N + \mu_4(t)\hat{Y}_{N-1}\hat{Z}_N \\
&\quad + \cdots + \mu_{2N-1}(t)\hat{X}_1\hat{Z}_2\cdots\hat{Z}_N + \mu_{2N}(t)\hat{Y}_1\hat{Z}_2\cdots\hat{Z}_N, \\
\hat{\mathscr{Y}}_N(t) &= \nu_1(t)\hat{X}_N + \nu_2(t)\hat{Y}_N + \nu_3(t)\hat{X}_{N-1}\hat{Z}_N + \nu_4(t)\hat{Y}_{N-1}\hat{Z}_N \\
&\quad + \cdots + \nu_{2N-1}(t)\hat{X}_1\hat{Z}_2\cdots\hat{Z}_N + \nu_{2N}(t)\hat{Y}_1\hat{Z}_2\cdots\hat{Z}_N.
\end{aligned} \tag{4.23}$$

The time-dependent coefficients $\mu_j(t)$'s and $\nu_j(t)$'s are functions of $J_i$'s and $B_i$'s. For generic sets $\{J_i\}$ and $\{B_i\}$, they can be obtained by recurrence formulas similar to those presented previously. In order to do so, one should determine the oriented graphs associated with $\hat{\mathscr{X}}_N(t)$ and $\hat{\mathscr{Y}}_N(t)$, which turn out to be linear. An example, for $N = 3$, is given in Fig. 4.5. Clearly, $\hat{Y}_N$ already appears in the graph corresponding to $\hat{X}_N$ and we do not need to construct another dedicated graph for it. By explicitly analysing $\mu_j(t)$'s for this specific model, we can write

$$\mu_j(t) = \sum_{l=0}^{\infty} \frac{(2t)^l}{l!} \mu_j^{(l)} \tag{4.24}$$

with

$$\begin{aligned}
\mu_1^{(l)} &= B_3\mu_2^{(l-1)}, & \mu_2^{(l)} &= -B_3\mu_1^{(l-1)} + J_2\mu_3^{(l-1)},\\
\mu_3^{(l)} &= -J_2\mu_2^{(l-1)} + B_2\mu_4^{(l-1)}, & \mu_4^{(l)} &= -B_2\mu_3^{(l-1)} + J_1\mu_5^{(l-1)},\\
\mu_5^{(l)} &= -J_1\mu_4^{(l-1)} + B_1\mu_6^{(l-1)}, & \mu_6^{(l)} &= -B_1\mu_5^{(l-1)}
\end{aligned} \tag{4.25}$$

and the condition $\mu_j^{(0)} = 0\,(1)$ for $j \neq 1\,(j = 1)$. Similar recurrence formulas hold for $v_j(t)$'s. It is easy to recognise that the information flux from $\hat{Y}_1$ ($\hat{X}_1$) to $\hat{X}_N$ ($\hat{Y}_N$) follows the same behaviour as the one $\hat{X}_1 \to \hat{X}_{2N}$ ($\hat{Y}_1 \to \hat{Y}_{2N}$) in an open $2N$-qubit chain ruled by

$$\hat{\mathscr{H}}_{eq} = \sum_{i=1}^{2N-1} J_i^{eq}(\hat{X}_i\hat{X}_{i+1} + \hat{Y}_i\hat{Y}_{i+1}) \tag{4.26}$$

with $J_i^{eq} = B_{(i+1)/2}$ ($J_i^{eq} = J_{i/2}$) for odd (even) $i$. As remarked previously, this model allows perfect state transfer [3]. The similarity between fluxes for the two types of interaction paves the way to the idea proposed here. In particular, if the parameters in Eq. (4.22) follow the patterns

$$J_i = \pm J\sqrt{4i(N-i)} \tag{4.27}$$

and

$$B_i = \pm J\sqrt{(2i-1)(2N-2i+1)} \tag{4.28}$$

(with the choice of signs consistent throughout the chain) and the initial state of all qubits but the first one is $|0\rangle$, the modulus of the information flux from $\hat{Y}_1$ ($\hat{X}_1$) to $\hat{X}_N$ ($\hat{Y}_N$) is equal to unity at time $t^* = \pi/(4J)$, suggesting that one can achieve perfect state transfer also with this interaction. $\mathscr{I}_N^{XY}(t)$ and $\mathscr{I}_N^{YX}(t)$ for $N = 3$ are shown in Fig. 4.6**a** and **b**, respectively. The unit fluxes have to be those between homonymous operators (i.e. the fluxes from $\hat{X}_1$ to $\hat{X}_N$ and from $\hat{Y}_1$ to $\hat{Y}_N$ need to be equal to 1), therefore we need to apply a single-qubit operation on the first spin, before the evolution due to $\hat{\mathscr{H}}_C$ in Eq. (4.22). Under this point of view, the information flux approach is quite non-conventional. In fact, instead of using a formal map between models in Eqs. (4.22) and (4.26), a quantitative analogy between the evolutions of specific sets of operators as driven by these two interactions allows the design of the optimal protocol. One can easily map the Hamiltonian in Eq. (4.22) onto the one in Eq. (4.21) and thus achieve perfect state transfer. This can be done with a further change of basis for all the qubits in the chain that transforms $|0\rangle_i \to |+\rangle_i = (|0\rangle_i + |1\rangle_i)/\sqrt{2}$.

For the sake of clarity, let us summarise the details of the protocol.

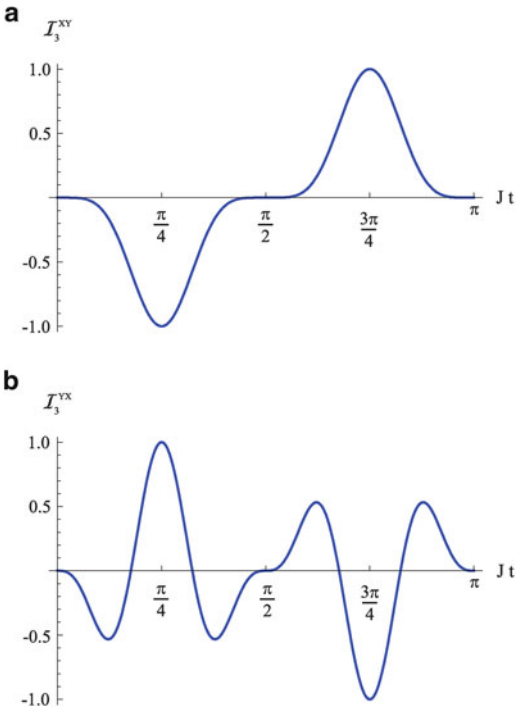


**Fig. 4.6** **(a)**: Information flux from $\hat{Y}_1$ to $\hat{X}_N$ for the Hamiltonian in Eq. (4.22), with $N = 3$, $J_i = \pm J\sqrt{4i\,(N-i\,)}$ and $B_i = \pm J\sqrt{(2i-1)(2N-2i+1)}$. Qubits 2 and 3 are prepared in $|00\rangle_{23}$. **(b)**: Information flux from $\hat{X}_1$ to $\hat{Y}_N$, for the same conditions as in panel **(a)** (Adapted from [6])

- The first qubit is prepared in $|\psi\rangle_1 = \alpha|0\rangle_1 + \beta|1\rangle_1$, while the rest of the chain is initialised in the tensor product state $\otimes_{i=2}^{N}|+\rangle_i$.
- *First step*: The operator $\hat{T}_1 \otimes \hat{H}_1 \otimes \hat{T}_1$ is applied to the first qubit of the chain, where

$$\hat{T} = \begin{pmatrix} 1 & 0 \\ 0 & e^{i\frac{\pi}{2}} \end{pmatrix} \tag{4.29}$$

  and $\hat{H}$ is the Hadamard gate

$$\hat{H} = \frac{1}{\sqrt{2}} \begin{pmatrix} 1 & 1 \\ 1 & -1 \end{pmatrix}. \tag{4.30}$$

- *Second step*: The chain evolves under the action of $\hat{\mathscr{H}}$ in Eq. (4.21) for a time $t^* = \pi/(4J)$.

In this way, the last qubit ends up in the state $|\psi\rangle_N$, while the rest of the chain is in $\otimes_{i=1}^{N-1}|+\rangle_i$, thus achieving perfect state transfer. The first step is necessary to cope with both the required basis changes (the first change to map the Hamiltonian $\hat{\mathscr{H}}$ onto $\hat{\mathscr{H}}_C$ and the second to obtain unit fluxes between homonymous operators) and

can be performed off-line. This corresponds to carrying out only the second step but using the initial state

$$|\tilde{\psi}\rangle_1 = \frac{1}{\sqrt{2}}[(\alpha + i\beta)|0\rangle_1 + (\beta + i\alpha)|1\rangle_1]. \tag{4.31}$$

Alternatively, the change of basis can be performed off-line at the end of the evolution driven by $\hat{\mathscr{H}}$.

## 4.4 State Transfer in a Chain with a Time-Dependent Hamiltonian

In order to present another strategy for state transfer in spin chains, instead of the pre-arrangement of the interaction strengths across the medium, we consider here a uniform distribution of time-dependent couplings [8]. The introduction of time-dependent terms allows to bypass the intrinsic rigidity of protocols based on pre-engineered spin chains. In fact, it is usually the case that spin media are arranged so as to implement a specific communication or computational task and cannot be "recycled" and used for a different one. Moreover, should an experimentally-prepared pattern of coupling strengths be found not accurate enough, the whole medium should be discarded (unless a non-ideal performance of the quantum protocol could be tolerated). Differently, by allowing the presence of time-dependent Hamiltonian terms, a more dynamical "adjustment" of the performances would be possible by implementing a simple feedback loop: state transmission can be tested using a given functional form of these terms and, according to the results, this can be tuned so as to converge towards better performances. A time-dependent scheme for quantum state transfer has been discussed by Lyakhov and Bruder in Ref. [9]. Building up on general results described in Ref. [10], they only let the first and the last pair of spins in a chain to experience time-dependent couplings. Our scheme, on the other hand, is different as we consider a fully homogeneous set of time-dependent interaction strengths.

The system we analyse is an open spin chain of $N$ elements, whose Hamiltonian reads

$$\hat{\mathscr{H}} = \sum_{i=1}^{N-1}[J_x(t)\hat{X}_i\hat{X}_{i+1} + J_y(t)\hat{Y}_i\hat{Y}_{i+1}] + \sum_{i=1}^{N} B(t)\hat{Z}_i\,. \tag{4.32}$$

For the sake of simplicity, we consider $N$ as an odd number. However, all the results presented here can be straightforwardly adapted to the case of an even number of spins in the chain. It is important to note that the inter-spin couplings and the amplitude of the magnetic field are site independent. This is a feature that differentiates the system at hand from a few previous proposals for perfect state

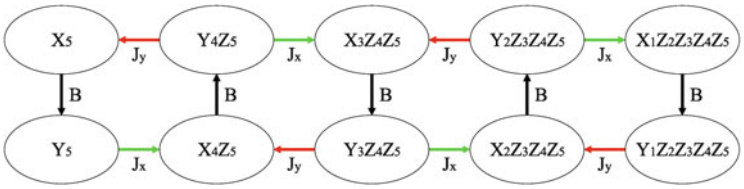


**Fig. 4.7** Oriented graph describing how the operators $\hat{X}_N$ and $\hat{Y}_N$ evolve under the action of $\hat{\mathscr{H}}$ in Eq. (4.32), with $N = 5$ (Adapted from [8])

transfer available in literature [2]. Although Eq. (4.32) is spatially unmodulated (in analogy with Ref. [4]), the price to pay in order to achieve unit transfer fidelity for any length of the chain is the time-dependence of the interaction strengths.

In general, also Eq. (4.32) does not preserve the number of spin-excitations. If we study by means of the information flux approach the evolution of the operators acting on the last spin, $\hat{\mathscr{X}}_N$ and $\hat{\mathscr{Y}}_N$ generate the oriented graph shown in Fig. 4.7 (where the case $N = 5$ has been considered). Here, we have exploited for the construction of the graph the same strategy as done for time-independent Hamiltonian models. This is possible because, as one can easily check, the operators involved in the decomposition do not change due to the time-dependence of the interaction. Clearly, we need to adapt the evaluation performed by means of the recurrence formulas. A straightforward way for this is by dividing the total evolution into short time steps. Within each of them, the interaction terms are taken as constant and numerically equal to the average values they assume in the respective time window (for smooth functions of time, the arithmetic means of the function values in the end-points of the time windows can also be used). The results obtained for each step are then used as initial conditions of the next. Clearly, the shorter is the time step with respect to the rate of variation of the interaction, the more accurate is the evaluation. The method is then iterated for each step and the total evolution of the operators is finally reconstructed. Let us study the action of $\hat{\mathscr{H}}$ in Eq. (4.32) when only one of the inter-spin coupling terms differs from zero and $N = 5$. The graph in Fig. 4.7 shows that, in these conditions, every node is linked at most to one nearest neighbour. In fact, the full oriented graph for the information flux analysis corresponding to Eq. (4.32) can be seen as the juxtaposition of three mutually disconnected subgraphs, each associated with only one of the coupling terms in $\hat{\mathscr{H}}$ and represented by a different colour in Fig. 4.7. It is easy to track the operator dynamics associated with these configurations. Let us consider, for instance, the case $B(t) \neq 0$ and $J_{x,y}(t) = 0\ \forall t$. Figure 4.7 (black colour) shows that $\hat{X}_5$ and $\hat{Y}_5$ are mutually linked and the evaluation by means of the recurrence formulas gives

$$\begin{aligned} \hat{\mathscr{X}}_5(t) &= \cos[2\beta(t)]\hat{X}_5 + \sin[2\beta(t)]\hat{Y}_5, \\ \hat{\mathscr{Y}}_5(t) &= -\sin[2\beta(t)]\hat{X}_5 + \cos[2\beta(t)]\hat{Y}_5 \end{aligned} \tag{4.33}$$

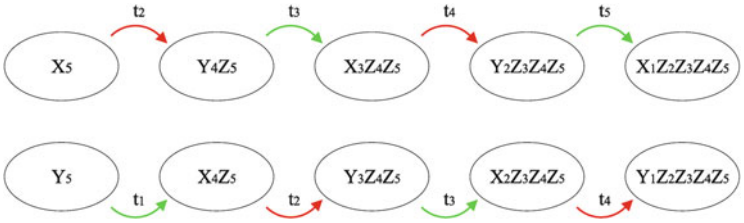


**Fig. 4.8** "Operator jumps" induced by $\hat{\mathscr{H}}$ in Eq. (4.32), when $J_x$ and $J_y$ are alternately different from zero. $J_x$ ($J_y$) is non-zero in the time intervals $t_i$ with an odd (even) value of $i$, and its integral over each of these intervals is equal to $\pi/4$ (Adapted from [8])

with $\beta(t) = \int_0^t B(t')dt'$. Clearly, an isolated node in a graph corresponds to an operator that is constant in time (for instance, $\hat{\mathscr{X}}_5(t) = \hat{X}_5$ when $J_x \neq 0$, $J_y = B = 0$, as in Fig. 4.7 (light green)). This result is the key to our investigation. If we let the interaction terms be alternatively non-zero for a time window $[0, \tau]$ such that $\beta(\tau) = \pi/4$, the action of $\hat{\mathscr{H}}$ in Eq. (4.32) will correspond to *kicks of information* between pairs of connected nodes of the graph discussed above. In Fig. 4.8 we show an example for $J_{x,y}(t)$ being alternately non-zero for five time intervals such that $\int_{t_{j-1}}^{t_j} J_x(t')dt' = \pi/4$ for $j = 1, 3, 5$ ($\int_{t_{j-1}}^{t_j} J_y(t')dt' = \pi/4$ for $j = 2, 4$), with $J_x(t) = 0$ [$J_y(t) = 0$] whenever $J_y(t) \neq 0$ [$J_x(t) \neq 0$]. The negligibility of the mutual overlaps of the coupling functions ensures that the information kicks occur according to the ordered scheme in Fig. 4.8. A similar transport of information from the leftmost to the rightmost part of the graph is achieved by kicking information using a pattern given by fixing $J_y = 0$ ($J_x = 0$) and alternately changing the amplitude of $J_x$ ($J_y$) and $B$ in a way so as to satisfy the conditions stated above. After a sequence of $N$ (for time-dependent $J_x$ and $J_y$) or $2N - 1$ kicks (for time-dependent $B$ and either $J_x$ or $J_y$), one obtains

$$\begin{aligned} \hat{\mathscr{X}}_5(\tau^*) &= \hat{X}_1\hat{Z}_2\hat{Z}_3\hat{Z}_4\hat{Z}_5, \\ \hat{\mathscr{Y}}_5(\tau^*) &= \hat{Y}_1\hat{Z}_2\hat{Z}_3\hat{Z}_4\hat{Z}_5, \end{aligned} \tag{4.34}$$

where $\tau^*$ is the total time of the evolution. By initially preparing the $j$-th spin of the chain (except the first) in an eigenstate of $\hat{Z}_j$, there is a complete end-to-end transport of information across the chain. This interaction can thus be exploited for perfect state transfer exactly as it happens for the Hamiltonian model of Ref. [3]. Depending on the details of a specific practical realisation of the intra-chain couplings, temporal control of the form highlighted here can be more convenient than pre-fabrication of a specific pattern of static coupling strengths. This is the case, for instance, for quasi-unidimensional optical lattices loaded with neutral atoms, where inter-site couplings are achievable in a time-controlled way via external optical potentials or cold atomic collisions. In perspective, this could also be a viable option in solid-state structures (such as arrays of Josephson junctions), where

fabrication of the pattern required for ideal state transfer would be demanding (if not prohibitive) already at moderate chain lengths. Achieving control via proper voltage/magnetic pulses inducing time-controlled information kicks would be a possibility to exploit instead. One can also show that the conditions on the time-dependence presented here can be further relaxed, if an almost-perfect state transfer is acceptable. This can be achieved, for instance, in a scenario where only the magnetic field is time-dependent while any other term is constant [8].

## 4.5 The Problem of Medium Initialisation

The ability to prepare a fiducial state of a quantum system that has to accomplish a task of quantum communication or computation is one of seven desiderata, more commonly known as *DiVincenzo's criteria* [11], that any reliable device for QIP should meet. One can summarise these requirements as:

- The availability of a scalable physical system with well-defined qubits.
- The ability to initialise the state of the qubits in a simple fiducial pure state.
- The possibility to arrange gate operations lasting much less than any decoherence time.
- The potentiality to implement a universal set of quantum gates.
- The achievability of qubit-specific measurements with high efficiency.
- The ability to interconvert stationary and flying qubits.
- The possibility to faithfully transmit flying qubits between specified locations.

However, even the innocent request for a pure reference state for the initialisation of a QIP device is not easily granted, in practice, mainly due to the difficulty of preparing pure states of multi-particle systems. A striking example is given by QIP in nuclear-magnetic-resonance systems [12], where the signal observed in an experiment comes from a chaotic ensemble of emitters, whose overall state is strongly mixed, and is "reinterpreted" quantum mechanically by relying on the concept of pseudo-purity [13]. Another very important instance is provided by the schemes for quantum state transfer in spin chains. The preparation of the spin medium in a fiducial pure state is an important step in the achievement of optimal transport fidelity. However, studies conducted on the effects of randomisation of the chain's state have revealed that the process' efficiency gets spoiled, in a way that quantitatively depends on the mechanism assumed for such randomisation [14].

The information flux approach can be exploited in order to show that the conditions on the initial state of a spin chain which enables perfect state transfer can be considerably reduced, without requiring fine dynamical control achieved through pulses over the chain [15]. Specifically, one can present a scheme for perfect state transfer that is able to bypass the initialisation of the spin medium in a *known pure* state [16]. The protocol requires only end-chain single-qubit operations and a *single* application of a global unitary evolution. It is thus fully within a scenario where the

control over the core part of the spin medium is relaxed in favour of controllability of the first and the last element of the chain. The flexibility of the scheme allows one to adapt it to various interaction models.

## 4.6 Perfect State Transfer Without State Initialisation for the Ising Model

Let us re-considered the spin-non-preserving Ising model in Eq. (4.21), with the parameters $J_i$'s and $B_i$'s following the patterns in Eqs. (4.27) and (4.28), respectively. As shown previously, it is possible to obtain perfect state transfer by means of this Hamiltonian. However, the transfer fidelity is sensitive to deviations of the initial state from the one being ideally required. The information flux approach is also useful in the study of multi-site correlation functions [17]. Here, for the purposes of the following investigation, we focus the analysis on the evolution of the two-site operators $\hat{\mathbb{1}}_i \hat{X}_{N-i+1}$, $\hat{Z}_i \hat{Y}_{N-i+1}$, and $\hat{Z}_i \hat{Z}_{N-i+1}$. At time $t^* = \pi/(4J)$, the evolved operators can be written as

$$\begin{aligned}
\hat{\mathbb{1}}_i(t^*)\hat{\mathscr{X}}_{N-i+1}(t^*) &= \hat{X}_i \hat{\mathbb{1}}_{N-i+1}, \\
\hat{\mathscr{Z}}_i(t^*)\hat{\mathscr{Y}}_{N-i+1}(t^*) &= \hat{Y}_i \hat{Z}_{N-i+1}, \\
\hat{\mathscr{Z}}_i(t^*)\hat{\mathscr{Z}}_{N-i+1}(t^*) &= \hat{Z}_i \hat{Z}_{N-i+1},
\end{aligned} \tag{4.35}$$

which are easily found by noticing that

$$\begin{aligned}
\hat{\mathscr{Y}}_i(t^*) &= -\hat{X}_1 \cdots \hat{X}_{N-i} \hat{Z}_{N-i+1} \hat{X}_{N-i} \cdots \hat{X}_N, \\
\hat{\mathscr{Z}}_i(t^*) &= \hat{X}_1 \cdots \hat{X}_{N-i} \hat{Y}_{N-i+1} \hat{X}_{N-i} \cdots \hat{X}_N.
\end{aligned} \tag{4.36}$$

Clearly, each of the two-site operators under investigation evolves in its swapped version, without any dependence on other chain's operators. This paves the way to the core of the proposed protocol, which is now described qualitatively. Qubit 1 is initialised in the input state $\rho^{in}$ (either a pure or mixed state) that has to be transferred and qubit $N$ is projected onto an eigenstate of $\hat{Z}$. Then the interaction in Eq. (4.21) is switched on for a time $t^* = \pi/(4J)$, after which the chain ends up in a particular entangled state. The amount of entanglement shared by the elements of the chain depends critically on their initial state, as it will be discussed later on. Regardless of the amount of entanglement being set, a $\hat{Z}$-measurement over the first spin projects the $N$-th one onto a state that is locally-equivalent to $\rho^{in}$. More specifically, if the product of the measurement outcomes at 1 after the evolution and at $N$ before the evolution is $+1$ $(-1)$, the last spin ends up in $\rho^{in}$ $(\hat{X}\rho^{in}\hat{X})$. Here, outcome $+1$ $(-1)$ of the measurement on spin $N$ before the evolution implies that spin $N$ is initialised

in $|0\rangle$ ($|1\rangle$). In all cases, apart from a simple single-spin transformation, perfect state transfer is achieved.

The proposal can now be quantitatively assessed. First, let us suppose that spins $2, \ldots, N-1$ are all prepared in unknown eigenstates of the $\hat{Z}$ operator. For simplicity, we assume that a pure state

$$|\psi\rangle = \alpha|0\rangle + \beta|1\rangle \tag{4.37}$$

should be transmitted and the last spin is initialised in state $|0\rangle$. These assumptions can be relaxed and the scheme can be generalised straightforwardly. For definiteness, a representative of the initial state of the medium is written as

$$|\psi_0\rangle_{2,\ldots,N-1} = |a_2 \ldots a_{N-1}\rangle_{2,\ldots,N-1} \tag{4.38}$$

with $|a_i\rangle_i$ the state of spin $i$ ($a_i = 0, 1$). The final state of the chain

$$|\Psi\rangle_F = e^{-i\hat{\mathscr{H}}t^*}|\psi\rangle_1|a_2 \ldots a_{N-1}\rangle_{2,\ldots,N-1}|0\rangle_N \tag{4.39}$$

can be cast as

$$\begin{aligned} |\Psi\rangle_F = \frac{1}{\sqrt{2}}[&|0\rangle_1|a_{N-1} \ldots a_2\rangle_{2,\ldots,N-1}|\psi\rangle_N \\ &+ i|1\rangle_1|a_{N-1}^{\perp} \ldots a_2^{\perp}\rangle_{2,\ldots,N-1}(\hat{X}|\psi\rangle_N)], \end{aligned} \tag{4.40}$$

where $\langle a_i^{\perp}|a_i\rangle = 0$, $\forall i$. Thus, upon measurement of the first spin in the $\hat{Z}$ eigenbasis, the state of the last spin is clearly locally-equivalent to $|\psi\rangle$ and separable with respect to the subsystem $\{2, \ldots, N-1\}$. More specifically, if spin 1 is measured in $|0\rangle$ ($|1\rangle$), spin $N$ collapses in $|\psi\rangle$ ($\hat{X}|\psi\rangle$). Therefore, if the result of the measurement on spin 1 is $-1$, a single $\hat{X}$ operator applied on the last spin is sufficient to retrieve the original input state. The form of $|\Psi\rangle_F$ reveals the core of the proposed mechanism. In fact, before the measurement stage, a fraction of genuine $N$-party entanglement of GHZ form [18] is shared by the elements of the chain. Such fraction is maximum for $\langle\psi|\hat{X}|\psi\rangle = 0$ and disappears if $|\psi\rangle$ is taken as an eigenstate of $\hat{X}$, showing that the state to be transmitted acts as a knob for the entanglement in the chain. This consideration can be extended to any other spin of the medium. Indeed, suppose that one of the central spins, labelled $j$, is prepared in an eigenstate $|\pm\rangle_j$ of $\hat{X}$. The final state of the chain after the evolution is

$$\begin{aligned} \frac{1}{\sqrt{2}}|\pm\rangle_{N-j+1}[&|0\rangle_1|a_{N-1} \ldots a_2\rangle_{(2,\ldots,N-1)'}|\psi\rangle_N \\ &+ i|1\rangle_1|a_{N-1}^{\perp} \ldots a_2^{\perp}\rangle_{(2,\ldots,N-1)'}(\hat{X}|\psi\rangle_N)], \end{aligned} \tag{4.41}$$

where $(2,\ldots,N-1)'$ denotes the set of all spins from 2 to $N-1$, spin $N-j+1$ excluded. This shows that, in general, the GHZ entanglement shared by the elements of the chain before the measurement stage does not include the spins that are mirror-symmetrical with respect to any element initially prepared in an eigenstate of $\hat{X}$.

One can now extend the analysis to the case of an initial mixed state of the spin medium. As before, for simplicity, the state of the last spin is $|0\rangle$. By following the same steps above, the final state of the system is

$$\begin{aligned}\rho_F = \frac{1}{2}[&|0\rangle_1\langle 0| \otimes \rho \otimes \rho_N^{in} + |1\rangle_1\langle 1| \otimes \hat{\mathscr{S}}_2\rho \otimes \hat{\mathscr{T}}_2\rho_N^{in} \\ &- (i\,|0\rangle_1\langle 1| \otimes \hat{\mathscr{S}}_1\rho \otimes \hat{\mathscr{T}}_1\rho_N^{in} + h.c.)]\end{aligned} \tag{4.42}$$

with $\rho$ the density matrix of the spins from 2 to $N-1$ obtained by applying a mirror-inversion operation to their initial state and $\rho^{in}$ the density matrix of the state to transfer. Here, the following notation has been used

$$\begin{aligned}&\hat{\mathscr{S}}_1\rho = \rho\prod_{i=2}^{N-1}\hat{X}_i\ , \quad \hat{\mathscr{S}}_2\rho = \prod_{i=2}^{N-1}\hat{X}_i\rho\prod_{j=2}^{N-1}\hat{X}_j\ , \\ &\hat{\mathscr{T}}_1\rho_N^{in} = \rho_N^{in}\hat{X}_N\ , \quad \hat{\mathscr{T}}_2\rho_N^{in} = \hat{X}_N\rho_N^{in}\hat{X}_N.\end{aligned} \tag{4.43}$$

Again, the crucial point is that, regardless of the amount of entanglement established between the spin medium and the extremal elements of the chain (i.e. spins 1 and $N$), upon $\hat{Z}$-measurement of qubit 1, the last spin is disconnected from the rest of the system, *whose initial state is inessential to the performance of the protocol* and could well be, for instance, a thermal state of the chain in equilibrium at finite temperature. In fact, the key requirements for this scheme are the arrangement of the proper time evolution (to be accomplished within the coherence times of the system) and the performance of clean projective measurements on spin 1 and, preventively, on spin $N$.

The last requirement is particularly important and, in order to estimate its relevance, one should evaluate the performance of the protocol against the purity of the initial state of spin $N$. For the sake of simplicity, we focus the investigation on the case in which a pure state is transmitted, the case of mixed states being easily deduced from this. The tool to evaluate the performance of the scheme will be the input-output transfer fidelity

$$\mathscr{F}_{1N} =_1 \langle\psi|\rho_N^{out}|\psi\rangle_1. \tag{4.44}$$

Here, $\rho_N^{out}$ is the state of the last qubit after the protocol. It is straightforward to obtain that

$$\mathscr{F}_{1N} = p_{00} + (1-p_{00})\langle\psi|\hat{X}|\psi\rangle, \tag{4.45}$$

where $p_{00} \in [0, 1]$ is the population of $|0\rangle$ in the density matrix describing the initial state of spin $N$, decomposed over the $\hat{Z}$-basis. The independence of the transfer fidelity from the coherences of the initial state of spin $N$ implies that it is effectively the same to work with a pure state

$$|\phi\rangle_N = \sqrt{p_{00}}|0\rangle_N + e^{i\varphi}\sqrt{1 - p_{00}}|1\rangle_N \tag{4.46}$$

or the mixed one

$$\rho_N = \begin{pmatrix} p_{00} & \gamma \\ \gamma^* & 1 - p_{00} \end{pmatrix} \tag{4.47}$$

with $\gamma$ an arbitrary value such that $\rho_N$ embodies a legitimate density matrix. Any error in the transfer process has to be ascribed to the fact that, for a non-unit value of $p_{00}$, the perfectly-transmitted state $|\psi\rangle$ has a component coming from the "wrong" state $\hat{X}|\psi\rangle$. This explains the dependence of $\mathscr{F}_{1N}$ on the state to be transmitted and, more precisely, on $\langle\psi|\hat{X}|\psi\rangle$.

## 4.7 Perfect State Transfer Without State Initialisation for the XX Model

As anticipated, the results on state transfer without initialisation are not bound to the specific instance of interaction model that has been considered. More generally, such findings depend on the way two-site operators evolve in time. Under different couplings, the behaviour of objects like

$$\hat{\mathscr{O}}_i(t^*)\hat{\mathscr{O}}'_{N-i+1}(t^*), \tag{4.48}$$

with $\hat{O}_i$ and $\hat{O}'_i$ single-qubit operators acting on spin $i$, can be found to be very similar to what has been observed above. If this is the case, it is then easy to adapt the protocol also to these interactions. In fact, with minor adjustments to the procedure previously described, one can apply the scheme to the open $N$-qubit XX model

$$\hat{\mathscr{H}} = \sum_{i=1}^{N-1} J_i(\hat{X}_i\hat{X}_{i+1} + \hat{Y}_i\hat{Y}_{i+1}) \tag{4.49}$$

with $J_i = J\sqrt{i(N-i)}$. As already remarked, this interaction allows $1 \to N$ perfect state transfer when the initial state of all the spins but the first one is $|0\rangle$. Here we focus on the use of the information flux approach in order to bypass the initialisation of the spin medium. As done for the Ising model, we look at the dynamics of two-site operators that are symmetrical with respect to the center of the chain. At time $t^* = \pi/(4J)$ and for any $N$, one has

$$\hat{\mathbb{1}}_i(t^*)\hat{\mathscr{Z}}_{N-i+1}(t^*) = \hat{Z}_i\,\hat{\mathbb{1}}_{N-i+1}. \tag{4.50}$$

On the other hand, for even $N$

$$\begin{aligned}\hat{\mathscr{X}}_i(t^*)\hat{\mathscr{X}}_{N-i+1}(t^*) &= \hat{X}_i\,\hat{X}_{N-i+1},\\ \hat{\mathscr{X}}_i(t^*)\hat{\mathscr{Y}}_{N-i+1}(t^*) &= \hat{Y}_i\,\hat{X}_{N-i+1}.\end{aligned} \tag{4.51}$$

For an odd number of spins in the chain, we find

$$\begin{aligned}\hat{\mathscr{X}}_i(t^*)\hat{\mathscr{X}}_{N-i+1}(t^*) &= \hat{Y}_i\hat{Y}_{N-i+1},\\ \hat{\mathscr{X}}_i(t^*)\hat{\mathscr{Y}}_{N-i+1}(t^*) &= -\hat{X}_i\,\hat{Y}_{N-i+1}.\end{aligned} \tag{4.52}$$

Due to this difference, one should adjust the procedure depending on the chain's length. In particular, the last spin has to be projected onto

$$|\pm_N\rangle = \frac{1}{\sqrt{2}}(|0\rangle \pm e^{iN\frac{\pi}{2}}|1\rangle). \tag{4.53}$$

In the following, we associate the outcome $+1$ $(-1)$ to a projection onto $|+_N\rangle$ $(|-_N\rangle)$. After the evolution $e^{-i\hat{\mathscr{H}}t^*}$, the first spin is measured over the $\hat{X}$ basis. The resulting output state depends, as for the Ising model, on the product of the measurement outcomes at site 1 after the evolution and at site $N$ before the evolution. If such product is $+1$ $(-1)$, the transmitted state is $(\hat{T}^N)^\dagger\rho^{in}(\hat{T}^N)$ $[\hat{Z}(\hat{T}^N)^\dagger\rho^{in}(\hat{T}^N)\hat{Z}]$ with $\hat{T}$ as in Eq. (4.29). As before, perfect state transfer is achieved (modulo a single-spin transformation). For the XX model, the final state of the system before the measurement stage (for the sake of simplicity, here the last spin is considered in $|+_N\rangle$) can be cast into the form

$$\begin{aligned}\rho_F = \frac{1}{2}\{&|+\rangle_1\langle+|\otimes\tilde{\rho}\otimes\tilde{\rho}_N^{in} + |-\rangle_1\langle-|\otimes\hat{\mathscr{S}}_4\tilde{\rho}\otimes\hat{\mathscr{T}}_4\tilde{\rho}_N^{in}\\ &- [i(-1)^N|+\rangle_1\langle-|\otimes\hat{\mathscr{S}}_3\tilde{\rho}\otimes\hat{\mathscr{T}}_3\tilde{\rho}_N^{in} + h.c.]\}\end{aligned} \tag{4.54}$$

with $|+\rangle = \frac{|0\rangle+|1\rangle}{\sqrt{2}}$, $|-\rangle = \frac{|0\rangle-|1\rangle}{\sqrt{2}}$, and

$$\begin{aligned}&\tilde{\rho} = \hat{A}^\dagger\rho\hat{A}\ ,\ \tilde{\rho}^{in} = (\hat{T}^N)^\dagger\rho^{in}(\hat{T}^N),\\ &\hat{A} = \prod_{i=2}^{N-1}\hat{T}_i^N,\\ &\hat{\mathscr{S}}_3\tilde{\rho} = \tilde{\rho}\prod_{i=2}^{N-1}\hat{Z}_i\ ,\ \hat{\mathscr{S}}_4\tilde{\rho} = \prod_{i=2}^{N-1}\hat{Z}_i\tilde{\rho}\prod_{j=2}^{N-1}\hat{Z}_j,\\ &\hat{\mathscr{T}}_3\tilde{\rho}_N^{in} = \tilde{\rho}_N^{in}\hat{Z}_N\ ,\ \hat{\mathscr{T}}_4\tilde{\rho}_N^{in} = \hat{Z}_N\tilde{\rho}_N^{in}\hat{Z}_N.\end{aligned} \tag{4.55}$$

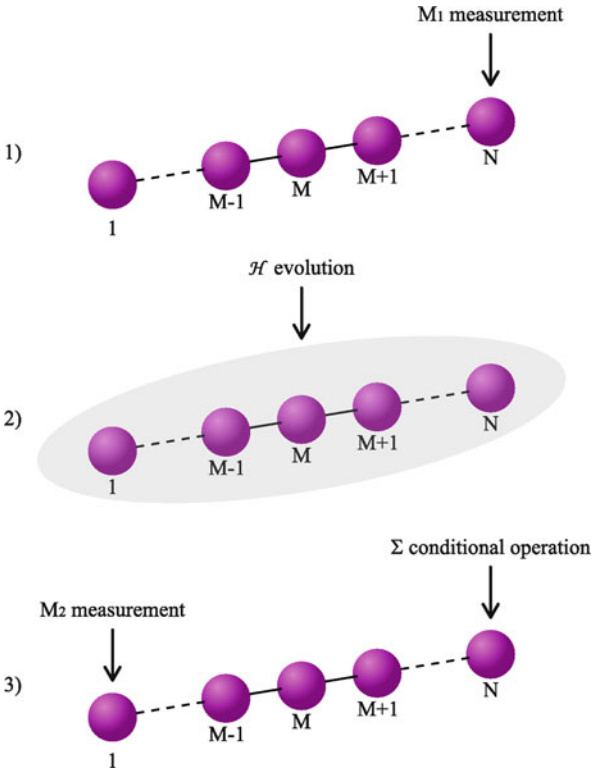


**Fig. 4.9** Sketch of the general scheme for perfect state transfer without state initialisation. $M_1$ and $M_2$ are measurements performed over a fixed basis, $\Sigma$ is a conditional operation, and $\hat{\mathscr{H}}$ is the Hamiltonian. The information encoded in the first spin is perfectly transmitted to the last one, regardless of the state of the other spins (Adapted from Phys. Rev. Lett. **101**, 230502 (2008))

## 4.8 Complete Conditions for the Success of the Protocol

The protocol for state transfer without initialisation can be adapted to any Hamiltonian for which it is possible to find a triplet of single-spin operators $\hat{\mathscr{B}}, \hat{C}, \hat{D}$ such that, for symmetric spin pairs, the conditions

$$\hat{\mathscr{B}}_i^{j_O}(t^*)\hat{C}_{N-i+1}\hat{\mathscr{O}}_{N-i+1}(t^*) = O_i\,\hat{D}_{N-i+1}^{k_O} \tag{4.56}$$

hold. Here, $\hat{\mathscr{B}}_i$ ($\hat{D}_{N-i+1}$) provides the eigenbasis for the measurement over spin $i$ ($N-i+1$) of the chain after (before) the evolution, $\hat{C}_{N-i+1}$ is a decoding operation, $\hat{O}_i = \hat{\mathscr{O}}_i(0) = \hat{X}, \hat{Y}, \hat{Z}$ and $j_O, k_O = 0, 1$, depending on the coupling model. For instance, Eqs. (4.35) are retrieved by taking $\hat{\mathscr{B}}_i = \hat{\mathscr{Z}}_i$, $\hat{C}_{N-i+1} = \mathbb{1}$, $\hat{D}_{N-i+1} = \hat{Z}_{N-i+1}$ with $j_X = k_X = 0$ and $j_{Y,Z} = k_{Y,Z} = 1$. A sketch of the general scheme is presented in Fig. 4.9. Clearly, also time-dependent Hamiltonian can be used. If we consider, for example, the interaction in Eq. (4.32), with the conditions for which Eqs. (4.34) hold, the two-site evolved operators are exactly those obtained for the XX model studied above, and the same strategy can thus be followed.

As noticed previously, the nature and amount of the entanglement generated during the performance of the protocol depend on the form of the initial state of the spins. Multi-partite entanglement shared by all or some of the elements of the chain, as well as only bi-partite entanglement involving the first and the last spin, can be generated. Nevertheless, one can achieve unit transfer fidelity when the proper time evolution and perfect hard projections are performed. This strongly supports the idea that state transfer protocols do not crucially rely on the specific nature and quality of the entanglement generated throughout the many-body dynamics, in stark contrast with other schemes for QIP.

On the other hand, the counter-intuitive fact that $\mathscr{F}_{1N} = 1$ regardless of the initial state of the medium could remind one, at first sight, of the idea of *deterministic quantum computation with one quantum bit* (DQC1) proposed in Ref. [19]. In this model, a single pure two-level system and arbitrarily many ancillae prepared in a maximally mixed state are used in order to solve problems for which no efficient classical algorithm is known. The apparent similarity with the case analysed here is dissipated by observing that, in DQC1, the initial state is restricted to that particular instance. In fact, the pure single-qubit state and the maximally mixed state of all the other qubits can be seen as the "fiducial" state invoked in one of DiVincenzo's criteria. Differently, the scheme presented here completely relaxes the knowledge required on the state of the spin medium, which might well be completely unknown to the agents that perform the state transfer process. The achievement of quantum computation with initial mixed states has also been analysed in Ref. [20], where it has been shown that a single qubit supported by a collection of qubits in an arbitrary mixed state is sufficient to efficiently implement Shor's factorisation algorithm. In that case, however, the performance of the protocol depends on the input state. Indeed, the average efficiency over all the possible random states, mixed or pure, is evaluated. However, for some particular input states, for instance $\otimes_{i=2}^{N}|0\rangle_i$, this can drop below the classical limit. The scheme described above, on the other hand, does not depend on the initialisation of the spin medium and, therefore, its efficiency cannot be spoiled by any input state.

It is also worth clarifying another important aspect. The procedures presented here might remind one of the general scheme for one-way quantum computation put forward in Ref. [21]. In both cases, the optimal result of a protocol depends on the performance of perfect projective measurements onto specific elements of a register and the feed-forward of a certain amount of classical information (in the case of the protocol presented here, the outcome of the measurements over spin 1 and the initial projection of spin $N$). Moreover, as in the one-way model, in this proposal the "pattern" of quantum correlations depends on the initial state of the elements of the system. However, such an analogy cannot be pushed too much as, remarkably, the use of quantum entanglement in the two protocols is different. The one-way model relies on a pre-built multi-partite entangled resource, the graph state [22], which is progressively destroyed by a proper program of measurements. On the other hand, in the scheme proposed here, multi-partite entanglement, if any, is built while the protocol is running. A single measurement is needed for the processing of the information encoded at the input state. In addition, differently from a graph

state, the preparation of some of the spins in the medium in a state that prevents their participation to a multi-partite entangled state does not spoil the efficiency of the protocol, as it has been demonstrated. This is not the case for a graph state built out of pairwise Ising interactions: the wrong initialisation of a part of the register excludes it from the overall entangled state, and actually "blocks" the transfer of information through that region of the register.

Finally, it is important to stress the difference between this approach and those achieving perfect state transfer via mirror-inverting coupling model [23]. In the general protocol proposed here, mirror inversion is "induced" in models which otherwise would not allow it, by adjusting the pattern of quantum interferences within the spin medium via the local encoding/decoding stages. By means of these, one can avoid the pre-engineered fulfilment of precise conditions on the spectrum of each interacting spin which, combined with reflection symmetry, are required for mirror-inversion. These models satisfy just the second of these conditions, perfect transfer without initialisation being achieved through the encoding and decoding steps previously described.

## 4.9 Conclusions

We have reviewed the information flux method for the investigation of quantum multi-particle systems embodied by spin chains. We have shown that this approach allows to highlight in a clear way features of the dynamics of the system that are otherwise buried in the complexity of the interaction models. Besides being useful in the study of quantum open-system dynamics [24], the method can be effective for the design of coherent strategies for quantum state transfer. A simple encoding-decoding scheme can be designed in a way that perfect state transfer is achievable without the necessity for quantum state initialisation of the spin medium. The protocol requires only end-chain single-qubit operations and a single application of a global unitary evolution. The efficiency of the scheme arises from the establishment of correlations between the first and last spin of the chain. The designed protocol is very flexible and can be adjusted to be used in various interaction models. This study considerably relaxes the prerequisites for obtaining reliable transfer of quantum information across interacting spin systems, a fundamental step in order to shorten the time for the achievement of realistic QIP with limited resources. It allows one to loose the requirements for information protection from environmental effects. Instead of utilising demanding always-on schemes for the shielding of the information content of a system, this could be done only during the running-time of the protocol.

Our scheme has been the subject of further developments. A recent proposal [25] has addressed a protocol similar to ours where the necessity for "remote coordination" between sending and receiving agents is bypassed. In this case, the state to transmit is codified in the first two spins of the chain: the logical $|0\rangle_l$ corresponds to the physical state $|10\rangle_{1,2}$, while $|1\rangle_l$ is represented by $|01\rangle_{1,2}$. Therefore, the general

state $|\psi\rangle_l = \alpha|0\rangle_l + \beta|1\rangle_l$ is encoded into the entangled state $\alpha|10\rangle_{1,2} + \beta|01\rangle_{1,2}$. By assuming the Hamiltonian model in Eq. (4.49) (with $J_i = J\sqrt{i(N-i)}$), perfect state transfer can be achieved. No measurement is required and no classical communication has to be sent from one end of the chain to the other. The price to pay, however, is the increased control over the system. Two spins for each end of the chain have to be accessed, and the protocol requires the use of an entangled resource in order to encode the state to send.

**Acknowledgements** CDF and MP's work was supported by the UK EPSRC with a grant under the "New Directions for EPSRC Research Leaders" initiative (EP/G004759/1). MSK's work was supported by the grant NPRP 4-554-1-094 from Qatar National Research Fund. MP thanks the UK EPSRC for a Career Acceleration Fellowship.

## References

1. C. Di Franco, M. Paternostro, G. M. Palma, M. S. Kim, Phys. Rev. A **76**, 042316 (2007); C. Di Franco, M. Paternostro, G. M. Palma, Int. J. Quant. Inf. **6**(Supp. 1), 659 (2008)
2. S. Bose, Contemp. Phys. **48**, 13 (2007)
3. M. Christandl, N. Datta, A. Ekert, A. J. Landahl, Phys. Rev. Lett. **92**, 187902 (2004); C. Albanese, M. Christandl, N. Datta, A. Ekert, Phys. Rev. Lett. **93**, 230502 (2004); G. M. Nikolopoulos, D. Petrosyan, P. Lambropoulos, Europhys. Lett. **65**, 297 (2004); G. M. Nikolopoulos, D. Petrosyan, P. Lambropoulos, J. Phys.: Condens. Matter **16**, 4991 (2004); M. Christandl, N. Datta, T. C. Dorlas, A. Ekert, A. Kay, A. J. Landahl, Phys. Rev. A **71**, 032312 (2005)
4. S. Bose, Phys. Rev. Lett. **91**, 207901 (2003)
5. S. Sachdev, *Quantum Phase Transitions* (Cambridge University Press, Cambridge, 1999); E. Lieb, T. Schultz, D. Mattis, Ann. Phys. **16**, 407 (1961)
6. C. Di Franco, M. Paternostro, D. I. Tsomokos, S. F. Huelga, Phys. Rev. A **77**, 062337 (2008)
7. Y. Makhlin, G. Schön, A. Schnirman, Rev. Mod. Phys. **73**, 357 (2001); D. Vion, A. Aassime, A. Cottet, P. Joyez, H. Pothier, C. Urbina, D. Esteve, M. H. Devoret, Science **296**, 886 (2002); D. I. Tsomokos, M. J. Hartmann, S. F. Huelga, M. B. Plenio, New J. Phys. **9**, 79 (2007)
8. C. Di Franco, M. Paternostro, M. S. Kim, Phys. Rev. A **81**, 022319 (2010)
9. A. O. Lyakhov, C. Bruder, Phys. Rev. B **74**, 235303 (2006)
10. A. Wojcik, T. Luczak, P. Kurzynski, A. Grudka, T. Gdala, M. Bednarska, Phys. Rev. A **72**, 034303 (2005)
11. D. P. DiVincenzo, in *Mesoscopic Electron Transport*, eds. by L. Kowenhoven, G. Schön, L. Sohn (Kluwer, Dordrecht, 1997).
12. N. Gershenfeld, I. L. Chuang, Science **275**, 350 (1997)
13. S. L. Braunstein, C. M. Caves, R. Jozsa, N. Linden, S. Popescu, R. Schack, Phys. Rev. Lett. **83**, 1054 (1999)
14. G. De Chiara, D. Rossini, S. Montangero, R. Fazio, Phys. Rev. A **72**, 012323 (2005); D. Burgarth, Eur. Phys. J. Special Topics **151**, 147 (2007); M. Wiesniak, arXiv:0711.2357; L. Zhou, J. Lu, T. Shi, C. P. Sun, arXiv:quant-ph/0608135
15. J. Fitzsimons, J. Twamley, Phys. Rev. Lett. **97**, 090502 (2006)
16. C. Di Franco, M. Paternostro, M. S. Kim, Phys. Rev. Lett. **101**, 230502 (2008); C. Di Franco, M. Paternostro, M. S. Kim, LNCS **6519**, 168 (2011)
17. C. Di Franco, M. Paternostro, M. S. Kim, Phys. Rev. A **77**, 020303(R) (2008)
18. D. M. Greenberger, M. A. Horne, A. Zeilinger, in *Bell Theorem, Quantum Theory, and Conceptions of the Universe*, ed. by M. Kafatos (Kluwer, Dordrecht, 1989)

19. E. Knill, R. Laflamme, Phys. Rev. Lett. **81**, 5672 (1998)
20. S. Parker, M. B. Plenio, Phys. Rev. Lett. **85**, 3049 (2000)
21. R. Raussendorf, H.-J. Briegel, Phys. Rev. Lett. **86**, 5188 (2001)
22. M. Hein, J. Eisert, H.-J. Briegel, Phys. Rev. A **69**, 062311 (2004); H.-J. Briegel, D. E. Browne, W. Dür, R. Raussendorf, M. Van den Nest, Nat. Phys. **5**, 19 (2009)
23. M.-H. Yung, S. Bose, Phys. Rev. A **71**, 032310 (2005); P. Karbach, J. Stolze, Phys. Rev. A **72**, 030301(R) (2005)
24. T. J. G. Apollaro, A. Cuccoli, C. Di Franco, M. Paternostro, F. Plastina, P. Verrucchi, New J. Phys. **8**, 083046 (2010)
25. M. Markiewicz, M. Wiesniak, Phys. Rev. A **79**, 054304 (2009); see also A. Kay, Int. J. Quant. Inf. **8**, 641 (2010)

# Chapter 5
# Robustness of Spin-Chain State-Transfer Schemes

**Joachim Stolze, Gonzalo A. Álvarez, Omar Osenda, and Analia Zwick**

**Abstract** Spin chains are linear arrangements of qubits (spin-1/2 objects) with interactions between nearest or more distant neighbors. They have been considered for quantum information transfer between subunits of a quantum information processing device at short or intermediate distances. The most frequently studied task is the transfer of a single-qubit state. Several protocols have been developed to achieve this goal, broadly divisible into two classes, fully-engineered and boundary-controlled spin chains. We discuss state transfer induced by the natural dynamics of these two classes of systems, and the influence of deviations from the ideal system configuration, that is, manufacturing errors in the nearest-neighbor spin couplings. The fidelity of state transfer depends on the chain length and the disorder strength. We observe a power-law scaling of the fidelity deficit, i.e. the deviation from perfect transfer. Boundary-controlled chains can provide excellent fidelity under suitable circumstances and are potentially less difficult to manufacture and control than fully-engineered chains. We also review other existing theoretical work on the robustness of quantum state transfer as well as proposals for experimental implementation.

J. Stolze (✉)
Institut für Physik, Technische Universität Dortmund, 44221 Dortmund, Germany
e-mail: joachim.stolze@tu-dortmund.de

G.A. Álvarez · A. Zwick
Department of Chemical Physics, Weizmann Institute of Science, 76100 Rehovot, Israel
e-mail: gonzalo.a.alvarez@weizmann.ac.il; analia.zwick@weizmann.ac.il

O. Osenda
Facultad de Matemática, Astronomía y Física, Universidad Nacional de Córdoba,
5000 Córdoba, Argentina
e-mail: osenda@famaf.unc.edu.ar

G.M. Nikolopoulos and I. Jex (eds.), *Quantum State Transfer and Network Engineering*,
Quantum Science and Technology, DOI 10.1007/978-3-642-39937-4_5,

## 5.1 Introduction

### *5.1.1 Spin Chains*

Spin chains have been an important topic in the theory of magnetism ever since the pioneering works of Ising [1] and Bethe [2]. From a theoretical point of view they are historically early and simple, yet highly nontrivial examples of interacting quantum many-body systems. Their dynamics was studied early on by theoretical and later on also by experimental means. Neutron scattering [3] has been an important tool to study elementary excitations in magnetic systems in general and low-dimensional systems in particular, especially since the discovery of high-temperature superconductivity [4], where magnetic excitations in spin chains, ladders, and planes are among the prime suspects believed to be involved in the mechanism of superconductivity. However, purely one-dimensional magnetism has also generated a lot of activity. One famous crystal of $KCuF_3$ has been around ever since the 1970s and the magnetic excitations of the spin-1/2 chains formed by the Cu ions have been measured over and over with increasing precision at every new neutron-scattering facility; for a list of relevant publications, see [5]. In the mid-1990s, $CuGeO_3$, the first inorganic compound showing a spin-Peierls transition [6] caused a renewed wave of interest in one-dimensional magnetism.

The ground state of a one-dimensional ferromagnetic spin-1/2 chain is the all-up state

$$|\uparrow\rangle_1 \otimes |\uparrow\rangle_2 \otimes \ldots \otimes |\uparrow\rangle_N = |\uparrow\uparrow \ldots \uparrow\rangle. \tag{5.1}$$

Here, the states $|\uparrow\rangle_i$ and $|\downarrow\rangle_i$ are the eigenstates of the Pauli spin operator $\sigma_i^z$ acting at site $i$ of an $N$-site chain, with eigenvalues $+1$ and $-1$, respectively. Without an external magnetic field this state is of course degenerate with the all-down state. For simplicity we focus on the state (5.1). A very simple excited state is then created by flipping a single spin; $\sigma_j^-|\uparrow\uparrow \ldots \uparrow\rangle$, where $\sigma_j^- = \frac{1}{2}(\sigma_j^x - i\sigma_j^y)$. This state breaks translational invariance, which may be restored, however, by the superposition

$$|\psi_k\rangle := \frac{1}{\sqrt{N}} \sum_{j=1}^{N} \mathrm{e}^{ikj} \sigma_j^- |\uparrow\uparrow \ldots \uparrow\rangle. \tag{5.2}$$

Here $k = \frac{2\pi\nu}{N}$ $(\nu = 0, \ldots, N-1)$ is a dimensionless wave number, and we have temporarily assumed periodic boundary conditions. The state (5.2) is called a (single-) spin-wave state in magnetism [7]; in quantum information science it has been rediscovered and called "twisted W state" [8]. Spin waves are often found to be low lying excited energy eigenstates of spin chain models, with the energy-momentum relation (dispersion relation) $\omega(k)$ depending on the detailed nature of the model Hamiltonian. With the appropriate caution these considerations also apply to antiferromagnetic spin chains if a suitable unitary transformation is applied to,

say, all even lattice sites. The ferromagnetic state then transforms into the Néel state $|\uparrow\downarrow\uparrow\downarrow\ldots\uparrow\downarrow\rangle$. Note, however, that the Néel state is *not* the ground state of the antiferromagnetic nearest-neighbor Heisenberg chain, as noticed by Bethe [2].

Since a single spin wave has no beginning or end in space-time, or, to say it more quantum mechanically, since it is a stationary state (of a suitable model), it cannot be used to transmit information. To that end temporal structure has to be introduced by generating pulses. Clearly the Fourier relation (5.2) may be inverted to represent a localized single spin-flip state

$$\sigma_j^-|\uparrow\uparrow\ldots\uparrow\rangle \tag{5.3}$$

as a superposition of spin-wave states $|\psi_k\rangle$. Obviously (5.3) is the most sharply localized state available in a spin chain.

The change from low-dimensional magnetism to quantum information science is basically just a change of language. The single spin-1/2 system is called a quantum bit (qubit), its states $|\uparrow\rangle$ and $|\downarrow\rangle$ are mapped to the basis states $|0\rangle$ and $|1\rangle$ of the qubit, respectively, and the all-up ferromagnetic state is mapped to the computational basis state $|\mathbf{0}\rangle = |00\ldots0\rangle$ of the $N$-qubit chain. The state (5.3) then is interpreted as one of the $N$ computational basis states with a single non-zero qubit at site $j$:

$$\sigma_j^-|\uparrow\uparrow\ldots\uparrow\rangle =: |\mathbf{j}\rangle. \tag{5.4}$$

As stated above the state (5.4) may be expressed as a superposition of spin wave states (5.2) each of which propagates in space-time with amplitude $\mathrm{e}^{\mathrm{i}(kj-\omega t)}$, that is, with a phase velocity

$$v_\phi = \frac{\omega(k)}{k} \tag{5.5}$$

which in general varies with $k$ if the dispersion relation $\omega(k)$ is nonlinear. Dispersion then takes its toll by broadening and flattening the pulse in the course of time, an effect well-known also from the study of Gaussian free-particle wave packets in elementary quantum mechanics.

The simplicity (though sometimes deceptive) of quantum spin chains has made these systems extremely popular in quantum information science, the main topical fields being the statics and dynamics of entanglement, and the transport, storage, and processing of quantum information, the transport of quantum information being the focus of the present volume.

The popularity of quantum spin chain models in quantum information science is aptly illustrated by the fact that a list of pertinent journal publications and preprints comprises more than 400 items (J. Stolze, Entanglement in quantum chain models, 2012, Unpublished notes). It is obvious that in the present chapter we will not be able to do justice to all the work which has been done in the field, even when we narrow our focus to the robustness of spin-chain transfer schemes,

and we apologize in advance to all colleagues whose work is not reported here, our only excuse being the rapid and exciting evolution of quantum information science combined with the finiteness of our time and energy resources. In the remainder of this introduction we will sketch some of the main lines of attack on the problem of quantum information transfer via quantum spin chains. All those proposals work well under ideal "design" conditions. Robustness of some of the schemes under less than ideal conditions is discussed subsequently. In Sect. 5.2 we will present the main results of our theoretical studies [9–11] on the effects of static perturbations ("manufacturing errors") on quantum information transfer in quantum spin chains. Section 5.3 reviews theoretical work by other authors, and Sect. 5.4 describes experimental work, or rather proposals for experimental work.

### 5.1.2 *Quantum Information Transfer in Ideal Quantum Spin Chains*

To set the stage we define the following general nearest-neighbor coupled spin-1/2 chain Hamiltonian:

$$H = \frac{1}{2}\sum_{i=1}^{N} J_i \left[(1+\gamma)\sigma_i^x \sigma_{i+1}^x + (1-\gamma)\sigma_i^y \sigma_{i+1}^y + \Delta\sigma_i^z \sigma_{i+1}^z\right] + \sum_{i=1}^{N} h_i \sigma_i^z. \quad (5.6)$$

We identify site 1 with the fictitious site $N+1$, that is, $\sigma_{N+1}^{\alpha} \equiv \sigma_1^{\alpha}$ ($\alpha = x, y, z$). Then $H$ describes a ring for $J_N \neq 0$ and an open chain of $N$ spins for $J_N = 0$. If $J_i$ (for $i \neq N$) and $h_i$ do not depend on $i$ we call the system homogeneous, otherwise it is inhomogeneous. The symmetry of the spin-spin interaction is controlled by the anisotropy parameters $\Delta$ and $\gamma$. For $\gamma = 0$ and $\Delta = 1$ the model is the original Heisenberg model, also known as XXX model, because all spin components experience the same coupling to their nearest neighbors. For $\gamma = 0$ and $\Delta \neq 1$ the model is called XXZ model, the important special case $\Delta = 0$ being known as XX model.[1] $\gamma = 0$ implies conservation of the total $z$ spin component, a case of obvious importance in quantum information transfer, since the number of ones in the state of the $N$-qubit system as expressed in the computational basis is then a constant of motion. If $\gamma \neq 0$ and $\Delta \neq 0, 1$ the model is referred to as the general XYZ chain, the ground-state properties of which are related to the thermal properties of the eight-vertex model, a classical two-dimensional model [12]; the dynamical properties of the XYZ chain, however, have never been studied in detail. Finally, for $\gamma \neq 0$ and $\Delta = 0$ the model is known as the XY chain, a special case being $\gamma = \pm 1$ where we have an Ising chain in a transverse magnetic field (TI chain). As shown

[1] Some authors also use the name XY model; we would like to reserve the term XY model for the anisotropic case, $\Delta = 0, \gamma \neq 0$.

by Lieb et al. [13] and Katsura [14] the $\Delta = 0$ case of (5.6) may be mapped to a model of noninteracting spinless lattice fermions with nearest-neighbor hopping by means of a Jordan-Wigner transformation [15], with the number of fermions being conserved for the XX case, $\gamma = 0$. Hence the XX chain has been quite popular as a model for quantum information transfer due to its simple dynamics.

The earliest example [16] for quantum information transfer in a spin chain, however, employed a ferromagnetic Heisenberg chain in its ground state with homogeneous couplings to whose ends a "sender" and a "receiver" spin can be coupled by the experimenters, Alice and Bob, after Alice has prepared the sender spin in the single-qubit state she wishes to transmit. As the state of the combined system evolves, information is transferred to the other end of the chain, where Bob at some suitable time decouples the receiver spin from the rest of the system and measures or further processes it. The fidelity of this process is less than perfect, but higher than the maximal value of 2/3 [17] for classical transmission of a quantum state, for $N \leq 80$. Osborne and Linden [8] pointed out the deleterious effect of dispersion on single-qubit quantum state transfer and proposed to encode the quantum information to be transmitted not in the state of a single spin, but in a spin-wave packet constructed so as to involve only the approximately linear part of the dispersion relation $\omega(k)$ of the spin-wave excitations in a homogeneous Heisenberg model ring. Burgarth and Bose [18] and Burgarth et al. [19] suggested to improve the Heisenberg chain transfer protocol by using two or more chains in parallel and performing measurements in order to increase the fidelity of transfer. That "multirail" protocol is treated in Chap. 3 of the present book, by Burgarth and Giovannetti. Besides the presence of dispersion effects the homogeneous Heisenberg chain has another disadvantage which limits its usefulness and which was pointed out by, among others, Subrahmanyam [20]: two flipped spins in the ground state of a ferromagnetic Heisenberg chain interact with each other, leading to distortions of a two spin-flip state. More technically speaking, this means that while single spin-wave states are energy eigenstates, two spin-wave states are not, making their treatment more complicated and ultimately leading to the intricacies of the Bethe Ansatz [2].

Interactions between elementary excitations can be avoided by going from the Heisenberg chain to the XX chain by dropping the $z$ part of the nearest-neighbor interaction, but dispersion cannot be avoided as long as homogeneous chains ($J_i \equiv J$ in (5.6)) are considered. This precludes *perfect state transfer* (to be discussed below) for all but very short chains [21]. However, recent work on *pretty good state transfer* [22] shows that arbitrarily patient observers will obtain fidelities arbitrarily close to 1 in homogeneous XX chains of length $N = P-1, 2P-1$ with $P$ a prime, or $N = 2^M - 1$. The waiting time depends on the required deviation from unity and seems to grow exponentially with the chain length.

Haselgrove [23] discussed an interesting scheme involving time-dependent manipulation of the nearest-neighbor couplings between both sender and receiver qubits and the rest of the chain. Near-perfect transfer can be achieved by that method even for chains with slightly irregular couplings, provided those couplings are known and the chain dynamics in the single-excitation subspace can be simulated

beforehand. Another attempt at improving the transfer fidelity of homogeneous quantum chains is the application of a sequence of two-qubit gates (switchable interactions) between the end of the spin-chain "wire" and the receiving qubit [24]; some results on the stability of this scheme against disorder were reported in [25]. These schemes involving time-dependent couplings or external fields are at the border of quantum optimal control theory, an extremely rapidly developing field of research which, however, is not within the scope of the present chapter.

Zenchuk [26] suggested to consider not perfect state transfer but "complete information transfer": The state of the sender system $S$ (a subsystem of the communication system under study) is encoded in the initial reduced density operator $\rho_S(0)$ of $S$. The quantum time evolution of a fairly arbitrary chain system then performs a linear mapping of $\rho_S(0)$ to $\rho_R(t)$, the reduced density operator of the receiver subsystem $R$. If the Hilbert space of $R$ is at least as large as that of $S$ the linear mapping $\rho_S(0) \mapsto \rho_R(t)$ can be inverted for almost all times $t$ and the original information may be reconstructed.

The comprehensive review by Bose [27] covers the development of spin-chain quantum information transfer until the end of 2006. The special class of homogeneously coupled spin chains is discussed in Chap. 1 of the present book, by Bose et al.

Since quantum information transfer in strictly homogeneous chains suffers from dispersion effects as explained above, two main strategies have been developed, both based on the natural dynamics of inhomogeneous qubit chains. One approach uses "fully engineered" chains, where $\mathcal{O}(N)$ coupling constants or local fields have to be assigned specific values in order to achieve perfect state transfer (PST). The other approach employs "boundary-controlled" chains in which only $\mathcal{O}(1)$ coupling constants connecting sender and receiver qubits to the transmitting "wire" have to be adjusted in order to achieve optimized state transfer (OST). Both strategies will be explained below, before we turn to their robustness against static randomness in Sect. 5.2.

#### 5.1.2.1 Perfect State Transfer in Fully Engineered Chains

Perfect state transfer in engineered chains is based on the simple observation that a quantum system generates periodic dynamics if its energy spectrum displays only commensurate energy differences. Simple examples are the harmonic oscillator with energies $E_n = \hbar\omega(n + 1/2)$ $(n \geq 0)$ or the infinite square well with $E_n = n^2 E_1$ $(n \geq 1)$. A popular exercise in elementary quantum mechanics shows that arbitrary wave functions develop periodically (up to a global phase) under a harmonic force:

$$\psi(x,t) = -\psi\left(x, t + \frac{2\pi}{\omega}\right). \tag{5.7}$$

More interesting in the present context, but less often discussed in quantum mechanics courses is the relation

$$\psi\left(x, t+\frac{\pi}{\omega}\right) = -\mathrm{i}\psi(-x, t), \tag{5.8}$$

meaning that in one half period the state of the oscillator develops into a perfect spatial mirror image of the original state. This mirroring property of the quantum oscillator (which is trivial for the classical oscillator) rests on the commensurate energy spectrum and on the alternating parities of successive energy eigenstates. If these two properties can be carried over to a one-dimensional array of quantum mechanical objects that array can be used for perfect quantum state transfer.

A charged spin-$J$ particle in a magnetic field in $z$ direction shows a finite equidistant energy spectrum of $2J + 1$ levels, the energy eigenstates being the eigenstates of $J_z$. Transitions between these states are caused by the transverse spin components $J_x$ and $J_y$. In a 1979 paper Cook and Shore [28] employed the analogy between a spin-$J$ system and a $(2J + 1)$-level atom to derive a model for stepwise laser excitation, obtaining periodic solutions which permitted complete population inversion. Nikolopoulos et al. [29] turned population inversion into spatial inversion by suggesting an array of quantum dots able to accomodate an electron each, with tunneling between neighboring quantum dots adjusted so as to mimic the dynamics of the spin-$J$ system. The same line of thought was followed by Christandl et al. [21] who found PST in an inhomogeneous open $N$-spin XX chain with couplings[2] $J_i = \tilde{J}\sqrt{i\,(N-i\,)}$ and equidistant energy levels in the single spin-flip sector. Albanese et al. [30] generalized the concept to other state-mirroring systems using earlier results [31] on the construction of finite quantum systems with periodic dynamics. Shi et al. [32] discussed other spin chains involving external fields and displaying a commensurate energy spectrum.

Yung and Bose [33] and Karbach and Stolze [34] suggested a systematic approach to the construction of PST chains with a desired energy spectrum by solving a special type of Jacobian inverse eigenvalue problem [35, 36]. The basic point is the following: Given a set of $N$ real numbers $E_1 < E_2 < \ldots < E_N$, it is always possible to construct a unique *persymmetric Jacobi matrix*, that is, a real symmetric tridiagonal matrix with diagonal entries $a_1, \ldots, a_N$ and strictly positive super-/subdiagonal entries $b_1, \ldots, b_{N-1}$, with the additional symmetry conditions $a_i = a_{N+1-i}$ and $b_i = b_{N-i}$ which has the prescribed numbers $E_i$ as eigenvalues. Note that the number of given eigenvalues equals the total number of independent matrix elements $a_i$ and $b_i$. In an XX chain the $b_i$ are related to the nearest-neighbor couplings $J_i$ and the $a_i$ are related to the local fields $h_i$ in (5.6). The persymmetry of the matrix corresponds to the spatial symmetry of the spin chain and makes sure that successive eigenvalues correspond to eigenvectors of opposite parities. The eigenvalue spectrum can be chosen freely, as long as the energy differences are commensurate, to ensure PST. That freedom of choice may be used to provide

[2]The constant $\tilde{J}$ defines the energy scale.

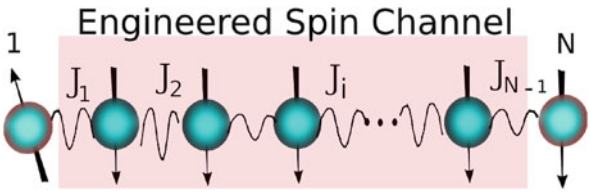


**Fig. 5.1** Fully engineered spin channel. Each coupling between neighbouring spins is tailored to allow for perfect state transfer

the system with other desirable properties besides PST. In [34] it was shown, for example, that it is possible to perform PST in chains with nearly homogeneous couplings, deviating from $J_i$ =const only on the few percent scale. If the diagonal matrix elements $a_i$ (the local fields $h_i$ in the XX chain) vanish, the eigenvalues are symmetrically distributed about zero, that is, $E_i = \pm|E_i|$ and the number of unknowns in the inverse eigenvalue problem is greatly reduced. For that special case, a simple algorithm was recently proposed by Wang et al. [37]; for the more general case, many interrelated algorithms are known [35, 36].

A simple spin-1/2 XX chain with PST thus is given by

$$H = \frac{1}{2}\sum_{i=1}^{N-1} J_i(\sigma_i^x\sigma_{i+1}^x + \sigma_i^y\sigma_{i+1}^y) \quad (J_i = J_{N-i}), \tag{5.9}$$

with the $J_i$ chosen appropriately, as shown in Fig. 5.1. Let us pause briefly to point out some important facts about this system. By the Jordan-Wigner transformation [15] (5.9) is equivalent to the Hamiltonian of noninteracting lattice fermions with hopping elements $J_i$. The number of fermions corresponds to the number of down spins and the ferromagnetic all-up state corresponds to the fermion vacuum. The Jacobi matrix discussed above in the context of the inverse eigenvalue problem is the Hamiltonian restricted to the subspace of a single fermion. All single-fermion states are transferred to their spatial mirror images at the same instant of time, and so are all many-fermion states, since the Jordan-Wigner fermions do not interact. This means that in contrast to many other quantum information transfer schemes, PST in the system (5.9) is not restricted to single-qubit states, as already noted in [30]. Entangled states of many qubits are transformed into their spatial mirror images, as are mixed (for example thermal) states [34]. It is also implied that only those qubits have to be prepared in the beginning which carry the information to be transferred; no initialization whatsoever of the remaining qubits of the chain is needed. Whatever those qubits contain in the beginning is just mirrored away "out of sight".

A generalization of the above PST systems was suggested by Kostak et al. [38] who discuss Hamiltonians which generate permutations between the sites of a network and can thus be employed for single-qubit perfect state transfer. A generalization of the PST concept in the mathematical sense is "almost PST" as defined recently [39] by replacing the periodic functions in the time evolution of the quantum system with almost periodic functions. A useful review on various aspects of PST was written by Kay [40].

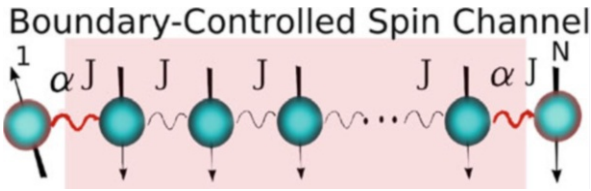


**Fig. 5.2** Boundary-controlled spin channel. Only boundary spin-couplings are tailored while all other couplings have the same strength $J$

#### 5.1.2.2 Optimized State Transfer in Boundary-Controlled Chains

The second strategy employing spin chains, boundary-controlled chains, is restricted to the transfer of single-qubit states by construction. In this strategy the sender qubit $A$ and the receiver qubit $B$ are only weakly coupled to the large system used to transfer the quantum information, the "quantum data bus", for example, a homogeneous spin chain as shown in Fig. 5.2.

An early example for that concept was given in [41], where a ring of coupled harmonic oscillators was assumed to have attached two additional oscillators acting as sender and receiver, respectively. To lowest order these sites only couple to the center of mass mode of the ring which thus provides distance-independent state transfer. Within the single-excitation subspace the coupled oscillator chain is equivalent to a spin-1/2 XX chain. A very clear picture of what is going on in the weak-coupling scenario was given in the short paper by Wójcik et al. [42]. There a homogeneous $N$-site XX chain with $J_i \equiv 1$ is coupled to two end spins with coupling strength $\alpha < 1$. The eigenvalues and eigenvectors responsible for single-excitation transfer are determined analytically and it is found that for very small values of $\alpha$ only two or three (when $N$ is odd) closely-spaced energy levels in the center of the spectrum are important. Oscillations between these states determine the quantum information transfer, and the transfer time increases as $\alpha$ decreases, while the deviation of the fidelity from unity scales as $\alpha^2 N$. The transfer time is $\mathcal{O}(\alpha^{-2})$ for even $N$ and $\mathcal{O}(N\frac{1}{2}\alpha^{-1})$ for odd $N$. Furthermore it is observed that after half the transfer time the two end spins become entangled for even $N$.

Another system proposed [43] to be used as a data bus is a spin ladder. Due to the excitation gap above the ladder's ground state, perturbation theory can be used to eliminate the ladder to lowest order and to replace it by an effective coupling between qubits $A$ and $B$. The ground-state entanglement between the end spins in some spin chains was suggested [44] to be used for teleportation or state transfer even at finite temperature $T$, as long as $T$ is smaller than the smallest excitation gap which depends on the chain length. Under suitable conditions, end spins $A$ and $B$ weakly coupled to an intermediate chain can then be approximated by an effective two-spin model. Similar approximations are also considered in more recent spin bus scenarios [45]. The same general strategy, of separating the sender-receiver Hilbert space of the spins $A$ and $B$ from the rest of the system, was followed in [46]. The specific system studied there was a chain with all pairs of spins coupled by a long-ranged generalized dipolar coupling. The end spins $A$ and $B$ can then be approximately decoupled from the intermediate chain by eliminating

the two spins next to $A$ and $B$, respectively. Since the nature of the transfer medium connecting $A$ and $B$ is to a large extent irrelevant, as long as certain conditions are fulfilled, that medium may even be a spin chain with random couplings, according to [47]. The separation of end spins from the remainder of the system may also be achieved by applying strong local fields to the end spins [48]. Thereby, two states of opposite parities and both strongly localized at the boundary spins are created, which are spectrally separated from the remainder of the Hilbert space, and which may be used for near-perfect state transfer [49]. This last example shows very clearly a drawback common to many of the boundary-controlled scenarios. The smaller the coupling between sender/receiver and data bus, the better is the quality of transfer. At the same time, unfortunately, the energy differences driving the dynamics become smaller and smaller and the transfer slows down, increasing the danger of the quantum information being destroyed by fluctuating interactions with the environment before it is transferred completely.

The boundary-controlled scenarios discussed up to now may be termed "weak-coupling" scenarios. We now briefly discuss the "optimal-coupling" scenario discovered in a numerical study by Zwick and Osenda [50] and at the same time developed analytically by Banchi et al. [51, 52]. As in [42], a homogeneous $N$-site XX chain with $J_i \equiv 1$ is coupled to two end spins with coupling strength $\alpha < 1$, however, $\alpha$ is optimized in a different way. For $\alpha = 1$, i.e. a completely homogeneous XX chain with $N + 2$ sites, the energy eigenvalues in the single-excitation subspace are proportional to $\cos k$, with $k = \frac{n\pi}{N+3}$, $(n = 1, \ldots, N + 2)$, while the corresponding eigenvector amplitudes at site $i$ of the chain are $u_k(i) = \sqrt{\frac{2}{N+3}} \sin ki$. Note that in the vicinity of $k = \frac{\pi}{2}$ the energies are approximately linear in $k$, so that packets of spin waves from that region are approximately free from dispersion. For $\alpha \neq 1$ the situation changes, but it is still possible to treat the eigenvalue problem analytically. It turns out [52] that the initial state with the sender spin down (and all others up) corresponds to a wave packet with approximately Lorentzian probability distribution in $k$, with center and width depending on $\alpha$. Since the energy spectrum also depends on $\alpha$ it is possible to jointly optimize the width of the wave packet and the linearity of the energy spectrum in order to achieve near-perfect state transfer. It turns out that the optimal value of $\alpha$ scales as $N^{-\frac{1}{6}}$. Further optimization is possible [53] if not only the first and last, but also the second and second to last bonds may be adjusted.

## 5.2 Fully-Engineered Versus Boundary-Controlled Chains

### *5.2.1 Introduction*

The topic of the present book chapter is the transfer of quantum information solely by the natural dynamics of a spin chain with fixed couplings, as explained in Sect. 5.1.2. Although the perfect-transfer schemes of Sect. 5.1.2.1 are able to transfer

multi-qubit states, we shall restrict our attention to the most frequently discussed case, single-qubit state transfer. Since nothing in this world is perfect, including computer hardware and software, both classical and quantum, information transport in spin chains is vulnerable to two main sources of irregularity: external dynamic randomness, that is, fluctuating fields caused by the environment, and internal static randomness, caused by inaccurate implementation of the theoretical design of the chain. Here we shall exclusively deal with static randomness and with the robustness of both the perfect state transfer chains from Sect. 5.1.2.1 and the optimized state transfer chains from Sect. 5.1.2.2 against this kind of "manufacturing errors".

In the following we will describe the general idea behind our approach before going into technical detail to some extent. The work of other groups on state transfer in disordered spin chains will be discussed mainly in Sect. 5.3.

For a study of weakly disordered systems we start with those systems which achieve PST in the conceptually simplest way when not subject to imperfections. That brings to mind the system first studied by Christandl et al. [21], that is, an open $N$-spin XX chain with couplings $J_i = \tilde{J}\sqrt{i(N-i)}$ and equidistant energy levels in the single-excitation sector. Indeed, that chain was studied early on by De Chiara et al. [54] who focused on the statistical changes in the energy spectrum when disorder is present. (For more detail see Sect. 5.3 below.) They found a particular scaling behavior of the transfer fidelity with the chain length $N$ and the strength of the disorder for that particular system. However, as pointed out in [33, 34], there are infinitely many ways to design perfect transfer chains which may or may not all behave differently under the influence of disorder. To shed some light on this question we focus on a particular subclass of perfect transfer chains and study in a systematic way which properties of the systems are most important for stability of state transfer in the presence of static randomness. The class of systems we selected for our study [9] generalizes the system studied by De Chiara et al. [54]. The (single-excitation) spectrum of that system shows a linear relation between the energy and the energy-ordering quantum number, and we studied systems with a more general power-law energy spectrum replacing the linear one. The robustness of this class of spin chains, that is, the ability to reliably transmit states even in the presence of static perturbations, is then determined by certain properties of the ordered system in combination with the statistical properties of the energy spectrum of the disordered system. We could identify two characteristics of the ordered system which support robustness: (1) there must be eigenvectors localized at the ends of the chain, near the sender and receiver qubits and, (2) the spectrum of the corresponding eigenvalues must be as linear as possible.[3] Both of these properties are shared by the boundary-controlled chains mentioned in Sect. 5.1.2.2. Therefore we studied whether these systems are robust under perturbations and if so, how their properties compare to

[3]The second point is relevant only if more than two or three eigenvectors contribute to the state transfer. As long as only two eigenvalues are involved, every spectrum is linear. This applies to the quadratic PST system discussed below in Sect. 5.2.3.1.

those of the power-law PST chains. These questions were studied in [10, 11]; some of the results are reviewed below.

The remainder of this section is organized as follows. After briefly defining the fidelity as a figure of merit and introducing the kind of disorder to be considered, we present a detailed analysis of the non-disordered spin chain properties that are most relevant to our analysis, in particular the distribution of the eigenvectors. Then we will focus on the statistical properties of the spectra. Finally we analyze the behaviour of the fidelity of transmission, in particular how this function scales with the extensive and intensive parameters of the chain, i.e. with the length of the chain and the strength of the noise, respectively.

### 5.2.2 Methods

We consider two different types of spin chains for state transfer: boundary-controlled [10, 42, 50–52], and perfect state transfer (PST) type [9, 21, 30, 34, 37, 55, 56]. Both are described by a XX Hamiltonian

$$H = \frac{1}{2}\sum_{i=1}^{N-1} J_i \left(\sigma_i^x \sigma_{i+1}^x + \sigma_i^y \sigma_{i+1}^y\right) \tag{5.10}$$

where $\sigma_i^{x,y}$ are the Pauli matrices, $N$ is the chain length, and $J_i > 0$ are the time-independent exchange interaction couplings between neighboring spins. The $J_i$ are allowed to vary in space, but we assume mirror symmetry with respect to the center of the chain, $J_i = J_{N-i}$. This guarantees the alternating parity of successive energy eigenstates which is necessary for PST (see Sect. 5.1.2.1 and references cited there) and simplifies the situation for boundary-controlled systems.

The boundary-controlled spin chains are a mono-parametric family of chains, such that

$$J_1 = J_{N-1} = \alpha J, \quad \text{and} \quad J_i = J, \ \forall i \neq 1, N-1. \tag{5.11}$$

The parameter $\alpha$ modifies the strength of the exchange interaction of the boundary spins with their respective nearest-neighbor spins; otherwise the chains are homogeneous.

In contrast, the PST spin chains are chains designed, or engineered, to allow for perfect state transmission at some instant of time. The engineering involves the tailoring of all the spin-spin exchange interaction strengths. Actually the design proceeds by imposing rules on the spin chain energy spectrum and then the spin-spin couplings are obtained uniquely by solving an inverse eigenvalue problem [35, 36].

#### 5.2.2.1 The Fidelity as a Figure of Merit

The aim is to transmit a quantum state $|\psi_0\rangle$ stored on the first spin ($i = 1$) to the last spin of the chain ($i = N$), where $|\psi_0\rangle = \alpha\,|0\rangle + \beta\,|1\rangle$ is a given superposition of a spin up and down, respectively, and the remaining spins of the chain are initialized in the spin up state. The Hamiltonian (5.10) preserves the total magnetization along the $z$-axis because $[H, \Sigma_i \sigma_i^z] = 0$, i.e., the number of excited spins is conserved. Because the initial state $|\Phi_0\rangle = |\psi_0\rangle \otimes |00\ldots0\rangle$ of the $N$-spin system is a superposition of the eigenstate $|\mathbf{0}\rangle = |00\ldots0\rangle$ and the state $|\mathbf{1}\rangle = |1_1 0\ldots\ldots0\rangle$, the component $|\mathbf{0}\rangle$ is conserved and the component $|\mathbf{1}\rangle$ evolves within the one excitation subspace spanned by the basis states $|\mathbf{i}\rangle = |0\ldots01_i0\ldots0\rangle$. The state of the system at a given time $t$ is

$$|\Phi(t)\rangle = \mathrm{e}^{-\mathrm{i}Ht/\hbar}|\Phi_0\rangle = \alpha|\mathbf{0}\rangle + \beta\sum_{i=1}^{N} f_i(t)|\mathbf{i}\rangle, \tag{5.12}$$

where $f_i(t) = \langle\mathbf{i}|\mathrm{e}^{-\mathrm{i}Ht/\hbar}|\mathbf{1}\rangle$. To measure the effectiveness of state transfer between sites 1 and $N$, we determine the state-dependent fidelity $\mathscr{F}(t) = \langle\Phi_N|\rho_N(t)|\Phi_N\rangle$, where $|\Phi_N\rangle = |00\ldots0\rangle\otimes|\psi_0\rangle$ and $\rho_N(t)$ is the density operator of the $N$-site chain which develops from $\rho_N(0) = |\Phi_0\rangle\langle\Phi_0|$ after time $t$. Since $\mathscr{F}(t)$ still depends on the initial state we average it over all possible single-spin initial states $|\psi_0\rangle$ distributed uniformly over the Bloch sphere, and obtain [16]

$$F(t) = \frac{|f_N(t)|\cos\gamma}{3} + \frac{|f_N(t)|^2}{6} + \frac{1}{2}, \tag{5.13}$$

where $\gamma = \arg|f_N(t)|$. Because the phase $\gamma$ can be controlled by an external field once the state is transferred, we consider $\cos\gamma = 1$. PST is achieved when $F(t) = 1$ for some time, meaning that every single-qubit state of the sender spin is perfectly transmitted to the receiver spin.

For a spin chain possessing mirror symmetry with respect to the center, i.e., $J_i^2 = J_{N-i}^2$, the matrix element $f_N(t)$ can be expressed in terms of the energies $E_k$ and the eigenstates $|k\rangle$:

$$f_N(t) = \sum_k P_{k,1}\mathrm{e}^{-\mathrm{i}E_k t/\hbar}(-1)^k, \tag{5.14}$$

where $P_{k,1} = |\langle k|\mathbf{1}\rangle|^2$ is the occupation probability of site 1 for a qubit in the $k$th eigenstate. Evidently the fidelity of state transfer thus depends crucially on the structures of the energy spectrum and of the eigenstates; examples will be discussed in Sect. 5.2.3.1 below. Perfect state transfer (PST) occurs if at some time $t_{PST}$ all contributions to the sum (5.14) are in phase. This happens if and only if

$$E_{k+1} - E_k = \pi\hbar(2m_k + 1)/t_{\mathrm{PST}}, \tag{5.15}$$

where the set of eigenenergies $\{E_k\}$ is ordered, $E_k < E_{k+1}$. The condition (5.15) must be fulfilled for all pairs of successive energies, where the $m_k$ may be arbitrary integers. The shortest time $t_{\mathrm{PST}}$ for which (5.15) is fulfilled is the first time at which PST is achieved [34, 40]. Since (5.15) implies strictly periodic time evolution, PST occurs again and again, at all odd multiples of $t_{\mathrm{PST}}$.

#### 5.2.2.2 Static Disorder

Static disorder in the couplings within the transfer channel is described by $J_i \rightarrow J_i + \Delta J_i$ $(i = 2, \ldots, N-2)$ with $\Delta J_i$ a random variable. Two possible coupling disorder models are of particular interest: (a) *relative static disorder*, where each coupling is allowed to fluctuate by a certain fraction of its ideal size, $\Delta J_i = J_i \delta_i$ [9, 10, 54, 57], and (b) *absolute static disorder,* where all couplings may fluctuate within a certain fixed range which we measure in terms of $J_{max} = \max J_i$: $\Delta J_i = J_{max} \delta_i$ [10, 58]. Each $\delta_i$ is an independent and uniformly distributed random variable in the interval $[-\varepsilon_J, \varepsilon_J]$. The parameter $\varepsilon_J > 0$ characterizes the strength of the disorder. The two coupling disorder models are equivalent for the *boundary-controlled spin chains* spin chains since all couplings are equal there for $i = 2, \ldots, N-2$. However, in the fully engineered PST systems $J_{max} - J_{min}$ depends on the type of system and tends to increase with $N$ so that *absolute disorder* is expected to be more damaging than the relative one in these systems. Which kind of disorder is relevant depends on the particular experimental method used to engineer the spin chains [59]. In the present review we focus on the case of relative static disorder for reasons of clarity. The main results on absolute disorder are only briefly discussed and further details can be found in references [9, 10].

### 5.2.3 *Selected Systems: Linear and Quadratic PST Compared to Optimized and Weak Boundary Coupling*

Every set of integers $m_k$ in (5.15) leads to a unique energy spectrum enabling PST and hence to a unique set of coupling constants $J_i$. Therefore, there are infinitely many spin chains allowing for PST. But, are all of them equally efficient for transferring information? How is their PST capability affected by perturbations through inaccuracies in the coupling constants or from coupling to external degrees of freedom? What properties are necessary to stabilize the system against such perturbations?

#### 5.2.3.1 Properties of Ideal Systems (Without Randomness)

In Sect. 5.2.1 we claimed that localization properties of the single-excitation eigenstates and linearity of their energy spectrum are important for robust high-fidelity

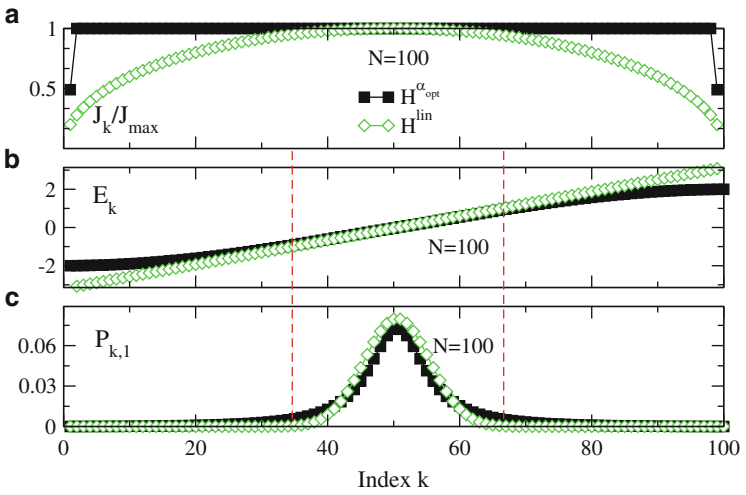


**Fig. 5.3** Properties of the $H^{\alpha_{opt}}$ system with $\alpha_{opt} = 0.49$ (*dark solid squares*) and the $H^{lin}$ system (*light open diamonds*) for chain length $N = 100$. (**a**) Exchange couplings $\frac{J_k}{J_{max}}$. (**b**) Eigenenergies $E_k$. (**c**) Probabilities $P_{k,1}$ of the initial state $|\Phi_0\rangle = |\mathbf{1}\rangle$. The *dashed vertical lines* define the region of dominant energy eigenstates $|k\rangle$ that contribute to the state transfer. $P_{k,1}^{\alpha_{opt}}$ is approximately Lorentzian [52] and $P_{k,1}^{lin}$ is approximately Gaussian [11]

quantum information transfer. We now illustrate these properties by two pairs of examples. The first system to be considered is the PST chain with strictly linear spectrum, that is, (5.10) with $J_i = \tilde{J}\sqrt{i(N-i)}$, first studied in [21]. We call this system $H^{lin}$ and we compare its properties to those of the optimized boundary-controlled system $H^{\alpha_{opt}}$, that is, (5.10) with couplings given by (5.11) and with boundary coupling strength parameter optimized ($\alpha = \alpha_{opt} \approx 1.06\, N^{-1/6}$) [50–52].

Figure 5.3 shows the properties of the two systems for chain length $N = 100$, where $\alpha_{opt} = 0.49$. The upper panel (a) clearly shows the large differences in the spin coupling distribution $J_i$ (normalized to the maximum coupling $J_{max}$ present in the chain). Despite these differences, the physical properties determining the quality of state transfer are suprisingly similar, as obvious from panels (b) and (c). The energy spectrum of $H^{lin}$ is strictly linear by construction, while the spectrum of $H^{\alpha_{opt}}$ is approximately linear in the central energy region. In order to make that similarity between the spectra more obvious we have rescaled the eigenvalues plotted in Fig. 5.3b. For $H^{\alpha_{opt}}$ we plot $E_k/J_{max}$, while for $H^{lin}$ we plot $(\pi/2)E_k/J_{max}$. In panel (c) we show the relative importance of the energy eigenstates for the information transfer problem at hand, by plotting the occupation probability $P_{k,1}$ of a qubit in the $k$th eigenstate at site 1 of the chain. For both systems, the initial state $|\mathbf{1}\rangle$ of the quantum information transfer protocol obviously is a superposition of energy eigenstates from a relatively narrow range of states in the central region of the spectrum. Correspondingly, the relevant part of the energy spectrum of $H^{\alpha_{opt}}$ is (approximately) linear so that one may expect that system

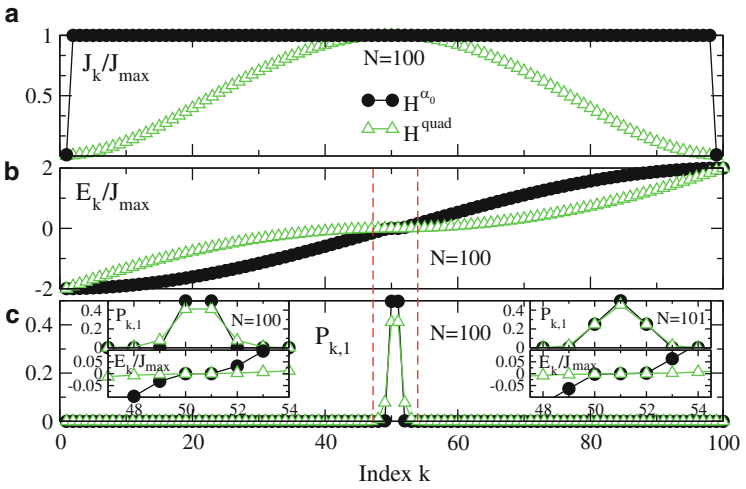


**Fig. 5.4** Properties of the $H^{\alpha_0}$ system with $\alpha_0 = 0.01$ (*dark solid circles*) and the $H^{quad}$ system (*light open triangles*) for chain length $N = 100$. (**a**) Exchange couplings $\frac{J_k}{J_{max}}$. The couplings for the $H^{quad}$ system are determined by solving the inverse eigenvalue problem. (**b**) Eigenenergies $E_k$. (**c**) Probabilities $P_{k,1}$ of the initial state $|\Phi_0\rangle = |\mathbf{1}\rangle$. The *dashed vertical lines* enclose the few dominant energy eigenstates $|k\rangle$ that contribute to the state transfer. A magnified view of this region is displayed in the *left inset*. The *right inset* shows the same region for odd $N = 101$

to show (approximately) PST. For large $N$ the probability distribution $P_{k,1}$ is a Gaussian with width $\sim N^{1/2}$ for $H^{lin}$ [11] and a Lorentzian with width $\sim N^{2/3}$ for $H^{\alpha_{opt}}$ [52], respectively.

The next pair of systems whose state transfer properties we are going to compare is the subject of Fig. 5.4. The fully engineered system $H^{quad}$ is defined by its quadratic energy spectrum, that is,

$$E_k = \mathrm{sgn}x \left[ (x - \delta \mathrm{sgn}x)^2 - \delta \right] \frac{\pi\hbar}{t_{PST}}, \tag{5.16}$$

with $x = k - \frac{N+1}{2}$, $\delta = \begin{cases} \frac{1}{2} & \text{for even } N \\ 0 & \text{for odd } N \end{cases}$, and $k = 1, \ldots, N$. That spectrum is obviously commensurate (i.e. it fulfills (5.15)) and thus enables PST. The corresponding couplings $J_i$ are determined by solving an inverse eigenvalue problem, see Sect. 5.1.2.1.

The boundary-controlled system $H^{\alpha_0}$ to which we compare is a weak-coupling system, that is, the couplings are again given by (5.11), but now the parameter $\alpha$ is small; for $N = 100$ we have chosen $\alpha = 0.01$. The coupling distributions in panel (a) of Fig. 5.4 are again quite different for the two systems. As can be seen from panel (b), even the energy spectra are clearly different. However, these differences do not really matter, the reason for that being visible in panel (c). It turns out that for

$H^{\alpha_0}$ and even $N$ two eigenstates completely dominate the probability distribution $P_{k,1}$ and the corresponding energies are very close together. This is easily explained by a second-order perturbation calculation in $\alpha$. The quantum information transfer process thus depends on a single parameter, the energy difference $\Delta E$ between those two states, which is proportional to $\alpha^2$. Similarly, the probability distribution $P_{k,1}$ of $H^{quad}$ is also dominated (however, less strictly) by the two states closest to the center of the energy band. Again, the difference $\Delta E = \pi\hbar/t_{PST}$ between these states is small, and the two states next in energy which still contribute visibly to $P_{k,1}$ are already at a distance $3\Delta E$ to the two dominant states.

The situation changes slightly for odd $N$, for example, $N = 101$, compare left and right insets in panel (c) of Fig. 5.4. The "unperturbed" $H^{\alpha_0}$ system ($\alpha = 0$) now has three zero-energy states (two isolated end sites and one state of the $N = 99$ chain) which for $\alpha \neq 0$ split into three states with energies zero and $\pm\Delta E$ in first order in $\alpha$. These states again dominate the quantum information transfer. Similarly, $H^{quad}$ for odd $N$ has one zero-energy eigenstate which, together with the two adjacent (in energy) states dominates quantum information transfer. This change in the structure of states and spectra makes us expect significant even-odd effects in these two systems.

It should be noted that when only two or three energy eigenstates contribute to the quantum information transfer, the overall properties of the energy spectrum become rather unimportant. This feature relates the weak-coupling boundary-controlled chain $H^{\alpha_0}$ to the various spin-bus type systems mentioned in Sect. 5.1.2.2.

The time evolution of the average transfer fidelity (5.13) is shown in Fig. 5.5 for all four systems discussed above, in the absence of disorder. A glance at the time axis immediately shows that the time scales involved differ by orders of magnitude even though all chains considered have basically the same length. Note, however, that the choice of time scales contains some arbitrariness since time must be expressed in units related to a typical energy scale of the system; here we choose to measure times in units of $J_{max}^{-1}$, where $J_{max}$ is the maximum nearest-neighbor coupling along the spin chain. For the boundary-controlled chains $J_{max}$ is the strength of $\mathcal{O}(N)$ bonds and only $\mathcal{O}(1)$ bonds have a different strength, while in the power-law PST chains the couplings vary over a broad range and only $\mathcal{O}(1)$ bonds with $J = J_{max}$ occur. Another reasonable choice of time unit could have been $J_{min}^{-1}$, the inverse minimum nearest-neighbor coupling, or $\Delta E_{min}^{-1}$ the inverse minimum energy difference in the single-excitation spectrum. As long as we discuss theoretical models, the choice of time units is basically a matter of taste. However, when it comes to comparing experimental implementations, technical possibilities define limitations on the available time and energy scales, and the range of possible information transfer rates is an important issue, of course.

Panel (a) of Fig. 5.5 shows the average fidelity $F(t)$ (5.13) for the systems $H^{\alpha_{opt}}$ ($\alpha_{opt} = 0.49$) and $H^{lin}$ with chain length $N = 100$. Note that $H^{lin}$ reaches $F(t) = 1$ while for $H^{\alpha_{opt}}$ the maximum value of $F(t)$ is smaller than unity. The perfect transfer time $t_{PST}$ is determined by the condition (5.15) with $m_k = 0$, leading to $t_{PST} = \frac{\pi N}{4J_{max}}$ [21]. Perfect transfer recurs periodically, at all odd multiples of $t_{PST}$, due to the perfectly periodic dynamics of the system. In contrast, $H^{\alpha_{opt}}$ reaches only

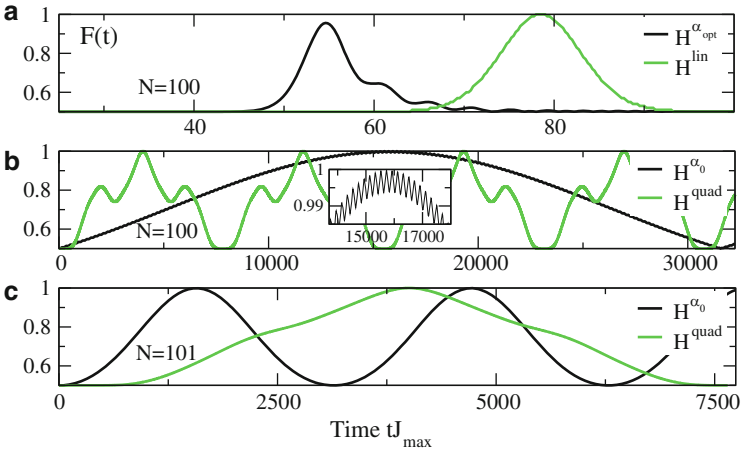


**Fig. 5.5** Evolution of the average state transfer fidelity. (**a**) $F^{\alpha_{opt}}(t)$ (*dark line*) and $F^{lin}(t)$ (*light line*) for chain length $N = 100$. The behavior of the fidelity is not affected by the parity of $N$ for these systems. However, for $F^{quad}(t)$ (*light line*) and $F^{\alpha_0}(t)$ (*dark line*), the parity of $N$ matters, as panels (**b**) (for $N = 100$), and (**c**) (for $N = 101$) demonstrate. Note the different time scales. The *inset* in (**b**) shows the fast small-amplitude oscillation observed in $F^{\alpha_0}_{N_{even}}(t)$ for even $N$, as explained in the main text

$F(t) \approx 0.955$ and with each revival of the signal the peak height decreases. The characteristic time scale $\tau^{\alpha_{opt}} \approx \frac{N}{2J_{max}}$ [50] is determined by the maximum group velocity of the elementary excitations in a homogeneous XX chain with nearest-neighbor coupling $J_{max}$. Attenuated revivals of $F(t)$ occur at odd multiples of $\tau^{\alpha_{opt}}$, since the signal has to perform a round trip through the chain before it revives. Note that since $t_{PST} \approx \frac{\pi}{2}\tau^{\alpha_{opt}}$, the boundary-controlled system is a little faster than the fully-engineered system, but transfer is less than perfect. The maximum value of the fidelity increases for shorter chains [50].

The fully-engineered system with quadratic spectrum, $H^{quad}$, and the weakly-coupled boundary-controlled system $H^{\alpha_0}$ (with $\alpha_0 = 0.01$) are compared in panels (b) and (c) of Fig. 5.5, for $N = 100$ and $N = 101$, respectively. The perfect state transfer time $t_{PST}$ of $H^{quad}$ is about the same for $N = 100$ and 101, but the optimal transfer times $\tau$ for $H^{\alpha_0}$ differ by an order of magnitude. This strong even-odd effect can be understood [42] from perturbation theory in $\alpha$. The unperturbed system consists of a homogeneous XX chain with nearest-neighbor coupling $J_{max}$, plus two isolated spins next to the chain ends, corresponding to two zero-energy eigenstates. The $N-2$ single-excitation energies of the chain are symmetrically distributed about zero; there is no zero-energy eigenstate if $N$ is even. In that situation the two isolated spins couple to the intermediate chain only in second order and the corresponding energies are proportional to $\alpha^2 J_{max}$. For odd $N$, in contrast, there are three zero-energy eigenstates in the unperturbed system, because the intermediate $(N-2)$-spin chain has a zero-energy eigenstate with nonvanishing amplitude at its first and

last spins. In this situation, first-order degenerate perturbation theory yields two eigenvalues $\approx \pm\frac{\alpha J_{max}}{\sqrt{N}}$ and one zero eigenvalue. Speaking more pictorially, we have (fast) resonant state transfer for odd $N$ and (slow) non-resonant state transfer for even $N$. The transfer times related to the energy differences just discussed, $\tau_{even}^{\alpha_0} \approx \frac{\pi}{2\alpha_0^2 J_{max}}$ and $\tau_{odd}^{\alpha_0} \approx \frac{\pi\sqrt{N}}{2\alpha_0 J_{max}}$ match the numbers which may be read off from Fig. 5.5. For even $N$ one observes, on top of the slow oscillation (with period $2\tau_{even}^{\alpha_0}$), a faster small-amplitude oscillation, see inset of panel (b). The slow oscillation is related to the two formerly degenerate zero-energy eigenstates mainly responsible for the quantum information transfer, while the faster oscillation is caused by a small admixture of the two eigenstates of the intermediate $(N-2)$-spin chain with energies closest to zero, $E \approx \pm\frac{\pi J_{max}}{N}$. For the situation in Fig. 5.5 that energy is much larger than that of the two dominant states and thus the period of the fast oscillation is approximately given by $\frac{2N}{J_{max}}$. For the PST system $H^{quad}$ the dynamics of state transfer is determined by the energy differences between the dominant and subdominant eigenvalues, as discussed above. These differences are $\Delta E = \pi\hbar/t_{PST}$ and $3\Delta E$, and indeed the shape of $F^{quad}(t)$ in both panels (b) and (c) of Fig. 5.5 is well described by something like $\frac{1}{2}[1 - a\cos\omega t - (1-a)\cos 3\omega t]$ with suitable values for $a$ and $\omega$.

#### 5.2.3.2 Fidelity in the Presence of Randomness

We now turn to the central point of our topic, the influence of random static disorder (see Sect. 5.2.2.2) on the state transfer properties of the PST and OST systems discussed above. Some additional results on PST systems with more general power-law energy spectra may be found in [9]. As discussed in Sect. 5.2.2.2 we focus on the case of relative disorder and only mention some main differences to the case of absolute disorder (further details in [9, 10]). Thus, every coupling is allowed to fluctuate around its nominal value: $J_i \rightarrow J_i(1+\delta_i)$, where each $\delta_i$ is an independent and uniformly distributed random variable in the interval $[-\varepsilon_J, \varepsilon_J]$. For given perturbation strength $\varepsilon_J$ we have first calculated the Bloch-sphere averaged fidelities $F(t)$ (5.13) for $N_{av}$ realizations of the disordered systems and then have taken the ensemble average over the $N_{av}$ disordered configurations.

Figure 5.6 shows the ensemble-averaged fidelity $\overline{F}$ at the time $\tau$ defined by the nominal transfer time of the unperturbed system; that is, $\tau = t_{PST}$ for the fully-engineered PST systems, while $\tau$ is the time of the first maximum of $F(t)$ in the boundary-controlled systems, as discussed in Sect. 5.2.3.1. Note that for every single disordered chain configuration both the time and the height of the maximum in $F(t)$ may deviate from $\tau$ and $\overline{F}(\tau)$, respectively. Figure 5.6a shows $\overline{F}(\tau)$ as a function of the disorder strength $\varepsilon_J$ in comparison for the four systems discussed in Sect. 5.2.3.1. Note that we have selected the odd-length versions for the $H^{quad}$ and $H^{\alpha_0}$ systems because they provide much faster state transfer than their even counterparts, see Fig. 5.5. For $\varepsilon_J = 0$ the two PST systems achieve $\overline{F}(\tau) = 1$ as expected, but the weak-coupling system $H^{\alpha_0}(\alpha_0 = 0.01)$ also reaches almost

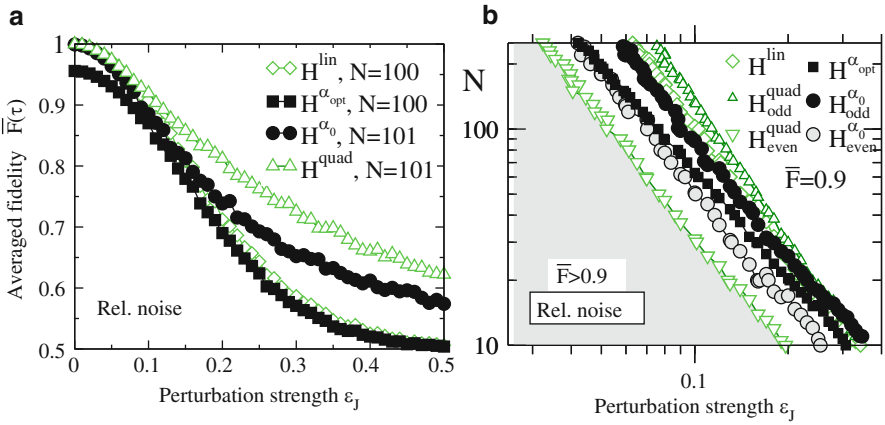


**Fig. 5.6** Ensemble-averaged fidelity at time $\tau$ as a function of the perturbation strength $\varepsilon_J$ for boundary-controlled state transfer channels (*filled symbols*) and fully-engineered perfect state transfer channels (*open symbols*). The average is over $N_{av} = 10^3$ realizations. (**a**) Chain lengths $N = 100,101$. (**b**) *Contour lines* of the average transfer fidelity $\overline{F}(\varepsilon_J, N) = 0.9$. In the *shaded region* to the left of the symbols the average transfer fidelity $\overline{F} > 0.9$ for all systems considered here

perfect transfer, while $H^{\alpha_{opt}}$ only achieves $\overline{F}(\tau) \approx 0.955$, as already observed in Fig. 5.5. For small $\varepsilon_J$ values $\overline{F}(\tau)$ apparently decreases quadratically. $H^{quad}$ achieves the highest $\overline{F}(\tau)$ values for all $\varepsilon_J$. The next most robust system is $H^{\alpha_0}$, which for small $\varepsilon_J$ shows the same behavior as $H^{lin}$. However, $H^{lin}$ becomes less robust as $\varepsilon_J$ grows and then its fidelity is as low as that of $H^{\alpha_{opt}}$, the least robust system, but the fastest one. Note that $\overline{F}(\tau)$ values below, say, 0.9 become increasingly meaningless, since fidelity 2/3 may be reached by classical means anyway [17].

In Fig. 5.6b we show the robustness of state transfer as a function of both chain length and disorder strength. In their pioneering study [54] De Chiara et al. found that the fidelity of $H^{lin}$ scales as

$$1 - \overline{F}(\tau) \sim N\varepsilon_J^2 \tag{5.17}$$

for small $N\varepsilon_J^2$ and hence the lines of constant $\overline{F}(\tau)$ in the $(\varepsilon_J, N)$ plane should be $N \sim \varepsilon_J^{-2}$ for fidelities close to unity. The symbols in Fig. 5.6b show the locations in the $(\varepsilon_J, N)$ plane where $\overline{F}(\tau) = 0.9$, confirming and generalizing the results from Fig. 5.6a. Again the most robust system is the odd $H^{quad}$, providing high $\overline{F}(\tau)$ values for the longest and most disordered chains. Note that in contrast, $H^{quad}$ for even-length systems is the least robust system. The data show power-law scaling $N \sim \varepsilon_J^{-\beta}$ with $\beta$ close to 2; for more detailed results we refer our readers to [11]. The shaded grey area in the lower left of Fig. 5.6b is the "safe region" where all systems considered offer fidelities larger than 0.9.

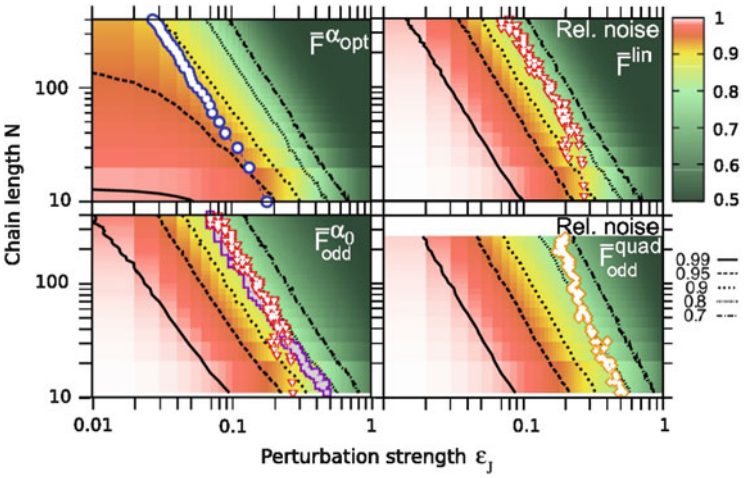


**Fig. 5.7** Average fidelities $\overline{F}^{\alpha_{opt}}, \overline{F}^{lin}, \overline{F}^{\alpha_0}_{odd}$ and $\overline{F}^{quad}_{odd}$ as functions of disorder strength $\varepsilon_J$ and chain length $N$. Average was taken over $N_{av} = 10^3$ realizations of relative static disorder. The *black contour lines* denote $\overline{F} = 0.99, 0.95, 0.9, 0.8, 0.7$. The *colored symbols* show crossings between the different systems, as explained in the text. Note that for the boundary-controlled systems relative and absolute disorder are identical

A more detailed picture of the fidelity landscape (for relative disorder) in the $(\varepsilon_J, N)$ plane is shown in Fig. 5.7 for the four system types of Fig. 5.6a in a set of combined contour and color plots.[4] All panels show contour lines corresponding to $\overline{F}$ values of 0.99, 0.95, 0.9, 0.8, and 0.7, respectively. The contours are straight lines, representing power-law scaling as discussed above, with deviations for the boundary-controlled $\alpha_{opt}$ system at weak disorder. The additional colored symbols show various crossovers. The blue circles in the upper left panel indicate where the fidelities of $H^{\alpha_{opt}}$ and $H^{lin}$ are equal for the case of *absolute* disorder, while all other crossovers marked by symbols in the figure refer to relative disorder. To the left of the symbols $\overline{F}^{lin} > \overline{F}^{\alpha_{opt}}$, and to the right $\overline{F}^{lin} < \overline{F}^{\alpha_{opt}}$. For relative disorder, we always have $\overline{F}^{lin} > \overline{F}^{\alpha_{opt}}$, see Fig. 5.6a for an example. The red triangles in the upper right and lower left panels show where $H^{\alpha_0}$ and $H^{lin}$ have equal fidelities. To the left of the symbols $\overline{F}^{lin}$ is marginally greater than $\overline{F}^{\alpha_0}$, while to the right $\overline{F}^{lin} < \overline{F}^{\alpha_0}$. The open squares in the lower left panel denote the fidelity crossover between $H^{\alpha_0}_{odd}$ and $H^{\alpha_0}_{even}$ (no further results shown for the latter system), where $\overline{F}^{\alpha_0}_{odd} > \overline{F}^{\alpha_0}_{even}$ in the high-fidelity region to the left of the symbols. Finally, the diamonds in the lower right panel indicate where $\overline{F}^{\alpha_0}_{even}$ (no results shown) is equal to $\overline{F}^{quad}_{odd}$, with $\overline{F}^{quad}_{odd} > \overline{F}^{\alpha_0}_{even}$ to the left of the symbols. While the system $H^{quad}$ (for

[4]Note that we have inverted the customary traffic-light symbolics: Here red means everything is fine, while green signals danger, that is, low fidelity.

odd $N$) shows the best robustness under relative disorder (see Fig. 5.6b), it is very sensitive against absolute disorder. This reflects the large variation in magnitude of the nearest-neighbor couplings in the system (see Fig. 5.4): small couplings are more severely affected by fluctuations of a given size than strong ones.

For absolute disorder we found [10] that there is almost always a boundary-controlled system with fidelity larger than that of the PST systems. Only for very small perturbation strength can PST systems be better than OST systems, but the fidelities are similarly close to unity in that range.

The results shown in Figs. 5.6 and 5.7 and in [9,10] show that there is no "simply the best" spin chain for quantum information transfer. The desired fidelity, speed, and distance of transfer are important factors in system design, as are the disorder model (relative or absolute, see Sect. 5.2.2.2) and disorder strength. If fidelity very close to unity is desired, complete engineering of the couplings and careful protection from disorder seem to be the path to choose. Weakly coupled boundary spins ($H^{\alpha_0}$) can be an alternative: as $\alpha_0$ is reduced, the fidelity increases, but so does the transfer time. However, if only moderate fidelity is needed (or possible, due to unavoidable high levels of disorder) a boundary-controlled system might do. If the transfer speed is primarily important, the fastest transfer is achieved by the boundary-controlled system $H^{\alpha_{opt}}$, closely followed by the fully-engineered system $H^{lin}$, while the other systems are significantly slower. On the whole one may say that in many situations boundary-controlled systems are serious competitors of fully-engineered chains, especially in view of the fact that ideally the required degree of fine-tuning is much smaller for the former.

For all systems with $\overline{F} \to 1$ in the clean limit $\varepsilon_J \to 0$ we find a power law behavior $N\varepsilon_j^{\beta} = \text{const}$ for the contours of constant fidelity, with $\beta$ close to 2. This generalizes the scaling law found in [54] for $H^{lin}$. In order to get some insight into the mechanisms behind this behavior and also behind the different levels of robustness in the systems considered, we now analyze in more detail how the relevant system properties are affected by randomness.

#### 5.2.3.3 Spectral Sensitivity

In Sect. 5.2.3.1 we found that the quantum information transfer performance of a spin chain is determined by simple properties of the single-excitation energies and eigenstates. There must be a reasonably small number of energy eigenstates which are strongly localized near the boundaries of the system, where the sender and receiver qubits are situated. That means, the occupation probability $P_{k,1}$ of site 1 in the $k$th energy eigenstate should consist of a single narrow peak (compare Figs. 5.3 and 5.4). Then the initial state of the transfer protocol is a superposition of only a few energy eigenstates. In the systems studied here the energies of these states were always close to the center of the energy band. The robustness of quantum information transfer then is determined by the degree of change of these dominant energies and eigenstates under the influence of disorder, a property which one

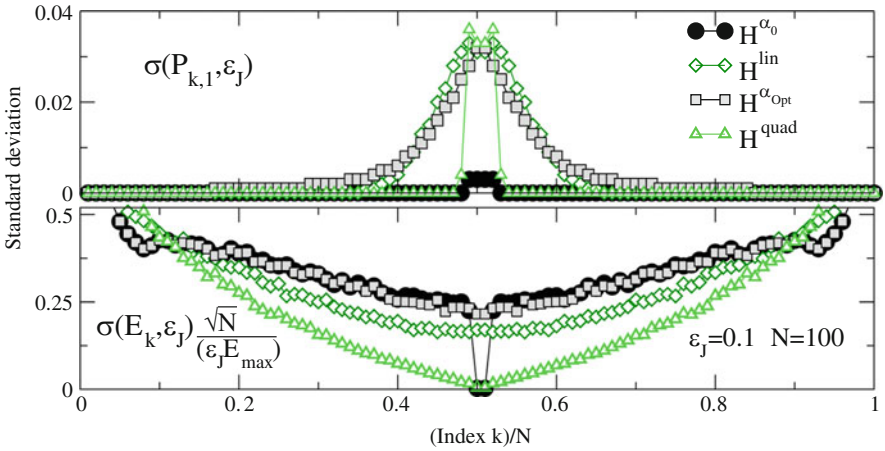


**Fig. 5.8** Standard deviation of the eigenvector probabilities $\sigma(P_{k,1}, \varepsilon_J)$ and of the energy levels $\sigma(E_k, \varepsilon_J) = \frac{1}{\sqrt{N_{av}-1}} \sqrt{\sum_{i=1}^{N_{av}} (E^i_{k,\varepsilon_J} - E_{k,0})^2}$ due to randomness with strength $\varepsilon_J = 0.1$ for chain length $N = 100$, $N_{av} = 10^3$ realizations and boundary-controlled state transfer channels (*filled symbols*) and fully-engineered perfect state transfer channels (*open symbols*)

might call spectral sensitivity. In order to estimate that sensitivity we studied how the probabilities $P_{k,1}$ and the energies $E_k$ are distributed in disordered chains. To understand the numerical results it is useful to recall some essential properties of the eigenvalue problem we are discussing. At zero disorder the spin chain is spatially symmetric, meaning that the Hamiltonian matrix in the single-excitation subspace is persymmetric (see Sect. 5.1.2.1). The matrix is also symmetric, tridiagonal and has zero diagonal elements. Hence the eigenvectors have definite parities and the parity alternates between successive (in energy) eigenvectors. For PST systems the energy eigenvalues have to be commensurate. Because of the zero diagonal the eigenvalues come in pairs, $E_k = \pm|E_k|$, the two eigenvectors of each pair are related to each other by a sign change of all even- (or odd-) numbered components. At nonzero disorder, the spatial symmetry of the system is broken and persymmetry of the matrix is lost, along with the parity of the eigenvectors. Commensurability of the eigenvalue spectrum of the PST systems is no longer guaranteed. However, the energy eigenvalues are still distributed symmetrically about zero and the corresponding eigenvectors are still related by a collective sign change of half of the components.

The symmetry in energy is clearly displayed by the data in Fig. 5.8, where we show the standard deviations $\sigma(P_{k,1}, \varepsilon_J)$ of the occupation probabilities $P_{k,1}$ (upper panel) and the standard deviations $\sigma(E_k, \varepsilon_J)$ of the energy eigenvalues $E_k$ (lower panel) as functions of $k/N$ for a chain of length $N = 100$ with disorder strength $\varepsilon_J = 0.1$ and ensemble size $N_{av} = 10^3$. The standard deviation $\sigma(P_{k,1}, \varepsilon_J)$ with disorder resembles the shape of $P_{k,1}$ without disorder (see Figs. 5.3 and 5.4) for the systems $H^{lin}$ and $H^{\alpha_{opt}}$ for which $P_{k,1}$ is a relatively broad distribution. Note

that $\sigma(P_{k,1}, \varepsilon_J)$ is the same order of magnitude as $P_{k,1}$ itself for $\varepsilon_J = 0.1$, that is, $P_{k,1}$ fluctuates significantly. For the system $H^{quad}$ again $\sigma(P_{k,1}, \varepsilon_J)$ and $P_{k,1}$ show similar shapes, but the values of $P_{k,1}$ are significantly larger than those of $\sigma(P_{k,1}, \varepsilon_J)$, making the relative fluctuations rather small. This is even more so for $H^{\alpha_0}$, where $\sigma(P_{k,1}, \varepsilon_J)$ is extremely small, this probably being related to the almost completely isolated sender and receiver qubits.

The standard deviations of the energy eigenvalues show a different pattern. In the relevant region close to the center of the energy band the two boundary-controlled systems show comparable levels of fluctuations, with one exception: The energies of the two central states of $H^{\alpha_0}$ do not fluctuate significantly, because they are proportional to $\pm\alpha_0^2$ to lowest order in $\alpha$ and thus very close to zero regardless of what the remainder of the chain does. The PST system $H^{lin}$ shows somewhat smaller standard deviation (in the normalization chosen here), while for the $H^{quad}$ system $\sigma(E_k, \varepsilon_J)$ shows a broad minimum, dropping to zero in the important region in the center of the energy band: the most important energies show the smallest fluctuations. Note, however, that this does not automatically single out $H^{quad}$ as the most robust system; Fig. 5.6b indicates that for many values of $N$ or $\varepsilon_J$ $H^{quad}$ is the best system if $N$ is odd, but the worst one if $N$ is even, although the $\sigma(E_k, \varepsilon_J)$ of $H^{quad}$ for odd $N$ show a behavior similar to the lower panel of Fig. 5.8 (compare Fig. 8 of [9]). The difference between even and odd may thus be more important than that between different system types.

The maximum achievable fidelity is only one of several critical issues in quantum information transfer. Other important points are the speed of transmission which we discussed already, and the necessary precision in timing [56] when reading out the transferred state at the receiver qubit. Figure 5.5 shows that the duration during which $F(t)$ is close to its maximum value varies enormously between the different systems. For ordered PST systems that time scale can be determined by calculating the quantity $|f_N(t)|^2$ (see Sect. 5.2.2.1) at time $t = t_{PST} + \delta t$, where $t_{PST}$ is given by (5.15). Starting from (5.14) and observing the spatial symmetry of PST systems as well as the PST condition (5.15), we obtain

$$|f_N(t_{PST}+\delta t)|^2 = \sum_{k,s} P_{k,1} P_{s,1} \mathrm{e}^{-\mathrm{i}(E_k - E_s)\frac{\delta t}{\hbar}} \approx 1 - \frac{1}{2}\left(\frac{\delta t}{\hbar}\right)^2 \sum_{k,s} P_{k,1} P_{s,1} (E_k - E_s)^2. \tag{5.18}$$

Thus $|f_N(t)|^2$ stays close to unity for a long time if $P_{k,1}$ is concentrated on a small number of states in a spectral region with particularly small energy differences. This favors the PST system with quadratic spectrum among several PST systems with power-law spectra [9]. In the $H^{\alpha_0}$ system the dynamics of $F(t)$ is determined by a single sinusoidal oscillation between two states with very small energy difference, leading to both long transfer times and long time windows for readout. The $H^{\alpha_{opt}}$ system, in contrast, is similar to the $H^{lin}$ system by construction.

## 5.3 Other Theoretical Approaches

In this section we review some studies dealing with the robustness of quantum information transfer schemes. We are restricting ourselves to the transfer of single-qubit states and we consider only static randomness inherent in the system, that is, fabrication errors. Furthermore, although interesting schemes involving different kinds of qubit networks [60–65] have been suggested, we will discuss only strictly one-dimensional systems. Despite these restrictions we are sure to have missed some important contributions in this rapidly developing field.

Nikolopoulos et al. [29, 66] proposed a model for electron transport in a linear array of tunnel-coupled quantum dots. Single-electron transport in that model is equivalent to single-qubit transfer along a nearest-neighbor spin-1/2 XX chain. Both constant couplings and a set of couplings leading to perfect state transfer [21] were considered. The influence of disorder and interactions was studied in numerical simulations for small systems. The robustness of that scheme against disorder was studied again in [67] (see also [29, 66]). Two types of disorder were considered. Diagonal (local) disorder is caused by hyperfine interactions in each dot which can be modelled by a random (Gaussian) classical Overhauser field acting on the spins. Off-diagonal disorder results in the nearest-neighbor Heisenberg exchange interactions fluctuating in time more or less rapidly. Numerical simulations of short ($N \leq 10$) chains showed diagonal disorder to be more dangerous than off-diagonal disorder and antiferromagnetic chains to be more robust than ferromagnetic ones.

An influential early paper is the study [54] by De Chiara et al. who considered the influence of disorder on the state transfer properties of the PST chain with linear energy spectrum [21], that is, the model called $H^{lin}$ in Sect. 5.2.3. Both the nearest-neighbor couplings $J_i$ and the local $z$ fields $h_i$ ($h_i = 0$ in the ideal case) were assumed random. Borrowing from the language of single-particle transport in a one-dimensional tight-binding chain, one might call the disorder in $h_i$ diagonal and the disorder in $J_i$ off-diagonal. These two kinds of disorder are known to have fundamentally different effects on the localization and transport properties of nearest-neighbor coupled tight-binding chains [68, 69]. In fact, these two kinds of disorder also turn out to be very different for the spin chains in [54]: Coupling constant disorder is the more detrimental the longer the chains become, while magnetic field disorder apparently averages out for longer chains. Numerical evidence and perturbation calculations for weak disorder show that the fidelity[5] is a decreasing function of the two variables $N\varepsilon_J^2$ and $\varepsilon_h^2/N$, where $\varepsilon_J$ measures the strength of the (relative) coupling disorder (see Sect. 5.2.2.2) and $\varepsilon_h$ does the same for the (absolute) field disorder. Note that the ideal coupling values $J_i = \tilde{J}\sqrt{i(N-i)}$ scale with the chain length so that a given relative disorder strength $\varepsilon_J$ entails larger absolute changes in the couplings for longer chains.

[5] To be precise: the fidelity between the first and last spins, averaged over the Bloch sphere with respect to the first spin, calculated at $t_{PST}$ and averaged over the disorder.

In contrast the random fields $h_i$ do not scale with $N$, and $\varepsilon_h^2/N$ is what the central limit theorem yields for the variance of the (zero) average field $\frac{1}{N}\sum_i h_i$.

Burrell and Osborne [70] investigated correlations in an infinite XX chain with random nearest-neighbor interactions and a random magnetic field and showed that all correlations are exponentially suppressed outside of an effective "light cone" whose radius grows at most logarithmically in time (and hence is no light cone at all). This means that information transfer out of a region of given size will take exponentially long times in the limit of an infinite system. This is Anderson localization at work: In one dimension all states go localized at arbitrarily small diagonal disorder [68], but things are different for off-diagonal disorder [69] since in that case there is always a delocalized state at the center of the band. Localization effects were also discussed by Keating et al. [71], unfortunately without clear distinction between the two kinds of disorder. However, localization can be overcome for finite systems. In fact, it has been shown [72] how to employ quantum error correction techniques to send a qubit with high fidelity using several imperfect spin chains in parallel, over distances large compared to the individual chain's localization length. In temporally fluctuating fields things are different, see [73] for a study of localization properties in that case.

An early example for robustness considerations is the paper by Kay [56], which contains a section about manufacturing errors. This paper considers couplings beyond nearest neighbors in XX chains and also discusses the influence of, for example, timing errors when reading out the transmitted state. The advantages of the linear-spectrum PST chain [21] are stressed.

Creation and dynamics of entanglement in linear arrays of Josephson qubits were studied in [74] for short ($N \sim 10$) and intermediate-length ($N = 40$) chains. Coupling disorder was concluded to be less detrimental than noise from separate bosonic baths coupled to each qubit.

Three different scenarios of quantum information transfer along XX spin chains are covered in [57]. The first scenario involves sequential SWAP operations effected by switching in turn every single spin coupling for an appropriate duration. The second scenario employs the natural dynamics of the PST system $H^{lin}$ without any external driving, while the third one achieves adiabatic state transfer by slowly switching all even and odd couplings appropriately. The transfer times for all these schemes scale as $\tau \sim N/J_{max}$, where $J_{max}$ is the maximum coupling available. All three scenarios are studied in the presence of diagonal (magnetic field) and off-diagonal (exchange coupling) static randomness. It turns out that the sequential SWAP scheme is most susceptible to randomness, especially of the off-diagonal type. The PST system $H^{lin}$ is more robust than the sequential SWAP scheme, but the adiabatic state transfer scheme is most noise-tolerant, at least for the system sizes ($N \leq 51$) studied.

Another scheme involving external driving was suggested in [75]. A special chain of corner-sharing squares of spins 1/2 with nearest-neighbor XX couplings can be mapped to an array of separate short chain sections whose natural dynamics is assisted by regular global pulses which achieve the transfer between separate

subchains. The pulses are supposed to be slightly random in timing, and also in the effective direction of the applied field. It turns out that the state transfer is more robust when the noise contains some amount of correlations.

Ronke et al. [58] performed a comprehensive study of robustness of state transfer in short PST chains ($N \leq 15$) with linear spectrum [21]. The built-in perturbations considered were randomness in the nearest-neighbor couplings, site-dependent random magnetic fields, interactions between travelling excitations and unwanted next-nearest neighbor spin couplings. In addition, also handling errors, such as readout timing errors were studied. It was found that next-nearest neighbor spin couplings had the strongest detrimental affair on the quality of state transfer. The general behavior of the transfer fidelity was found to be consistent with an exponential decay with chain length and a Gaussian dependence on the disorder strength.

Bruderer et al. [76] suggested a smart hybrid approach unifying advantages of the fully-engineered and boundary-controlled state transfer schemes. Their idea amounts to optimizing the temporal structure (commensurate spectrum leading to perfect periodicity) and the spatial structure (boundary-localized states insensitive to perturbations from the interior of the chain) at the same time. As an example, consider an odd-$N$ XX chain without external magnetic field and with a linear energy spectrum with spacing $\Delta E = M$ (integer, in appropriate units), and with the well-known [21] nearest-neighbor spin couplings. Since $N$ is odd, there is a zero energy eigenvalue. Now shift all positive (negative) eigenvalues down (up) by $M-1$, creating three equidistant energy eigenvalues $0, \pm\Delta E/M$ in the middle of the spectrum. The spectrum is still commensurate, with the perfect state transfer time extended by a factor $M$. Solution of the inverse eigenvalue problem corresponding to the modified spectrum shows that the two boundary couplings are significantly reduced and that two strongly localized boundary states emerge, which are mainly responsible for the state transfer and which are not too sensitive to disorder in the couplings, as numerical results show.

A striking effect is displayed [76] by a chain with an "inverted quadratic" spectrum,

$$E_k = k(N-1-|k|) \quad k = -\frac{N-1}{2}, \ldots, \frac{N-1}{2}. \tag{5.19}$$

Note that the spectrum is very different from the "quadratic" spectrum (5.16) discussed earlier. In (5.19) the largest energy differences occur in the middle of the spectrum, whereas in (5.16) they show up at the boundaries of the spectrum. If the spectrum (5.19) is "contracted" towards the center as discussed above for the linear spectrum, only three states dominate the state transfer and the overlap $|f_N(t)|$ (see (5.12) and (5.13)) is an almost purely sinusoidal function with a broad maximum at $t_{PST}$, in contrast to the chain with the original spectrum (5.19), where $|f_N(t)|$ displays a needle-like peak at the same time. The spectral manipulation thus effectively removes the overwhelming majority of all Fourier components from the

function $f_N(t)$, making the system much more robust with respect to timing errors in the readout process.

The influence of static randomness on short isotropic Heisenberg (XXX) antiferromagnetic chains was studied in [45]. These chains can be used as spin buses if the sender and receiver spins (qubits) $A$ and $B$ are coupled weakly to two nodes of the $N$-spin chain, not necessarily the first and $N$th ones. If the gaps between the low-lying states of the isolated chain are sufficiently large, perturbation theory can be used to calculate the effects on the spins $A$ and $B$. For even $N$ it turns out that the chain can be replaced by an effective coupling between $A$ and $B$, while for odd $N$ the chain effectively reduces to a single spin coupled to $A$ and $B$. Oh et al. [45] performed a detailed study on how randomness in nearest-neighbor couplings and local magnetic fields influences the energy gaps and effective couplings governing the spin-bus performance. Numerical results for short chains of both even and odd lengths were reported. Note that long chains in this scheme become increasingly problematic since the relevant energy gaps close with growing $N$, making it more and more difficult to fulfill the condition under which perturbation theory is applicable.

An approach similar in spirit to the boundary-controlled system $H^{\alpha_0}$ was studied very recently in [77], where boundary-localized states were created by erecting high magnetic field barriers on sites close to the ends of a homogeneous XX chain. The system was shown to be reasonably robust against small random static magnetic fields in the interior of the chain.

Also very recently the PST scheme suggested by Christandl et al. [21] was implemented in an array of 9 [78] or 19 [79] laterally coupled parallel waveguides. In this optical implementation transitions in time between neighboring sites of the spin chain are mapped to transitions between neighboring waveguides, taking place along the longitudinal coordinate of the waveguides. In the experiment, reasonable fidelity was observed despite some imperfections in the spacing, and thus the coupling, of the waveguides.

## 5.4 Experimental Implementations

In this section we review some of the experimental implementations of state transfer using protocols based on spin chain channels and show their present limitations. Every proposal for physical qubits that allows to couple them permanently can be used to develop spin chains. Therefore, in solid-state systems, there are proposals to implement qubit chains using superconducting nanocircuits, such as charge qubits [80, 81], Josephson junctions [74, 82, 83] or flux qubits [84, 85]. The advances in semiconductor technology allow to couple quantum dots, so there are proposals using chains of charged quantum dots [29, 66, 86] or alternatively, excitons in quantum dots [87, 88]. Spin chains can be also simulated in optical lattices [78, 79, 89–94] or with nuclear spin systems in NMR [95–97]. Nitrogen vacancy centers in diamond [47, 98–101] constitute another promising solid-state system.

However, only very few of these systems have actually developed into experimental implementations of quantum spin channels and in particular NMR was the pioneer setup for testing these protocols.

The main limitation to make these quantum channels a reality is decoherence, which not only affects the survival time of the quantum information [102], but also affects the distance over which it can be transmitted [54, 70–72, 103–107]. Perfect or high fidelity state transfer can be obtained by many of the theoretical methods described so far. However, if the ideal control Hamiltonian or system for the state transfer is affected by decoherence, the transfer fidelity can be remarkably reduced. Decoherence effects can come from either time dependent perturbations or even static ones. In order to show this, let us consider the simplest quantum channel of two qubits, where a SWAP operation transfers the state from one qubit to the other. The experimental implementation of a SWAP operation was first addressed within the field of liquid state NMR [108–110]. However, pioneering solid state NMR experiments performed by Müller et al. [111] can now be identified as a SWAP operation. Even in this simple two-qubit channel the swapping oscillation is damped by a decoherence rate that depends on the rate of interaction with the environment. Even worse, if the interaction rate with the environment becomes larger than the ideal swapping frequency between the two spins, the swap is frozen, manifesting an overdamped dynamics due to localization effects of the initial excitation [106, 112, 113].

Ideally quantum communication is expected to be performed by means of pure-state transfers. Consequently most of the theoretical approaches focused on pure-state communication processes, but experimental realization of pure states is a major challenge for present technologies. Just recently a lot of progress has been made with superconducting devices, semiconductor technologies, optical lattices and Nitrogen vacancy centers where pure states can be generated and controlled, even at the single qubit level [114–119]. However, the first implementations of quantum computation were based on ensemble quantum computing using mixed states that mimic pure-state quantum evolutions, in particular with NMR setups [96, 97, 120]. State transfer in a solid state system has been observed in a ring of spins with dipolar (many-body) interactions [121, 122]. An initial polarization localized in a specific spin of the ring propagates around the ring and after a time related to the ring length, a constructive interference reappears in the form of an echo [121,122]. This mesoscopic echo [123] reflects the quantum nature of the finite quantum spin-ring. However, the many-body nature of these spin-spin interactions made these systems sensitive to perturbations which strongly reduce the amplitude of the echo [124]. In order to improve the state transfer fidelity an effective XX interaction Hamiltonian[6] has been experimentally implemented in a spin chain by Mádi et al. [95] by using global-pulse rotations of the spins in a liquid state sample. In Ref. [95], the evolution of the initial excitation was monitored in all the spins of

[6]Many experimental references employ the term XY or planar interaction for what we call XX interaction here.

the quantum channel. In that work two important features deserve special attention. On the one hand it is relevant to be able to generate, even if artificially, the simple one-body XX Hamiltonian for state transfer because it increases the transfer fidelity in comparison to more complicated many-body Hamiltonians. On the other hand, by comparing the experimentally observed evolution of polarization transfer to the ideal design, one can assess the decoherence effects reducing the transfer fidelity. These decoherence effects originate from the finite precision of control pulses and from interactions with external degrees of freedom changing the coupling strengths between the spins and/or their Zeeman energies.

Due to the non scalability of liquid state NMR, more recently, implementations of spin chains were attempted in solid-state NMR [125–130] which mimic the XX state transfer evolution. This approach is based on experimentally generating a double quantum Hamiltonian where the evolution of a locally prepared initial state can be mapped to the one generated by an XX interaction [131]. However, these systems do not allow individual addressing of the qubits, engineering of the coupling strengths or local manipulations for generating PST.

Up to now, PST protocols could only be implemented in systems of very few spins, mainly in trivial cases of 2 [108–110] and 3 [132, 133] spins interacting by a homogeneous XX interaction. Again, the XX interaction was not natural and in particular in these cases it was engineered by controlling the spins individually and generating the desired effective Hamiltonian. Similarly, but only requiring global control-pulses on a 6-spin system, effective chains of 2, 3, and 6 spins were generated for implementing PST protocols [134]. In this case the selective spin-spin coupling networks were created by exploiting selective quantum interferences in the time domain to filter out the undesired couplings while leaving intact the desired ones [134]. The process can be interpreted as a time-domain analog of Bragg gratings that filter the non-selected coupling strengths [135, 136]. Alternative state transfer protocols with spin chains for achieving arbitrarily high fidelities were constructed applying iterative state transfer [24] along chains of 3 and 4 spins by controlling only the boundary spins [137, 138]. Again, in all these cases decoherence by external degrees of freedom or finite precision control changes the coupling strengths or induces energy fluctuations of the spins affecting the transfer fidelity.

The decoherence effects also are the main limitation on the chain lengths. Decoherence effects increase as the number of qubits increases [105, 107, 139–142]. The sensitivity of the quantum states grows with the number of spins, causing imperfections, disorder or external influence on the couplings within the spin channel to induce localization of the quantum information [54, 70–72, 103–105, 107, 143]. These localization effects were recently observed experimentally in three-dimensional spin-network topologies with about 7,000 spins, where the localization effects were induced by finite precision control of the quantum gates driving the information transfer [105, 107]. Thus it is clear that the only way of building quantum computers or quantum simulators has to be based on developing robust methods of controlling the information and in particular the state transfer [144].

**Acknowledgements** A. Z. and O. O. acknowledge support from SECYT-UNC and CONICET. A. Z. thanks for support by DAAD, G. A. A. for support by Alexander von Humboldt Foundation; both acknowledge the hospitality and support of Fakultät Physik of TU Dortmund.

## References

1. E. Ising, Z. Phys. **31**, 253 (1925)
2. H.A. Bethe, Z. Phys. **71**, 205 (1931)
3. E. Balcar, S.W. Lovesey, *Theory of Magnetic Neutron and Photon Scattering*. Oxford Series on Neutron Scattering in Condensed Matter (Oxford University Press, Oxford, 1989)
4. J.G. Bednorz, K.A. Müller, Z. Phys. B Condens. Matter **64**, 189 (1986)
5. J. Deisenhofer, M. Schmidt, Z. Wang, C. Kant, F. Mayr, F. Schrettle, H.A. Krug von Nidda, P. Ghigna, V. Tsurkan, A. Loidl, Ann. Phys. (Berl.) **523**, 645 (2011)
6. K. Uchinokura, J. Phys. Condens. Matter **14**, R195 (2002)
7. D.C. Mattis, *The Theory of Magnetism I – Statics and Dynamics*. Springer Series in Solid-State Sciences, vol. 17 (Springer, Berlin, 1981)
8. T.J. Osborne, N. Linden, Phys. Rev. A **69**, 052315 (2004)
9. A. Zwick, G.A. Álvarez, J. Stolze, O. Osenda, Phys. Rev. A **84**, 022311 (2011)
10. A. Zwick, G.A. Álvarez, J. Stolze, O. Osenda, Phys. Rev. A **85**, 012318 (2012)
11. A. Zwick, G.A. Álvarez, J. Stolze, O. Osenda, Optimal quantum state transfer in disordered spin chains. Preprint arXiv:1306.1695
12. J.D. Johnson, S. Krinsky, B.M. McCoy, Phys. Rev. A **8**, 2526 (1973)
13. E. Lieb, T. Schultz, D. Mattis, Ann. Phys. **16**, 407 (1961)
14. S. Katsura, Phys. Rev. **127**, 1508 (1962)
15. P. Jordan, E. Wigner, Z. Phys. **47**, 631 (1928)
16. S. Bose, Phys. Rev. Lett. **91**, 207901 (2003)
17. M. Horodecki, P. Horodecki, R. Horodecki, Phys. Rev. A **60**, 1888 (1999)
18. D. Burgarth, S. Bose, Phys. Rev. A **71**, 052315 (2004)
19. D. Burgarth, V. Giovannetti, S. Bose, J. Phys. A Math. Gen. **38**, 6793 (2005)
20. V. Subrahmanyam, Phys. Rev. A **69**, 034304 (2004)
21. M. Christandl, N. Datta, A. Ekert, A.J. Landahl, Phys. Rev. Lett. **92**, 187902 (2004)
22. C. Godsil, S. Kirkland, S. Severini, J. Smith, Phys. Rev. Lett. **109**, 050502 (2012)
23. H.L. Haselgrove, Phys. Rev. A **72**, 062326 (2005)
24. D. Burgarth, V. Giovannetti, S. Bose, Phys. Rev. A **75**, 062327 (2007)
25. D. Burgarth, Eur. Phys. J. Spec. Top. **151**, 147 (2007)
26. A.I. Zenchuk, J. Phys. A Math. Gen. **45**, 115306 (2012)
27. S. Bose, Contemp. Phys. **48**, 13 (2007)
28. R.J. Cook, B.W. Shore, Phys. Rev. A **20**, 539 (1979)
29. G.M. Nikolopoulos, D. Petrosyan, P. Lambropoulos, J. Phys. Condens. Matter **16**, 4991 (2004)
30. C. Albanese, M. Christandl, N. Datta, A. Ekert, Phys. Rev. Lett. **93**, 230502 (2004)
31. N.M. Atakishiyev, E.I. Jafarov, S.M. Nagiyev, K.B. Wolf, Rev. Mex. de Fis. **44**, 235 (1998)
32. T. Shi, Y. Li, Z. Song, C.P. Sun, Phys. Rev. A **71**, 032309 (2005)
33. M.H. Yung, S. Bose, Phys. Rev. A **71**, 032310 (2005)
34. P. Karbach, J. Stolze, Phys. Rev. A **72**, 030301(R) (2005)
35. G.M.L. Gladwell, *Inverse Problems in Vibration*, 2nd edn. (Kluwer, Dordrecht, 2004)
36. M.T. Chu, G.H. Golub, *Inverse Eigenvalue Problems: Theory, Algorithms, and Applications* (Oxford University Press, Oxford, 2005)
37. Y. Wang, F. Shuang, H. Rabitz, Phys. Rev. A **84**, 012307 (2011)
38. V. Kostak, G.M. Nikolopoulos, I. Jex, Phys. Rev. A **75**, 042319 (2007)
39. L. Vinet, A. Zhedanov, Phys. Rev. A **86**, 052319 (2012)

40. A. Kay, Int. J. Quantum Inf. **8**, 641 (2010)
41. M.B. Plenio, F.L. Semião, New J. Phys. **7**, 73 (2005)
42. A. Wójcik, T. Łuczak, P. Kurzyński, A. Grudka, T. Gdala, M. Bednarska, Phys. Rev. A **72**, 034303 (2005)
43. Y. Li, T. Shi, B. Chen, Z. Song, C.P. Sun, Phys. Rev. A **71**, 022301 (2005)
44. L. Campos Venuti, C. Degli Esposti Boschi, M. Roncaglia, Phys. Rev. Lett. **99**, 060401 (2007)
45. S. Oh, Y.P. Shim, J. Fei, M. Friesen, X. Hu, Phys. Rev. B **85**, 224418 (2012)
46. G. Gualdi, V. Kostak, I. Marzoli, P. Tombesi, Phys. Rev. A **78**, 022325 (2008)
47. N. Yao, L. Jiang, A.V. Gorshkov, Z.X. Gong, A. Zhai, L.M. Duan, M.D. Lukin, Phys. Rev. Lett. **106**, 040505 (2011)
48. A. Casaccino, S. Lloyd, S. Mancini, S. Severini, Int. J. Quantum Inf. **7**, 1417 (2009)
49. T. Linneweber, J. Stolze, G.S. Uhrig, Int. J. Quantum Inf. **10**, 1250029 (2012)
50. A. Zwick, O. Osenda, J. Phys. A Math. Gen. **44**, 105302 (2011)
51. L. Banchi, T.J.G. Apollaro, A. Cuccoli, R. Vaia, P. Verrucchi, Phys. Rev. A **82**, 052321 (2010)
52. L. Banchi, T.J.G. Apollaro, A. Cuccoli, R. Vaia, P. Verrucchi, New J. Phys. **13**, 123006 (2011)
53. T.J.G. Apollaro, L. Banchi, A. Cuccoli, R. Vaia, P. Verrucchi, Phys. Rev. A **85**, 052319 (2012)
54. G. De Chiara, D. Rossini, S. Montangero, R. Fazio, Phys. Rev. A **72**, 012323 (2005)
55. M. Christandl, N. Datta, T.C. Dorlas, A. Ekert, A. Kay, A.J. Landahl, Phys. Rev. A **71**, 032312 (2005)
56. A. Kay, Phys. Rev. A **73**, 032306 (2006)
57. D. Petrosyan, G.M. Nikolopoulos, P. Lambropoulos, Phys. Rev. A **81**, 042307 (2010)
58. R. Ronke, T.P. Spiller, I. D'Amico, Phys. Rev. A **83**, 012325 (2011)
59. T. Ladd, F. Jelezko, R. Laflamme, Y. Nakamura, C. Monroe, J.L. O'Brien, Nature **464**, 45 (2010)
60. M.A. Jafarizadeh, R. Sufiani, Phys. Rev. A **77**, 022315 (2008)
61. D.I. Tsomokos, M.B. Plenio, I. de Vega, S.F. Huelga, Phys. Rev. A **78**, 062310 (2008)
62. S.I. Doronin, E.B. Fel'dman, A.I. Zenchuk, Phys. Rev. A **79**, 042310 (2009)
63. V. Kendon, C. Tamon, J. Comput. Theor. Nanosci. **8**, 422 (2011)
64. D.I. Tsomokos, Phys. Rev. A **83**, 052315 (2011)
65. A. Ajoy, P. Cappellaro, Phys. Rev. B **87**, 064303 (2013)
66. G.M. Nikolopoulos, D. Petrosyan, P. Lambropoulos, Europhys. Lett. **65**, 297 (2004)
67. S. Yang, A. Bayat, S. Bose, Phys. Rev. A **82**, 022336 (2010)
68. B. Kramer, A. MacKinnon, Rep. Prog. Phys. **56**, 1469 (1993)
69. M. Inui, S. Trugman, E. Abrahams, Phys. Rev. B **49**, 3190 (1994)
70. C.K. Burrell, T.J. Osborne, Phys. Rev. Lett. **99**, 167201 (2007)
71. J.P. Keating, N. Linden, J.C.F. Matthews, A. Winter, Phys. Rev. A **76**, 012315 (2007)
72. J. Allcock, N. Linden, Phys. Rev. Lett. **102**, 110501 (2009)
73. C.K. Burrell, J. Eisert, T.J. Osborne, Phys. Rev. A **80**, 052319 (2009)
74. D.I. Tsomokos, M.J. Hartmann, S.F. Huelga, M.B. Plenio, New J. Phys. **9**, 79 (2007)
75. F. Benatti, R. Floreanini, V. Karimipour, Phys. Rev. A **86**, 062335 (2012)
76. M. Bruderer, K. Franke, S. Ragg, W. Belzig, D. Obreschkow, Phys. Rev. A **85**, 022312 (2012)
77. S. Lorenzo, T.J.G. Apollaro, A. Sindona, F. Plastina, Phys. Rev. A **87**, 042313 (2013)
78. M. Bellec, G.M. Nikolopoulos, S. Tzortzakis, Opt. Lett. **37**, 4504 (2012)
79. A. Perez-Leija, R. Keil, A. Kay, H. Moya-Cessa, S. Nolte, L.C. Kwek, B.M. Rodríguez-Lara, A. Szameit, D.N. Christodoulides, Phys. Rev. A **87**, 012309 (2013)
80. A. Romito, R. Fazio, C. Bruder, Phys. Rev. B **71**, R100501 (2005)
81. F.W. Strauch, C.J. Williams, Phys. Rev. B **78**, 094516 (2008)
82. J. Majer, J.M. Chow, J.M. Gambetta, J. Koch, B.R. Johnson, J.A. Schreier, L. Frunzio, D.I. Schuster, A.A. Houck, A. Wallraff, A. Blais, M.H. Devoret, S.M. Girvin, R.J. Schoelkopf, Nature **449**, 443 (2007)
83. M.A. Sillanpää, J.I. Park, R.W. Simmonds, Nature **449**, 438 (2007)
84. A. Lyakhov, C. Bruder, New J. Phys. **7**, 181 (2005)
85. A.O. Lyakhov, C. Bruder, Phys. Rev. B **74**, 235303 (2006)
86. D. Petrosyan, P. Lambropoulos, Opt. Commun. **264**, 419 (2006)

87. I. D'Amico, Microelectron. J. **37**, 1440 (2006)
88. T.P. Spiller, I. D'Amico, B.W. Lovett, New J. Phys. **9**, 20 (2007)
89. U. Dorner, P. Fedichev, D. Jaksch, M. Lewenstein, P. Zoller, Phys. Rev. Lett. **91**, 073601 (2003)
90. L.M. Duan, E. Demler, M.D. Lukin, Phys. Rev. Lett. **91**, 090402 (2003)
91. M.J. Hartmann, F.G.S.L. Brandão, M.B. Plenio, Phys. Rev. Lett. **99**, 160501 (2007)
92. M. Lewenstein, A. Sanpera, V. Ahufinger, B. Damski, A. Sen(De), U. Sen, Adv. Phys. **56**, 243 (2007)
93. S. Ospelkaus, A. Pe'er, K.K. Ni, J.J. Zirbel, B. Neyenhuis, S. Kotochigova, P.S. Julienne, J. Ye, D.S. Jin, Nat. Phys. **4**, 622 (2008)
94. B.P. Lanyon, C. Hempel, D. Nigg, M. Müller, R. Gerritsma, F. Zähringer, P. Schindler, J.T. Barreiro, M. Rambach, G. Kirchmair, M. Hennrich, P. Zoller, R. Blatt, C.F. Roos, Science **334**, 57 (2011)
95. Z.L. Mádi, B. Brutscher, T. Schulte-Herbrüggen, R. Brüschweiler, R.R. Ernst, Chem. Phys. Lett. **268**, 300 (1997)
96. D.G. Cory, A.F. Fahmy, T.F. Havel, Proc. Natl. Acad. Sci. USA **94**, 1634 (1997)
97. N.A. Gershenfeld, I.L. Chuang, Science **275**, 350 (1997)
98. P. Cappellaro, L. Jiang, J.S. Hodges, M.D. Lukin, Phys. Rev. Lett. **102**, 210502 (2009)
99. P. Neumann, R. Kolesov, B. Naydenov, J. Beck, F. Rempp, M. Steiner, V. Jacques, G. Balasubramanian, M.L. Markham, D.J. Twitchen, S. Pezzagna, J. Meijer, J. Twamley, F. Jelezko, J. Wrachtrup, Nat. Phys. **6**, 249 (2010)
100. N.Y. Yao, L. Jiang, A.V. Gorshkov, P.C. Maurer, G. Giedke, J.I. Cirac, M.D. Lukin, Nat. Commun. **3**, 800 (2012)
101. Y. Ping, B.W. Lovett, S.C. Benjamin, E.M. Gauger, Phys. Rev. Lett. **110**, 100503 (2013)
102. W. Zurek, Rev. Mod. Phys. **75**, 715 (2003)
103. A. Pomeransky, D. Shepelyansky, Phys. Rev. A **69**, 014302 (2004)
104. T. Apollaro, F. Plastina, Open Syst. Inf. Dyn. **14**, 41 (2007)
105. G.A. Álvarez, D. Suter, Phys. Rev. Lett. **104**, 230403 (2010)
106. G.A. Álvarez, E.P. Danieli, P.R. Levstein, H.M. Pastawski, Phys. Rev. A **82**, 012310 (2010)
107. G.A. Álvarez, D. Suter, Phys. Rev. A **84**, 012320 (2011)
108. M.A. Nielsen, E. Knill, R. Laflamme, Nature **396**, 52 (1998)
109. Z.L. Madi, R. Brüschweiler, R.R. Ernst, J. Chem. Phys. **109**, 10603 (1998)
110. N. Linden, H. Barjat, E. Kupce, R. Freeman, Chem. Phys. Lett. **307**, 198 (1999)
111. L. Müller, A. Kumar, T. Baumann, R.R. Ernst, Phys. Rev. Lett. **32**, 1402 (1974)
112. G.A. Álvarez, E.P. Danieli, P.R. Levstein, H.M. Pastawski, J. Chem. Phys. **124**, 194507 (2006)
113. G.A. Álvarez, P.R. Levstein, H.M. Pastawski, Physica B **398**, 438 (2007)
114. T.D. Ladd, F. Jelezko, R. Laflamme, Y. Nakamura, C. Monroe, J.L. O'Brien, Nature **464**, 45 (2010)
115. J.I. Cirac, P. Zoller, Nat. Phys. **8**, 264 (2012)
116. I. Bloch, J. Dalibard, S. Nascimbène, Nat. Phys. **8**, 267 (2012)
117. R. Blatt, C.F. Roos, Nat. Phys. **8**, 277 (2012)
118. A. Aspuru-Guzik, P. Walther, Nat. Phys. **8**, 285 (2012)
119. A.A. Houck, H.E. Türeci, J. Koch, Nat. Phys. **8**, 292 (2012)
120. E. Knill, R. Laflamme, Phys. Rev. Lett. **81**, 5672 (1998)
121. H.M. Pastawski, P.R. Levstein, G. Usaj, Phys. Rev. Lett. **75**, 4310 (1995)
122. H.M. Pastawski, G. Usaj, P.R. Levstein, Chem. Phys. Lett. **261**, 329 (1996)
123. V.N. Prigodin, B.L. Altshuler, K.B. Efetov, S. Iida, Phys. Rev. Lett. **72**, 546 (1994)
124. P.R. Levstein, G. Usaj, H.M. Pastawski, J. Chem. Phys. **108**, 2718 (1998)
125. P. Cappellaro, C. Ramanathan, D.G. Cory, Phys. Rev. A **76**, 032317 (2007)
126. P. Cappellaro, C. Ramanathan, D.G. Cory, Phys. Rev. Lett. **99**, 250506 (2007)
127. E. Rufeil-Fiori, C.M. Sanchez, F.Y. Oliva, H.M. Pastawski, P.R. Levstein, Phys. Rev. A **79**, 032324 (2009)
128. W. Zhang, P. Cappellaro, N. Antler, B. Pepper, D.G. Cory, V.V. Dobrovitski, C. Ramanathan, L. Viola, Phys. Rev. A **80**, 052323 (2009)

129. P. Cappellaro, L. Viola, C. Ramanathan, Phys. Rev. A **83**, 032304 (2011)
130. C. Ramanathan, P. Cappellaro, L. Viola, D.G. Cory, New J. Phys. **13**, 103015 (2011)
131. S.I. Doronin, E.B. Fel'dman, Solid State Nucl. Magn. Reson. **28**, 111 (2005)
132. J. Zhang, G.L. Long, W. Zhang, Z. Deng, W. Liu, Z. Lu, Phys. Rev. A **72**, 012331 (2005)
133. A. Ajoy, R.K. Rao, A. Kumar, P. Rungta, Phys. Rev. A **85**, 030303 (2012)
134. G.A. Álvarez, M. Mishkovsky, E.P. Danieli, P.R. Levstein, H.M. Pastawski, L. Frydman, Phys. Rev. A **81**, 060302(R) (2010)
135. A. Ajoy, G.A. Álvarez, D. Suter, Phys. Rev. A **83**, 032303 (2011)
136. A. Ajoy, P. Cappellaro, Phys. Rev. Lett. **110**, 220503 (2013)
137. J. Zhang, N. Rajendran, X. Peng, D. Suter, Phys. Rev. A **76**, 012317 (2007)
138. J. Zhang, M. Ditty, D. Burgarth, C.A. Ryan, C.M. Chandrashekar, M. Laforest, O. Moussa, J. Baugh, R. Laflamme, Phys. Rev. A **80**, 012316 (2009)
139. H.G. Krojanski, D. Suter, Phys. Rev. Lett. **93**, 090501 (2004)
140. H.G. Krojanski, D. Suter, Phys. Rev. Lett. **97**, 150503 (2006)
141. H.G. Krojanski, D. Suter, Phys. Rev. A **74**, 062319 (2006)
142. M. Lovric, H.G. Krojanski, D. Suter, Phys. Rev. A **75**, 042305 (2007)
143. C. Burrell, J. Eisert, T. Osborne, Phys. Rev. A **80**, 052319 (2009)
144. P. Hauke, F.M. Cucchietti, L. Tagliacozzo, I. Deutsch, M. Lewenstein, Rep. Prog. Phys. **75**, 082401 (2012)

# Chapter 6
# Implementation of State Transfer Hamiltonians in Spin Chains with Magnetic Resonance Techniques

**Paola Cappellaro**

**Abstract** Nuclear spin systems and magnetic resonance techniques have provided a fertile platform for experimental investigation of quantum state transfer in spin chains. From the first observation of polarization transfer, predating the formal definition of quantum state transfer, to the realization of state transfer simulations in small molecules and in larger solid-state spin systems, the experiments have drawn on the strengths of nuclear magnetic resonance (NMR), in particular on its long history of well-developed control techniques. NMR implementations have been invaluable both as proof-of-principle demonstrations of quantum state transfer protocols and to explore dynamics occurring in real systems that go beyond what can be analytically solved or numerically simulated. In addition, control techniques developed in these systems to engineer the Hamiltonians required for transport can be adopted in potentially scalable quantum information processing architectures. In this contribution we describe recent results and outline future directions of research in magnetic-resonance based implementations of quantum state transfer in spin chains.

## 6.1 Introduction

The goal of quantum state transfer (QST) is to map quantum information from one qubit to a distant one, for example in quantum communication protocols or in distributed quantum information processing (QIP) architectures. While photons are ideal carriers of quantum information, when state transfer is required in solid-state systems, between not too distant qubits, an alternative strategy [1] relies only on the natural evolution of a permanently coupled chain of quantum systems.

P. Cappellaro (✉)
Nuclear Science and Engineering Department, Research Laboratory of Electronics, Massachusetts Institute of Technology, Cambridge, MA 01239, USA
e-mail: pcappell@mit.edu

G.M. Nikolopoulos and I. Jex (eds.), *Quantum State Transfer and Network Engineering*, Quantum Science and Technology, DOI 10.1007/978-3-642-39937-4_6,

Various systems have been proposed as experimental implementation of this scheme, including Josephson junction arrays [2], excitons and spins in quantum dots [3, 4], electrons in Penning traps [5] and ultracold atoms in a 1D optical lattice [6, 7]. Among all the proposed experimental systems, spins-1/2 stand out as the most natural one, thanks to the direct mapping from the theoretical model. Using electronic or nuclear spins as the physical basis for quantum wires can in addition take advantage of the well-developed techniques of magnetic resonance.

Spin systems are also at the center of many QIP proposals, starting from the famous scheme by Kane [8] and arriving to more recent proposals, including for example the Nitrogen Vacancy center in diamond [9]. In this context, it might be beneficial to use some of these spin qubits as quantum wires.

While no current implementation of magnetic resonance spin-based QIP has reached the level of control and complexity required for a scalable architecture, smaller-scale processors have been used to investigate quantum algorithms, including spin transport [10–13]. In general, magnetic resonance (and in particular nuclear magnetic resonance, NMR) plays an important role as a test-bed for a variety of questions related to QIP, from advanced control techniques to decoherence study, and it can make similar contributions in the study of quantum state transfer.

More fundamentally, NMR has long been interested in the dynamics of transport, as transport of polarization and of correlated spin states can on one side elucidate the geometrical structure of molecules and crystals of interest [14], and on the other side it constitutes a crucial step in dynamic nuclear polarization (DNP) [15–17], which is used to achieve enhanced sensitivity. Thus, the investigation of quantum state transfer in NMR systems connects to and draws upon these prior studies and it can as well contribute to their advance.

This contribution is structured as follows. We first review in Sect. 6.2 the basic principles of NMR, focusing on their applications to QIP problems. We present in particular liquid-state and solid-state NMR implementations of qubit systems, in Sects. 6.2.1 and 6.2.2, respectively. We then review in Sect. 6.3 demonstrations of quantum state transfer in small liquid-state quantum information processors (Sect. 6.3.1) and in larger solid-state crystal systems (Sect. 6.3.2). We conclude the chapter with an outlook of the potential contribution of magnetic-resonance implementations both to the investigation of quantum state transfer beyond solvable models (exploring for example questions of decoherence) and to scalable QIP architectures.

## 6.2 NMR Quantum Information Processing

Spin systems have been proposed as promising quantum information processing devices [8, 9, 18, 19] based on NMR techniques. Since the very start of experimental QIP, NMR has played an important role in implementing the first proof-of-principle demonstrations, thanks to the fact that it is a mature technology [19–22]. Indeed, NMR is unique in that simple implementations based on liquid-state NMR

**Table 6.1** Spin-$\frac{1}{2}$ nuclei commonly used in NMR QIP experiments. We report their isotopic natural abundance (%), their gyromagnetic ratios $\gamma$ and their Larmor frequencies $\omega_L = \gamma B$ at two typical NMR magnetic field strengths

| Nucleus | Natural abundance | $\gamma$ (MHz/T) | $\omega_L$ at 9.4 T (MHz) | $\omega_L$ at 7.05 T (MHz) |
|---|---|---|---|---|
| $^{1}$H | 99.99 | 42.58 | 400 | 300 |
| $^{13}$C | 1.1 | 10.71 | 100.7 | 75.5 |
| $^{15}$N | 0.366 | −4.316 | 40.6 | 30.4 |
| $^{19}$F | 100 | 40.05 | 376.5 | 282.4 |

have been able to control up to 12 spin qubits [23] with commercially available technology. There are three main reasons for the success of NMR QIP: well-defined qubits (and well characterized Hamiltonians), relatively long coherence times and a tradition of well developed (pulsed) control techniques.

**Spins** – In NMR-based QIP, qubits are simply spin-1/2 nuclei, thus the mapping from logical to physical qubit is straightforward. The most common nuclear spins used in NMR are shown in Table 6.1. Spins interact with magnetic fields via the Zeeman interaction [24–26], thus precessing at their Larmor frequency, set by the gyromagnetic ratio, $\omega_L = \gamma B$, which is proper of each isotope.

**Experimental apparatus** – The magnetic field is usually generated by a superconducting coil, which can create fields up to 23.5 T with very good homogeneities. NMR QIP can take advantage of the mature technology, commercially available for NMR spectroscopy, as the basics operations are common for both tasks. The main components of the experimental apparatus are shown in Fig. 6.1.

**Measurement** – The spin magnetization is measured inductively by a pick-up coil. The measurement is weak, thus in contrast to projective measurements the state is only weakly perturbed by the measurement and we can follow the evolution of the spin magnetization. The measurement is thus well-described by a simple model of a classical dipole, where the transverse spin magnetization couples to the coil via magnetic induction. Only the portion of the spin state that is dipolar and oriented along the coil axis will couple and be detected (although other parts of the density operator might evolve into detectable states during the measurement evolution time). The signal is the ensemble average of the transverse polarization over the whole sample.

**Pulse control** – The pick-up coil is used as well to manipulate the spins. The most common control technique in NMR is the use of short bursts of magnetic field at the spin radio-frequency (RF) frequency $\omega_0$ in a transverse plane (with respect to the large, static magnetic field, by convention aligned with the z-axis). In the rotating wave approximation, the Hamiltonian describing the interaction of the spins with the RF field is given by:

$$\mathscr{H}_{ext} = e^{-i\varphi(t)\Sigma_z}\left(\tfrac{1}{2}\,\omega_{\mathrm{RF}}(t)\,\textstyle\sum_h \sigma_x^h\right) e^{\,i\varphi(t)\Sigma_z} \tag{6.1}$$

where $\sigma_i$ are the usual Pauli matrices, $\Sigma_z = \sum_k \sigma_z^k$ and we set (here and in the following) $\hbar = 1$. Here $\varphi(t) = \omega_0 t + \phi(t)$ is a time-dependent phase and

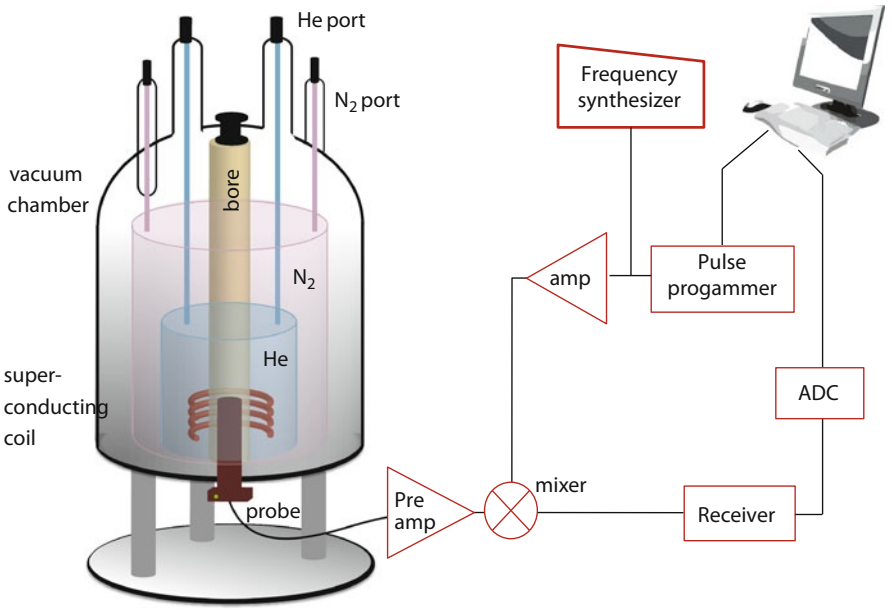


**Fig. 6.1** Schematic of the principal components of a NMR system. The sample is placed inside a probehead that carries a resonant circuit. The probehead is inserted in the bore of a superconducting magnet, kept at low temperature by liquid He (in turns kept cold by liquid Nitrogen). A radio-frequency (RF) field is amplified and gated by a computer-controlled timing unit and delivered via the resonant circuit to the sample. The time-dependent magnetic field produced by the sample is picked-up by the same coil, amplified, digitized and analysed by a computer. Components not shown here also allow for quadrature detection, phase, frequency and amplitude modulation of the RF field as well as the generation of gradient pulses

$\omega_{\mathrm{RF}}(t)$ is a time-dependent amplitude. The phase and amplitude can be controlled independently, allowing a high level of flexibility. Several methods such as shaped pulses [27], composite pulses [28] or numerically-optimized pulse shapes [29–31] have been used in NMR.

A host of pulse sequences have been developed in NMR to achieve various spectroscopic goals, as well as to improve the coherence properties of the system. These same techniques have had an influence on the further development of control strategies for QIP. We will now describe in more detail NMR experimental techniques applied to quantum information processing, making a distinction depending on the type of sample studied, either liquid- or solid-state.

### *6.2.1 Liquid-State NMR*

Most of NMR spectroscopy deals with samples at the liquid state, investigating the spins in molecules. In liquid-state NMR the qubits are defined as magnetically

distinct spins-$\frac{1}{2}$ of a given molecule immersed in a solvent. Because of easy identification of qubits, good knowledge of their Hamiltonians and of the relaxation superoperator, high level of control already developed by the NMR community and long decoherence times, liquid-state NMR is recognized as one of the most flexible test-beds for QIP. One of its limitations is the exponential decrease in signal for each qubit added to the system, which is associated with the use of mixed states in ensemble QIP. Although not a scalable approach to quantum computation because of the limited number of frequency-resolved spins, liquid-state NMR has made it possible over the years to test experimentally quantum algorithms and to study issues of control and fault-tolerant quantum computation.

**Spin qubits** – In liquid-state NMR, the spin-carrying nuclei are part of molecules dissolved in a solvent. As the couplings among molecules are weak and averaged to zero to first order by random motion, the molecules can be considered independent. The NMR sample is then an ensemble of a large number ($N_m \approx 10^{18}$) of independent molecules, or, in QIP terms, an ensemble of $N_m$ independent quantum processors.

**Hamiltonian** – The $N$ spins in each molecule are magnetically distinct: Not only different chemical species have different gyromagnetic ratios, but also the resonances of homonuclear spins depend on the local chemical environment. These differences in frequencies are called *chemical shifts* and are usually on the order of 10–100 part-per-million (ppm) of the resonance frequency.

The spins interact with each other indirectly, the coupling being mediated by the electrons forming the molecular orbital between nuclei. The interaction strength is given by the *scalar (weak) coupling* constants $J_{k,h}$, which can range from a few Hz to hundreds of Hz.

The internal Hamiltonian of a molecule's nuclear spins in a large external magnetic field along the z-axis is then:

$$\mathscr{H}_{int} = \frac{1}{2}\sum_{k=1}^{N}\omega_k \boldsymbol{\sigma}_z^k + \frac{\pi}{2}\sum_{k\neq h} J_{k,h}\boldsymbol{\sigma}^k \cdot \boldsymbol{\sigma}^h \tag{6.2}$$

where $\sigma_\alpha^k$ are Pauli matrices for the $k$th spin.

It is usual in NMR to work in the so-called *rotating* frame, an interaction frame defined by the RF driving frequency $\omega_0$ and the total spin in the $z$-direction, $\Sigma_z = \sum_k \sigma_z^k$. Thus the frequencies $\omega_k$ in Eq. (6.2) are to be interpreted as: $\omega_k = \omega_L^k + \delta\omega_k - \omega_0$, where $\omega_L^k$ is the Larmor frequency of the $k$th nucleus and $\delta\omega_k$ its chemical shift.

The values of the chemical shifts and J-couplings of a molecule's nuclear spins can be derived directly from their spectrum. For example, in Fig. 6.2 are the parameters of the internal Hamiltonian of one molecule used in QST experiments [13, 32].

**Coherence Times** – Spin-1/2 systems have particularly long coherence times since they only couple to magnetic (and not electric) fields. In addition, they are shielded by the surrounding electronic spins. Thus the only source of decoherence

| | H | $C_1$ | $C_2$ | $T_1$ | $T_2$ |
|---|---|---|---|---|---|
| H | 3,233 | | | 4.7s | 0.24s |
| $C_1$ | 201 | 14,660 | | 3.8s | 0.40s |
| $C_2$ | 9 | 103 | 15,566 | 4.2s | 0.21s |

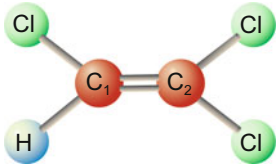


**Fig. 6.2** Carbon-13 labeled trichloroethylene. This molecule has been used for liquid-state NMR QIP experiments [13, 32]. The table on the *left* shows the NMR parameters. The diagonal terms in the table are the chemical shifts in Hz with respect to the reference frequencies 500.13 and 125.76 MHz, for $^1$H and $^{13}$C respectively. The non-diagonal terms are the $J$ coupling constants in Hz. Also reported are the measured [32] $T_1$ and $T_2$ times for each spin. The spins are labeled as in the figure on the *right*

is the coupling to other spins in the system. The longitudinal relaxation time $T_1$ – which describes energy exchange with the lattice and determines the relaxation to thermal equilibrium – can be extremely long, especially in solid-state systems, where it can reach minutes. The transverse relaxation time $T_2$ is instead usually shorter in solid crystals, due to the dipolar couplings among spins. At the liquid-state, instead, because of the fast molecular reorientation, most of the spin couplings to other molecules are averaged, thus yielding $T_2$ coherence times of the order of hundreds of millisecond.

#### 6.2.1.1 Liquid-State NMR Quantum Information Processing

Liquid-state NMR has been one of the first techniques that has been able to demonstrate experimentally the concepts of quantum information processing. Thanks to the discovery of pseudo-pure states [33, 34] in 1997, many simple algorithms have been implemented in small NMR molecular systems. These include Deutsch's algorithm [35], which was implemented on homonuclear [36, 37] and heteronuclear [38] spin systems, as well as its generalization, the Deutsch-Josza algorithm [39], which was implemented on systems comprising from one to five spins [40] (the first implementation being on three spins [41]). Grover's quantum search algorithm [42] was implemented both in liquid-state NMR systems [43, 44] and in a liquid-crystal system [45]. The quantum Fourier transform was as well demonstrated in liquid-state NMR [46] as well as Shor's factorization algorithm [47]. Besides these algorithms, NMR was also used to study quantum simulations [48–50], quantum random walks [51], quantum games [52, 53] and quantum chaos [54]. Most of these results have been made possible by the creation of pseudo-pure states (see next section), which play as well a role in the demonstration of quantum state transport.

One of the most important contributions of NMR QIP has been in the precision with which qubits can be controlled. This includes advances in error-correction techniques, based on both active quantum error correction [55] and on passive protection via decoherence-free subsystems [56–61]; and development of robust control techniques (see Sect. 6.2.1.3) to avoid coherent gate errors. These control

techniques have also enabled the implementation of QST in small molecular systems and will be more generally useful in many future implementations of quantum state transfer.

#### 6.2.1.2 Pseudo-pure States

The simulation of small quantum algorithms by ensemble liquid-state NMR has been made possible by techniques for the preparation of so-called pseudo-pure states that are able to simulate the dynamics of pure states:

$$\rho_{\text{pps}} = \frac{1-\alpha}{2^N}\mathbb{1} + \alpha|0\rangle\langle 0|^{\otimes N}, \tag{6.3}$$

where $N$ is the number of spins. Since the identity operator $\mathbb{1}$ is left unchanged by the usual unital evolution of NMR and does not contribute to the signal, the evolution of this pseudo-pure states is completely equivalent to the evolution of the associated pure states.

Pseudo-pure states can be obtained either by spatial [33] or temporal averaging [62] or by logical labeling [34]. In general, one needs to use a non-coherent evolution in order to obtain $\rho_{\text{pps}}$ from the thermal-equilibrium state,

$$\rho_{th} = \frac{e^{-\beta\mathscr{H}}}{Z} \approx \frac{\mathbb{1} - \epsilon\Sigma_z}{2^N}, \tag{6.4}$$

where $\epsilon = \beta\hbar\omega \ll 1$, with $\beta = (k_b T)^{-1}$ the Boltzmann factor and $\Sigma_z = \sum_{k=1}^{N} \boldsymbol{\sigma}_z^k$. Since $\alpha < \epsilon$, pseudo-pure states are still highly mixed states and they usually entail a signal loss.

For example, in temporal averaging one repeats the experiment several times with different preparation steps. The signal from each experiment measurement is averaged to give the final answer. Provided the preparation steps are chosen such that the average of the prepared input states is a pseudo-pure state, the signal average is the same as for a pure input state. This technique is somewhat reminiscent of phase cycling in NMR [63, 64], in which the same sequence is repeated several times with different pulse phases, in order to select only a particular subsystem of the state (e.g. only the double-quantum terms [26]).

#### 6.2.1.3 Control

NMR experiments have contributed greatly to the development of control strategies for QIP. Drawing on the expertise of NMR spectroscopy, the first algorithms were implemented by decomposing complex quantum gates into simpler units that could be implemented by a combination of RF pulses and evolution under the internal Hamiltonian. In addition, composite pulses [28], adiabatic pulses [65] and shaped

pulses [66] were adopted in early NMR QIP experiments to better compensate for static and RF field inhomogeneities.

Since then, more sophisticated control techniques have been introduced. A particular promising direction has been in the development of numerical searches for the optimal excitation profile [67], either based on strongly modulated pulses [29] or by optimal pulse shapes [31]. The first method uses a numerical optimization to find strong control fields, which performs a desired spin-selective unitary operation, without any additional corrections being required to account for decay or inhomogeneities. The second method, based on optimal control theory (OCT), finds analytical solutions to time-optimal realization of unitary operation, by optimization techniques based either on gradient methods [31] or on Krotov's numerical method [68].

NMR QIP has also contributed greatly to the development of dynamical decoupling techniques [69–71], which are aimed at improving the coherence times of quantum systems and build upon long-established NMR techniques such as spin echo [72] and CPMG sequence [73, 74].

### 6.2.2 Solid-State NMR

Solid-state NMR presents some differences that are advantageous for QIP. With spins fixed in a solid matrix, the dipolar interactions are not averaged out. This provides much stronger couplings for faster gates, but also a shorter phase coherence time, which can be increased only by special purpose pulse sequences. In addition, the spin polarization can be increased by dynamic nuclear polarization [16, 17], increasing the sensitivity.

The dominant interaction in spin-$\frac{1}{2}$ nuclear systems in a rigid crystal is the magnetic dipole-dipole interaction. The dipolar Hamiltonian is given by

$$\mathscr{H}_{dip} = \sum_{i<j} \frac{\hbar \gamma_i \gamma_j}{|r_{ij}|^3} \left( \frac{3(\boldsymbol{\sigma}_i \cdot \mathbf{r}_{ij})(\boldsymbol{\sigma}_j \cdot \mathbf{r}_{ij})}{|\mathbf{r}_{ij}|^2} - \boldsymbol{\sigma}_i \cdot \boldsymbol{\sigma}_j \right) \tag{6.5}$$

where $\mathbf{r}_{ij}$ is the intra-spin vector and $\gamma_i$ the gyromagnetic ratio of the $i$th spin.

In a large magnetic field along the z axis, we only consider the energy-conserving *secular* part of the dipolar Hamiltonian, that is, the terms that commute with the stronger Zeeman Hamiltonian (and therefore conserve the total magnetization along the z direction). The dipolar Hamiltonian then takes the form:

$$\mathscr{H}_{dip} = \sum_{ij} b_{ij} [\sigma_z^i \sigma_z^j - \frac{1}{2}(\sigma_x^i \sigma_x^j + \sigma_y^i \sigma_y^j)] \tag{6.6}$$

where the dipolar coupling coefficients are given by:

$$b_{i,j} = \frac{1}{2}\frac{\hbar\gamma_i\gamma_j\left[3\cos(\vartheta_{ij})^2 - 1\right]}{|\mathbf{r}_{ij}|^3} \tag{6.7}$$

with $\vartheta_{ij}$ the angle between intra-spin vector and the external magnetic field direction, $\cos(\vartheta_{ij}) \propto \hat{\mathbf{z}} \cdot \mathbf{r}_{ij}$.

This many-body Hamiltonian drives a very complex dynamics; of particular relevance for quantum information transport are the dynamics of spin diffusion [17, 75–77] and of multiple quantum coherences [78–80]. The dynamics can be further tailored by multiple-pulse sequences. Various tools have been developed to describe the subsequent complex evolution and to guide in the design of pulse sequences, most notably average Hamiltonian theory (AHT) [81, 82]. This technique also plays an important role in engineering QST Hamiltonians.

#### 6.2.2.1 Average Hamiltonian Theory and Hamiltonian Engineering

The effects of a series of pulses and delays, organized in a cyclic sequence, can be best evaluated using Average Hamiltonian Theory (AHT) [81–83] which is an important tool in the construction of special purpose pulse sequences. The basic idea is that the evolution of the system under the applied periodic train of pulses may be described as if occurring under a time-independent effective Hamiltonian $\overline{\mathscr{H}}$. In a multiple pulse sequence, the cycle propagator over the duration $T_c$ of each control cycle reads

$$U(T_c) = \mathscr{T}\exp\left(-i\int_0^{T_c}[\mathscr{H}_{dip} + \mathscr{H}_{\mathrm{RF}}(s)]ds\right) = e^{-i\overline{\mathscr{H}}T_c}, \tag{6.8}$$

where $\hbar = 1$, $\mathscr{T}$ denotes the time-ordering operator and $\mathscr{H}_{\mathrm{RF}}(t)$ is the time-dependent Hamiltonian describing the RF pulses. By invoking the Magnus expansion [82], the actual Hamiltonian $\overline{\mathscr{H}}$ may be expressed as $\overline{\mathscr{H}} = \sum_{\ell=0}^{\infty}\bar{\mathscr{H}}^{(\ell)}$, where the lowest-order term must yield the desired target Hamiltonian. We thus want to impose the condition:

$$\sum_k R_k\mathscr{H}_{dip}R_k^\dagger = \mathscr{H}_{des}, \tag{6.9}$$

where $R_k$ are collective rotations of all the spins given by the RF pulses. For cyclic and periodic pulse sequences, the long-time evolution over many cycles can be evaluated by simply calculating the evolution over one cycle, which in turn is well-approximated by the lowest-order AHT expansion. The higher order terms can be usually neglected, since $\left\|\bar{\mathscr{H}}^{(\ell)}\right\| = \mathscr{O}(T_c^\ell)$.

In addition, if the pulse cycle is time-symmetric all odd-order corrections vanish [84], and the leading error term in the cycle propagator is of order $\mathcal{O}(\|\bar{\mathcal{H}}^{(2)}T_c\|)$. Remarkably, this is true even when considering ideal and finite-width pulses. Average Hamiltonian techniques are invaluable in achieving Hamiltonian engineering [85, 86] that can be used for a variety of QIP goals. Here we will use this technique to guide the engineering of the transport Hamiltonian [11].

#### 6.2.2.2 Multiple Quantum Coherences

Evolution under complex multiple-pulse sequences usually lead to the creation of many-body spin states. While creating these correlations is not in general the goal of quantum state transfer, one can gather further insight in the transport dynamics by characterizing these states experimentally. Since solid-state NMR does not allow single-spin readout, as required for example for state tomography, other techniques have been developed to characterize these many-spin states. In particular, it is critical to distinguish the presence of correlation among the spins, specially coherences.

In NMR, coherences between two or more spins are usually called *multiple quantum coherences* (MQC), to distinguish them from the single quantum coherence operators, which are the usual (direct) observables. Quantum coherence in general refers to a state where the phase differences among the various constituent of the system wavefunction can lead to interference. In particular, quantum coherences often refer to a many-body system, whose parties have interacted and therefore show a correlation, a well defined phase relationship. When the system is quantized along the $z$ axis, so that the Zeeman magnetic moment along $z$ is a good quantum number, a quantum coherence of order $q$ is defined as the transition between two states $|m_1\rangle$ and $|m_2\rangle$, such that the difference of the magnetic moment along z of these states is $\propto m_1 - m_2 = q$. The matrix element in the system's density operator $|m_2\rangle\langle m_1|$ is also called a coherence of order $q$.

Quantum coherences can also be classified based on their response to a rotation around the z axis: A state of coherence order $q$ will acquire a phase proportional to $q$ under a z-rotation:

$$e^{-i\varphi\Sigma_z/2}\rho_q e^{i\varphi\Sigma_z/2} = e^{-iq\varphi}\rho_q \tag{6.10}$$

This property can be used to selectively detect a particular quantum coherence order.

Since higher quantum coherences are sensitive to the number, geometry and interconnectivity among nuclei, they can be used to access information about these properties, which are otherwise hidden in a simpler experiment. In particular, since a $q$-quantum coherence can only form in a cluster of $q$ or more spins, it is also possible to estimate the number of spins interacting at a given evolution time; this kind of experiments are called *spin-counting* experiments [80].

MQC intensities cannot be measured directly, since the NMR spectrometer coil is only sensitive to single body, single quantum coherences. MQC created in the

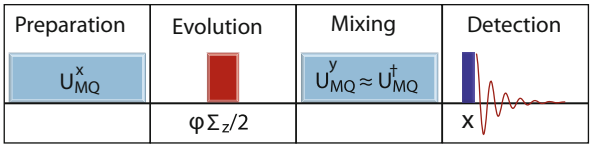


**Fig. 6.3** NMR pulse sequence for the creation and detection of MQC. The usual multiple quantum experiment is composed of four steps: The MQC are first excited during the preparation period (for example by a multiple quantum propagator $U^x_{MQ}$, see also Fig. 6.7). MQC evolve during the evolution period. In the simplest case a simple $\varphi$ rotation along the $z$ axis ($\varphi\Sigma_z/2$) is applied to flag each coherence in the system state. MQC are then refocused during the mixing periods (by $U^\dagger_{MQ}$) prior to measurement, obtained by a $\pi/2$ rotation followed by acquisition

system must therefore be tagged before bringing them back to observable operators, in order to separate the contributions of different MQC into the signal. The usual MQC experiment thus involves four steps (see Fig. 6.3).

During the preparation time, a pulse sequence creates a propagator $U_{MQ}$ that generates high coherence orders. The evolution period lets the system evolve to better characterize the MQC as required by each specific experiment. The refocusing step brings back the MQC to single-spin states, ideally by a propagator $U^\dagger_{MQ}$; finally, after a $\pi/2$ pulse, the signal is measured during the detection period. In the most simple experiment, the evolution period consists in the acquisition of a phase $\varphi$ (either by an off-resonance, free evolution period or more simply, by a phase shift of all the following pulses). The experiment than reveals the intensities of MQC created in the preparation time. Starting from the thermal state $\rho(0) \propto \mathbb{1} - \epsilon\delta\rho_0$, where $\delta\rho_0 = \Sigma_z$, the observed signal is indeed given by:

$$\begin{aligned} S_\varphi(t) &= \mathrm{Tr}\left\{U^\dagger_{MQ} e^{-i\varphi\Sigma_z/2} U_{MQ}\,\delta\rho_0\, U^\dagger_{MQ} e^{i\varphi\Sigma_z/2} U_{MQ}\,\Sigma_z\right\} \\ &= \mathrm{Tr}\left\{e^{-i\varphi\Sigma_z/2}\rho_{MQC} e^{i\varphi\Sigma_z/2}\rho_{MQC}\right\} = \textstyle\sum_q e^{iq\varphi}\mathrm{Tr}\left\{\rho_q\rho_{-q}\right\} \end{aligned} \tag{6.11}$$

where $\rho_q$ is the $q$th-quantum coherence component in the state $\rho_{MQC} = U_{MQ}\,\Sigma_z U^\dagger_{MQ}$. In the last step we used Eq. (6.10) and the fact that $\mathrm{Tr}\left\{\rho_p\rho_q\right\} = \delta_{p,-q}$ to simplify the expression. By varying the angle $\varphi$ between 0 and $2\pi$ in steps of $\pi/M$ ($M$ being the maximum coherence number to be measured), it is possible to obtain the intensities of the MQC contributions, by Fourier-transforming the signal with respect to $\varphi$:

$$I_q(t) = \sum_{m=1}^{2M} S_{\varphi_m}(t) e^{-iqm\pi/M}, \tag{6.12}$$

where $S_{\varphi_m}(t) = \mathrm{Tr}\{\rho_m(t)\rho_i\}$ is the signal acquired in the $m$th measurement for $\varphi_m = m\pi/M$.

### 6.2.3 *Liquid Crystals*

To benefit from advantages of both liquid-state NMR (small number of spins with addressable frequencies) and solid-state NMR (strong dipolar couplings) molecules can be embedded in a liquid crystal matrix that fixes their orientations. Then, the dipolar couplings inside the molecules are not averaged out providing faster dynamics.

Liquid crystals are like liquids in that the constituent molecules undergo rapid translational diffusion, and they are like solids in that the molecules demonstrate some amount of long-range ordering. The NMR spectrum of a typical liquid crystal material is very broad due to the many non-equivalent dipolarly coupled protons. However, when a smaller, rigid molecule is dissolved in a liquid crystal solvent, the solute adopts the orientational ordering of the solvent and the resolved peaks of the solute spectrum appear on top of a broad baseline due to the liquid crystal solvent. Multiple pulse sequences can remove the unwanted signal from the solvent while leaving a complicated spectrum of many resolved transitions due to the dissolved molecules. The dominant features in the resolved spectrum arise due to the presence of strong magnetic dipolar couplings among nuclear spins in the solute material. This strong dipolar interaction is the principal difference between liquid and liquid crystal solvents NMR.

For an ensemble of rigid molecules, the inter-nuclear distances are fixed by the structure of the molecule, and the angular terms in the dipolar coupling strength are averaged over the distribution of molecular orientations in the ensemble $\langle b_{ij} \rangle = \frac{1}{2} \frac{\hbar \gamma_i \gamma_j \langle 3 \cos(\theta_{ij})^2 - 1 \rangle}{|\mathbf{r}_{ij}|^3}$. In both liquid and liquid crystal solvents, the solute molecules move about with rapid, diffusive translational motion, which averages the intermolecular dipolar couplings to zero. In addition, the molecules in a liquid solvent are randomly rotating, averaging out the intramolecular dipolar couplings as well. By contrast, a molecule dissolved in a liquid crystal has a preferred orientation, so rotational motion is restricted, and intramolecular dipolar couplings are retained, as the average $\langle b_{ij} \rangle$ is non-zero.

The solute material in a liquid crystal solvent system can be used for NMR quantum information processing with the main advantage given by resolved, large dipolar couplings. This yields not only faster computing speed, but also the potential for larger spin systems, thanks to the resolved couplings. Both of these advantages can be exploited in small-scale demonstrations of quantum state transfer [87].

## 6.3 Quantum State Transfer in Spin Systems

The many contributions of NMR to quantum information processing have also extended to the area of quantum state transfer. There have been two main directions of exploration.

Liquid-state NMR systems have enabled proof-of-principle experiments demonstrating the concept of quantum state transfer (see Sect. 6.3.1). While the system size is usually small, the long coherence time and high degree of control in these systems have allowed, for example, testing various QST strategies, such as faster transport with 3-body interaction and improved fidelity with end-chain control.

In solid-state NMR it is instead possible to explore larger spin systems and thus potentially longer chains. Exploiting the geometry of some crystals, which approximate one dimensional systems, it has been possible to achieve direct simulations of QST protocols (see Sect. 6.3.2). In particular, this has increased the interest in quantum state transfer via mixed-state spin wires (Sect. 6.3.2.3). Current studies have focused on overcoming the constraints imposed by the collective control available in these systems to achieve the state preparation and readout required to observe quantum state transfer (Sect. 6.3.2.4). This has opened the possibility to gather further insight in the transport dynamics, taking into account effects that go beyond the solvable models (Sect. 6.3.2.5), an area where experimental implementations, such as those based on solid-state NMR, could give important contributions.

### 6.3.1 Simulations with Liquid-State NMR

As a testament to the versatility of liquid-state NMR experiments, the first observation of coherent transport by NMR was performed even before proposals for QST were put forward. Polarization transport (a "spin wave") was observed [10] in a five spin chain associated with Lysine (see Fig. 6.4). The dynamics was driven by the XX Hamiltonian,

$$\mathscr{H}_{xx} = \sum_{i,j} \frac{1}{2} b_{i,j} (\sigma_i^x \sigma_j^x + \sigma_i^y \sigma_j^y) = \sum_{i,j} b_{i,j} (\sigma_i^+ \sigma_j^- + \sigma_i^- \sigma_j^+) \tag{6.13}$$

obtained from the natural weak-coupling interaction via a multiple-pulse sequence. The initial perturbation state was created by transferring polarization from a proton spin to the first C-13 spin in the chain. The amount of polarization was monitored by measuring each spin (which are spectroscopically distinguished) and it showed the well-known behavior for polarization transport [11] for equal coupling chain ($J = 55\,\text{Hz}$).

For small spin chains, as found in small molecules observed by liquid-state NMR techniques, quantum state transfer can be obtained by manipulating individual spins to implement quantum gates, such as SWAP [88, 89] gates. In addition, CNOT gates [88] can be used to sequentially map the excitation of one spin at the end of the chain onto the other spins in the chain; this strategy, introduced in [90] to amplify the signal from a single spin, was implemented with NMR techniques [90–93].

However, the same transfer (and amplification) can be obtained relying on the evolution driven by spin-spin couplings; this alternative strategy can in principle lead to a transfer speed-up [94–96] thanks to optimal control techniques. More

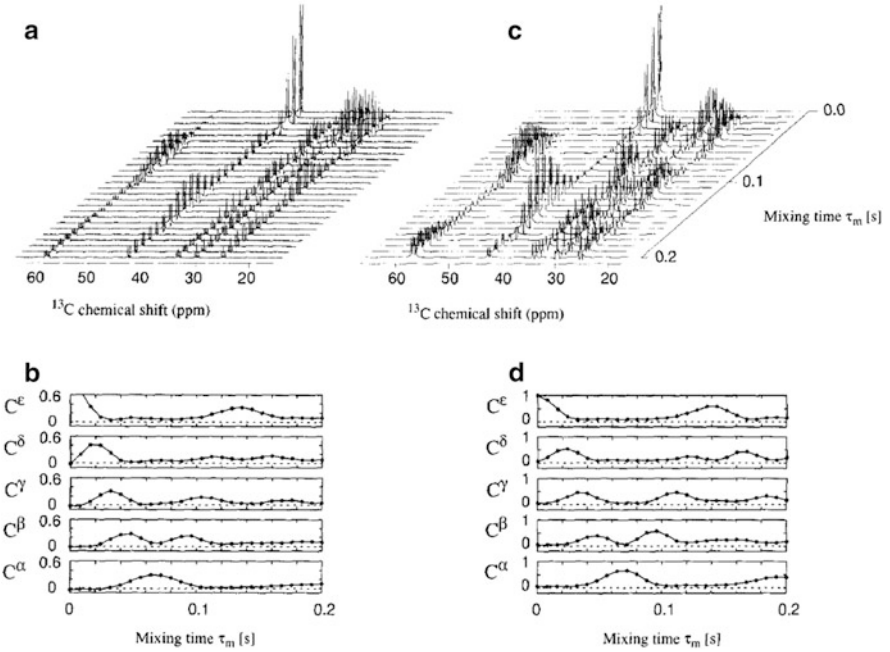


**Fig. 6.4** Experimental and simulation results reproduced with permission from Ref. [10]. (**a**) shows experimental spectra (stacked plots) with soft pulse excitation on the first carbon in the chain ($C_\epsilon$) recorded with increasing mixing time $\tau_m$ and (**b**) gives the corresponding peak integrals. (**c**) and (**d**) show the computer-simulated spectra and integrals using the experimental parameters (pulse widths, delays, chemical shifts and J couplings). The spectra were recorded at 100.6 MHz $^{13}$C Larmor frequency, selective excitation was achieved by a 2.5 ms Gaussian shaped pulse. (Reprinted from Madi et al. [10], pp. 300–305, Copyright (1997), with permission from Elsevier)

generally, QST driven by interactions between spins in the chain, without the requirement of single-spin control, is a more powerful paradigm that can in principle be implemented in larger spin chains. Thus, several authors have used liquid-state NMR, and the high degree of control that it provides, to simulate this scenario, even when individual control of spins was available – or indeed required to obtain the desired evolution.

J. Zhang and coworkers [13, 32] simulated QST driven by a simple XX Hamiltonian with equal coupling [97] in a 3-spin chain embodied by the spins in a trichloroethylene (TCE) molecule (see Fig. 6.2). The experiments used a sample of $^{13}$C -labeled TCE dissolved in d-chloroform analysed in a Bruker DRX 500 MHz spectrometer. The proton spin $^1$H is taken as qubit 2, the $^{13}$C directly connecting to it is denoted as qubit 1, and the other $^{13}$C is qubit 3. The Hamiltonian of this system,

$$\mathscr{H}^{TCE} = \sum_{k=1}^{3} \omega_k \sigma_z^k + \frac{1}{2} \sum_{k,j>k} J_{kj} \sigma_z^k \sigma_z^j \tag{6.14}$$

is quite different from the XX Hamiltonian $\mathscr{H}_{XX}$ on 3 spins required for transport. Thus the authors decompose the transport propagator, $U_{XX} = \exp(-it\mathscr{H}_{XX})$ into unitary propagators that can be implemented by liquid-state NMR techniques. Indeed, thanks to the difference in chemical shifts and $J$-coupling (Fig. 6.2), universal control can be achieved [98–100] and thus any propagator can be obtained. In the first implementation [32], the desired evolution was decomposed as:

$$U_{XX} = e^{-i\frac{\pi}{8}\sigma_x^1\sigma_z^2\sigma_y^3} e^{-i\frac{J_I}{\sqrt{2}}\sigma_x^1\sigma_x^2} e^{i\frac{\pi}{8}\sigma_x^1\sigma_z^2\sigma_y^3} e^{-i\frac{\pi}{8}\sigma_y^1\sigma_z^2\sigma_x^3} e^{-i\frac{J_I}{\sqrt{2}}\sigma_x^2\sigma_x^3} e^{i\frac{\pi}{8}\sigma_y^1\sigma_z^2\sigma_x^3} \tag{6.15}$$

where each unitary is obtained by a combination of selective and non-selective RF pulses, interleaved by period of free evolution. It was realized that in this decomposition three-body interaction terms emerge naturally. These couplings are not present in the natural Hamiltonian, but can be introduced by the method proposed in [49]. The main limitation in the experimental results was due to the length of the pulse sequence, so that the fidelity of transport was limited by $T_2$-decay. Indeed the implementation via the decomposition in Eq. (6.15) was found to be longer and more complex than applying two SWAP gates, as needed for transport in a 3-spin chain.

The authors thus studied how to speed up the transport [13] exploiting these three-body Hamiltonian (see Fig. 6.5). They found that adding a term

$$\mathscr{H}_3 = \frac{\lambda}{2}(\sigma_x^1\sigma_z^2\sigma_x^3 - \sigma_y^1\sigma_z^2\sigma_y^3) \tag{6.16}$$

to the Hamiltonian $\mathscr{H}_{XX}^{TCE}$ speeds up the transfer time for a wide range of the $\lambda$ parameter strength. This lead to a different decomposition of the transport propagator,

$$U_{XX}^{TCE} = U_C U_D = e^{-i2\sqrt{2}\mathbf{L}_C\cdot\mathbf{n}_C} e^{-i2\sqrt{2}\mathbf{L}_D\cdot\mathbf{n}_D} \tag{6.17}$$

where $\mathbf{L}_C = [\sigma_x^1\sigma_x^2/2, \sigma_y^2\sigma_y^3/2, \sigma_x^1\sigma_z^2\sigma_y^3/2]$, $\mathbf{L}_D = [\sigma_x^2\sigma_x^3/2, \sigma_y^1\sigma_y^2/2, \sigma_y^1\sigma_z^2\sigma_x^3/2]$, $\mathbf{n}_C = \frac{1}{\sqrt{2}}[1, 1, \frac{4}{\lambda}]$ and $\mathbf{n}_D = \frac{1}{\sqrt{2}}[1, 1, -\frac{4}{\lambda}]$. The propagators where further decomposed in single-qubit operations and free evolution under the spin-spin coupling $e^{i\vartheta\sigma_z^i\sigma_z^k}$, which can be achieved by NMR techniques. Quantum state transfer was observed for initial mixed states, $\delta\rho_\alpha = \sigma_\alpha^3$ (with $\alpha = \{x, y, z\}$). These states were obtained using RF pulses and gradients to erase the polarization of spins 1–2. While in principle this is equivalent to following the state transfer evolution for a set of different initial states of the chain [13], no correction was taken to account for the phase arising in different excitation manifolds [101–104]. Despite the good agreement of the experimental data with the simulations shown in Fig. 6.5, the transport fidelity (measured by the correlation of the experimental state with the theoretical state) were quite low, $C \approx 0.2$–$0.3$. As in [32], the relatively low fidelity was due to relaxation processes, since the experimental implementation time ($t = 210$–$280$ ms) exceeds the dephasing time $T_2^*$. Further reductions arise

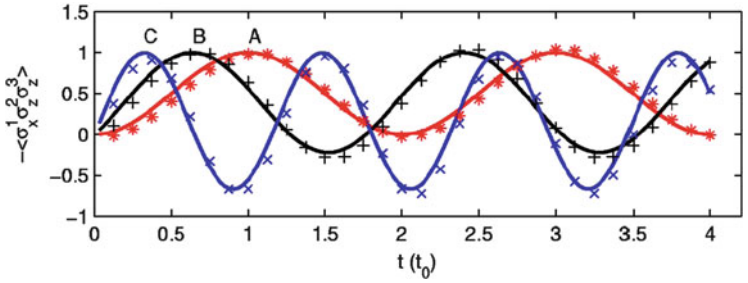


**Fig. 6.5** Implementation of QST in a molecule of TCE as obtained by Zhang et al. [13]. Overlap of the evolved density operator $\delta\rho(0) = \sigma_x^3$ with the target state $\sigma_x^1\sigma_z^2\sigma_z^3$, for different strengths of the three-body coupling as a function of time. Time is normalized to the transport time $t_0$ in the absence of the three-body interaction. Experimental data for $\lambda = 0,\ 1.5$ and 4 are marked by $\star$, $+$ and $\times$ respectively. The *solid lines* represent the theoretical results. Points *A, B,* and *C* indicate the maxima corresponding to the transfer times $C_3 \rightarrow C_1$. This clearly demonstrates the speed-up of the transfer by the three-body interaction (Reprinted figure with permission from J. Zhang et al. [13] , Copyright (2006) by the American Physical Society)

from pulse errors and from the effects of strong couplings, which were ignored in the implementation. Thus, the speed-up offered by three-body terms is not enough in this case to avoid relaxation effects; in addition, it is hard to efficiently extend this strategy to longer chains, when a three-body Hamiltonian is not naturally present and single-spin addressability is not available.

Instead of relying on extensive single-spin control, Alvarez and coworkers [105] proposed to achieve perfect QST relying only on well-selected times of evolution under a (engineered) $\mathscr{H}_{XX}$ Hamiltonian and single-spin rotation about the $z$-axis, obtained by free evolution under the chemical shift. The alternation between these two evolution periods is able to select only the spin-spin couplings desired, thus the authors were able to implement QST along different pathways comprising different $^{13}$C spins in a leucine molecule backbone. Although the proposed method requires knowledge of system parameters and distinct frequencies for each spin in the chain as given by the chemical shifts, it is more general than the methods used in [13,32], since it does not require selective qubit manipulations. This strategy is indeed closer to the Hamiltonian engineering strategy introduced in [85] for dipolarly coupled spin networks, where a combination of evolution under the double-quantum Hamiltonian and linear gradient is able to engineer an optimally-coupled [97] spin chain from a complex spin network.

Liquid-state NMR has also been used to simulate particular QST protocols, such as the strategy proposed in [106]. In this scheme, control gates are applied on the end-spins of the chain, which act as qubits; even in the presence of arbitrary couplings in the chain, the protocol achieves perfect transport fidelity by multiple iterations of spin chain evolution and two-qubit gate operations. The scheme was first implemented in a 3-spin chain in ethyl 2-fluoroacetoacetate [107] and later in a four-qubit chain based on orthochlorobromobenzene ($C_6H_4ClBr$) dissolved in the

liquid-crystal solvent ZLI-1132 [87]. This last implementation exploited the larger spin couplings afforded by liquid-crystal NMR and adopted numerically optimized pulses (with the GRAPE algorithm [31]) to achieve higher fidelity of transport starting from an initial pseudo-pure state.

### *6.3.2 Spin Chains in Solid-State NMR*

Transport in complex many-body spin systems has been widely studied as it manifests itself as spin diffusion [76, 108, 109]. In a solid, diffusive behaviour driven by the naturally occurring secular dipolar Hamiltonian arises from energy-conserving flip-flops of anti-aligned spin pairs, which produce a dynamics analogous to a random walk. Spin diffusion has been studied extensively as it is a critical step of dynamic nuclear polarization [15–17], an important technique to increase the sensitivity of NMR. Unfortunately, the dipolar Hamiltonian-driven transport of magnetization in three dimensions appears indistinguishable from an incoherent process [110–112]. The polarization appears to decay to its thermodynamic equilibrium and thus spin diffusion cannot be used for QST. It was however realized early on that the dynamics can be different in one-dimensional, finite systems, where quasi-equilibrium regimes might emerge [113,114]. This type of coherent behaviour was first observed in a ring of protons [115]. The six protons belonged to a benzene molecule; polarization was initially transferred to one of the proton spins by cross-polarization with a $^{13}$C nucleus and eventually detected after mapping the evolved polarization intensity onto the $^{13}$C . As the benzene molecule was dissolved in a liquid crystal matrix of ZLI-1167, the spins interacted via the dipolar Hamiltonian which drove (imperfect) polarization transfer during a period of free evolution. The authors were thus able to contrast the polarization transfer in this small system – showing polarization oscillations – with the spin diffusion behaviour that leads to a polarization decay.

Still, the transport under the full dipolar Hamiltonian is slower than ballistic and dispersive and thus still not directly suitable for QST. However, solid-state NMR proved to be a good experimental test-bed for QST, since multiple pulse sequences can engineer the desired transport Hamiltonian. In the following we will describe a particular physical system, apatite crystals, that has been proven fruitful for the exploration of QST with solid-state NMR. We will then describe how a transport Hamiltonian can be engineered from the natural Hamiltonian and how transport can be studied even in the usual experimental NMR conditions, at room temperature with thermal equilibrium states. Control strategies for the manipulation of the equilibrium state allow the preparation of the initial state of interest for QST. Finally, we will describe how NMR techniques have allowed further exploration of the transport dynamics and its limitations arising from control errors and interactions with the environment.

#### 6.3.2.1 Apatite Crystals for NMR-Based QST

Owing to their unique geometry [116, 117], nuclear spin systems in apatite crystals have emerged as a rich test-bed to probe quasi-one-dimensional (1D) spin dynamics, including transport and decoherence [12, 118–120].

Apatite crystals have a hexagonal geometry with space group $P6_3/m$ [116, 121] (see Fig. 6.6). The main components of the apatite family are chlorapatite [ClAp, $Ca_{10}(PO_4)_6Cl_2$] and carbonated apatites: hydroxyapatite [HAp, $Ca_{10}(PO_4)_6(OH)_2$] and fluorapatite [FAp, $Ca_{10}(PO_4)_6F_2$]. The last two varieties have been studied extensively in NMR as they contain fluorine $^{19}$F nuclear spins (FAp) or protons $^1$H (HAp).

Crystals of FAp can be obtained easily as they occur naturally (e.g. well-known locations are in Durango, Mexico; Quebec, Canada; New Mexico or Connecticut, USA; Epirus, Greece) [122]. FAp and HAp can also be synthetically grown. For example, large single crystals of FAp have been grown by the Czochralski method [123, 124] and more recently by the flux method [125–127]. This same method has also been used to grow HAp [128]. Apatites have many diverse applications, from solid-state laser to fluorescent lamps, from phosphorus chemistry to geological probes. Calcium apatites have also applications in biology, since they form the mineral part of bone and teeth. FAp and HAp have thus become common as biocompatible materials for bone replacement and coating of bone prostheses and their growth methods have been optimized [128].

The parameters of the unit cell of FAp are $a = b = 9.367\,\text{Å}$ ; $c = 6.884\,\text{Å}$; $\hat{a} = \hat{b} = 90°$ and $\hat{g} = 120°$[129]. The $^{19}$F nuclei form linear chains along the $c$-axis, each one surrounded by six other chains. The distance between two intra-chain $^{19}$F nuclei is $d = c/2 = 3.442\,\text{Å}$ and the distance between two cross-chain $^{19}$F nuclei is $D = a = 9.367\,\text{Å}$. Due to the $1/r^3$ dependence of dipolar coupling, there is a large difference between the in-chain and cross chain couplings. The largest ratio between the strongest intra- and cross-chain couplings is obtained when the crystalline $c$-axis is oriented parallel to the external field,

$$\frac{|3\cos(\vartheta_{in})^2 - 1|/r_{in}^3}{|3\cos(\vartheta_{\times})^2 - 1|/r_{\times}^3} = \frac{2/d^3}{1/D^3} \approx 40$$

Thus, to first approximation, in this crystal orientation the 3D $^{19}$F system may be treated as a collection of identical 1D spin chains. For a single chain oriented along $z$, we have $b_{j\ell} = -(\mu_0/\pi)(\gamma^2\hbar/c^3|j-\ell|^3)$. HAp crystals have a similar geometry, with parameters $D = 9.42\,\text{Å}$ and $d = 3.44\,\text{Å}$ [130].

Naturally occurring defects in the sample (such as vacancies or substitutions [122, 131–133]) cause the chains to be broken into many shorter chains. Natural crystals usually contain more impurities (as manifested by a shorter $T_1$ time and a yellow color) and are thus expected to have shorter chain lengths. Synthetically grown crystals present quite long $T_1$ times (e.g. $T_1$=1,100 s for $^{19}$F [134]) indicating a low concentration of paramagnetic impurities; although other defects interrupting the chains, such as vacancies, are expected to be present, the chain length is likely longer.

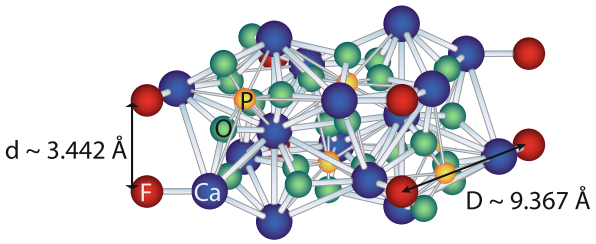


**Fig. 6.6** Unit cell of fluorapatite crystal $[Ca_5(PO_4)_3F]$, highlighting the geometry of the fluorine chains (*red spheres*). *Blue spheres* are calcium atoms, *green* are oxygen atoms and *yellow*, phosphorus atoms

The dynamics of these spin chains have been studied by various nuclear magnetic resonance (NMR) techniques [120, 121, 130, 135–141].

This system first attracted the attention of experimentalists and theoreticians interested in characterizing the NMR spectrum of solid-state systems. While this is a formidable task for 3D systems, this quasi-1D system allowed the comparison of various approximation models, in particular the moment approximation, with numerical calculations and experiments [121,135,136]. Magic-angle spinning NMR was later used to characterize this crystal system, in particular various defects and dopant sites of technological interest [137, 141]. Multiple quantum coherence techniques were used to further characterize the system [138]; conversely, the system was used to gain a better insight into the dynamics of MQC [120, 130, 139] and discrepancies with theoretical models adopted for MQC growth in 3D systems lead to further theoretical analysis [142,143]. More recently, FAp crystals have been proposed as a quantum information processing platform [18, 144] and used to study quantum information transport [12, 101, 118, 119, 134] in a quasi-1D nuclear spin system, as we will present in the following.

#### 6.3.2.2 Double-Quantum Hamiltonian for Spin Transport

Most of the theoretical proposals for QST focused on the XX Hamiltonian, $\mathscr{H}_{XX}$ (Eq. 6.13), as the interaction driving the transport [145], whereas some studied the Heisenberg isotropic Hamiltonian [1] or the Ising Hamiltonian with a transverse field [104]. Unfortunately none of these Hamiltonian can be obtained from the naturally occurring dipolar Hamiltonian $\mathscr{H}_{dip}$ using only collective rotations, which are experimentally available. Indeed, following Average Hamiltonian Theory, we can obtain a desired Hamiltonian from the naturally occurring $\mathscr{H}_{dip}$ by piece-wise constant evolution under rotated versions of $\mathscr{H}_{dip}$, $\sum_k R_k \mathscr{H}_{dip} R_k^\dagger = \mathscr{H}_{des}$ (see Eq. 6.9). To highlight its rotation properties, we can write a general Hamiltonian for 2 spin-$\frac{1}{2}$ particles in terms of spherical tensors $T_{l,m}$ [146] (see Table 6.2):

$$\mathscr{H} = \sum_{l,m} (-1)^m A_{l,m} T_{l,m} \tag{6.18}$$

**Table 6.2** Spherical tensors for two spin-1/2 ($a$ and $b$) [146]. $\sigma_\alpha$ are the usual Pauli operators

| | |
|---|---|
| $\mathbb{1}$ | $T_{00} = (\sigma_x^a\sigma_x^b + \sigma_y^a\sigma_y^b + \sigma_z^a\sigma_z^b)/\sqrt{3}$ |
| $T_{10}^a = \sigma_z^a/2$ | $T_{10}^b = \sigma_Z^b/2$ |
| $T_{11}^a = \sigma_+^a/\sqrt{2}$ | $T_{1-1}^a = \sigma_-^a/\sqrt{2}$ |
| $T_{11}^b = \sigma_+^b/\sqrt{2}$ | $T_{1-1}^b = \sigma_-^b/\sqrt{2}$ |
| $T_{11} = (\sigma_+^a\sigma_z^b - \sigma_z^a\sigma_+^b)/2$ | $T_{1-1} = (\sigma_-^a\sigma_z^b - \sigma_z^a\sigma_-^b)/2$ |
| $T_{10} = (\sigma_+^a\sigma_-^b - \sigma_-^a\sigma_+^b)/2$ | $T_{20} = (2\sigma_z\sigma_z - \sigma_x^a\sigma_x^b - \sigma_y^a\sigma_y^b)/\sqrt{6}$ |
| $T_{21} = (\sigma_+^a\sigma_z^b + \sigma_z^a\sigma_+^b)/2$ | $T_{2-1} = (\sigma_-^a\sigma_z^b + \sigma_z^a\sigma_-^b)/2$ |
| $T_{22} = \sigma_+^a\sigma_+^b/2$ | $T_{2-2} = \sigma_-^a\sigma_-^b/2$ |

where the coefficients $A_{l,m}$ depend on the type of spin-spin interaction and the external field. Since collective rotations conserve the rank $l$ of each spherical tensor [82], there are limitations to which Hamiltonians can be engineered. In particular, $T_{00}$ (the isotropic Hamiltonian) commutes with collective rotations: its contribution is thus a constant of the motion and, conversely, it cannot be introduced in the desired Hamiltonian if it is not present in the natural one. An Ising Hamiltonian $\mathscr{H}_I = \sigma_z\sigma_z$ is instead expanded as $\mathscr{H}_I = (T_{00} + \sqrt{2}T_{20})/\sqrt{3}$, so that only the second part can be modulated. Conversely, the secular dipolar Hamiltonian is given by $T_{20}\sqrt{6}$, thus it cannot produce a Hamiltonian containing $T_{00}$, for instance we cannot generate the XX Hamiltonian $\mathscr{H}_{XX} = (T_{00} - T_{20}/\sqrt{2})/\sqrt{3}$. We can instead generate the Hamiltonian

$$\mathscr{H}_{DQ} = \sum_{i,j} \frac{1}{2} b_{i,j}(\sigma_i^x\sigma_j^x - \sigma_i^y\sigma_j^y) = \sum_{i,j} b_{i,j}(\sigma_i^+\sigma_j^+ + \sigma_i^-\sigma_j^-) \tag{6.19}$$

which is usually called double quantum (DQ) Hamiltonian, since it can increase the coherences number by steps of two. As we will see, this Hamiltonian can be used to simulate QST. The DQ Hamiltonian can be prepared from the secular dipolar Hamiltonian by using a simple sequence consisting of two time intervals, $t_1 = t_2/2$ with the Hamiltonian rotated by a $\pi/2$ rotation around the y axis ($\frac{\pi}{2}\big|_y$) in second time period, to yield: $\sqrt{6}T_{2,0}t_1 + \left[\frac{3}{8}(T_{2,2} + T_{2,-2}) - \sqrt{\frac{1}{2}}T_{2,0}\right] t_2 \propto \mathscr{H}_{DQ}$. Symmetrized versions of this simple sequence are routinely used in NMR experiments [78, 147]. The primitive pulse cycle is given by $\mathrm{P2} = \frac{\delta}{2} - \frac{\pi}{2}|_x - \delta' - \frac{\pi}{2}|_x - \frac{\delta}{2}$, where $\delta' = 2\delta + w$, $\delta$ is the delay between pulses and $w$ is the width the $\pi/2$ pulse (see Fig. 6.7). To first order average Hamiltonian, this sequence simulates the DQ Hamiltonian, while the 8-pulse sequence, $\mathrm{P8} = \mathrm{P2}\cdot\overline{\mathrm{P2}}\cdot\overline{\mathrm{P2}}\cdot\mathrm{P2}$, where $\overline{\mathrm{P2}}$ is the time-reversed version of P2, gives $\overline{\mathscr{H}}_{\mathrm{DQ}}$ to second order and the 16-pulse sequences, $\mathrm{P8}\cdot\overline{\mathrm{P8}}$, compensates for pulse errors.

While the XX and DQ Hamiltonian are quite different (the first one conserves the total $\Sigma_z$ quantum number, whereas the second one can create high coherence terms) they differ by just a similarity transformation, $V_{XX}^{DQ}$. This transformation is

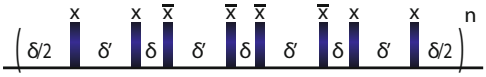


**Fig. 6.7** NMR pulse sequence for the creation of the DQ Hamiltonian. Here we show a 8-pulse sequence used in the experiments to create the DQ Hamiltonian, generating the propagator $U^x_{MQ}$. Bars are $\pi/2$-pulses along the $x$ or $\bar{x} = -x$ axis. The time delays between pulses are $\delta$ and $\delta' = 2\delta + w$, where $w$ is the duration of the $\pi/2$ pulses. Shifting the pulse phases by $\pi/2$ (that is, pulsing along $y$) we obtain the propagator $U^y_{MQ} = (U^x_{MQ})^\dagger$

particularly simple in one dimension, where a $\pi$ rotation of every other spin around the $y$ axis transforms $\mathscr{H}_{XX}$ into $\mathscr{H}_{DQ}$. This fact was used in [11, 148] to deduce the dynamics induced by $\mathscr{H}_{DQ}$ based on the well-known eigenvalue structure of $\mathscr{H}_{XX}$ [149]. In addition, it was realized [11] that for chains at thermal equilibrium, the initial state and the desired observable (magnetization of the end-chain spins) are left unchanged by the transformation $V^{DQ}_{XX}$ linking the XX and DQ Hamiltonian. This opened the possibility to study QST via solid-state NMR techniques.

#### 6.3.2.3 Transport with Mixed-State Spin Chains

With some notable exceptions (e.g., [104, 150–152]) where protocols for perfect state transfer without state initialization have been investigated under the assumption of sufficient end-chain control, existing analyses have primarily focused on transport in the one-spin excitation manifold. However, the assumption of reduced control on the spin chain, which is commonly used, may also naturally entail an imperfect initialization of the spin chain, possibly in a mixed state. Allowing QST via a mixed-state chain can considerably relax the experimental requirements and indeed it allowed its implementation via solid-state NMR.

We can generalize the spin excitation transport usually considered in QST to mixed-state chains by studying polarization transport. Thus, instead of an initial state $|00\ldots1_j\ldots0\rangle$, we take the state

$$\rho = \frac{1}{2^n}(\mathbb{1} + \epsilon\, \delta\rho^j_z), \quad \delta\rho^j_z = \mathbb{1}_{j-1} \otimes \sigma^j_z \otimes \mathbb{1}_{n-j}. \tag{6.20}$$

This state represents a completely mixed-state chain with a single spin partially polarized along the z axis. To quantify the transport efficiency from spin $j$ to spin $l$, instead of the transport fidelity we evaluate the correlation between the resulting time-evolved state and the intended final state, that is, $M_{jl}(t) = \mathrm{Tr}\left\{\rho_j(t)\rho_l\right\}$. As long as the dynamics is unital, this is equivalent to $C_{jl}(t) = \mathrm{Tr}\left\{\delta\rho^j_z(t)\delta\rho^l_z\right\}/\mathrm{Tr}\left\{\delta\rho^j_z(0)^2\right\}$, since we only need to follow the evolution of the traceless deviation $\delta\rho$ from the identity. Since the state in Eq. (6.20) does not reside in the lowest excitation manifold, in which QST is usually calculated, we need to evaluate the dynamics of the transport Hamiltonian in all the manifolds.

We consider first the XX-Hamiltonian (Eq. (6.13)): as it conserves the spin excitation number, it can be diagonalized in each excitation subspace. We denote the eigenstates in the first excitation subspace by $|E_k\rangle$. Then, eigenfunctions of the higher manifolds can be exactly expressed in terms of Slater determinants of the one-excitation manifold. For example, given a basis for the 2-excitation manifold, $|pq\rangle = \left|0\ldots 1_p..0..1_q\ldots 0\right\rangle$, the eigenstates $|E_{kh}\rangle$ are

$$|E_{kh}\rangle = \frac{1}{2}\sum_{pq}\left(\langle E_k|p\rangle\langle E_h|q\rangle - \langle E_k|q\rangle\langle E_h|p\rangle\right)|pq\rangle\,, \tag{6.21}$$

with eigenvalues $E_{kh} = \hbar(\omega_k + \omega_h)$. We can then calculate the time evolution as [101]

$$U_{xx}(t)\,|pq\rangle = \sum_{k,h} e^{-i(\omega_k+\omega_h)t}\langle E_{kh}|pq\rangle\langle rs|E_{kh}\rangle\,|rs\rangle = \sum_{r,s} A_{pq,rs}(t)\,|rs\rangle\,, \tag{6.22}$$

where

$$A_{pq,rs}(t) = \begin{vmatrix} A_{pr}(t) & A_{ps}(t) \\ A_{qr}(t) & A_{qs}(t) \end{vmatrix}, \tag{6.23}$$

and $A_{pr}(t)$ describes the amplitude of the transfer in the one-excitation manifold, $A_{pr}(t) = \langle r|\,U_{xx}(t)\,|p\rangle$. Notice that the transport fidelity from spin $i$ to spin $j$ is then $F_{ij} = |A_{1N}|^2$.

More generally, for an arbitrary initial eigenstate of $\Sigma_z$, $|\mathbf{p}\rangle = |p_1, p_2, \ldots\rangle$, with $p_k \in \{0, 1\}$, the transfer amplitude to the eigenstate $|\mathbf{r}\rangle$ is given by

$$A_{\mathbf{pr}}(t) = \begin{vmatrix} A_{p_1r_1}(t) & A_{p_1r_2}(t) & \ldots \\ A_{p_2r_1}(t) & A_{p_2r_2}(t) & \ldots \\ \ldots & \ldots & \ldots \end{vmatrix}. \tag{6.24}$$

We can then evaluate the transfer of any initial mixed state $\rho_a = \sum_{\mathbf{p},\mathbf{q}} a_{\mathbf{pq}}\,|\mathbf{p}\rangle\,\langle\mathbf{q}|$ to another mixed state $\rho_b$ by calculating the relevant correlation between the evolved state and the final desired state,

$$M_{ab}(t) = \sum_{\mathbf{r},\mathbf{s},\mathbf{p},\mathbf{q}} b_{\mathbf{rs}}\,a_{\mathbf{pq}}A_{\mathbf{pr}}(t)A^*_{\mathbf{qs}}(t). \tag{6.25}$$

To implement QST in solid-state NMR with mixed-state chains, we are interested in the transport features of DQ-Hamiltonian. As this Hamiltonian does not conserve the spin excitation number, $[\mathscr{H}_{DQ}, \Sigma_z] \neq 0$, we would not expect it to support the transport of single-spin excitations. However, the DQ-Hamiltonian commutes with the operator $\tilde{\Sigma}_z = \sum_j (-1)^{j+1}\sigma_z^j$ and it can be block-diagonalized following the subspace structure defined by the (degenerate) eigenvalues of $\tilde{\Sigma}_z$. Different non-spin-excitation conserving Hamiltonians have been proposed in [104, 153, 154] taking advantage of other conserved quantities. The DQ-Hamiltonian allows for

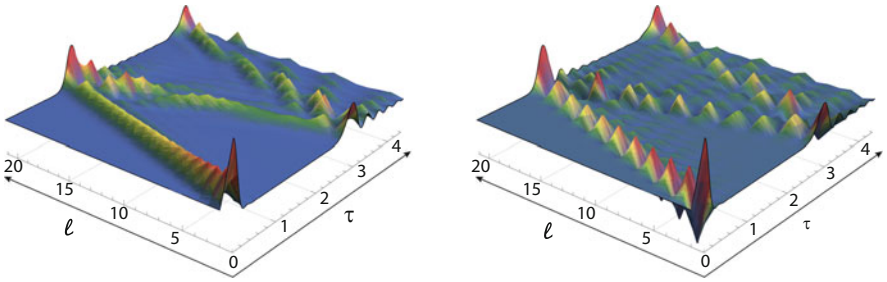


**Fig. 6.8** (*Left*) Transport of polarization under the XX-Hamiltonian. We assumed all equal couplings $b_{j,j+1} = b$. Shown is the intensity of the polarization at each spin site $C^{xx}_{1,\ell}(t) = P^{xx}_{1,\ell}(t)$ as a function of normalized time $\tau = bt$ for a propagation starting from spin 1. The chain length was $n = 21$ spins. (*Right*) Transport of polarization under the DQ-Hamiltonian $C^{DQ}_{1,\ell}(t)$ with the same parameters as in (*Left*)

the mirror inversion of states contained in each of the subspaces defined by the eigenvalues of $\tilde{\Sigma}_z$ (the equivalent of single-spin excitation and higher excitation manifolds for $\Sigma_z$). For pure states, these states do not have a simple interpretation as local spin excitation states, and the DQ-Hamiltonian is thus of limited practical usefulness for state transfer. Interestingly, however, the situation is more favorable for the transport of spin polarization in mixed-state chains. Indeed, states such as $\delta\rho^j_z$ are invariant, up to a sign change, under the similarity transformation from $\mathscr{H}_{xx}$ to $\mathscr{H}_{DQ}$. Thus we can recover the results obtained for the polarization transport under the XX-Hamiltonian for any coupling distribution:

$$C^{DQ}_{jl}(t) = (-1)^{j-l}|A_{jl}(t)|^2. \tag{6.26}$$

In Fig. 6.8 we illustrate the transport of polarization from spin $j = 1$ as a function of the spin number $\ell$ and time. Comparing transport under the equal-coupling XX- and DQ-Hamiltonians, we see enhanced modulations due to the positive-negative alternation of the transport on the even-odd spin sites. Despite this feature, transport properties of the two Hamiltonians are equivalent.

While polarization transfer follows the same dynamics as the transport of a single-spin excitation, a similar mapping cannot be carried further in such a simple way. Thus we can transfer one bit of classical information, by encoding it in the sign of polarization, but we cannot use for example the state $\delta\rho^j_x = \mathbb{1}_{j-1} \otimes \sigma^j_x \otimes \mathbb{1}_{n-j}$ to simulate the transfer of a coherent pure state such as $|+\rangle\,|00\ldots\rangle$, where $|+\rangle = (|0\rangle + |1\rangle)/\sqrt{2}$. The problem is that the evolution of this state creates a highly correlated state, as $\sigma^1_x$ evolves to $\prod_{i=1}^{n-1}\sigma^i_z\sigma_\alpha$, where $\alpha = x(y)$ for $n$ odd (even) [155]. Although particle-conserving Hamiltonians (such as the ones considered) allow for state transfer in any excitation manifold (and mirror-symmetric Hamiltonians achieve perfect state transfer), a manifold-dependent phase is associated with the evolution [102, 156–158], thus only states residing entirely in one of these manifolds can be transferred.

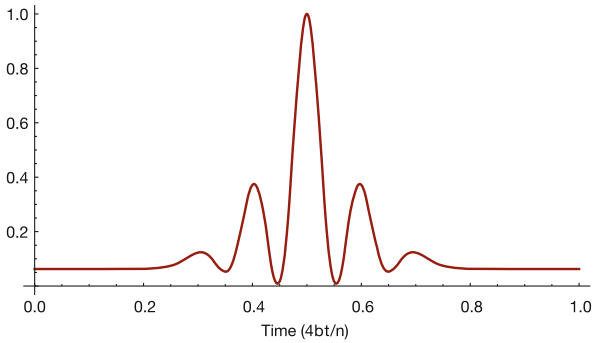


**Fig. 6.9** Transport fidelity of the logical entangled state $(|00\rangle_L + |11\rangle_L)/\sqrt{2} = (|0000\rangle + |1111\rangle)/2$ in a completely mixed chain of $n = 11$ spins. Here we assumed that the spins in the chain were coupled in a optimal way, with $b_{j,j+1} = b\sqrt{j(n-j)}/n$ [97, 101] and we plotted the fidelity as a function of the normalized time $bt/n$

To overcome this problem in mixed-state chain QST, two strategies have been proposed. Although the evolved state contains complex many-body correlations, quantum information can still be extracted from it with just a measurement [104], at the cost of destroying the initial state and of introducing classical communication and conditional operations. The second strategy is a simple two-qubit encoding [101, 151]. For evolution under the XX-Hamiltonian, the encoding corresponds to the zero-eigenvalue subspace of the operator $\sigma_z^1 + \sigma_z^2$, which corresponds to an encoded pure-state basis $|0\rangle_L^{xx} = |01\rangle$ and $|1\rangle_L^{xx} = |10\rangle$. Instead, for transport via the DQ-Hamiltonian, the required encoding is given by the basis $|0\rangle_L^{DQ} = |00\rangle$ and $|1\rangle_L^{DQ} = |11\rangle$, as follows from the similarity transformation between XX- and DQ-Hamiltonians. With this encoding we can transport a full operator basis,

$$\begin{aligned} \sigma_L^{DQ} &= \tfrac{\sigma_x^1\sigma_x^2 - \sigma_y^1\sigma_y^2}{2} & \sigma_{yL}^{DQ} &= \tfrac{\sigma_y^1\sigma_x^2 + \sigma_x^1\sigma_y^2}{2} \\ \sigma_{zL}^{DQ} &= \tfrac{\sigma_z^1 + \sigma_z^2}{2} & \mathbb{1}_L^{DQ} &= \tfrac{\mathbb{1} + \sigma_z^1\sigma_z^2}{2}. \end{aligned} \tag{6.27}$$

thus we can transport one qubit of quantum information. This encoding protocol is quite versatile. For example, it can be extended to more than a single logical qubit, to encode an entangled state of two logical qubits into four spins [60, 159], such as an encoded Bell state $|\psi\rangle = (|01\rangle_L + |10\rangle_L)/\sqrt{2}$. With a small encoding overhead, in principle this allows perfect transport of entanglement through a completely mixed chain (see Fig. 6.9).

#### 6.3.2.4 Chain Initialization and Readout

As explained in the previous section, transport of quantum information is possible even via a completely mixed-state spin chain. Still, one spin at the end of the chain

should act as a qubit and initially encode the quantum information to be transferred. In a distributed architecture, the qubit might be a different physical system that is put in contact with the spin wire when transport is required. In NMR-based experimental efforts to demonstrate QST, the qubit is often the spin at the end of the chain [12, 134]. Thus we would like to initialize it in a state of interest for the transfer of either classical or quantum information, while leaving the rest of the spin chain in the maximally mixed state. In the first case, we would like to prepare the state $\delta\rho_z^1$ (see Eq. 6.20); whereas in the second case we would like to prepare one of the logical states, e.g., $\delta\rho_y^L = \frac{\sigma_y^1\sigma_x^2+\sigma_x^1\sigma_y^2}{2} \otimes \mathbb{1}_{n-2}$ (see Eq. 6.27). Unfortunately, collective control of all the pulses in the chains, as given by on-resonance RF pulses, seems to preclude the preparation of these states. However exploiting the spin natural dynamics and a combination of coherent and incoherent control it is possible not only to prepare [12], but even to detect these types of states [134]. This was one critical step toward the demonstration of QST in a solid-state NMR platform.

The key insight was to realize that even in the absence of frequency addressability, the dynamics of the end-chain spins under the internal dipolar Hamiltonian is different from the bulk spins, as the end-spins have only one nearest neighbour.

Polarization initially in the transverse plane, $\delta\rho = \sum_{k=1}^{N} \sigma_x^k$ (prepared from the thermal state by a $\pi/2$ pulse), evolves under the internal dipolar Hamiltonian at different rates. The end-spin evolution rate is slower by a factor $\approx 1/\sqrt{2}$ as compared to the rest of the chain, due to fewer numbers of couplings with neighbouring spins. Thus, there exist a time $t_1$ when the state of the end-spins is still mainly $\sigma_x$, whereas the rest of the spins have evolved to many-body correlations. A second $\pi/2$ pulse brings the end-spin magnetization back to the longitudinal axis, while an appropriate phase cycling scheme cancels out other terms, thus obtaining the state

$$\delta\rho_{end} = \delta\rho_z^1 + \delta\rho_z^N . \tag{6.28}$$

We note that the chain geometry prevents breaking the symmetry between spin 1 and $N$. Here the phase cycling achieves a similar result of temporal averaging in the preparation of pseudo-pure states. The sequence that prepares this state can thus be written as

$$\left.\frac{\pi}{2}\right|_{\alpha} - t_1 - \left.\frac{\pi}{2}\right|_{-\alpha}, \tag{S1}$$

with $\alpha = \{-x, y\}$, to average out terms that do not commute with the total magnetization $\Sigma_z$. As the phase cycling does not cancel zero-quantum coherences, they will be the main source of errors in the initialization scheme [12, 118].

A similar control strategy can be as well used to read out the spins at the end of the chain even if the observable in inductively measured NMR is the collective magnetization of the spin ensemble, $\Sigma_z$. To measure a different observable, the desired state must be prepared prior to acquisition. Thus we want to turn $\Sigma_z$

into the end-chain state, Eq. (6.28). In general, the sequence used for readout cannot be a simple inversion of the end-selection step since this is not a unitary – reversible – operation. It is however sufficient to ensure that the state prior to the end-selection sequence has contributions mainly from population terms ($\propto \sigma_z^k$) for the sequence (S1) to work as a readout step. A two-step phase cycling [63] is enough to select populations and zero quantum terms, which in turn can be eliminated by purging pulses [160]. However, since the states created by evolution under the DQ Hamiltonian are already of the form $\propto \sigma_z^k$, the (S1) sequence with a two-step phase cycling is enough for the end-readout step.

The initialization technique described above was first introduced in [12] (see also [118, 161]); Kaur [134] later demonstrated both the initialization and readout techniques in a pure, single crystal of FAp grown by the flux method [125] and placed in a 7 T wide-bore magnet with a 300 MHz Bruker Advance Spectrometer and a probe tuned to 282.4 MHz for $^{19}$F measurement. The effectiveness of the initialization and readout methods was verified by probing the transport dynamics, as driven by the DQ Hamiltonian, comparing the end-polarized states and observables with the thermal-equilibrium state. To this goal, the collective or end-chain magnetization was measured as the evolution time was increased under the DQ Hamiltonian. The 8-pulse sequence [78] in Fig. 6.7 was used to implement the DQ Hamiltonian with a 1.45 μs $\pi/2$ pulse length. The evolution time was incremented by varying the inter-pulse delay from 1 to 6.2 μs and repeating the sequence from 1 to 12 times. The evolution was restricted to a timescale where the ideal model applies and errors arising from discrepancies from the ideal model (leakage to other chains and next-nearest neighbor couplings) are small [118]. In this timescale, the initial perturbation travels across $\approx$ 17 spins [119], however only polarization leaving one end of the chain could be observed: a clear signature of the polarization reaching the other end is erased by the distribution of chain lengths. Still, the experimental verification of initial state preparation is possible even at these short time scales thanks to marked differences in the signal arising from the evolution of thermal and end-polarized state under DQ Hamiltonian.

Figure 6.10 (blue) shows the observed evolution of the collective magnetization $\Sigma_z$ under the DQ Hamiltonian, starting from the thermal initial state, $\delta\rho_{th} = \Sigma_z$; the signal is given by $S^{th}(t) \propto \mathrm{Tr}\left\{U_{MQ}\delta\rho_{th}U_{MQ}^\dagger \Sigma_z\right\}$, with $U_{MQ}(t) = e^{-i\overline{\mathscr{H}}_{DQ}t}$. Modelling the physical spin system by an ensemble of equivalent and independent spin chains with nearest-neighbour couplings only, we can derive analytical formulas for the evolution to fit the experimental data. Under this approximation, the DQ Hamiltonian is exactly solvable by invoking a Jordan-Wigner mapping onto a system of free fermions [149, 162]. The analytical solution for the evolution of the thermal state, when measuring the collective magnetization, is given by [119, 134]:

$$S^{th}(t) = \sum_{p=1}^{N} f_{p,p}(2t), \tag{6.29}$$

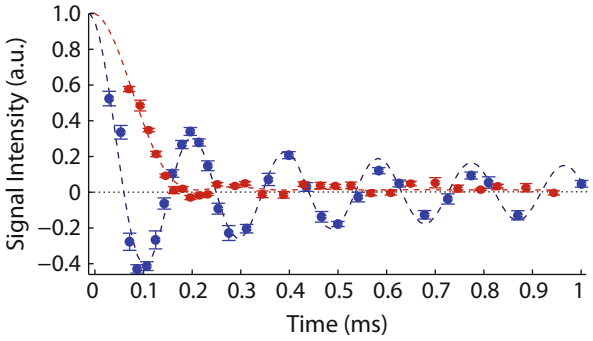


**Fig. 6.10** Transport under the DQ Hamiltonian, first reported in [134]. *Blue*: Initial state $\delta\rho_{th}$; readout, collective magnetization, $\Sigma_z$. *Red*: Initial state, $\delta\rho_{end}$; readout, end readout. Data points are the experimental data (*Blue*: collective magnetization; *Red* end of chain magnetization), with error bars obtained from the offset of the signal from zero. The measurement was done using a single scan (*blue*) and four scans (*red*) as required by using twice the two-step phase cycling of sequence S1. The lines are the fits using the analytical model. The fitting gives the following values for the dipolar coupling: 8.165 (*blue*, thermal state), and 8.63 (*red*) $\times 10^3$ rad/s. The *two curves* highlight the differences arising from the different initial state and readouts

with

$$\begin{aligned} f_{j,q}(t) = &\sum_{m=0}^{\infty}[i^{m\nu+\delta}J_{m\nu+\delta}(2bt) - i^{m\nu+\sigma}J_{m\nu+\sigma}(2bt)] \\ &+ \sum_{m=1}^{\infty}[i^{m\nu-\delta}J_{m\nu-\delta}(2bt) - i^{m\nu-\sigma}J_{m\nu-\sigma}(2bt)], \end{aligned} \tag{6.30}$$

where $\nu = 2(N+1), \delta = q - j, \sigma = q + j$ and $J_n$ are the $n$th order Bessel functions of the first kind. The data points in Fig. 6.10 were fitted to this analytical function (Eq. 6.29).

The red data in Fig. (6.10) show the evolution of the end polarized initial state under the DQ-Hamiltonian, measured using the readout strategies outlined above, $S^{sre} \propto \mathrm{Tr}\left\{U_{MQ}\delta\rho_{end}U_{MQ}^{\dagger}\delta\rho_{end}\right\}$. The fitting function used is given by

$$S^{sre}(t) = f_{1,1}^2(t) + f_{1,N}^2(t), \tag{6.31}$$

which has the same form as the transport of a single excitation in a pure state chain [97, 101], $|\langle 1_N|\, U_{xx}(t)\,|1_1\rangle|$. This experiment is thus a direct simulation of quantum state transport.

To further validate the initialization and readout method, in Fig. 6.11 (blue, open circles) we plot the system dynamics when starting from an end-polarized state, Eq. (6.28) (where polarization is localized at the ends of the chain) and reading out the collective magnetization, $S^{se} \propto \mathrm{Tr}\left\{U_{MQ}\delta\rho_{end}U_{MQ}^{\dagger}\Sigma_z\right\}$. The red (filled circle) data in Fig. 6.11 show a complementary measurement where we start from thermal initial state, given by the collective magnetization, and read out the ends of the

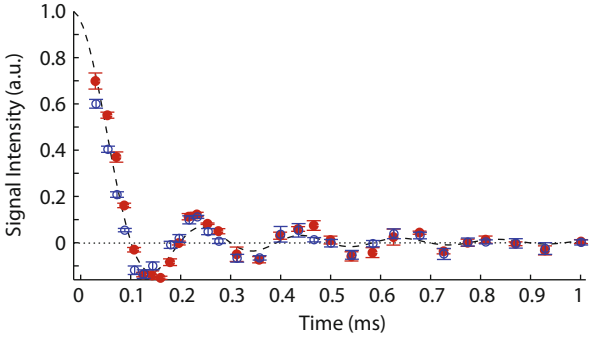


**Fig. 6.11** Evolution under the DQ Hamiltonian, first reported in [134]. *Blue*, *open circles*: Initial state, $\delta\rho_{end}$; readout, collective magnetization, $\Sigma_z$. *Red, filled circles*: Initial state, $\delta\rho_{th}$; readout, end-spin readout. Data points are the experimental data (*Blue*: collective magnetization; *Red* end of chain magnetization). Error bars are given by the offset of the signal from zero. The measurement was done using two scans as required by the two step phase cycling in sequence S1. The lines are the fits using the analytical model. The fitting gives the following values for the dipolar coupling: 8.172 (*blue*) and $8.048 \times 10^3$ rad/s (*red*). The experimental data shows remarkable agreement between the two schemes, thus confirming the validity of the initialization and readout methods

chains after evolution under the DQ Hamiltonian, $S^{re} \propto \mathrm{Tr}\left\{U_{MQ}\delta\rho_{th}U_{MQ}^{\dagger}\delta\rho_{end}\right\}$. Both these data sets were fitted by the analytical expression

$$S^{se}(t) = S^{re}(t) = \sum_{p=1}^{N} f_{1,p}^2(t), \tag{6.32}$$

As it is evident from the near perfect fitting, the analytical model explains the experimental data quite precisely.

Figures 6.10 and 6.11 show very different chain dynamics for the two initial states (with and without end selection), giving an experimental validation of our initialization method. Furthermore, the data and fittings for end selection and end readout measurements, Fig. 6.11, are very similar. This indicates the robustness of the readout step.

The small discrepancy in the fitting parameter (coupling strength) in the spin transport experiment (Fig. 6.10, red data) is due to accumulation of imperfections of the end-select and readout schemes. Unfortunately, the phase cycling scheme does not cancel out zero-quantum terms. Thus, residual polarization on spins 2 and N−1 ($\sigma_z^2 + \sigma_z^{N-1}$) and correlated states of the form $\sigma_j^z(\sigma_{j-1}^+\sigma_{j+1}^- + \sigma_{j-1}^-\sigma_{j+1}^+)$ lower the fidelity with the desired state. This effect is more important for the last experiment, since not only errors in the two selection steps accumulate but the readout step is further degraded by the fact that it is not applied to the ideal state expected after transport. Still, the agreement of the experimental data with the analytical model indicates that these errors are small and do not invalidate the scheme.

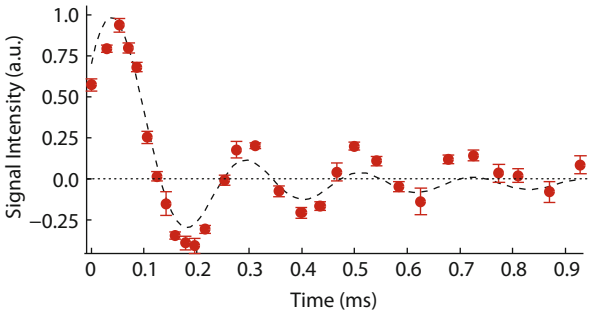


**Fig. 6.12** Evolution of the logical state $\delta\rho_y^L$ (Eq. 6.27) under the transport Hamiltonian, first reported in [134]. The logical initial state was prepared using the sequence (S2) and its evolution under the DQ Hamiltonian monitored by observing the collective magnetization. *Circles* represent the experimental data and the *dashed line* is the fit to the analytical model of Eq. (6.33). The fitting of the data points gives a dipolar coupling value of $7.551 \times 10^3$ rad/s

The end-selection scheme presented above can not only prepare the end-chain polarized states, but also the logical states – introduced in Eq. (6.27) – required for quantum information transport. First we prepare the end polarized state $\delta\rho_{end}$ by the sequence (S1). Then this evolves under the DQ Hamiltonian for a very short time $t_{\mathrm{DQ}} = 14.7\,\mu\mathrm{s}$, thus creating a two-spin correlated state as required. We can write this initialization sequence as

$$\frac{\pi}{2}\Big|_{\alpha} - t_1 - \frac{\pi}{2}\Big|_{\beta} - \mathrm{DQ}^{\gamma}, \tag{S2}$$

where $\mathrm{DQ}^{\gamma=x}$ is propagation under $U_{MQ}(t_{\mathrm{DQ}}) = e^{-i\overline{\mathscr{H}}_{DQ}t_{DQ}}$ and $\mathrm{DQ}^{\gamma=y}$ under $U_{MQ}^{\dagger}$. Setting $[\alpha, \beta, \gamma] = [-x, x, x]$, the state after the sequence (S2) is approximately given by zero and double quantum coherences, $\delta\rho_{end}(t_{\mathrm{DQ}}) \approx \sigma_{1,2}^{\mathrm{zq}} + \sigma_{n-1,n}^{\mathrm{zq}} + \sigma_{1,2}^{\mathrm{DQ}} + \sigma_{n-1,n}^{\mathrm{DQ}}$, where $\sigma_{i,j}^{\mathrm{zq}} = (\sigma_x^i\sigma_y^j - \sigma_y^i\sigma_x^j)$ and $\sigma_{i,j}^{\mathrm{DQ}} = (\sigma_x^i\sigma_y^j + \sigma_y^i\sigma_x^j)$. A double quantum filter given by the four-step phase cycling scheme,

$$[\alpha, \beta, \gamma] = \{[-x, x, x]; [y, -y, x]; [-x, -x, y]; 1[y, y, y]\}$$

cancels out the zero-quantum terms and selects the double-quantum terms, which is our desired state: $\delta\rho_y^L \propto \sigma_{1,2}^{\mathrm{DQ}} + \sigma_{n-1,n}^{\mathrm{DQ}}$. Figure 6.12 shows the evolution of this state under the DQ Hamiltonian. We note that this experiment implements the transport of quantum information via a maximally mixed quantum channel. The dynamics was monitored by measuring the collective magnetization, $S^L \propto \mathrm{Tr}\left\{U_{MQ}\delta\rho_y^L U_{MQ}^{\dagger}\sigma_z\right\}$. The data points were fitted by the expression

$$S^{yL}(t) = f_{1,2}(2t) + f_{N-1,N}(2t), \tag{6.33}$$

showing good agreement with the analytical model.

#### 6.3.2.5 Experimental Insight into Transport Dynamics

Implementing experimentally quantum state transfer, even with the constraints described above regarding state initialization and readout, is critical further learn about practical features and limitations that do not arise in the idealized model. It is thus possible to gather further insight into the transport dynamics, for example by studying more in depth the state created during transport [119, 134] and its decay [140, 163]. In addition it is possible to explore the effects that discrepancies from the ideal model, such as longer-range couplings and couplings to external spins, have on transport [118]. These phenomena often go beyond analytical solutions and are thus best explored experimentally.

**Multiple quantum coherence dynamics** – To gather further insight into the transport dynamics it would be interesting to completely characterize the evolved state, as it is done in state tomography [164]. Unfortunately, given the large dimension of the system considered and measurement constraints, this is not possible. We can still infer more information on the state by measuring not only the system's polarization (either collective polarization, $\Sigma_z$ or the end-spin polarization, $\delta\rho_{end}$) but also spin correlations encoded in multiple quantum coherences. As these MQC intensities present a beating every time the polarization is transferred from spin 1 to $N$, it would be possible in principle to monitor state transfer driven by the DQ Hamiltonian by measuring the MQC intensities, which are more easily detected [11]. Although this signature is washed out by a distribution of chain lengths [118], MQC intensities still retain information about the state that is transported, for example distinguishing between the thermal and end-polarized state, as shown in Fig. 6.13.

The figure shows the evolution of the MQC intensities experimentally measured for different initial states and readouts. Here the signal is slightly different than what presented in Eq. (6.12). When the initial state $\rho_i$ and observable $\rho_{obs}$ are different, the signal $S^{obs}_{\varphi_m} = \mathrm{Tr}\left\{\rho^m_f(t)\rho_{obs}\right\}$ yields the coherence order intensity

$$I'_q(t) = \sum_{m=1}^{M} S_{\varphi_m}(t)e^{-iq\varphi_m} = \mathrm{Tr}\left\{\rho_i(t)^q\rho_{obs}(t)^{-q} + \rho_i(t)^{-q}\rho_{obs}(t)^q\right\}, \quad (6.34)$$

where $\rho_i(t) = U_{MQ}\rho_i U^\dagger_{MQ}$ and $\rho_{obs}(t) = U_{MQ}\rho_{obs}U^\dagger_{MQ}$. Figure 6.13a shows the usual MQC signal, obtained by measuring the collective magnetization and starting from an initial thermal state (Eq. 6.4). The data points are fitted by the functions predicted by the analytic model [11, 148, 162]:

$$\begin{aligned} J^{th}_0(t) &= \frac{1}{N}\sum_k \cos^2[4bt\cos(\psi_k)], \\ J^{th}_2(t) &= \frac{1}{2N}\sum_k \sin^2[4bt\cos(\psi_k)], \end{aligned} \quad (6.35)$$

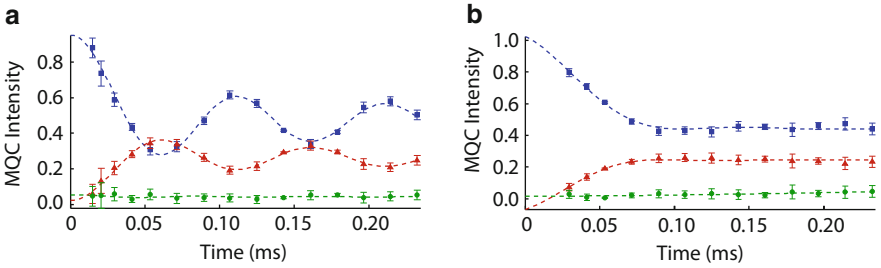


**Fig. 6.13** Evolution of multiple quantum coherences $I'_n(t)$ (0Q *blue squares*, 2Q *red triangles*, 4Q *green circles*) first reported in [134]: (**a**) Initial state: $\delta\rho_{th}$. Readout: collective magnetization. (**b**) Initial state: $\delta\rho_{end}$. Readout: end-readout. Data points are the experimental data (collective magnetization in (**a**) and end of chain magnetization in (**b**)). The measurement was done using a single scan in (**a**) and four scans in (**b**) for the four step phase cycling. The error bars are estimated from the deviation of 1st order quantum coherence from zero. The first two data points were measured using a 4 pulse sequence to implement the DQ Hamiltonian (instead of a standard 8 pulse sequence), leading to greater error bars. The data points are fitted by analytical functions (*blue* and *red lines*) obtained from the DQ Hamiltonian with NN couplings (Eqs. (6.35) and (6.36) for figures (**a**) and (**b**) respectively). The 4Q coherences (which should be zero in the ideal model) were simply fitted with a constant. Fitting of the data gives dipolar coupling: 7.971 (**a**) and 8.492 (**b**) $\times 10^3$ rad/s

where $N$ is the number of spins in the chain and $\psi_k = k\pi/(N+1)$.

The data for the case where we initialize the ends of the chains before letting the system evolve under DQ Hamiltonian and then read out the ends is shown in Fig. 6.13b. The data is fitted to the normalized MQC intensities given by the analytical model [11]:

$$\begin{aligned} J_0^{sre}(t) &= \tfrac{4}{(N+1)^2} \sum_{k,h} \sin^2(\kappa)\sin^2(\eta)\cos^2(\psi_k+\psi_h)(1+\cos[(N+1)\kappa]\cos[(N+1)\eta]), \\ J_2^{sre}(t) &= \tfrac{2}{(N+1)^2} \sum_{k,h} \sin^2(\kappa)\sin^2(\eta)\sin^2(\psi_k+\psi_h)(1+\cos[(N+1)\kappa]\cos[(N+1)\eta]). \end{aligned} \tag{6.36}$$

The fitting yielded a dipolar coupling strength b=8.492 $\times 10^3$ rad/s [134], a slightly higher value than what is obtained from other independent experiments on the same system. As mentioned, this is due to accumulation of errors in the initialization and readout steps.

MQC intensities provide further insight into the dynamics of various initial states driven by the transport Hamiltonian. In particular, these experiments yield an independent validation of the initialization and readout steps. Unfortunately, MQC are not enough to fully reconstruct the system's state. For example, during the course of the evolution, multi-spin correlations are created [119], as the polarization wavepacket spreads out. This effects is due to the fact that for a Hamiltonian with all-equal coupling transport is eventually dispersive [165]. In order to reach perfect state transfer one needs to study alternative strategies, including static [97, 101] or

dynamic [85, 105] engineering of optimal couplings or a weakening of the coupling between the bulk spins and the end-chain spins [152, 166–169]. Still, it would be interesting to study the sequential growth of multi-spin correlations in the case of equal-coupling Hamiltonians, not only to characterize the dynamics but also to further study the decay of these correlations [140], which might be faster than for single-spin states [170, 171].

Ramanathan et al. [119] experimentally characterized the sequential growth of multi-spin correlations using an x-basis encoding of MQC [147]. In standard MQC experiments, as explained in Sect. 6.2.2.2, we encode the coherence order with respect to $\Sigma_z$ eigenstates. The encoding is simply obtained by the phase shift acquired during a collective rotation of the spins about the z-axis. Similarly, a collective rotation about the x-axis results in an encoding of MQC with respect to eigenstates of $\Sigma_x = \sum_k \sigma_x^k$. Higher order coherences in the x-basis are a signature of the presence of multi-spin correlations [147]. It was observed (see Fig. 4 in [119]) that during the evolution under the DQ Hamiltonian, in a one-dimensional system after the initial rapid creation of 3-spin correlations (and concomitant reduction in the single spin term), the coherence orders change quite slowly. This confirms that although the equal-coupling DQ Hamiltonian is dispersive, the rate of dispersion is quite slow, thus one can still achieve high fidelity transport over short distances.

**Errors and decoherence** – The greatest contribution of experimental implementations of QST, even in systems with practical limitations, for example not allowing scalability, is in the study of effects that go beyond the ideal analytic models. Indeed, while transport in the one-excitation manifold (and its generalization to mixed states) via local Hamiltonian can be either solved analytically or efficiently simulated on a classical computer, more realistic models, closer to possible physical implementations, in general cannot be solved. Thus it becomes interesting to simulate experimentally possible discrepancies of a real system from the ideal model, as many of these effects will be common to many different physical systems. These include long-range couplings inside the chain and interaction of the chain spins with an environment and possibly with other nearby chains, as it would happen in a distributed quantum computing architecture.

Using fluorapatite as a model system, W. Zhang and coworkers [118] examined how the ideal model (an isolated spin chain, with a nearest-neighbor only DQ Hamiltonian) compares to the physical system's evolution. They used both experimental and numerical methods to break down the various contributions to the observed deviation from the ideal model. In addition to errors introduced in state initialization, that we mentioned above, they analyzed experimental errors introduced during the DQ Hamiltonian engineering as well as by the presence of longer-range couplings, both within a single chain and between adjacent spin chains, and by a distribution of chain lengths.

It was found that pulse errors were the main cause of the deviation of the engineered Hamiltonian (via the sequence in Fig. 6.7) from the ideal DQ Hamiltonian, Eq. (6.19), while the experimental implementation of the sequence is enough to reduce the effects of second-order terms in AHT. Despite the experimental Hamiltonian is not ideal, the effects are only felt at long times, much longer than

usually explored during transport experiments and thus it is not a limitation for studying transport over 10–20 spins (we note that the fidelity of transport would decrease sensibly for longer chains even in the ideal model with equal couplings).

A larger contribution to the deviation of the experimental signal from the expected ideal behavior over the timescale of interest was due to long-range couplings. The main results were the creation of spurious terms in the evolved state, as signaled by the appearance of four-quantum coherences, which are not expected in the ideal model, and a decay of the signal toward its long-time average value (that is, a damping of its coherent oscillation amplitude). It was found that the effects of in-chain couplings were hardly distinguishable from cross-chain couplings, even if they have different strengths, since six neighboring chains contribute to the second effect. These results are important for the experimental implementation of QST in any physical platform, as they indicate that much attention should be paid not only to isolating the chain from the environment and other nearby spin wires, but also to carefully engineer the transport Hamiltonian, for example by filtering out next-nearest neighbor couplings [85] that would otherwise decrease the transport fidelity [154].

## 6.4 Conclusions and Outlook

NMR systems and techniques have provided a fertile platform for experimental investigation of quantum state transfer in spin chains. From the first observation of polarization transfer, predating the formal definition of QST [10], to the realization of QST simulations in small molecules and in larger solid-state spin systems, the experiments have drawn on the strength of NMR, in particular on its long history of well-developed control techniques. Thus, NMR implementations have been invaluable both as proof-of-principle demonstrations of QST protocols and to explore dynamics occurring in real systems that go beyond what can be analytically solved or numerically simulated.

Some challenges and limitations of NMR-based implementations of QST remain. On the one side, liquid-state implementations have been limited in size by the number of spins in the molecules. Although larger molecules exist, a more fundamental challenge derives from the difficulty of controlling the natural Hamiltonian in larger systems in order to obtain the desired transport interaction. In addition, the weakness of the scalar couplings makes transport in liquid-state molecules a slow process that quickly competes with decoherence. Still, liquid-state implementations might be well-suited to demonstrate control-intensive protocols, to refine the control techniques that will be as well required in larger systems and to study the effects of limitations and constraints in the control.

QST in larger systems and at a faster rate has been obtained using solid-state NMR. However, in these systems the constraints imposed by collective control and by ensemble measurements have prevented the experimental characterization of transport fidelity: indeed, due to the chain length distribution, the signal averaged

over the chain ensemble does not provide information about the transport fidelity. Using different systems, for example $^{1}$H doped FAp (or $^{19}$F-doped HAp), combined with control techniques could provide a solution to this problem [134].

Both traditional liquid- and solid-state NMR systems are not well suited to move beyond simple demonstrations of QST and toward its actual implementation in the context of a QIP architecture. Still, the techniques and insight developed on these systems can help the design of potentially scalable systems. For example, NMR techniques could be used in hybrid systems, comprising electronic and nuclear spins or combining magnetic resonance and optical techniques for initialization and readout.

A spin-based distributed quantum information processor can be based on single-crystal molecular monolayers as proposed in [19, 172]. The individual registers are organic molecules with a localized free-radical electron spin, which interacts with a small number of nuclear spins via an anisotropic hyperfine interaction [100]. These molecules can be made into single-crystal molecular monolayers using either a Langmuir-Blodgett process [173], or by self-assembly [174]. This system could be used to explore QST or, conversely, using some of the registers to form a wire could enable building larger architectures based on this model.

Another system that has emerged as a potential candidate for QIP architectures is the Nitrogen-Vacancy (NV) center in diamond [9], thanks to its long coherence times and the possibility of optical initialization and readout even at room temperature. The NV center could be thus at the center of small quantum registers [175, 176], where nuclear spins play the role of long-time storage qubits with fast access and control provided by the NV electronic spin. To connect the registers, other spins in the diamond lattice could be used, for example Nitrogen electronic spins [101, 177, 178]. While Nitrogen implantation can be done with improving precision [179–182], the Nitrogen to NV conversion is limited, as vacancies need to recombine with single Nitrogens by annealing at high temperature. Thus although it is difficult to envision regular NV spin chains, the nitrogen defects (P1 centers [183]) are electronic spin-1/2 that can be used as quantum wires to connect the NV-center qubits. While NV centers can be initialized to their ground state and controlled individually by a combination of microwave and optical control [184], the P1 can only be controlled collectively and are found in their thermal (highly mixed) state. Using the P1 centers as quantum wires would enable larger separation between NV qubits and thus their individual addressing by sub-diffraction-limit optical techniques [184, 185]. Local operations at the NV center register would allow for quantum error correction and entanglement purification, with the potential of a fault-tolerant, room temperature quantum computer. The P1 centers interact via the dipolar interaction, which can be truncated to its secular part [101], Eq. (6.6), at high enough magnetic fields or even reduced to an Ising Hamiltonian thanks to gradients [177]. The transport Hamiltonian (either DQ or XX Hamiltonian) can then be engineered via the multiple-pulse techniques discussed in this chapter, while magnetic resonance control techniques can help in obtaining the desired couplings of the NV centers to the P1 spins (to achieve for example, the weak-coupling regime [152, 166–169, 186, 187]). While dephasing noise limits the

transport fidelity [178] material engineering and dynamical decoupling techniques that can increase the coherence time [188, 189] by orders of magnitude might make this scheme practical.

Alternatively, the NV centers could be used as single-spin detectors [190–192] to read out spins in various solid-state systems, either as a scanning head or as a substrate of surface spin networks [172, 193]. This would allow transforming some spin systems, which currently lack addressability, into potential candidate platforms for scalable QIP and in particular for QST. Combining local addressability with strong gradients can enable Hamiltonian engineering, inspired by NMR multiple-pulse control techniques [82], which allow state transfer in more general networks [85, 105].

From the examples we briefly discussed it follows that, as it is a long tradition in QIP, magnetic resonance techniques will continue to play an important role in advancing the experimental implementations of quantum state transfer.

**Acknowledgements** It is a pleasure to thank David Cory, Chandrasekhar Ramanathan and Lorenza Viola for a fruitful collaboration on magnetic-resonance based transport in spin chains. P.C. acknowledges partial support from the National Science Foundation under Grant No. DMR-1005926 and by AFOSR.

## References

1. S. Bose, Phys. Rev. Lett. **91**(20), 207901 (2003)
2. M. Mariantoni, H. Wang, T. Yamamoto, M. Neeley, R.C. Bialczak, Y. Chen, M. Lenander, E. Lucero, A.D. O'Connell, D. Sank, M. Weides, J. Wenner, Y. Yin, J. Zhao, A.N. Korotkov, A.N. Cleland, J.M. Martinis, Science **334**(6052), 61 (2011)
3. D. Loss, D.P. DiVincenzo, Phys. Rev. A **57**(1), 120 (1998)
4. X. Li, Y. Wu, D. Steel, D. Gammon, T.H. Stievater, D.S. Katzer, D. Park, C. Piermarocchi, L.J. Sham, Science **301**(5634), 809 (2003)
5. G. Ciaramicoli, I. Marzoli, P. Tombesi, Phys. Rev. A **75**, 032348 (2007)
6. L.M. Duan, E. Demler, M.D. Lukin, Phys. Rev. Lett. **91**(9), 090402 (2003)
7. J. Simon, W.S. Bakr, R. Ma, M.E. Tai, P.M. Preiss, M. Greiner, Nature **472**(7343), 307 (2011)
8. B.E. Kane, Nature **393**, 133 (1998)
9. J. Wrachtrup, F. Jelezko, J. Phys.: Condens. Matter **18**(21), S807 (2006)
10. Z. Madi, B. Brutscher, T. Schulte-Herbruggen, R. Bruschweiler, R. Ernst, Chem. Phys. Lett. **268**(3), 300 (1997)
11. P. Cappellaro, C. Ramanathan, D.G. Cory, Phys. Rev. Lett. **99**(25), 250506 (2007)
12. P. Cappellaro, C. Ramanathan, D.G. Cory, Phys. Rev. A **76**(3), 032317 (2007)
13. J. Zhang, X. Peng, D. Suter, Phys. Rev. A **73**, 062325 (2006)
14. D.D. Traficante, Concepts Magn. Reson. **3**(1), 49 (1991)
15. N. Bloembergen, Physica **15**, 386 (1949)
16. A. Abragam, M. Goldman, Rep. Prog. Phys. **41**(3), 395 (1978)
17. C. Ramanathan, App. Mag. Res. **34**(3), 409 (2008)
18. T.D. Ladd, J.R. Goldman, F. Yamaguchi, Y. Yamamoto, E. Abe, K.M. Itoh, Phys. Rev. Lett. **89**(1), 017901 (2002)
19. D. Cory, R. Laflamme, E. Knill, L. Viola, T. Havel, N. Boulant, G. Boutis, E. Fortunato, S. Lloyd, R. Martinez, C. Negrevergne, M. Pravia, Y. Sharf, G. Teklemariam, Y. Weinstein, W. Zurek, Fort. der Phys. **48**(9–11), 875 (2000)

20. B. Criger, G. Passante, D. Park, R. Laflamme, Phil. Trans. R. Soc. A **370**(1976), 4620 (2012)
21. C. Ramanathan, N. Boulant, Z. Chen, D.G. Cory, I. Chuang, M. Steffen, Quantum Inf. Process. **3**, 15 (2004)
22. J.A. Jones, Prog. Nucl. Magn. Reson. Spectrosc. **59**(2), 91 (2011)
23. C. Negrevergne, T.S. Mahesh, C.A. Ryan, M. Ditty, F. Cyr-Racine, W. Power, N. Boulant, T. Havel, D.G. Cory, R. Laflamme, Phys. Rev. Lett. **96**(17), 170501 (2006)
24. A. Abragam, *Principles of Nuclear Magnetism* (Oxford University Press, Oxford, 1961)
25. R. Ernst, G. Bodenhausen, A. Wokaun, *Principles of Nuclear Magnetic Resonance in One and Two Dimensions* (Clarendon Press, Oxford, 1987)
26. C.P. Slichter, *Principles of Magnetic Resonance*, 3rd edn. (Springer, New York, 1996)
27. P.T. Callaghan, *Principles of Nuclear Magnetic Resonance Microscopy* (Oxford Science Publications, Oxford, 1991)
28. M.H. Levitt, Prog. Nucl. Magn. Reson. Spectrosc. **18**(2), 61 (1986)
29. E.M. Fortunato, M.A. Pravia, N. Boulant, G. Teklemariam, T.F. Havel, D.G. Cory, J. Chem. Phys. **116**, 7599 (2002)
30. M.A. Pravia, N. Boulant, J. Emerson, A. Farid, E.M. Fortunato, T.F. Havel, R. Martinez, D.G. Cory, J. Chem. Phys. **119**, 9993 (2003)
31. N. Khaneja, T. Reiss, C. Kehlet, T. Schulte-Herbuggen, S. Glaser, J. Magn. Res. **172**, 296 (2005)
32. J. Zhang, G.L. Long, W. Zhang, Z. Deng, W. Liu, Z. Lu, Phys. Rev. A **72**, 012331 (2005)
33. D.G. Cory, A.F. Fahmy, T.F. Havel, Proc. Nat. Acad. Sci. **94**(5), 1634 (1997)
34. N.A. Gershenfeld, I.L. Chuang, Science **275**(5298), 350 (1997)
35. D. Deutsch, Proc. R. Soc. A **400**(1818), 97 (1985)
36. J.A. Jones, M. Mosca, J. Chem. Phys. **109**(5), 1648 (1998)
37. M.S. Anwar, J.A. Jones, D. Blazina, S.B. Duckett, H.A. Carteret, Phys. Rev. A **70**, 032324 (2004)
38. I.L. Chuang, L.M.K. Vandersypen, X. Zhou, D.W. Leung, S. Lloyd, Nature **393**(6681), 143 (1998)
39. R. Cleve, A. Ekert, C. Macchiavello, M. Mosca, Proc. R. Soc. Lond. A: Math. Phys. Eng. Sci. **454**(1969), 339 (1998)
40. M. Kawamura, T. Morimoto, T. Kumaya, R. Sawae, K. Takarabe, Y. Manmoto, Int. J. Quantum Chem. **105**(6), 750 (2005)
41. N. Linden, H. Barjat, R. Freeman, Chem. Phys. Lett. **296**(1–2), 61 (1998)
42. L. Grover, in *Proceedings of 28th Annual ACM Symposium on Theory of Computing (STOC)*, Philadephia, 1996, pp. 212–219
43. J.A. Jones, M. Mosca, R.H. Hansen, Nature **393**(6683), 344 (1998)
44. I.L. Chuang, N. Gershenfeld, M. Kubinec, Phys. Rev. Lett. **80**, 3408 (1998)
45. C.S. Yannoni, M.H. Sherwood, D.C. Miller, I.L. Chuang, L.M.K. Vandersypen, M.G. Kubinec, Appl. Phys. Lett. **75**(22), 3563 (1999)
46. Y. Weinstein, T. Havel, J. Emerson, N. Boulant, M. Saraceno, S. Lloyd, D.G. Cory, J. Chem. Phys. **121**, 6117 (2004)
47. L. Vandersypen, M. Steffen, G. Breyta, C. Yannoni, M. Sherwood, I. Chuang, Nature **414**, 883 (2001)
48. S.S. Somaroo, C.H. Tseng, T.F. Havel, R. Laflamme, D.G. Cory, Phys. Rev. Lett. **82**, 5381 (1999)
49. C.H. Tseng, S. Somaroo, Y. Sharf, E. Knill, R. Laflamme, T.F. Havel, D.G. Cory, Phys. Rev. A **61**, 012302 (1999)
50. J. Du, N. Xu, X. Peng, P. Wang, S. Wu, D. Lu, Phys. Rev. Lett. **104**, 030502 (2010)
51. C.A. Ryan, M. Laforest, J.C. Boileau, R. Laflamme, Phys. Rev. A **72**, 062317 (2005)
52. J. Du, H. Li, X. Xu, M. Shi, J. Wu, X. Zhou, R. Han, Phys. Rev. Lett. **88**, 137902 (2002)
53. A. Mitra, K. Sivapriya, A. Kumar, J. Magn. Reson. **187**(2), 306 (2007)
54. Y.S. Weinstein, S. Lloyd, J. Emerson, D.G. Cory, Phys. Rev. Lett. **89**, 157902 (2002)
55. D.G. Cory, M.D. Price, W. Maas, E. Knill, R. Laflamme, W.H. Zurek, T.F. Havel, S.S. Somaroo, Phys. Rev. Lett. **81**(10), 2152 (1998)

56. L. Viola, E.M. Fortunato, M.A. Pravia, E. Knill, R. Laflamme, D.G. Cory, Science **293**(5537), 2059 (2001)
57. E.M. Fortunato, L. Viola, J. Hodges, G. Teklemariam, D.G. Cory, New J. Phys. **4**(1), 5 (2002)
58. N. Boulant, L. Viola, E.M. Fortunato, D.G. Cory, Phys. Rev. Lett. **94**, 130501 (2005)
59. P. Cappellaro, J.S. Hodges, T.F. Havel, D.G. Cory, J. Chem. Phys. **125**, 044514 (2006)
60. J.S. Hodges, P. Cappellaro, T.F. Havel, R. Martinez, D.G. Cory, Phys. Rev. A **75**(4), 042320 (2007)
61. P. Cappellaro, J.S. Hodges, T.F. Havel, D.G. Cory, Phys. Rev. A **75**, 042321 (2007)
62. E. Knill, I. Chuang, R. Laflamme, Phys. Rev. A **57**(5), 3348 (1998)
63. G. Bodenhausen, H. Kogler, R. Ernst, J. Magn. Reson. **58**(3), 370 (1984)
64. J. Keeler, *Understanding NMR Spectroscopy* (Wiley, New York, 2010)
65. J. Baum, R. Tycko, A. Pines, Phys. Rev. A **32**, 3435 (1985)
66. R. Freeman, Prog. Nucl. Magn. Reson. Spectrosc. **32**(1), 59 (1998)
67. C.A. Ryan, C. Negrevergne, M. Laforest, E. Knill, R. Laflamme, Phys. Rev. A **78**(1), 012328 (2008)
68. V.F. Krotov, *Global Methods in Optimal Control Theory* (Marcel Dekker Inc., New York, 1996)
69. L. Viola, S. Lloyd, Phys. Rev. A **58**, 2733 (1998)
70. K. Khodjasteh, D.A. Lidar, Phys. Rev. Lett. **95**(18), 180501 (2005)
71. G.S. Uhrig, Phys. Rev. Lett. **98**(10), 100504 (2007)
72. E.L. Hahn, Phys. Rev. **80**(4), 580 (1950)
73. H.Y. Carr, E.M. Purcell, Phys. Rev. **94**(3), 630 (1954)
74. S. Meiboom, D. Gill, Rev. Sci. Instr. **29**(8), 688 (1958)
75. N. Bloembergen, R.V. Pound, Phys. Rev. **95**, 8 (1954)
76. W. Zhang, D.G. Cory, Phys. Rev. Lett. **80**, 1324 (1998)
77. G.S. Boutis, P. Cappellaro, H. Cho, C. Ramanathan, D.G. Cory, J. Magn. Reson. **161**, 132 (2003)
78. Y.S. Yen, A. Pines, J. Chem. Phys. **78**(6), 3579 (1983)
79. M. Munowitz, A. Pines, Principle and applications of multiple-quantum NMR, in *Advances in Chemical Physics*, vol. 66 (Wiley, New York, 1987)
80. M. Munowitz, A. Pines, M. Mehring, J. Chem. Phys. **86**(6), 3172 (1987)
81. J. Waugh, L. Huber, U. Haeberlen, Phys. Rev. Lett. **20**, 180 (1968)
82. U. Haeberlen, *High Resolution NMR in Solids: Selective Averaging* (Academic, New York, 1976)
83. U. Haeberlen, J. Waugh, Phys. Rev. **175**(2), 453 (1968)
84. W.K. Rhim, D.D. Elleman, K.U. Schreiber, R.W. Vaughan, J. Chem. Phys. **60**, 4595 (1974)
85. A. Ajoy, P. Cappellaro (2012). ArXiv:1208.3656
86. S. Schirmer, *Lagrangian and Hamiltonian Methods for Nonlinear Control 2006*. Lecture Notes in Control and Information Sciences, vol. 366 (Springer, Berlin/Heidelberg/New York, 2007), pp. 293–304
87. J. Zhang, M. Ditty, D. Burgarth, C.A. Ryan, C.M. Chandrashekar, M. Laforest, O. Moussa, J. Baugh, R. Laflamme, Phys. Rev. A **80**, 012316 (2009)
88. M.A. Nielsen, I.L. Chuang, *Quantum Computation and Quantum Information* (Cambridge University Press, Cambridge/New York, 2000)
89. J. Zhang, K.B. Whaley, Phys. Rev. A **71**(5), 052317 (2005)
90. P. Cappellaro, J. Emerson, N. Boulant, C. Ramanathan, S. Lloyd, D.G. Cory, Phys. Rev. Lett. **94**, 020502 (2005)
91. J.S. Lee, A.K. Khitrin, J. Chem. Phys. **121**(9), 3949 (2004)
92. J.S. Lee, A.K. Khitrin, Phys. Rev. A **71**, 062338 (2005)
93. J.S. Lee, T. Adams, A.K. Khitrin, New J. Phys. **9**(4), 83 (2007)
94. N. Khaneja, S.J. Glaser, Phys. Rev. A **66**, 060301 (2002)
95. H. Yuan, S.J. Glaser, N. Khaneja, Phys. Rev. A **76**(1), 012316 (2007)
96. M. Nimbalkar, R. Zeier, J.L. Neves, S.B. Elavarasi, H. Yuan, N. Khaneja, K. Dorai, S.J. Glaser, Phys. Rev. A **85**, 012325 (2012)

97. M. Christandl, N. Datta, T.C. Dorlas, A. Ekert, A. Kay, A.J. Landahl, Phys. Rev. A **71**(3), 032312 (2005)
98. S.G. Schirmer, H. Fu, A.I. Solomon, Phys. Rev. A **63**, 063410 (2001)
99. C. Altafini, J. Math. Phys. **43**(5), 2051 (2002)
100. J.S. Hodges, J.C. Yang, C. Ramanathan, D.G. Cory, Phys. Rev. A **78**(1), 010303 (2008)
101. P. Cappellaro, L. Viola, C. Ramanathan, Phys. Rev. A **83**(3), 032304 (2011)
102. S.R. Clark, C.M. Alves, D. Jaksch, New J. Phys. **7**, 124 (2005)
103. D. Burgarth, K. Maruyama, F. Nori, Phys. Rev. A **79**, 020305 (2009)
104. C. DiFranco, M. Paternostro, M.S. Kim, Phys. Rev. Lett. **101**(23), 230502 (2008)
105. G.A. Álvarez, M. Mishkovsky, E.P. Danieli, P.R. Levstein, H.M. Pastawski, L. Frydman, Phys. Rev. A **81**(6), 060302 (2010)
106. D. Burgarth, V. Giovannetti, Phys. Rev. Lett. **99**(10), 100501 (2007)
107. J. Zhang, N. Rajendran, X. Peng, D. Suter, Phys. Rev. A **76**, 012317 (2007)
108. G.S. Boutis, D. Greenbaum, H. Cho, D.G. Cory, C. Ramanathan, Phys. Rev. Lett. **92**(13), 137201 (2004)
109. D. Greenbaum, M. Kindermann, C. Ramanathan, D.G. Cory, Phys. Rev. B **71**, 054403 (2005)
110. G.R. Khutsishvili, Sov. Phys. Uspekhi **8**(5), 743 (1966)
111. A.G. Redfield, Phys. Rev. **116**(2), 315 (1959)
112. D.K. Sodickson, J.S. Waugh, Phys. Rev. B **52**, 6467 (1995)
113. J.b. Waugh, Mol. Phys. **95**(5), 731 (1998)
114. R. Bruschweiler, R. Ernst, Chem. Phys. Lett. **264**(3–4), 393 (1997)
115. A.K. Khitrin, B.M. Fung, J. Chem. Phys. **111**, 7480 (1999)
116. M.I. Kay, R.A. Young, A.S. Posner, Nature **204**(4963), 1050 (1964)
117. J.S. Prener, J. Electrochem. Soc. **114**(1), 77 (1967)
118. W. Zhang, P. Cappellaro, N. Antler, B. Pepper, D.G. Cory, V.V. Dobrovitski, C. Ramanathan, L. Viola, Phys. Rev. A **80**(5), 052323 (2009)
119. C. Ramanathan, P. Cappellaro, L. Viola, D.G. Cory, New J. Phys. **13**(10), 103015 (2011)
120. E. Rufeil-Fiori, C.M. Sánchez, F.Y. Oliva, H.M. Pastawski, P.R. Levstein, Phys. Rev. A **79**(3), 032324 (2009)
121. W.V. der Lugt, W. Caspers, Physica **30**(8), 1658 (1964)
122. N. Leroy, E. Bres, Eur. Cell Mater. **2**, 36 (2001)
123. R. Mazelsky, R. Hopkins, W. Kramer, J. Cryst. Growth **3–4**, 260 (1968)
124. R. Mazelsky, R.C. Ohlmann, K. Steinbruegge, J. Electrochem. Soc. **115**(1), 68 (1968)
125. S. Oishi, T. Kamiya, Nippon Kagaku Kaishi **9**, 800 (1994)
126. K. Teshima, S. Lee, K. Yubuta, Y. Kameno, T. Suzuki, T. Shishido, M. Endo, S. Oishi, Cryst. Growth Des. **9**(9), 3832 (2009)
127. K. Teshima, S. Lee, T. Ishizaki, S. Mori, C. Mori, K. Yubuta, T. Ichiki, T. Shishido, S. Oishi, Cryst. Eng. Comm. **13**(6), 1749 (2011)
128. K. Teshima, S. Lee, M. Sakurai, Y. Kameno, K. Yubuta, T. Suzuki, T. Shishido, M. Endo, S. Oishi, Cryst. Growth Des. **9**(6), 2937 (2009)
129. C.K. Hughes JM, Cameron M, Am. Miner. **74**, 870 (1989)
130. G. Cho, J.P. Yesinowski, Chem. Phys. Lett. **205**(1), 1 (1993)
131. Y. Pan, M.E. Fleet, Rev. Miner. Geochem. **48**(1), 13 (2002)
132. Y. Pan, N. Chen, J.A. Weil, M.J. Nilges, Am. Miner. **87**(10), 1333 (2002)
133. N. Chen, Y. Pan, J.A. Weil, Am. Miner. **87**(1), 37 (2002)
134. G. Kaur, P. Cappellaro, New J. Phys. **14**(8), 083005 (2012)
135. M. Engelsberg, I.J. Lowe, J.L. Carolan, Phys. Rev. B **7**, 924 (1973)
136. A. Sur, I.J. Lowe, Phys. Rev. B **12**, 4597 (1975)
137. L.B. Moran, J.K. Berkowitz, J.P. Yesinowski, Phys. Rev. B **45**, 5347 (1992)
138. L.B. Moran, J.P. Yesinowski, Chem. Phys. Lett. **222**(4), 363 (1994)
139. G. Cho, J.P. Yesinowski, J. Chem. Phys. **100**(39), 15716 (1996)
140. H.J. Cho, P. Cappellaro, D.G. Cory, C. Ramanathan, Phys. Rev. B **74**(22), 224434 (2006)
141. G. Cho, C.N. Chau, J.P. Yesinowski, J. Phys. Chem. C **112**, 6165 (2008)
142. E.B. Fel'dman, S. Lacelle, J. Chem. Phys. **107**(18), 7067 (1997)

143. A.K. Khitrin, Chem. Phys. Lett. **274**, 217 (1997)
144. J.R. Goldman, T.D. Ladd, F. Yamaguchi, Y. Yamamoto, E. Abe, K.M. Itoh, *Laser Spectroscopy* (World Scientific, Singapore, 2002), pp. 333–336
145. M. Christandl, N. Datta, A. Ekert, A.J. Landahl, Phys. Rev. Lett. **92**, 187902 (2004)
146. M.E. Rose, *Elementary Theory of Angular Momentum* (Wiley, New York, 1957)
147. C. Ramanathan, H. Cho, P. Cappellaro, G.S. Boutis, D.G. Cory, Chem. Phys. Lett. **369**, 311 (2003)
148. S. Doronin, I. Maksimov, E. Fel'dman, JETP **91**, 597 (2000)
149. E. Lieb, T. Schultz, D. Mattis, Ann. Phys. **16**, 407 (1961)
150. J. Fitzsimons, J. Twamley, Phys. Rev. Lett. **97**(9), 090502 (2006)
151. M. Markiewicz, M. Wiesniak, Phys. Rev. A **79**(5), 054304 (2009)
152. N.Y. Yao, L. Jiang, A.V. Gorshkov, Z.X. Gong, A. Zhai, L.M. Duan, M.D. Lukin, Phys. Rev. Lett. **106**(4), 040505 (2011)
153. A. Kay, Phys. Rev. Lett. **98**(1), 010501 (2007)
154. A. Kay, Int. J. Quantum Inf. **8**(4), 641 (2010)
155. G.M.P. C. Di Franco, M. Paternostro, Int. J. Quantum Inf. **6**, 659 (2008)
156. S.R. Clark, A. Klein, M. Bruderer, D. Jaksch, New J. Phys. **9**(6), 202 (2007)
157. D. Burgarth, K. Maruyama, F. Nori, New J. Phys. **13**(1), 013019 (2011)
158. C. Di Franco, M. Paternostro, M.S. Kim, Phys. Rev. Lett. **102**, 187203 (2009)
159. M.K. Henry, C. Ramanathan, J.S. Hodges, C.A. Ryan, M.J. Ditty, R. Laflamme, D.G. Cory, Phys. Rev. Lett. **99**(22), 220501 (2007)
160. A. Davis, G. Estcourt, J. Keeler, E. Laue, J. Titman, J. Magn. Reson. **105**(2), 167 (1993)
161. P. Cappellaro, Quantum information processing in multi-spin systems. PhD dissertation, Department of Nuclear Science and Engineering, Massachusetts Institute of Technology, 2006
162. E.B. Fel'dman, S. Lacelle, Chem. Phys. Lett. **253**(1–2), 27 (1996)
163. S. Doronin, E. Fel'dman, I. Maximov, J. Magn. Reson. **171**(1), 37 (2004)
164. D.F.V. James, P.G. Kwiat, W.J. Munro, A.G. White, Phys. Rev. A **64**(5), 052312 (2001)
165. T.J. Osborne, N. Linden, Phys. Rev. A **69**(5), 052315 (2004)
166. Y. Li, T. Shi, B. Chen, Z. Song, C.P. Sun, Phys. Rev. A **71**, 022301 (2005)
167. A. Wojcik, T. Luczak, P. Kurzynski, A. Grudka, T. Gdala, M. Bednarska, Phys. Rev. A **72**, 034303 (2005)
168. G. Gualdi, V. Kostak, I. Marzoli, P. Tombesi, Phys. Rev. A **78**(2), 022325 (2008)
169. A. Ajoy, P. Cappellaro (2012). ArXiv:1207.5580
170. B. Furman, in *HFI/NQI 2007*, ed. by A. Pasquevich, M. Rentería, E. Saitovitch, H. Petrilli (Springer/Berlin, Heidelberg, 2008), pp. 459–465
171. H.G. Krojanski, D. Suter, Phys. Rev. Lett. **93**(9), 090501 (2004)
172. T.W. Borneman, Control methods for spin-actuator multinode quantum information processing. Ph.D. thesis, Massachusetts Institute of Technology, 2012
173. J. Le Moigne, J.L. Gallani, P. Wautelet, M. Moroni, L. Oswald, C. Cruz, Y. Galerne, J.C. Arnault, R. Duran, M. Garrett, Langmuir **14**(26), 7484 (1998)
174. M. Mannini, L. Sorace, L. Gorini, F.M. Piras, A. Caneschi, A. Magnani, S. Menichetti, D. Gatteschi, Langmuir **23**(5), 2389 (2007)
175. M.V.G. Dutt, L. Childress, L. Jiang, E. Togan, J. Maze, F. Jelezko, A.S. Zibrov, P.R. Hemmer, M.D. Lukin, Science **316**, 1312 (2007)
176. P. Cappellaro, L. Jiang, J.S. Hodges, M.D. Lukin, Phys. Rev. Lett. **102**(21), 210502 (2009)
177. N. Yao, L. Jiang, A. Gorshkov, P. Maurer, G. Giedke, J. Cirac, M. Lukin, Nat. Commun. **3**, 800 (2012)
178. Y. Ping, B.W. Lovett, S.C. Benjamin, E.M. Gauger, Phys. Rev. Lett. **110**, 100503 (2013)
179. C.D. Weis, A. Schuh, A. Batra, A. Persaud, I.W. Rangelow, J. Bokor, C.C. Lo, S. Cabrini, E. Sideras-Haddad, G.D. Fuchs, R. Hanson, D.D. Awschalom, T. Schenkel, J. Vac. Sci. Technol. B **26**(6), 2596 (2008)
180. D.M. Toyli, C.D. Weis, G.D. Fuchs, T. Schenkel, D.D. Awschalom, Nano Lett. **10**(8), 3168 (2010)

181. B. Naydenov, V. Richter, J. Beck, M. Steiner, P. Neumann, G. Balasubramanian, J. Achard, F. Jelezko, J. Wrachtrup, R. Kalish, App. Phys. Lett. **96**(16), 163108 (2010)
182. P. Spinicelli, A. Drau, L. Rondin, F. Silva, J. Achard, S. Xavier, S. Bansropun, T. Debuisschert, S. Pezzagna, J. Meijer, V. Jacques, J.F. Roch, New J. Phys. **13**(2), 025014 (2011)
183. R. Hanson, F.M. Mendoza, R.J. Epstein, D.D. Awschalom, Phys. Rev. Lett. **97**(8), 087601 (2006)
184. P.C. Maurer, J.R. Maze, P.L. Stanwix, L. Jiang, A.V. Gorshkov, A.A. Zibrov, B. Harke, J.S. Hodges, A.S. Zibrov, A. Yacoby, D. Twitchen, S.W. Hell, R.L. Walsworth, M.D. Lukin, Nat. Phys. **6**, 912 (2010)
185. E. Rittweger, D. Wildanger, S.W. Hell, Europhys. Lett. **86**(1), 14001 (2009)
186. A. Wójcik, T. Łuczak, P. Kurzyński, A. Grudka, T. Gdala, M. Bednarska, Phys. Rev. A **75**, 022330 (2007)
187. L. Banchi, T.J.G. Apollaro, A. Cuccoli, R. Vaia, P. Verrucchi, New J. Phys. **13**(12), 123006 (2011)
188. P.C. Maurer, G. Kucsko, C. Latta, L. Jiang, N.Y. Yao, S.D. Bennett, F. Pastawski, D. Hunger, N. Chisholm, M. Markham, D.J. Twitchen, J.I. Cirac, M.D. Lukin, Science **336**(6086), 1283 (2012)
189. N. Bar-Gill, L.M. Pham, A. Jarmola, D. Budker, R.L. Walsworth (2012). ArXiv:1211.7094
190. J.M. Taylor, P. Cappellaro, L. Childress, L. Jiang, D. Budker, P.R. Hemmer, A. Yacoby, R. Walsworth, M.D. Lukin, Nat. Phys. **4**(10), 810 (2008)
191. P. Maletinsky, S. Hong, M.S. Grinolds, B. Hausmann, M.D. Lukin, R.L. Walsworth, M. Loncar, A. Yacoby, Nat. Nanotechnol. **7**(5), 320 (2012)
192. P. Rabl, S.J. Kolkowitz, F.H.L. Koppens, J.G.E. Harris, P. Zoller, M.D. Lukin, Nat. Phys. **6**(8), 602 (2010)
193. J. Cai, A. Retzker, F. Jelezko, M.B. Plenio, Nat. Phys. **9**(3), 168 (2013)

# Chapter 7
# State Transfer Hamiltonians in Photonic Lattices

**Matthieu Bellec, Georgios M. Nikolopoulos, and Stelios Tzortzakis**

**Abstract** Faithful communication is a necessary precondition for large scale all-optical networking and quantum information processing. Related theoretical investigations in different areas of physics have led to various proposals in which finite discrete lattices are used as channels for short-distance communication tasks. Here, in the framework of femtosecond-laser-written waveguide arrays, we present the first experimental realization of such a channel with judiciously engineered couplings. Various sources of imperfections and defects are identified, which are associated with the engineering procedure and affect the communication.

M. Bellec (✉)
Institute of Electronic Structure and Laser, Foundation for Research and Technology – Hellas, P.O. Box 1385, Heraklion GR-71110, Greece

Present address: Laboratoire Physique de la Matière Condensée, CNRS UMR 7336, Université Nice-Sophia Antipolis, 06100 Nice, France
e-mail: bellec@unice.fr

G.M. Nikolopoulos
Institute of Electronic Structure and Laser, Foundation for Research and Technology – Hellas, P.O. Box 1385, GR-71110 Heraklion, Greece
e-mail: nikolg@iesl.forth.gr

S. Tzortzakis
Institute of Electronic Structure and Laser, Foundation for Research and Technology – Hellas, P.O. Box 1385, GR-71110 Heraklion, Greece

Department of Materials Science and Technology, University of Crete, P.O. Box 2208, Heraklion GR-71003, Greece
e-mail: stzortz@iesl.forth.gr

G.M. Nikolopoulos and I. Jex (eds.), *Quantum State Transfer and Network Engineering*, Quantum Science and Technology, DOI 10.1007/978-3-642-39937-4_7,

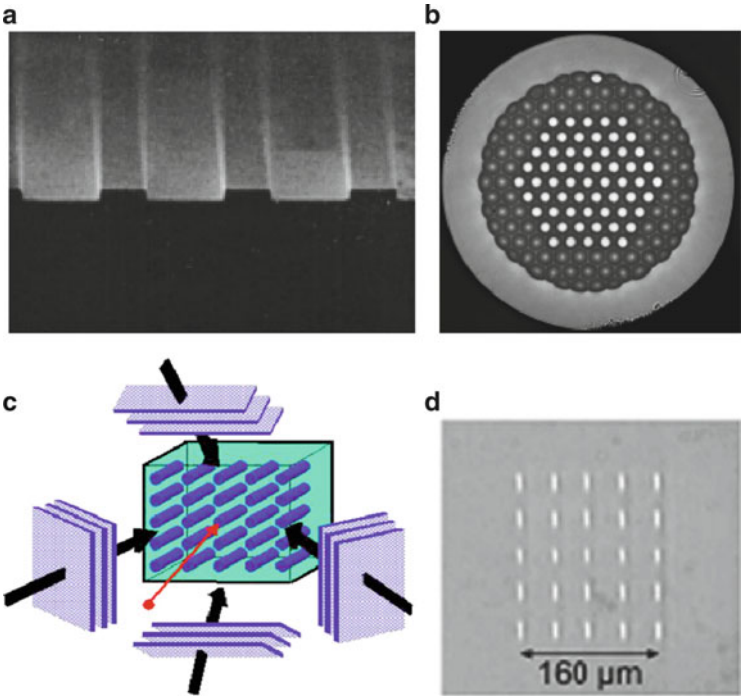


**Fig. 7.1** Typical photonic lattices. (**a**) A 1D arrangement in a AlGaAs array. (**b**) A 2D fiber array. (**c**) Optically induced structure in photorefractive crystal. (**d**) A 2D array in fused silica written by femtosecond laser. (**a,b,d**) Adapted by permission from The Optical Society of America [12, 13, 15]. (**c**) Adapted by permission from Macmillan Publishers Ltd: Nature [14], copyright (2003)

## 7.1 Introduction

Photonic lattices i.e., arrays of evanescently coupled waveguides, offer a remarkably simple and versatile tool for rigorous and transparent testing of various models associated mainly with tight-binding Hamiltonians [1–3]. Numerous phenomena encountered in various areas of physics, such as Bloch oscillations [4], Anderson localization [5–7], Glauber-Fock states displacement [8,9], have been demonstrated and studied experimentally in the context of linear photonic lattices. On the other hand, nonlinear lattices offer the prospect of creating and controlling optical discrete solitons [10] and filaments [11]. Various types of 1D and 2D waveguide arrays are depicted in Fig. 7.1. Throughout this chapter we focus on femtosecond-laser-written photonic lattices in fused silica. Besides their versatility, they offer scalability and compatibility with the widespread silica technologies. Hence, they are expected to play a pivotal role in the route towards all-optical networking [16] and large scale quantum information processing [17, 18].

The faithful transfer of signals is a necessary requirement for further developments in these directions, and has thus attracted considerable interest. Most of the proposed solutions, however, rely on boundary-free signal propagation, which implies that lattice truncation and edge effects will unavoidably lead to a considerable distortion of the transmission [19]. Intuitively speaking, even in the absence of disorder and dissipation, the initially well-localized wavepacket spreads as it propagates along the lattice, and splits into several smaller components that undergo reflections from the boundaries and give rise to interference phenomena.

One way to circumvent such diffraction problems is to prevent the uncontrollable spread of the wavepacket, by using discrete solitons as information carriers. This approach requires nonlinear photonic lattices and large intensities [1, 16]. Alternatively, in the context of linear discrete lattices one may resort to the segmentation of appropriate lattice sites [20–22], or to the engineering of judicious coupling constants between adjacent sites [19, 23, 24]. The latter scenario has been also studied thoroughly in the context of quantum networks [25,26], and various faithful-communication (state-transfer) Hamiltonians have been proposed, some of which are discussed in previous chapters. Many of these Hamiltonians have been obtained within the tight-binding approximation and various physical platforms have been proposed for their potential realization. As discussed in the chapter by Cappellaro, related experimental investigations so far have been focused on NMR systems with a few (up to four) sites (spins) and on schemes that do not require any coupling engineering [27–30].

Taking advantage of the versatility of photonic lattices, we have performed the first proof-of-principle experiment [31] on the state-transfer Hamiltonian proposed in [24, 32–35], for a sufficiently large number of sites so that coupling engineering is necessary (the realization of [27] was dealing with only three qubits and thus no engineering was required). In this chapter we review the underlying theory, and discuss our experimental observations in connection with the theoretical predictions, and the influence of disorder and losses.

## 7.2 Theory

In this section we review the coupled-mode theory which describes accurately arrays of evanescently coupled waveguides [36]. We derive the equations of motion describing the spatial evolution of a wave in such an array, and we compare them to the corresponding equations describing the time evolution of a single excitation in a one-dimensional lattice within the tight-binding and nearest-neighbour (NN) approximations.

### 7.2.1 Plane-Wave Propagation in an Array of Coupled Waveguides

The materials under consideration are non-magnetic and isotropic.[1] The permittivity $\varepsilon$ of such a material is a scalar that is modified spatially for the formation of the waveguide array. The propagation of a monochromatic plane wave along the $z$ direction, in such an inhomogeneous medium is governed by

$$\left[\nabla^2 + \frac{\omega^2}{c^2}\tilde{n}^2(x, y, z)\right]\mathbf{E}(x, y, z; t) = -\nabla\left[\frac{1}{\varepsilon}\mathbf{E}\cdot(\nabla\varepsilon)\right], \tag{7.1}$$

where $\mathbf{E}(x, y, z; t)$ is the electric field, $\omega$ is the frequency of the wave, $c$ is the speed of light in vacuum, and $\tilde{n}(x, y, z)$ is the refractive index of the material at the given frequency, which in general may depend on the spatial coordinates $(x, y, z)$.[2] The r.h.s of the wave equation depends on $\mathbf{E}\cdot(\nabla\varepsilon)$ and can be neglected if $\varepsilon$ varies only perpendicular to the polarization of the field, or if the fractional change of $\varepsilon$ within one wavelength is much smaller than 1. When at least one of these conditions is satisfied the wave equation reduces to

$$\left[\nabla^2 + \frac{\omega^2}{c^2}\tilde{n}^2(x, y, z)\right]\mathbf{E}(x, y, z; t) = 0. \tag{7.2}$$

The total power carried by the fields along the guide direction is obtained by integrating the $z$-component of the time-averaged Poynting vector over the cross-sectional area of the medium i.e.,

$$P = \int\int \langle\mathbf{S}\rangle dxdy, \tag{7.3}$$

where

$$\langle\mathbf{S}\rangle = \frac{1}{2}\mathrm{Re}\{\mathbf{E}\times\mathbf{H}^*\}\cdot\hat{\mathbf{z}} = \frac{1}{2}\mathrm{Re}\{\mathbf{E}_\perp\times\mathbf{H}_\perp^*\}\cdot\hat{\mathbf{z}}, \tag{7.4}$$

since only the transverse components of the field contribute, while $\mathbf{H}$ is the magnetic field.

[1] At present we ignore losses and consider a charge and current free configuration.

[2] As will be discussed later on, in the case of strong fields, the dependence of the refractive index (and of the permittivity) on the field strengths has to be taken into account.

### 7.2.2 Refractive Index Modifications

Consider an array of $N$ adjacent waveguides, which is fabricated by modifying the refractive index of a homogeneous, isotropic, non-magnetic slab along the $x$ and $y$ directions (see Fig. 7.2).[3] Let us denote by $n_j(x, y) = n_0 + \delta n_j(x, y)$ the linear refractive index distribution for the $j$th waveguide ($j = 1, \ldots, N$), with $n_0$ the unmodulated refractive index of the bulk. For the entire structure we have,

$$n(x, y) = n_0 + \sum_{j=1}^{N} \delta n_j(x, y), \tag{7.5}$$

where $\delta n_j \ll n_0$ is the localized perturbation at the position of the $j$th waveguide. So,

$$n^2(x, y) \approx n_0^2 + \sum_{j=1}^{N} \Delta n_j^2(x, y) \tag{7.6}$$

where $\Delta n_j^2(x, y) = 2n_0 \delta n_j$ and

$$\Delta n_j^2(x, y) := \begin{cases} n_j^2(x, y) - n_0^2, & \text{core } j, \\ 0, & \text{elsewhere.} \end{cases} \tag{7.7}$$

is the perturbation due to the presence of the $j$th waveguide. If one takes into account the nonlinearity, the refractive index of the array reads,

$$\tilde{n}^2(x, y) \approx n^2(x, y) + 2n_0 \kappa(x, y) |E(\mathbf{r}, t)|^2 \tag{7.8}$$

or

$$\tilde{n}^2(x, y) \approx n^2(x, y) + 2n_0 \bar{\kappa}(x, y) I(\mathbf{r}, t) \tag{7.9}$$

where $\kappa(x, y)$ (resp. $\bar{\kappa}(x, y)$) is the modified Kerr coefficient, $n^2(x, y)$ is given by Eq. (7.6), and we have dropped products of $\delta n_j$ and Kerr coefficients. The Kerr coefficient is proportional to third-order nonlinear susceptibility $\chi_3$, and is measured in $\mathrm{m}^2/\mathrm{V}^2$ (resp. $\mathrm{m}^2/\mathrm{W}$). For TE modes, in non-magnetic materials with small modifications of the refractive index, the conversion between $\kappa$ and $\bar{\kappa}$ is possible using the following expression:

$$\kappa[\mathrm{m}^2/\mathrm{V}^2] = \bar{\kappa}[\mathrm{m}^2/\mathrm{W}] \times n_0 \varepsilon_0 c/2. \tag{7.10}$$

[3] In general, however, one may modify the refractive index in all three directions (see e.g. [2, 37]).

The above formalism is valid for modifications of the refractive index along both $x$ and $y$ directions, although for the purposes of the present chapter, we assume modifications along the $x$ direction only.

### 7.2.3 Linear Coupled-Mode Theory

For the $j$th isolated (homogeneous and isotropic) waveguide, the corresponding propagating mode of interest is[4]

$$\mathscr{E}_j(x,y)\exp[i(\omega t-\beta_j z)], \tag{7.11}$$

where

$$\left[\nabla_\perp^2+\frac{\omega^2}{c^2}n_j^2(x,y)\right]\mathscr{E}_j(x,y)=\beta_j^2\mathscr{E}_j(x,y), \tag{7.12}$$

with $\beta_j$ denoting the corresponding propagation constant. We consider small modifications of the refractive index relative to the bulk, whereas the waveguides are not too close to each other. We can thus assume that the lowest (TE) modes of the waveguides are excited, and obey to the normalization condition

$$\alpha_j\int\int\mathscr{E}_j\cdot\mathscr{E}_j^*\,dxdy=1\quad\text{(Watts)}, \tag{7.13}$$

where

$$\alpha_j\equiv\frac{\beta_j}{2\omega\mu_0}=\frac{1}{2}n_j c\varepsilon_0\approx\frac{1}{2}cn_0\varepsilon_0. \tag{7.14}$$

The total electric field in the structure can be approximated by

$$\mathbf{E}(x,y,z;t)=\sum_{j=1}^{N}\psi_j(z)\mathscr{E}_j(x,y)\exp[i(\omega t-\beta_j z)], \tag{7.15}$$

and satisfies the wave-equation (7.2) with $\tilde{n}^2$ given by (7.6), whereas the mode amplitudes $\psi_j(z)$ are slowly varying with $z$. Assuming TE modes, in the limit of weak-confinement, we have for the power carried by the wave at distance $z$ from the input ($z=0$):

$$P(z)\approx\sum_{j=1}^{N}|\psi_j(z)|^2\left\{\alpha_j\int\int|\mathscr{E}_j(x,y)|^2dxdy\right\}, \tag{7.16}$$

[4]Throughout this chapter we consider monochromatic excitation of photonic lattices.

where we have assumed

$$\int\int \mathscr{E}_i(x,y)\mathscr{E}_j^*(x,y)dxdy \ll \int\int \mathscr{E}_j(x,y)\mathscr{E}_j^*(x,y)dxdy. \tag{7.17}$$

In view of the condition (7.13) we simply have

$$P(z) \approx \sum_{j=1}^{N} |\psi_j(z)|^2, \tag{7.18}$$

and thus all the information about the input peak power is obtained directly from the dimensionless amplitudes $\psi_k(z)$. When one of the waveguides (let us say the $k$th) is initially excited, the input power is given by

$$P_{\text{peak}} = |\psi_k(0)|^2. \tag{7.19}$$

Using Eqs. (7.15), (7.7) and (7.12) one obtains

$$\nabla^2\mathbf{E}(x,y,z;t) \approx -2i\sum_{j=1}^{N}\frac{d\psi_j}{dz}\beta_j\mathscr{E}_j(x,y)\exp[i(\omega t-\beta_j z)] - \frac{\omega^2}{c^2}n_0^2\mathbf{E}(x,y,z;t)$$
$$-\frac{\omega^2}{c^2}\sum_{j=1}^{N}\psi_j(z)\Delta n_j^2(x,y)\mathscr{E}_j(x,y)\exp[i(\omega t-\beta_j z)]. \tag{7.20}$$

where the Fresnel approximation has been employed.[5] Substituting Eq. (7.20) into Eq. (7.2), and using Eq. (7.6), one obtains

$$\frac{d\psi_k}{dz} \approx -i\frac{\omega^2\alpha_k}{2c^2\beta_k}\sum_{j=1}^{N}\psi_j(z)\exp[i(\beta_k-\beta_j)z]\int\int \mathscr{E}_k^*(x,y)\sum_{l\neq j}\Delta n_l^2(x,y)\mathscr{E}_j(x,y)dxdy, \tag{7.21}$$

where we have multiplied both sides by $\mathscr{E}_k^*(x,y)$, we have integrated over the entire $xy$ plane, while Eqs. (7.13) and (7.17) have been employed. This is the equation of motion for $\psi_k$ describing the dielectric perturbations to the $k$th waveguide as a result of the presence of the others, as well as the coupling of the $k$th waveguide to all the other waveguides. To proceed further we assume that the mode distributions, and the refractive index perturbations are highly peaked around the center of

[5] Variations of the mode amplitudes with $z$ are sufficiently small to allow for the omission of second-order derivatives with respect to $z$.

the waveguides.[6] In this case, we can keep only integrals that involve nearest neighbours, which are of the form:

$$\Omega_k \approx \frac{\omega\varepsilon_0}{4}\int\int \mathscr{E}_k^*(x,y)\Delta n_{k\pm1}^2(x,y)\mathscr{E}_k(x,y)dxdy, \tag{7.22}$$

$$\mathscr{J}_{k,k\pm1} \approx \frac{\omega\varepsilon_0}{4}\int\int \mathscr{E}_k^*(x,y)\Delta n_k^2(x,y)\mathscr{E}_{k\pm1}(x,y)dxdy. \tag{7.23}$$

The correction to the propagation constant is denoted by $\Omega_k$, while the coupling between the $k$th waveguide and its neighbours is denoted by $\mathscr{J}_{k,k\pm1}$. Hence, we have the following set of coupled differential equations for the amplitudes:

$$i\frac{d\psi_k}{dz} \approx \Omega_k\psi_k + \mathscr{J}_{k,k-1}\psi_{k-1}\exp[i(\beta_k-\beta_{k-1})z] + \mathscr{J}_{k,k+1}\psi_{k+1}\exp[i(\beta_k-\beta_{k+1})z]. \tag{7.24}$$

Setting $\psi_k(z) = \varphi_k(z)e^{-i\Omega_k z}$, we have

$$i\frac{d\varphi_k}{dz} \approx \mathscr{J}_{k,k-1}\varphi_{k-1}\exp[i(\beta'_k-\beta'_{k-1})z] + \mathscr{J}_{k,k+1}\varphi_{k+1}\exp[i(\beta'_k-\beta'_{k+1})z], \tag{7.25}$$

where $\beta'_k = \beta_k + \Omega_k$ is the modified wavenumber. For nearly identical waveguides, these equations are simplified to

$$i\frac{d\varphi_k}{dz} = \mathscr{J}_{k,k-1}\varphi_{k-1} + \mathscr{J}_{k,k+1}\varphi_{k+1}. \tag{7.26}$$

### 7.2.4 Nonlinear Coupled-Mode Theory

In the case of strong fields the dependence of the refractive index on the intensity has to be taken into account. Light propagation in the structure is governed by wave equation (7.2) with $\tilde{n}^2(x,y)$ given by Eq. (7.8). Assuming that the transverse profile of the field is the same as in the linear case (first-order perturbation theory), it satisfies Eq. (7.12) for $\beta_j \to \tilde{\beta}_j(\omega)$. Thus, following the same steps as before one obtains

[6] Formally speaking, for the $j$th waveguide this means that the typical sizes of $E_j(x,y)$ and $\Delta n_j^2(x,y)$, are much smaller than the separation of the $j$th waveguide from its neighbours.

$$i\frac{d\psi_k}{dz} = \Omega_k\psi_k + \mathscr{J}_{k,k-1}\psi_{k-1}\exp[i(\beta_k-\beta_{k-1})z] + \mathscr{J}_{k,k+1}\psi_{k+1}\exp[i(\beta_k-\beta_{k+1})z] + \frac{1}{2\beta_k}(\tilde{\beta}_k^2-\beta_k^2)\psi_k + \sum_{j,l,l'}\psi_l\psi_{l'}^*\psi_j\mathscr{K}_{k,j,l,l'}\exp[i(\beta_k+\beta_{l'}-\beta_j-\beta_l)z], \tag{7.27}$$

where

$$\mathscr{K}_{k,j,l,l'} = \frac{\omega^2 n_0}{c^2\beta_k}\frac{\int\int \mathscr{E}_{l'}^*(x,y)\mathscr{E}_k^*(x,y)\kappa(x,y)\mathscr{E}_j(x,y)\mathscr{E}_l(x,y)dxdy}{\int\int|\mathscr{E}_k|^2dxdy}. \tag{7.28}$$

Note here that the l.h.s. has units $m^{-1}$, and in order to be consistent with the r.h.s., the ratio of the integrals has to be dimensionless. This is indeed the case if $\kappa$ is in units of $m^2/V^2$. The last term in the equation of motion for $\psi_k$ can be simplified further if we drop terms that involve overlaps between nearest neighbours and beyond i.e., if we set

$$\mathscr{K}_{k,j,l,l'} \approx \frac{\omega^2 n_0\kappa_{\text{eff}}}{c^2\beta_k}\eta\delta_{l,l'}\delta_{k,j}\delta_{k,l} \tag{7.29}$$

where $\kappa(x,y)\approx\kappa_{\text{eff}}$ and

$$\eta = \frac{\int\int|\mathscr{E}_k(x,y)|^4dxdy}{\int\int|\mathscr{E}_k|^2dxdy}. \tag{7.30}$$

Using Eq. (7.13), we have

$$\eta = \frac{1[W]}{\alpha_k A_{\text{eff}}}, \tag{7.31}$$

where

$$A_{\text{eff}} = \frac{\left[\int\int|\mathscr{E}_k|^2dxdy\right]^2}{\int\int|\mathscr{E}_k(x,y)|^4dxdy} \tag{7.32}$$

is the effective core area. For TE modes and non-magnetic materials, $\alpha_k = \beta_k/(2\omega\mu_0) = n_k c\varepsilon_0/2[W/V^2]$ and thus

$$\frac{d\psi_k}{dz} \approx -i\,\Omega_k\psi_k - i\,\mathscr{J}_{k,k-1}\psi_{k-1}\exp[i(\beta_k-\beta_{k-1})z] - i\,\mathscr{J}_{k,k+1}\psi_{k+1}\exp[i(\beta_k-\beta_{k+1})z] - i\frac{1}{2\beta_k}(\tilde{\beta}_k^2-\beta_k^2)\psi_k - i\frac{2\pi\bar{\kappa}_{\text{eff}}[1W]}{\lambda A_{\text{eff}}}|\psi_k|^2\psi_k, \tag{7.33}$$

where $\lambda$ is the wavelength in vacuum. We have assumed $n_k \approx n_0$ and we have replaced $\kappa_{\text{eff}}$ by $\bar{\kappa}_{\text{eff}}$ according to Eq. (7.10). In the weakly-guiding approximation

$\tilde{\beta} \approx \beta$. Setting $\psi_k = \sqrt{P_{\text{peak}}}\psi_k$, where $P_{\text{peak}}$ is the input peak power, we can work with the normalized amplitudes

$$\frac{d\psi_k}{dz} \approx -i(\Omega_k + \gamma P_{\text{peak}}|\psi_k|^2)\psi_k - i\mathscr{J}_{k,k-1}\psi_{k-1}\exp[i(\beta_k - \beta_{k-1})z] \\ -i\mathscr{J}_{k,k+1}\psi_{k+1}\exp[i(\beta_k - \beta_{k+1})z], \tag{7.34}$$

where

$$\gamma = \frac{2\pi\bar{\kappa}_{\text{eff}}}{\lambda A_{\text{eff}}}. \tag{7.35}$$

Thus, we find that the propagation constant of the excited waveguide is shifted by $\gamma P_{\text{peak}}|\psi_k|^2$. For large input powers, this nonlinear shift is sufficiently large to prevent the communication of the initially excited waveguide with its neighbours. An estimate of the critical value of the input intensities can be obtained by looking at the band structure of the array (the nonlinear shift essentially moves the propagation constant into the gap above the first band). Roughly speaking, the ratio

$$\Lambda = \frac{\gamma}{\max\{\mathscr{J}_{\text{in}}\}}P_{\text{peak}} \tag{7.36}$$

is expected to play a pivotal role, where the maximum is estimated over all the couplings of the initially excited waveguide to its neighbours.

Setting $\psi_k(z) = \varphi_k(z)e^{-i\Omega_k z}$, we have

$$i\frac{d\varphi_k}{dz} \approx \gamma P_{\text{peak}}|\varphi_k|^2\varphi_k + \mathscr{J}_{k,k-1}\varphi_{k-1}\exp[i(\beta'_k - \beta'_{k-1})z] \\ + \mathscr{J}_{k,k+1}\varphi_{k+1}\exp[i(\beta'_k - \beta'_{k+1})z]. \tag{7.37}$$

where $\beta'_k = \beta_k + \Omega_k$ is the modified wavenumber. For nearly identical waveguides, these equations are simplified to

$$i\frac{d\varphi_k}{dz} \approx \gamma P_{\text{peak}}|\varphi_k|^2\varphi_k + \mathscr{J}_{k,k-1}\varphi_{k-1} + \mathscr{J}_{k,k+1}\varphi_{k+1}. \tag{7.38}$$

The dynamics of various physical systems in different contexts are described accurately by tight-binding Hamiltonians with NN couplings. The linear and nonlinear equations of motion that we have derived in the section (i.e., Eqs. (7.25) and (7.37)) are isomorphic to the equations of motion describing the evolution of excitations within the tight-binding and NN approximations. By employing this analogy, various tight-binding Hamiltonians have been simulated in the framework of photonic lattices [1–3]. In the following we focus on the simulation of a state-transfer Hamiltonian with NN couplings, but before this we discuss briefly the fabrication of photonic lattices in fused silica.

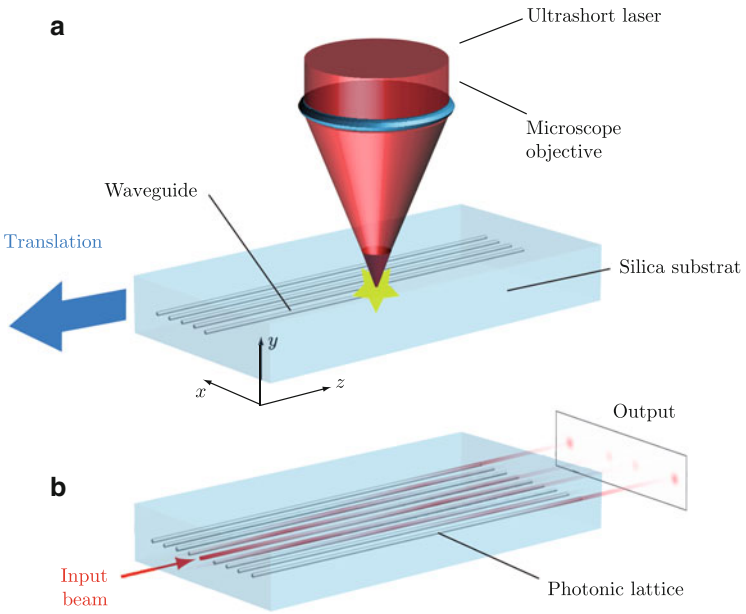


**Fig. 7.2** Fabrication of photonic lattices by means of a direct laser writing technique. (**a**) An ultrashort pulse is focused in a piece of glass, and the refractive index is locally modified. A single waveguide is written by translating the sample. (**b**) Light propagation in a 1D periodic lattice. The central waveguide is excited and the light experiences a discrete diffraction as it propagates in the lattice

## 7.3 Fabrication of Photonic Lattices in Fused Silica

The fabrication of photonic lattices in a transparent dielectric material (e.g. fused silica) can be achieved by means of a direct laser writing technique. When an ultrashort laser pulse is tightly focused in the material, a nonlinear absorption occurs leading to a microscopic permanent change of the optical properties of the material. For fused silica, used in our setup, the density increases locally, resulting in an increase of the refractive index by $\Delta n \sim 10^{-3}$ within a range of few $\mu$m [37]. By translating the sample, as sketched in Fig. 7.2a, a waveguide can be written [38]. In general, arbitrary waveguide paths can be written in this way allowing thus for the fabrication of photonic lattices with various configurations [2].

In our setup, the writing laser source pertained to 35 fs pulses at 800 nm with repetition rate 1 kHz. The beam was focused with a NA = 0.45 microscope objective 400 $\mu$m below the surface. Under these conditions, the laser energy was reduced to about 270 nJ using neutral density filters. The accuracy of the translation stage was 0.5 $\mu$m, and the sample was moved at $v = 0.05$ mm/s. The resulting waveguides had an elliptical cross section ($4 \times 16\,\mu\text{m}^2$) and the associated refractive index modification was estimated to about $5 \times 10^{-4}$ so that at $\lambda = 633$ nm a single mode

(the lowest TE mode) is excited. As illustrated in Fig. 7.2b, the input beam was launched in the lattice (here, the central waveguide) using a NA = 0.25 microscope objective, and its propagation in the lattice was monitored using a fluorescence microscopy technique [2]. This is a standard technique, which relies on local color centers that are created in fused silica during the writing process, and fluoresce at 650 nm when excited with light at 633 nm. Thus, one can visualize the evolution of the light distribution in a photonic lattice, by imaging the $xz$ plan on a CCD camera with a NA = 0.11 objective.

## 7.4 Simulation of a State-Transfer Hamiltonian in Photonic Lattices

The dynamics of a single excitation in a one-dimensional lattice with $N$ identical sites, within the tight-binding and NN approximations, is governed by a Hamiltonian of the form ($\hbar = 1$)

$$\hat{\mathscr{H}}_Q = \sum_{k=1}^{N-1} \mathscr{J}_{k,k+1}(\hat{a}_k^\dagger \hat{a}_{k+1} + \hat{a}_{k+1}^\dagger \hat{a}_k), \tag{7.39}$$

where $\hat{a}_k^\dagger$ is the creation operator for an excitation on the $k$th site. All of the $N$ sites are assumed to be on-resonant, and $\mathscr{J}_{k,l}$ is the coupling between the sites with indices $k$ and $l$. In the Schrödinger picture, the evolution of the excitation is described in terms of the amplitudes $A_k$, where $P_k = |A_k(t)|^2$ is the probability for the excitation to occupy the $k$th site at time $t$. The evolution of the amplitudes $A_k$ is governed by ($\hbar = 1$)

$$i\frac{\mathrm{d}A_k(t)}{\mathrm{d}t} = \mathscr{J}_{k-1,k}A_{k-1} + \mathscr{J}_{k,k+1}A_{k+1}. \tag{7.40}$$

In the framework of quantum communication, the excitation pertains to an information carrier prepared in a quantum state. In general, faithful transfer of the excitation does not imply faithful transfer of the state, but it is a necessary condition for the latter. However, as discussed in the previous chapters, as well as in the present introduction, the faithful transfer of the excitation between e.g., the two ends of a chain even in the absence of disorder and dissipation is a rather difficult task. The problem has attracted considerable interest in the community of quantum information processing over the last decade, and pertains to the quest of state-transfer Hamiltonians that achieve this task at a well-defined time [25, 26].

As discussed in the chapter by Nikolopoulos et al., when the couplings in the Hamiltonian (7.39) are chosen according to [24, 32–35]

$$\mathscr{J}_{k,k+1} = \mathscr{J}_0\sqrt{(N-k)k}, \tag{7.41}$$

the lattice operates as a perfect quantum channel, i.e., one can achieve ideally perfect transfer of the excitation from the $k$th to the $(N-k+1)$th site of the lattice at time $\tau = \pi/(2\mathscr{J}_0)$. For this particular coupling distribution, Hamiltonian (7.39) is isomorphic to the Hamiltonian that pertains to the rotation of a spin-$J$, system with $J = (N-1)/2$, around the $x$-axis i.e., $\hat{\mathscr{H}}_S = 2\mathscr{J}_0\hat{J}_x$, where $\hat{J}_x$ is the $x$-component of the spin vector [39–41].

The equivalence between Eqs. (7.40) and (7.26) is obvious. The energies of the sites correspond to the wavenumbers, the couplings between different sites are represented by the evanescent overlap between the transverse components of the field modes in adjacent waveguides, whereas the evolution of the wavepacket, in the case of photonic lattices, takes place in space instead of time. This, is a major advantage of photonic lattices since it allows for a direct observation of the light propagation. According to the previous discussion, in a lattice of $N$ waveguides of fixed length $L$, faithful (ideally perfect) power transfer from the $k$th to the $(N-k+1)$th waveguide can be achieved if the coupling distribution is chosen according to (7.41), with

$$\mathscr{J}_0 = \pi/(2L). \tag{7.42}$$

Moreover, the light propagation along the structure should be reminiscent of the rotation of a spin-$J$ system around a fixed axis.

In the weak-coupling regime, the coupling between any two adjacent waveguides is expected to depend exponentially on their separation i.e., we expect

$$\mathscr{J}^{\exp}_{k,k+1} = \mu \exp\left(-\xi d_{k,k+1}\right), \tag{7.43}$$

where $\mu, \xi$ are open parameters to be determined by fitting to related experimental data for a particular setup. To this end in our setup we wrote a number of couplers at different separations. Each coupler consisted of two identical waveguides of the same length $z = L$, separated by a constant distance $d$ (see Fig. 7.3a). When light is initially injected in one of the waveguides of the coupler, its evolution is governed by Eq. (7.26) for two amplitudes $\varphi_1$ and $\varphi_2$ corresponding to the two waveguides. Solving this set of equations one obtains for the coupling constant $\mathscr{J}$ between the waveguides:

$$\mathscr{J} = \frac{1}{L}\arctan\sqrt{\frac{I_2}{I_1}}, \tag{7.44}$$

when the waveguide 1 is initially excited (i.e. $\varphi_1(0) = 1$ and $\varphi_2(0) = 0$), where $I_1 = |\varphi_1(L)|^2$ and $I_2 = |\varphi_2(L)|^2$ are the output intensities (see Fig. 7.3a). We see therefore that for a given coupler of fixed length $L$ and separation $d$, the coupling between the waveguides can be determined by the ratio of the output intensities. For fixed $L$, this ratio depends only on the separation of the waveguides. Thus, by writing different couplers of the same length $L = 1$ cm with different separations,

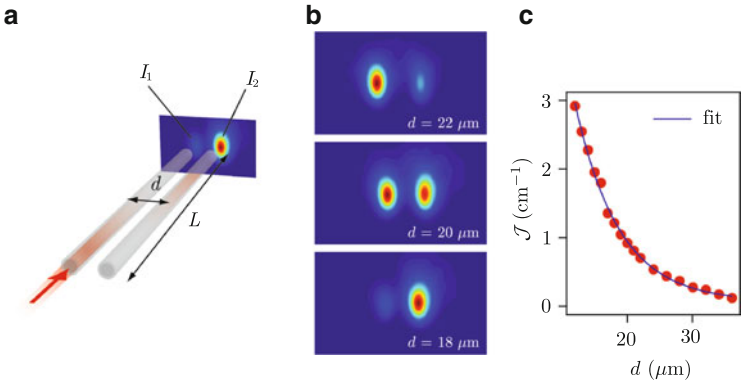


**Fig. 7.3** Coupling strength $\mathcal{J}$ versus the waveguide separation $d$. (**a**) Sketch of the coupler typically used in the estimation of the dependence of the coupling on the separation. The coupling at a given $d$ is determined by the ratio of the output intensities $I_2/I_1$ (see text). (**b**) Output images for various separations $d = 18, 20$ and $22\,\mu$m. (**c**) The coupling $\mathcal{J}$ for various separations $d$, and the corresponding exponential fit (see text for details)

one can measure the output intensities at different separations (few output images are depicted in Fig. 7.3b). The corresponding values of the coupling strength $\mathcal{J}$ are then readily obtained by Eq. (7.44). As shown in Fig. 7.3c, in our setup the experimental points $\mathcal{J}(d)$ were well approximated by the exponential law (7.43) with $\mu = 19.5\,\text{cm}^{-1}$ and $\xi = 0.152\,\mu\text{m}^{-1}$.

Let us assume now that we are interested in the realization of a particular NN coupling configuration $\{\mathcal{J}_{k,k+1}\}$ in the framework of photonic lattices. Having obtained the exponential law that governs the coupling of adjacent waveguides, one can readily show that the desired coupling distribution $\{\mathcal{J}_{k,k+1}\}$ is obtained in practise if the distance between successive waveguides follows the rule:

$$d_{k,k+1} = -\ln\left(\frac{\mathcal{J}_{k,k+1}}{\mu}\right)\xi^{-1}. \tag{7.45}$$

For the coupling configuration given by Eqs. (7.41) and (7.42) we obtain

$$d_{k,k+1} = \left[\ln(\mu/\mathcal{J}_0) - \ln(\sqrt{k(N-k)})\right]\xi^{-1}. \tag{7.46}$$

This relation gives the separations required for the realization of the coupling distribution (7.41) in a photonic lattice of fixed $N$ and $L$. In our setup, we had $N = 9$ waveguides of length $L = 10\,\text{cm}$, and the corresponding theoretical values of $\mathcal{J}_{k,k+1}$ and $d_{k,k+1}$ are shown in Fig. 7.4a and the Table 7.1. The photonic lattice was subsequently inscribed in fused silica using the femtosecond laser writing technique described in a previous section (see Fig. 7.4b).

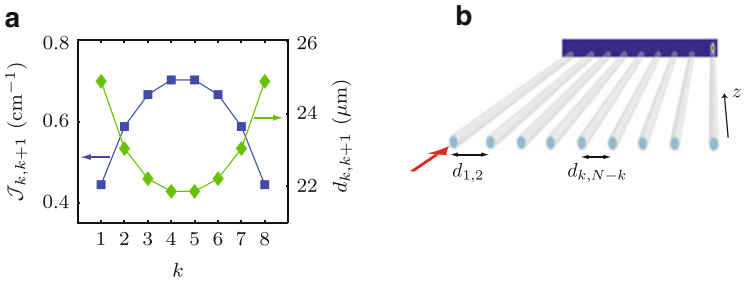


**Fig. 7.4** (**a**) Theoretical values of the couplings and the corresponding separations according to Eqs. (7.41), (7.42) and (7.46) for $N = 9$ and $L = 10\,\text{cm}$. (**b**) Schematic view of the photonic lattice with judiciously engineered couplings (i.e. distances)

**Table 7.1** Theoretical values of the couplings and the separations according to Eqs. (7.41), (7.42) and (7.46) for $N = 9$ and $L = 10\,\text{cm}$. Only data for the first four waveguides are shown since the configuration is symmetric with respect to $k = 5$

| $k$ | $\mathcal{J}_{k,k+1}$[a] [$\text{cm}^{-1}$] | $d_{k,k+1}$[a] [$\mu\text{m}$] |
|---|---|---|
| 1 | 0.4443 | 24.8796 |
| 2 | 0.5877 | 23.0387 |
| 3 | 0.6664 | 22.2120 |
| 4 | 0.7025 | 21.8655 |

[a] Numerical values with four-digit precision

## 7.5 Results and Discussion

In this section we discuss our main theoretical and experimental results pertaining to the realization of Hamiltonian (7.39) with couplings given by Eqs. (7.41) and (7.42), in a photonic lattice with $N = 9$ and $L = 10\,\text{cm}$.

Figure 7.5a, b present numerical results on the light propagation in the structure when one of the two outermost waveguides and the central waveguide respectively, are initially excited. The corresponding experimental observations are depicted in Fig. 7.5c, d, where we have normalized with respect to propagation losses in a single waveguide. Such losses are inherent in laser-written waveguides and are not related to the lattice or the associated coupling distribution. In our case they have been estimated to be in the order of 0.4 dB/cm, which is in agreement with reported values in the literature [2]. This means that 60 % of the input signal is lost after propagating along a 10 cm waveguide.

As depicted in Fig. 7.5, there is a rather good qualitative agreement with the theoretical predictions. Nevertheless, despite the fact that propagation losses along a waveguide have been taken into account, the power transfer from the $k$th to the mirror-symmetric waveguide is not complete, as opposed to the theoretical predictions. As shown in Fig. 7.6, in the case of Fig. 7.5c, about 39 % of the input intensity is transferred to the ninth waveguide, whereas in the case of Fig. 7.5d, this

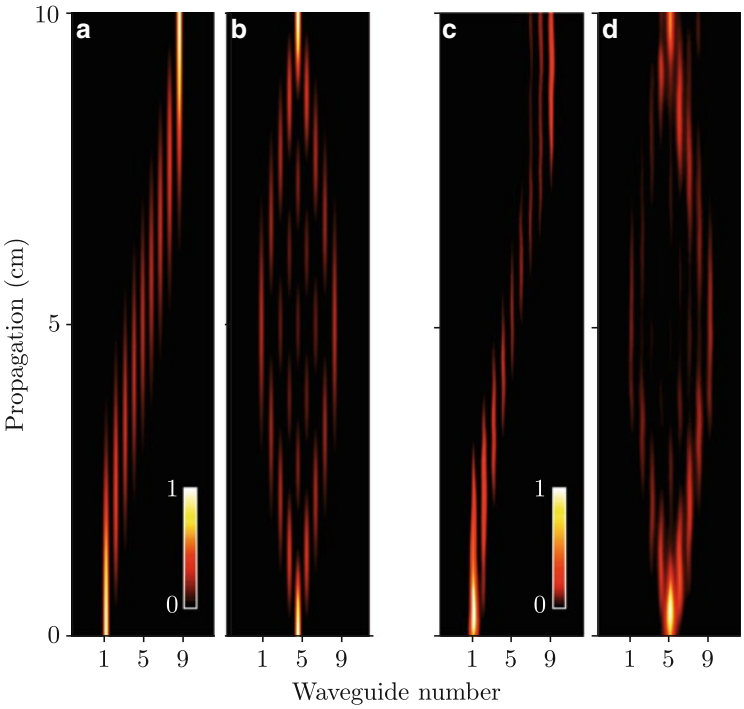


**Fig. 7.5** Light propagation in an array of $N = 9$ waveguides with coupling distribution shown in Fig. 7.4a. (**a,b**) Numerical results obtained by propagation of Eqs. (7.26) when the 1st and the 5th waveguide is initially excited, respectively. (**c,d**) Corresponding fluorescence images obtained in our experiment. Adapted from [31]

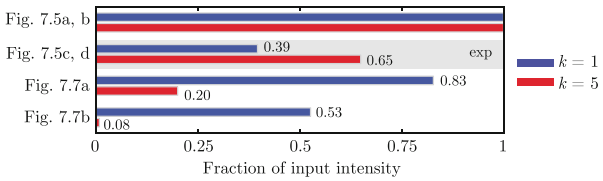


**Fig. 7.6** Fraction of the input intensity transferred from the $k$th to the $(N - k + 1)$th waveguide

percentage increases to about 65 %. In fact, a small fraction of the input power seems to have been transferred to waveguides adjacent to the $(N - k + 1)$th waveguide. This is an indication that the diffraction of the signal has been restricted but it has not been minimized. Such deviations can be attributed to experimental artefacts such as impurities and disorder induced in the lattice during the writing procedure.

The implemented photonic lattice gave us good qualitative agreement with the theoretical predictions, but it was not sufficiently pure to provide quantitative agreement. The observed deviations between the theory and the experimental results can be attributed mainly to two experimental parameters:

(i) One of our aims in the experiment was to follow the dynamics of the light in the lattice by means of a fluorescence microscopy technique. To this end, however, one needs sufficiently high intensity of the writing laser, since the fluorescence is associated with the formation of laser-induced color-centers. In our setup, the optimal input energy required for waveguides of good quality and with intense enough fluorescence signal was 270 nJ; a value that is quite close to the threshold intensity for damaging the sample (i.e, 300 nJ). As a result, and in view of the low repetition rate in our setup ($\sim$ 1 kHz), some of the waveguides in our lattice were inevitably damaged locally, due to small variations in the intensity during the writing process.[7] This means that most probably the waveguides were by no means identical, and thus the lattice was not mirror symmetric either. The use of a more appropriate laser sources with higher repetition rate[8] are expected to reduce considerably the writing time, facilitating thus the stability of the laser system and the induction of identical refractive index modulations.

(ii) The theoretical predictions for perfect transfer rely on a well-defined coupling distribution (i.e., Eqs. (7.41) and (7.42)), which can be achieved in practise only within a certain accuracy. In our setup, the translation stage of the writing procedure, did not allow us to implement the desired waveguide separations with accuracy better than 0.5 μm. Hence, the implemented coupling distribution also deviated from the theoretical values of Table 7.1. According to our simulations, however, such deviations may reduce the power transfer by at most 5 %; an estimate that can be reduced further by increasing the precision of the translation stage during the writing process.[9]

All of these imperfection mechanisms, together with the propagation losses mentioned above, are expected to be present in any realization of photonic lattices in fused silica, irrespective of the coupling distribution; albeit the details may vary from setup to setup. The propagation losses (estimated to be about 60 % of the input power after 10 cm of propagation) cannot be avoided, although there are techniques for their suppression [42]. Hence, the same amount of propagation losses are to be expected in a particular setup, irrespective of the implemented coupling distribution. On the contrary, diffraction losses do depend on the realized coupling configuration. As depicted in Fig. 7.6, the diffraction losses in the implemented configuration were about 61 and 35 % for Fig. 7.5c, d respectively. These losses would be significantly higher in the case of distributions that are not judiciously designed, such as the uniform one with $\mathscr{J}_{k,k+1} = \mathscr{J}_0$ or the harmonic distribution $\mathscr{J}_{k,k+1} = \mathscr{J}_0\sqrt{k}$ [8, 9]. Indeed, as depicted in Fig. 7.7, in these configurations

[7] The engineering of a lattice with $N = 9$ waveguides took us 8–9 h and the stability of the laser source was not guaranteed during this period.

[8] Standard amplifiers delivering few 100 kHz are usually employed and high-energy oscillators with a repetition rate up to few MHz become now available.

[9] Translation stages for laser micromachining applications with accuracy less than 0.1 μm are also available.

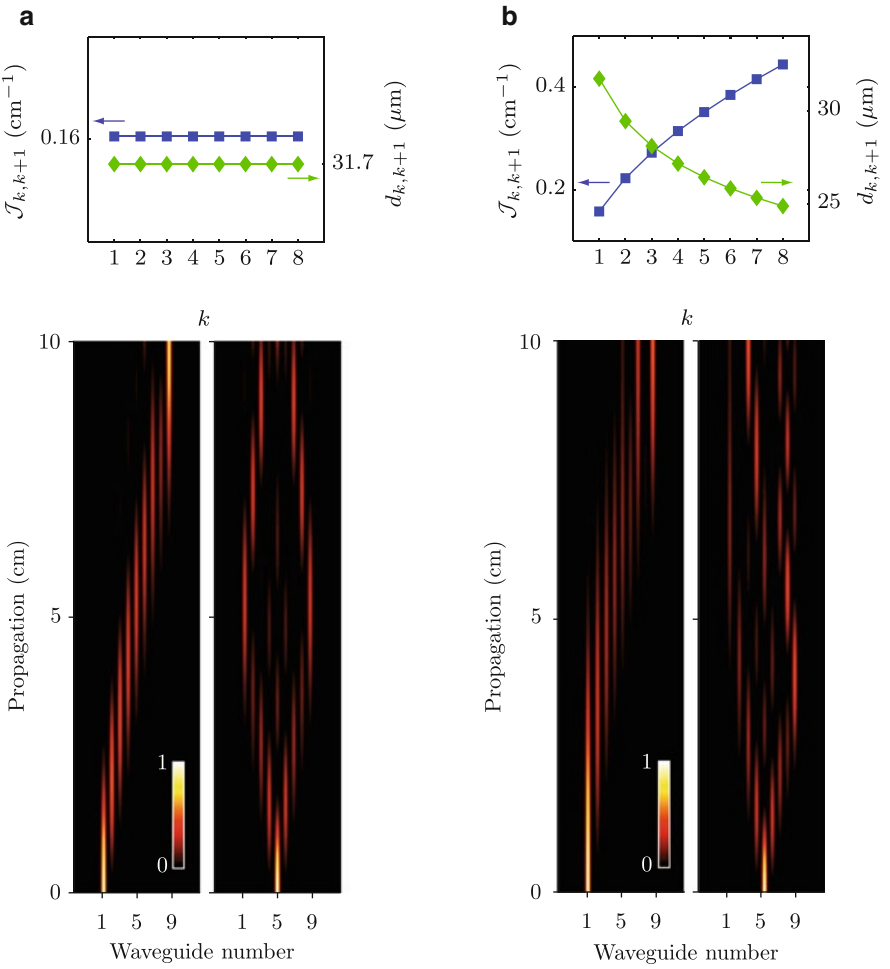


**Fig. 7.7** Numerical results on the light propagation in an array of $N = 9$ waveguides when the 1st and the 5th waveguide are initially excited, for two different coupling configurations: (**a**) $\mathcal{J}_{k,k+1} = 0.56\,\mathrm{cm}^{-1}$; (**b**) $\mathcal{J}_{k,k+1} = \mathcal{J}_0\sqrt{k}$ with $\mathcal{J}_0 \approx 0.3\,\mathrm{cm}^{-1}$. *Lower panels* have been adapted from [31]

the transfer from the 1st to the 9th waveguide does not ideally exceed 83 % of the input power, which are in contrast to the ideally perfect transfer expected in the case of distribution (7.41). Note that this percentage drops with increasing $N$, as opposed to the ideally perfect transfer. Moreover, as depicted in Fig. 7.7a, b, none of these schemes allows for self-imaging when the central waveguide is initially excited. This is a distinct feature of distribution (7.41) that has been also verified experimentally (see Fig. 7.5b, d).

We have seen that the dependence of the couplings on the separation of the waveguides follows an exponential law, with the two parameters determined by the particular experimental setup under consideration. This law imposes limitations on the size of photonic lattices that can be implemented for a given coupling configuration. For instance, the implementation of Hamiltonians with nearest-neighbours couplings requires sufficiently large separations between successive waveguides. In the case of the coupling distribution (7.41), the worst case scenario pertains to the central waveguides (with indices $q = \lceil (N+1)/2 \rceil$ and $q \pm 1$) where the distribution $\{d_{k,k+1}\}$ exhibits a minimum (see Eq. (7.46)). In particular, for $N \gg 1$, these waveguides are practically equally spaced i.e., $d_{q-1,q} \approx d_{q,q+1} = d_{\min}$ where

$$d_{\min} = \left[\ln(\mu/\mathscr{J}_0) - \ln(N/2)\right]\xi^{-1}. \tag{7.47}$$

Hence, in view of the exponential law (7.43), the NN approximation is justified if $e^{-\xi d_{\min}} = \epsilon$ for some finite $\epsilon \ll 1$, which implies that

$$N \leq \frac{2\mu\epsilon}{\mathscr{J}_0}, \tag{7.48}$$

where $\mathscr{J}_0$ is given by Eq. (7.42). For a given sample (i.e. fixed $L$ and $\mu$), this condition limits the number of waveguides for which the particular coupling distribution is implementable and at the same time, couplings beyond nearest neighbours can be neglected. The parameter $\epsilon$ basically quantifies the deviations from the NN Hamiltonian; the larger $\epsilon$ is, the larger deviations we expect. For the photonic lattice we implemented, $d_{\min} = d_{4,5} = (21.9 \pm 0.5)\,\mu\text{m}$ and thus $\epsilon \lesssim 0.038$; the NN couplings were almost two orders of magnitude larger than the couplings beyond nearest neighbours. Moreover, Eq. (7.48) reads $N \leq 248\epsilon$, which for $\epsilon = 0.1$ implies that the NN approximation will start breaking down for $N > 25$. This means that for a fixed $\mu$, the design of larger networks requires longer samples (i.e., larger $L$). Analogous limits are expected for the implementation of any NN-coupling configuration $\{\mathscr{J}_{k,k+1}(L,N)\}$. More precisely, when the spatial dependence of the coupling is expressed in the form of Eq. (7.43), we obtain

$$\max_k \{\mathscr{J}_{k,k+1}(L,N)\} \leq \epsilon\mu, \tag{7.49}$$

which is a sufficient condition for the neglect of interactions beyond nearest neighbours, and limits the number of waveguides that can be written in a sample of length $L$ and fixed $\mu$. The sample length, however, cannot be increased arbitrarily since, as discussed previously, propagation losses increase exponentially with $L$. Hence, for large-scale all-optical networking, one has to find the figure of merit between scalability and losses. It is also worth mentioning here that in general, the presence of couplings beyond NNs does not precludes the existence of faithful-state-transfer Hamiltonians [43, 44].

## 7.6 A Power-Sensitive Optical Switch

The previous results pertain to weak input powers and the linear regime of operation. As discussed in Sect. 7.2, in the optical domain, the nonlinear propagation regime arises as the input power is increased. The refractive index of the material depends on the input intensity according to the relations of Sect. 7.2.2. The spatio-temporal properties of the light are modified as it propagates, giving rise to novel phenomena such as optical discrete solitons [10] or lattice filaments [11]. Here, we focus on the effects of the Kerr nonlinearities on the transfer of signals.[10] Nonlinear light propagation in a photonic lattice with identical waveguides and NN couplings is governed by Eq. (7.38), with $\gamma$ given by Eq. (7.35) and $P_{\text{peak}}$ denoting the input peak power. The effective area $A_{\text{eff}}$ of the guided mode in the individual waveguides can be approximated by $\pi r^2$, where $r$ is the $1/e^2$-width of the mode. The effective Kerr coefficient $\kappa_{\text{eff}}$ is typically smaller than the bulk value $\kappa_0$. Note that, both $r$ and $\kappa$ depend on the writing velocities [2]; higher writing velocity implies smaller refractive index modification and thus weaker guiding (i.e., larger $r$). According to our writing conditions, for fused silica at $\lambda = 800\,\text{nm}$, one has $r \approx 10\,\mu\text{m}$ and $\bar{\kappa}_{\text{eff}} = 0.35\bar{\kappa}_0$ with $\bar{\kappa}_0 = 2.7 \times 10^{-20}\,\text{m}^2\,\text{W}^{-1}$.

We have investigated theoretically the performance of a photonic lattice with a coupling configuration given by Eqs. (7.41) and (7.42), with respect to the input peak power $P_{\text{peak}}$. In Fig. 7.8 we plot the distribution of the normalized intensity at the output ($L = 10\,\text{cm}$) of a lattice with $N = 9$ waveguides, as a function of $P_{\text{peak}}$, when the first waveguide is initially excited. Clearly, for low peak power, since the nonlinearity in Eq. (7.38) is weak and can be neglected (i.e. in Eq. (7.36), $\Lambda < 1$ which correspond to $P_{\text{peak}} < 190\,\text{kW}$), the lattice operates in the linear regime and the transfer to the ninth waveguide is perfect. When the peak power exceeds 800 kW, a discrete soliton is formed and the light is trapped in the excited waveguide. For intermediate input peak powers, we have partial transfer of the signal to other waveguides. Analogous results are expected for lattices of any $N$, when the coupling configuration is chosen so that in the linear regime the signal is transferred faithfully from the input waveguide to another. Therefore, such photonic lattices may operate as switches that are sensitive to the input peak power. For powers above a critical power, the signal remains trapped in the initially excited waveguide, whereas for input powers below another critical power, the signal is transferred perfectly from the input waveguide to another.

[10] Although throughout this theoretical model we consider monochromatic excitation of the lattice, in the case of broadband very short pulses temporal effects should be considered as well.

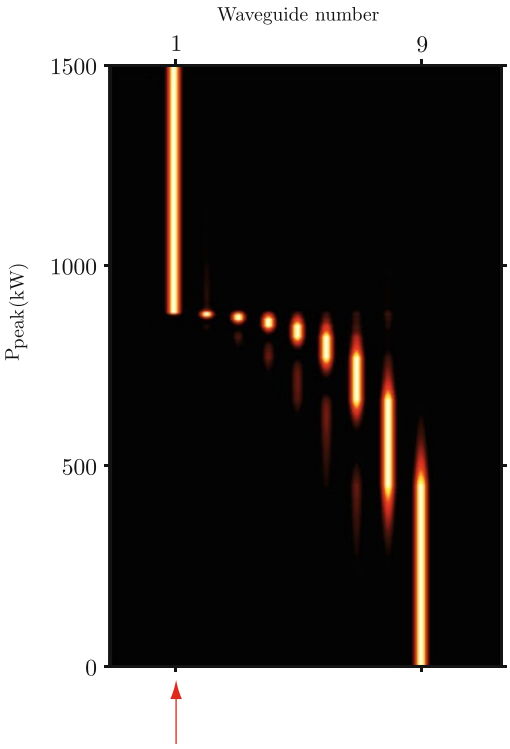


**Fig. 7.8** Numerical calculation of the output intensity as a function of the input peak power $P_{\text{peak}}$. The first waveguide is initially excited (*red arrow*). For weak input signals ($P_{\text{peak}} < 190\,\text{kW}$), the lattice operates in the linear regime and the signal is transferred from the first to the ninth waveguide. In the nonlinear regime ($P_{\text{peak}} \gtrsim 800\,\text{kW}$), a discrete soliton is formed, and the light stays confined in the initial waveguide

## 7.7 Conclusions

We have presented results on the realization of a state-transfer Hamiltonian with engineered couplings in photonic lattices [31]. Due to their simplicity and versatility, photonic lattices are excellent platforms for the implementation of various state transfer Hamiltonians. By contrast to NMR implementations, photonic lattices allow for the systematic engineering of networks of various topologies and coupling configurations. Moreover they offer scalability, as well as compatibility with the widespread silica technologies, which make them rather promising candidates for all-optical networking and large-scale quantum information processing.

The results presented in this chapter pertain to the optical analogue of a state-transfer Hamiltonian, and they emphasize that the problem of state transfer and the engineering of quantum networks goes beyond spin chains. In this first proof-of-principle experiment [31], there was no information encoded in the signal and thus, rigorously speaking the experiment was pertaining to the transfer of excitation rather than a quantum state. Yet, possible sources of imperfections and other limitations on the size of the networks have been revealed. Our experiment has been followed by analogous more elaborate experiments by other authors [45].

For purposes of quantum information processing one has eventually to encode information in the injected pulse, and study the transfer of non-classical quantum states. Femtosecond laser written waveguides in glasses are suitable for the manipulation of qubits with path [18] or polarization [46] encoding. Moreover, quadratically nonlinear waveguide arrays can be also fabricated by other means (see e.g. [10]), allowing for the generation of non-classically correlated biphotons, through spontaneous parametric down conversion [47]. Such ideas can be combined with ideas from the engineering of quantum networks and the problem of state-transfer, for the development of all-optical quantum chips that explore quantum phenomena to perform efficiently various tasks. The present results provide a benchmark case and guide for the planning of future experiments on all-optical networking and short-distance quantum communication.

## References

1. D.N. Christodoulides, F. Lederer, Y. Silberberg, Nature **424**, 817 (2003)
2. A. Szameit, S. Nolte, J. Phys. B **43**, 163001 (2010)
3. S. Longhi, Laser Photonics Rev. **3**, 243 (2009)
4. H. Trompeter, W. Krolikowski, D. Neshev, A. Desyatnikov, A. Sukhorukov, Y. Kivshar, T. Pertsch, U. Peschel, F. Lederer, Phys. Rev. Lett. **96**, 053903 (2006)
5. T. Schwartz, G. Bartal, S. Fishman, M. Segev, Nature **446**, 52 (2007)
6. Y. Lahini, A. Avidan, F. Pozzi, M. Sorel, R. Morandotti, D.N. Christodoulides, Y. Silberberg, Phys. Rev. Lett. **100**, 13906 (2008)
7. L. Martin, G. Di Giuseppe, A. Perez-Leija, R. Keil, F. Dreisow, M. Heinrich, S. Nolte, A. Szameit, A.F. Abouraddy, D.N. Christodoulides, B.E.A. Saleh, Opt. Express **19**, 13636 (2011)
8. A. Perez-Leija, H. Moya-Cessa, A. Szameit, D.N. Christodoulides, Opt. Express **35**, 2409 (2010)
9. R. Keil, A. Perez-Leija, F. Dreisow, M. Heinrich, H. Moya-Cessa, S. Nolte, D. N. Christodoulides, A. Szameit, Phys. Rev. Lett. **107**, 103601 (2011)
10. F. Lederer, G.I. Stegeman, D.N. Christodoulides, G. Assanto, M. Segev, Y. Silberberg, Phys. Rep. **463**, 1 (2008)
11. M. Bellec, P. Panagiotopoulos, D.G. Papazoglou, N.K. Efremidis, A. Couairon, S. Tzortzakis, Phys. Rev. Lett. **109**, 113905 (2012)
12. U. Peschel, R. Morandotti, J.M. Arnold, J.S. Aitchison, H.S. Eisenberg, Y. Silberberg, T. Pertsch, F. Lederer, J. Opt. Soc. Am. B **19**, 2637 (2002)
13. U. Röpke, H. Bartelt, S. Unger, K. Schuster, J. Kobelke, Opt. Express **15**, 6894 (2007)
14. J.W. Fleischer, M. Segev, N.K. Efremidis, D.N. Christodoulides, Nature **422**, 147 (2003)
15. A. Szameit, J. Burghoff, T. Pertsch, S. Nolte, A. Tünnermann, F. Lederer, Opt. Express **14**, 6055 (2006)
16. R. Keil, M. Heinrich, F. Dreisow, T. Pertsch, A. Tünnermann, S. Nolte, D.N. Christodoulides, A. Szameit, Sci. Rep. **1**, 94 (2011)
17. A. Politi, M.J. Cryan, J.G. Rarity, S. Yu, J.L. O'Brien, Science **320**, 646 (2008)
18. G.D. Marshall, A. Politi, J.C.F. Matthews, P. Dekker, M. Ams, M.J. Withford, J.L. O'Brien, Opt. Express **17**, 12546 (2009)
19. S. Longhi, Phys. Rev. B **82**, 041106(R) (2010)
20. S. Longhi, Opt. Lett. **33**, 473 (2008)

21. A. Szameit, F. Dreisow, M. Heinrich, T. Pertsch, S. Nolte, A. Tünnermann, E. Suran, F. Louradour, A. Barthélémy, S. Longhi, Appl. Phys. Lett. **93**, 181109 (2008)
22. R. Keil, Y. Lahini, Y. Shechtman, M. Heinrich, R. Pugatch, F. Dreisow, A. Tünnermann, S. Nolte, A. Szameit, Opt. Lett. **37**, 809 (2012)
23. Y. Joglekar, C. Thompson, G. Vemuri, Phys. Rev. A **83**, 063017 (2011)
24. R. Gordon, Opt. Lett. **29**, 2752 (2004)
25. S. Bose, Contemp. Phys. **48**, 13 (2007)
26. A. Kay, Int. J. Quantum Inf. **08**, 641 (2010)
27. J. Zhang, G. Lu Long, W. Zhang, Z. Deng, W. Liu, Z. Lu, Phys. Rev. A **72**, 012331 (2005)
28. J. Zhang, X. Peng, D. Suter, Phys. Rev. A **73**, 062325 (2006)
29. J. Zhang, N. Rajendran, X. Peng, D. Suter, Phys. Rev. A **76**, 012317 (2007)
30. J. Zhang, M. Ditty, D. Burgarth, C.A. Ryan, C.M. Chandrashekar, M. Laforest, O. Moussa, J. Baugh, R. Laflamme, Phys. Rev. A **80**, 012316 (2009)
31. M. Bellec, G.M. Nikolopoulos, S. Tzortzakis, Opt. Lett. **37**, 4504 (2012)
32. M. Christandl, N. Datta, A. Ekert, A. Landahl, Phys. Rev. Lett. **92**, 187902 (2004)
33. M. Christandl, N. Datta, T.C. Dorlas, A. Ekert, A. Kay, A.J. Landahl, Phys. Rev. A **71**, 032312 (2005)
34. G.M. Nikolopoulos, D. Petrosyan, P. Lambropoulos, Europhys. Lett. **65**, 297 (2004)
35. G.M. Nikolopoulos, D. Petrosyan, P. Lambropoulos, J. Phys.: Conds. Matter **16**, 4991 (2004)
36. A. Yariv, P. Yue, *Photonics: Optical Electronics in Modern Communications* (Oxford University Press, New York, 2006)
37. R.R. Gattass, E. Mazur, Nat. Photonics **2**, 219 (2008)
38. K.M. Davis, K. Miura, N. Sugimoto, K. Hirao, Opt. Lett. **21**, 1729 (1996)
39. J.H. Eberly, B.W. Shore, Z. Bialynicka-Birula, I. Bialynicki-Birula, Phys. Rev. A **16**, 2038 (1977)
40. Z. Bialynicka-Birula, I. Bialynicki-Birula, J.H. Eberly, B.W. Shore, Phys. Rev. A **16**, 2048 (1977)
41. R. Cook, B.W. Shore, Phys. Rev. A **20**, 539 (1979)
42. T. Fukuda, S. Ishikawa, T. Fujii, K. Sakuma, H. Hosoya, Proc. SPIE **5339**, 524 (2004)
43. V. Kostak, G. Nikolopoulos, I. Jex, Phys. Rev. A **75**, 042319 (2007)
44. G.M. Nikolopoulos, A. Hoscovec, I. Jex, Phys. Rev. A **85**, 062319 (2012)
45. A. Perez-Leija, R. Keil, A. Kay, H. Moya-Cessa, S. Nolte, L.C. Kwek, B.M. Rodríguez-Lara, A. Szameit, D.N. Christodoulides, Phys. Rev. A **87**, 012309 (2013)
46. L. Sansoni, F. Sciarrino, G. Vallone, P. Mataloni, A. Crespi, R. Ramponi, R. Osellame Phys. Rev. Lett. **105**, 200503 (2010)
47. A.S. Solntsev, A.A. Sukhorukov, D.N. Neshev, Y.S. Kivshar, Phys. Rev. Lett. **108**, 023601 (2012)

# Index




G.M. Nikolopoulos and I. Jex (eds.), *Quantum State Transfer and Network Engineering*, Quantum Science and Technology, DOI 10.1007/978-3-642-39937-4,

**E**



**F**



**G**



**H**



**I**



**J**



**K**



**L**

**M**



**N**



**O**



**P**



**Q**



**R**